2025

Journal of JART

—English edition—

2025

The Japan Association of Radiological Technologists

Journal of JART —English edition— 2025
The Japan Association of Radiological Technologists

CONTENTS

Note: The contents of this magazine are those that have been published in JART magazine.

Overview of the Japan Association of Radiological Technologists

The Japan Association of Radiological Technologists, a public interest incorporated association under the jurisdiction of the Ministry of Health, Labour and Welfare, was established in 1947 with the purpose of contributing to the health of citizens through raising the professional ethics of members, improving and furthering the study of medical radiology and medical radiological technology, and enhancing public health.

In light of the startling progress being made in the fields of image diagnostics and radiation therapy where radiological technologists work, it is necessary to stay constantly aware of the latest know-how and technology. JART collaborates with other certification agencies to enhance the capacity of all radiological technologists in general through providing lifelong learning seminars, short courses, academic conferences and numerous other learning opportunities. We believe that such activities constitute our obligation as medical professionals to the general public.

As the only medical profession that has “radiological” in its name, we strive to limit medical exposure, to raise the standing of our profession, and to realize a profession of specialist technologists that can be advertised. And we are committed to promoting services with you all for the provision of safe and secure medical care.

general principles

We will render our services to those in need of health care.

We will act as individual members of a health care team.

We will perform our duties in our field of specialty.

We will continue to study for the benefit of mankind.

We will respect and practice the policy of informed consent.

Regarding Publication of the English Edition

UEDA Katsuhiko (President)

The journal of the JART English version issues every year. It has a favorable reception for we members of the world and general people. As well as this issue, 13 articles to be useful for radiological technologists are issued.

We will feature clinical, educational, and research-based achievements by radiological technologists in the monthly issues of the JART journal, and continually work to improve the magazine. I truly hope that this English edition will benefit radiological technicians worldwide.

To give our radiological technologists from across the globe an insight into our business, I will briefly explain the history of the JART. In March 1896, we succeeded in taking the first X-ray image in Japan. In 1897, Shimadzu Corporation released an X-ray generator for educational use. In 1925, there were approximately 1,500 X-ray technicians. In 1927, the first Shimadzu X-ray Technician Training Institute was established, and evidence-based education was put in place. The JART was founded in 1947 to make “radiological technologist” a national qualification. Since its establishment, we have worked towards broad acceptance of this national qualification, in collaboration with the government, the Diet, the Japanese Medical Association, and occupational military authorities.

As a result in June 1951, we were finally able to see the promulgation of the Radiology X-ray Technicians Act, Act No.226 of 1951. Since then, we have responded to the changing needs of the society, revising the original act to get the Radiology X-ray Technicians Act of 1968 passed, and partially revising that to get the Radiology Technicians Act and Radiology X-ray Technicians Act of 1983 passed, and finally getting the Radiology Technicians Act, which is in place currently, passed. Back then, the scope of work was limited to general X-ray testing, television X-ray testing, angiography, X-ray computed tomography scanning, RI scanning, and radiation therapy. In 1993, the Radiology Technicians Act was further revised, and MRI scanning, ultrasonic testing, and non-mydriatic fundus camera examination were added to the list. In 2010, image interpretation assistance, radiation examination explanation, and consultation work were added. In April 2015, intravenous contrast agent injection using automated contrast injectors, needle removal and hemostasis, lower digestive tract examination (anal catheter insertion and administration of contrast medium), anal catheter insertion, and oxygen inhalation during radiation therapy were added as operations that could be performed by radiological technologists.

In October 2021, the needle insertion for examinations of contrasting of the examination for CT, MRI, Ultrasound and Radioisotope are added as the new operation that can be performed by radiological technologists.

The JART will continue to respond to the needs of the medical industry, and we hope to broaden the operational scope of radiological technologists based on our foundation in scientific evidence.

History of The Japan Association of Radiological Technologists (JART)

1947
- Establishment of JART (July 13)

1951
- Promulgation of the Act on Medical Radiographers (June 11)
- Authorization for Establishment of the Japan Association of Radiographers (June 13)

1954
- First national examination for Medical Radiographers (May 30)

1956
- Event to commemorate the 10th anniversary of founding, attended by Her Imperial Highness Princess Chichibunomiya

1962
- Event to commemorate the 15th anniversary of founding and 10th anniversary of enactment of the Act on Medical Radiographers, attended by Her Imperial Highness Princess Chichibunomiya

1968
- Promulgation of the Act to Partially Revise the Act on Medical Radiographers (establishment of two professions) (May 23)
- First national examination for radiological technologists

1969
- Renaming as the JART
- Staging of the 4th International Society of Radiographers & Radiological Technologist (ISRRT) World Congress at Tokyo Palace Hotel, attended by Her Imperial Highness Princess Chichibunomiya

1975
- Event to commemorate the 80th anniversary of the discovery of X-rays, attended by Her Imperial Highness Princess Chichibunomiya

1979
- Completion of the Education Center for JART

1983
- Partial revision of the Act on Medical Radiographers and the Act on Radiological Technologists (unification of the professions)

1985
- Event to commemorate the 90th anniversary of the discovery of X-rays, attended by Her Imperial Highness Princess Chichibunomiya
- Staging of the 1st Japan Conference of Radiological Technologists

1987
- General assembly resolution for establishment of the New Education Center and a four-year university

1989
- Completion of the New Education Center (Suzuka City)

1991
- Opening of Suzuka University of Medical Science

1993
- The Act to Partially Revise the Act on Radiological Technologists, and Ministerial Ordinance to Partially Revise the Enforcement Orders (April 28)

1994
- Appointment of the President of JART as the 11th President of ISRRT

1995
- Event to commemorate the 100th anniversary of the discovery of X-ray, attended by Her Imperial Highness Prince Akishinomiya

1996
- Start of the Medical Imaging and Radiologic Systems Manager certification system

1998
- Staging of the 11th ISRRT World Congress at Makuhari

1999
- Start of the Radiation Safety Manager certification system

2000

- "Presentation of the Medical Exposure Guidelines (Reduction Targets)" for patients

2001

- Start of the Radiological Technologists Liability Insurance System

2003

- Enactment of X-Ray Week

2004

- Relocation of offices to the World Trade Center Building in Tokyo

2005

- Start of the Medical Imaging Information Administrator certification system

2006

- Staging of a joint academic conference between Japan, South Korea, and Taiwan
- Revision of the Medical Exposure Guidelines

2008

- Establishment of the committee on Autopsy imaging (Ai)

2009

- Revision to the national examination for radiological technologists
- Launch of the Team Medicine Promotion Conference, with the President of JART as its representative
- Appointment of the President of JART as chairperson of the Central Social Insurance Medical Council specialist committee

2010

- Health Policy Bureau Director's notification concerning promotion of team medicine

2011

- Support activities following the Great East Japan Earthquake
- Staging of an extraordinary general meeting concerning transition to a public interest incorporated association

2012

- Registration of transition to a public interest incorporated association (April 1)
- Event to mark the 65th anniversary of founding and transition to a public interest incorporated association (June 2)
- Renaming as public interest incorporated association JART
- Launch of the Radiological Technologists Liability Insurance System with participation by all members

2013

- Signing of the Comprehensive Mutual Cooperation Agreement on Prevention of Radiation Exposure (September 21)

2014

- Consignment of work to measure personal exposure of residents
- Revision of the Act on Radiological Technologists, Government Ordinance to Partially Revise the Enforcement Orders, and Revision of the Enforcement Regulations (June 25)
- Launch of the radiation exposure advisor certification system

2015

- Event to commemorate the 120th anniversary of the discovery of X-rays

2017

- Event to mark the 70th anniversary of founding (June 2)

2018

- Notice from the Regional Medical Care Planning Division Director, Health Policy Bureau, Ministry of Health, Labour and Welfare, and Director of the Economic Affairs Division regarding Operational Considerations for Securing a System for Safety Management pertaining to Medical Equipment

2019

- Notice from the Health Policy Bureau on a Safety Management System for Medicinal Use of Radiation

2020

- Partial revision of the Ordinance on Prevention of Ionizing Radiation Hazards

2021

- Relocation of offices to the Mita Kokusai Building in Tokyo
- Revision of the Radiological Technologists Act expanded the scope of practice.
- Holding the 23th AACRT with 37th JCRT in Tokyo

2022

- Event to mark the 75th anniversary of founding (July 16)

Received July 10, 2023; accepted December 5, 2023

Proposal for training that does not use radiotherapy equipment and verification of training effects

MORI Yutaro[1], ISOBE Tomonori[1]*, NAGAI Yoshiaki[2], TOMITA Tetsuya[3], KOBAYASHI Daisuke[3], TAKEI Hideyuki[4], YANAGITA Satoshi[2], FUKUSHI Masahiro[2], YANAGAWA Noriyuki[2], SAKAE Takeji[1]

1) Institute of Medicine, University of Tsukuba
2) Department of Radiological Technology, Tsukuba International University
3) Department of Radiology, University of Tsukuba Hospital
4) National Institutes for Quantum Science and Technology

First Author: MORI Yutaro, E-mail: ymori@md.tsukuba.ac.jp
* Corresponding Author: ISOBE Tomonori, E-mail: tiso@md.tsukuba.ac.jp

Note: This paper is secondary publication, the first paper was published in the JART, vol. 71 no. 858: 22-29, 2024.

Key words: Undergraduate education, practical training, radiotherapy, dosimetry, particle beam therapy

【Abstract】
Purpose: The purpose of this study was to design effective radiotherapy training that can be used even in facilities without radiotherapy equipment and to verify its educational effects.
Methods: Practical training was planned and implemented for five themes: medical safety, brachytherapy, dosimetry, external irradiation, and proton therapy. After the practical training, a questionnaire survey was conducted to verify the educational effects.
Results: The Students scored 4 or higher out of 5 for all of the questionnaire items of each training theme. Interest in radiotherapy increased significantly after receiving the practical training.
Discussion: Many students evaluated the practical training highly, and it seemingly increased their interest in radiotherapy. In the future, it will be necessary to further examine the contents of hands-on training and aim to improve the training.

Introduction

In Japan, the regulations for the designation of radiological technologist schools and training institutes were modified in 2015 in response to business expansions due to the revision of the Radiological Technologists Act in 2014. Along with the modification, a review committee for improving the curriculum and other aspects of the training school for radiological technologists was established under the Ministry of Health, Labor and Welfare, and in March 2021, new guidelines for the training school were established. The purpose of the guidelines were to "improve the quality of clinical training for advanced medical personnel via by learning basic radiological techniques through practice in clinical settings in order for them to appropriately respond to patients with diverse needs." The current 10 units of clinical training will be expanded to 12 units. In addition, it has been proposed that "mandatory preclinical evaluations should be conducted in order to confirm in advance if applicants have the appropriate knowledge, skills, and attitudes desired for clinical training."

Clinical training in radiological technologist education is a valuable opportunity to convert the knowledge and skills learned thus far into practical ones. Basic knowledge is acquired via pre-practice education so that students can experience things that cannot be learned in classroom lectures in clinical practice. This is so they can find and organize the issues they need on their own. In addition, it is desirable for students to learn the atmosphere of an actual hospital. If an educational institution is equipped with sufficient medical equipment, it is possible to have students experience and learn in a way that is close to that of the real

world. But many facilities do not have radiotherapy equipment because it is expensive. Radiotherapy is a minimally invasive and low-impact cancer treatment, and its use is on the rise as the number of cancer patients increases. There are 6.2 million radiation treatments performed annually worldwide[1]. In recent years, there has been an increase in medical accidents due to over- or under-irradiation in radiotherapy, not only in Japan but also in many hospitals around the world. These have made people aware of the potential dangers of radiotherapy, which is in increasing demand, and called into question the need for awareness of medical safety[2]. The work of radiological technologists continues to increase and is becoming more complex, and the technology is expected to grow as medical care advances[3]. It is believed that the knowledge and abilities necessary for the implementation of accurate and safe treatment will change, and it has been reported that the education and training of radiological technologists need to be improved[4]. In the Japanese curriculum, the number of credits for radiotherapy technology was revised from six credits to seven credits. Specifically, students will be required to study the principles of radiotherapy and of particle beam therapy and the measurement and evaluation of absorbed doses. In this way, the importance of education of radiotherapy is being recognized again. Radiotherapy differs in the diagnostic field in many respects, such as the appearance of the device, handling of the brachytherapy source, quality control, and medical safety. Therefore, if clinical training starts without sufficient pre-training education, sufficient educational effects will not be obtained. In this study, we proposed an effective practical training protocol for radiological technologists before clinical training, even at educational facilities that do not have radiotherapy equipment. Moreover, the educational effect of the practical training was examined via a questionnaire survey.

Methods

1. Training content

In the FY 2021 Medical Radiological Technology Practicum I course at a four-year university with a clinical radiology department, an on-campus practical training titled "The Basics of Radiotherapy" was carried out. The targets were 89 students, and the practical training was divided into groups of about 10 people, with practical training sessions of 90 minutes × three sessions. The themes were (1) medical safety, (2) brachytherapy, (3)dosimetry (QA, QC), (4) external irradiation, and (5) proton therapy. These were implemented according to the schedule shown in Table 1.

The practical training study was conducted in three periods of 90 minutes each. The themes of medical safety, brachytherapy, dosimetry (QA, QC), external irradiation, and proton therapy were dealt with according to the schedule shown in the table.

The contents of each theme are detailed below.

① Medical safety

After lectures on medical safety, medical adverse events, and incident reports, the students were asked to write incident reports using examples.

② Brachytherapy

We outlined the flow of brachytherapy and gave a lecture on how to plan treatment. Af-

Table 1 Practice schedule
The practical training study was conducted in three periods of 90 minutes each. The themes of medical safety, brachytherapy, dosimetry (QA, QC), external irradiation, and proton therapy were dealt with according to the schedule shown in the table.

Time	Learning items
13:00–13:45	① Medical safety
13:45–14:30	② Brachytherapy
14:30–14:40	rest
14:40–16:10	③ Dosimetry (QA, QC)
16:10–16:20	rest
16:20–17:05	④ External irradiation
17:05–17:50	⑤ Proton therapy

ter that, for practical training, students were shown points A and B, which were important dose evaluation points in the Remote After Loading System, on an illustration of the uterus.

③ Dosimetry (QA, QC)

Lectures on dose measurement and standard dosimetry of the absorbed dose to water in external beam radiotherapy 12 were given with calculation problems. After that, we let the students experience the flow from dose measurement using Excel to monitor unit calibration.

④ External irradiation

Two videos (deep inspiration breath hold for left breast cancer and Intensity-Modulated Radiation Therapy for the head and neck) were shown to demonstrate actual radiotherapy. After watching the video, the students summarized the flow of radiotherapy.

⑤ Proton therapy

After explaining the characteristics of proton beam therapy, representative cases, and an overview of the treatment equipment, we practiced using Excel to create a spread-out Bragg peak from a monopeak.

2. Conducting the questionnaire survey

An anonymous questionnaire was conducted after the end of the on-campus clinical training. At the time of conducting the questionnaire, we informed students that the content of the answers had no effect on their grades. As shown in Fig. 1, the contents of the questionnaire were roughly divided into four parts: 1) Impressions of each training theme, 2) Whether or not the training was good for clinical training, 3) Interest in radiotherapy, and 4) Free comments. Responses were evaluated on a 5-point scale, wherein 5: strongly agree, 4: agree, 3: neither agree nor disagree, 2: disagree, and 1: strongly disagree. The reason for using the five-case method, which includes intermediate values, is because we thought that (1) we would obtain data from an intermediate group that could not be judged either way, and (2) a certain number of students would find it difficult to give a negative answer due to their position as students.

1) Impressions of each training theme
  [1] Explanation was sufficient and easy to understand
  [2] Handouts were thorough
  [3] The time given for the training content was appropriate
  [4] I understood the content
  [5] I am satisfied with the content
2) Are you glad to have received this training in preparation for your clinical training?
3) Interest in radiotherapy
  [1] Were you interested in radiotherapy before taking this practice?
  [2] Are you interested in radiotherapy after taking this practice?
4) Other, free comments

Fig. 1 Training questionnaire contents

Except for free comments, responses were evaluated on a 5-point scale, wherein 5: Strongly agree, 4: Agree, 3: Neither agree nor disagree, 2: Disagree, and 1: Strongly disagree.

3. Changes in grades before and after practical training

In parallel with this practical training, a lecture on radiotherapy technology II was being held as a subject for the first semester of the third year. In order to evaluate the learning effect of the practical training, we compared the final examination results of 2020, before this practical training was conducted, and the results of 2021, when the practical training was conducted.

4. Data analysis/statistics

In the content 2(Conducting the questionnaire survey), in order to verify the content of Question 3) Interest in radiotherapy, we examined the significance of the planned practice via Wilcoxon's signed-rank test with matched samples. In the content 3(Changes in grades before and after practical training), Welch's t-test with independent samples was used to examine the significance of the change in performance before and after the practical training. SPSS ver.28.0.0.0 (IBM) was used for all

of the statistical processing, and the statistical significance level was set at 5%.

5. Research ethics

This research was conducted with the approval of the president after review by the ethics committee of the research institution (approval number R04-8). The author and all co-authors have no conflicts of interest directly relevant to the content of this article. The research was explained to the target students during the guidance time. At that time, we informed them that the survey would be anonymous and that the results of their responses would have no bearing on their grades, and obtained their written consent. An outline of the study was also posted on a bulletin board, and sufficient time was allowed for withdrawal of consent.

Results

Fig. 2 shows the questionnaire results for each training theme. Across all of the ques-

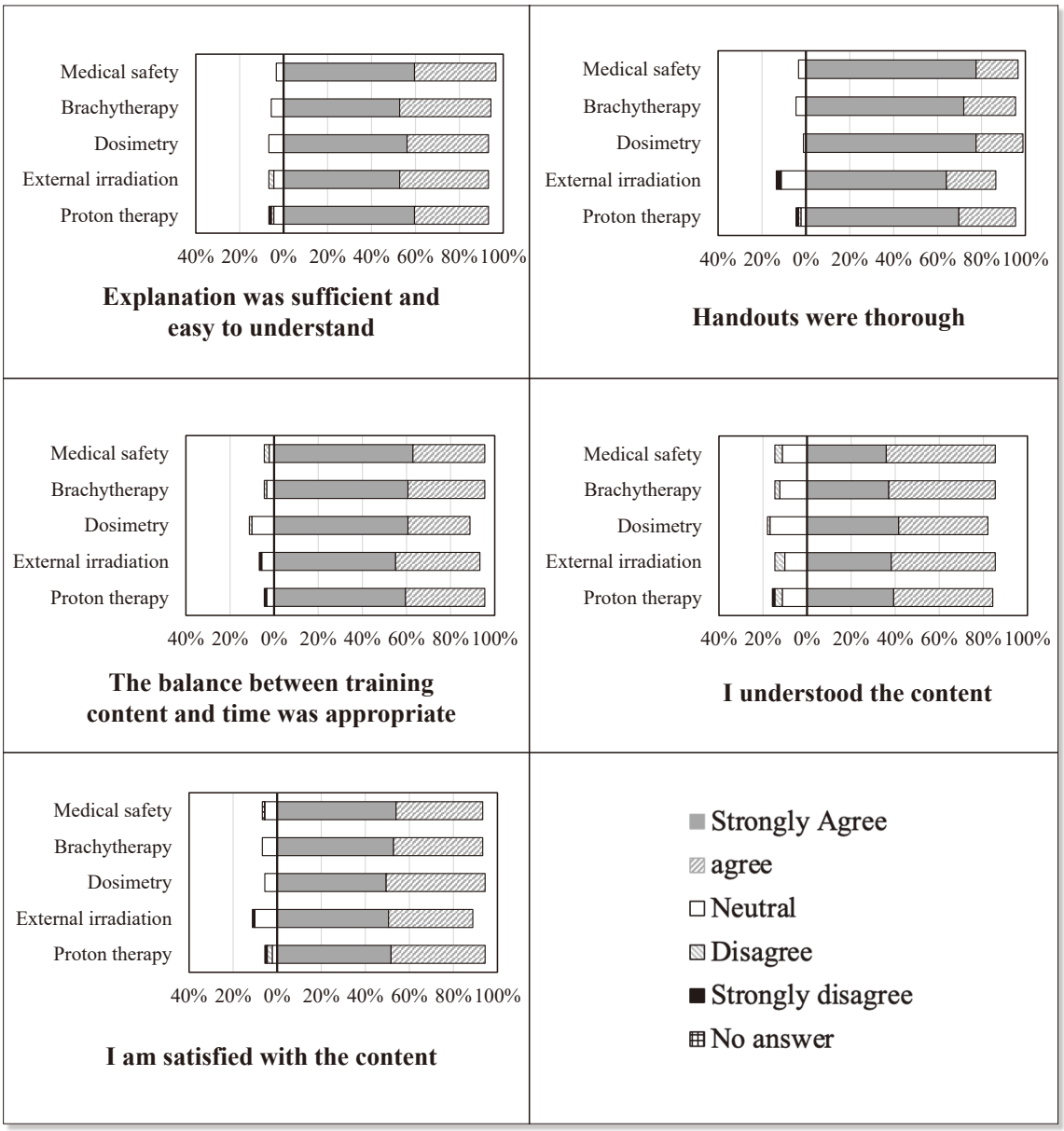

Fig. 2 Practical questionnaire results

The results of the "impressions of each training" theme in the training questionnaire are shown. More than 80% of the students answered "strongly agree" or "agree" to all of the question items.

tion items, the total number of students that strongly agreed or agreed fell no lower than 73 (82.0%). In other words, more than 80% of the students gave a high evaluation of the course content overall. More than 90% of the students answered that they were "satisfied" with the theme other than external irradiation (79 students [88.8%] for external irradiation). There was no significant difference in the number of respondents who answered "strongly agreed" or "agreed" for each theme. The least number of respondents answered "strongly agreed" or "agreed" for the question "I understood the content" among all themes.

There was no negative answer to the question "Are you glad to have received this training in preparation for your clinical training?", and more than 80% of the students answered that they strongly thought so (Fig. 3).

Fig. 4 shows the interest in radiotherapy before and after the practical training. The number of respondents who answered "strongly agree" and "agree" increased significantly, which indicates that the interest in radiotherapy significantly improved after the training (before training: 3.5, after training: 4.2; $p < 0.001$).

In terms of free comments, we received the following: "I felt that the appearance of the engineer in the video was very cool. Through this practical training, my awareness of hospital training increased, and I felt that I would like to make use of it in the actual workplace." In addition to such positive opinions, we also received other opinions, including the following: "I wanted to be more active than as a participants in classroom lectures. I wish there were more discussions with teachers and between students." Other opinions were also received.

Fig. 5 shows a comparison of the results of the final examination of radiotherapy technology II between the 2020 third-year students, who did not have practical training, and the

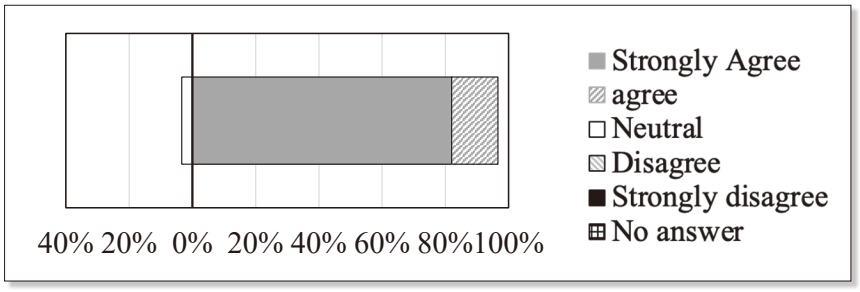

Fig. 3 Practical questionnaire results

—Are you glad to have received this training?—
This figure shows the results of the practical training questionnaire, "Was it good to receive this training for clinical training?" More than 80% of the students answered "strongly agree."

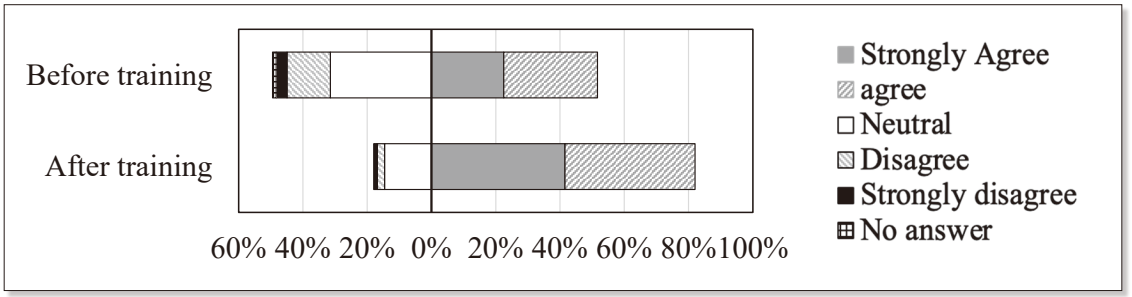

Fig. 4 Practical questionnaire results

—Are you interested in radiotherapy?—
The results of "interest in radiotherapy" in the practice questionnaire are shown. The interest in radiotherapy increased significantly after the practical training.

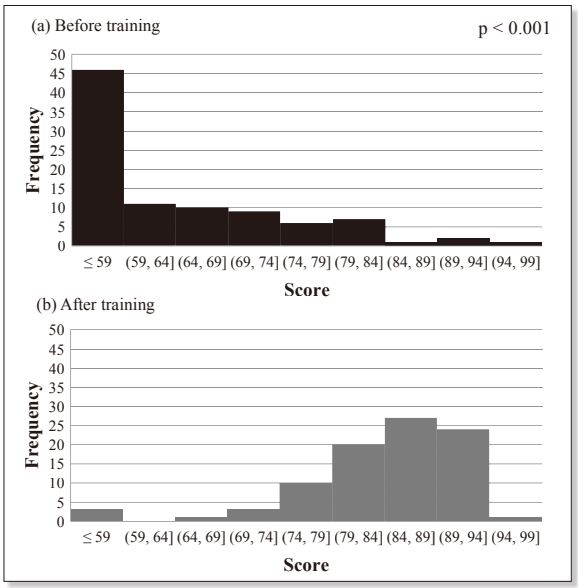

Fig. 5 Comparison of radiotherapy technology II test results

A comparison of the final examination results of radiotherapy technology II (third-year students) in 2020, before practical training was not conducted, and in 2021, when this practical training was conducted, is shown.

2021 third-year students, who had this practical training. Compared to the previous year, the results significantly improved, and the median score increased by 26.9 points.

Discussion

Many students gave the practical training a high evaluation, and their interest in radiotherapy increased. It is thought that this training could serve as a bridge to clinical training. With regard to the method of clinical training, it is said that a format in which clinical trainees participate as members of the medical care team is desirable[5]. It is thought that this practical training was also highly evaluated because it was possible to get a real feeling of practical training by incorporating a lot of time to actually move hands on multiple themes.

One of the reasons for the improvement in the results of the radiotherapy technology II examination was that the students' understanding of the lectures was further deepened by the lectures being held at the same time as the practical training. Lecture-style guidance can convey a lot of information in a limited amount of time, but it tends to be a one-way communication of information, and students are likely to be passive and less motivated[6-8]. The themes dealt with in this practical training, such as dose calculation and irradiation methods, are difficult to convey in classroom lectures, so it is effective to have students learn by actually using their own hands. The synergistic effect of classroom lectures and practical training can be applied to other fields, suggesting the possibility of greatly contributing to the improvement of educational effects. In order to further enhance the effectiveness of learning and training, it is important not only to improve quality independently, but also to deepen the relationship by being aware of both sides of the issue and complementing each other. However, the improvement in scores in this study was a comparison of different grades, and it is possible that differences in backgrounds such as the level of the students and their interest in radiotherapy may have contributed to the improvement in scores. Although a comparison between the groups that received the practical training and those who did not is effective in evaluating the improvement in performance, the practical training is a required course to all students, and it is difficult to obtain data on groups that do not experience practical training.

Regarding the reason why the theme of external irradiation was rated lower than the others, the content was mainly video, and there were few handouts compared to other themes. In addition, the teacher stopped the videos one by one and added explanations. These were considered to be the factors that lowered the level of satisfaction. In order to raise the level of "understandability" to that of the other practical training themes, the contents of the videos need to be further improved.

One of the other points to be improved in this training was that as a result of pursuing

things that can be easily done without a linear accelerator, desk work has become the main focus. In the questionnaire results, the number of respondents who strongly agreed or agreed with "I understood the content" was smaller than the others. This was thought to be because although teachers provided sufficient explanations and materials to the students, the students lacked the motivation to actively deepen their understanding due to the decrease in opportunities for students to think and speak for themselves. In the educational evaluation of clinical training, it is desirable to use an evaluation method that enables close communication between clinical training instructors and trainees, indicates specific goals, and confirms the process of self-development[9,10]. To incorporate the opinions of students who wanted to be more active and engaged in discussions, we recommend introducing Objective Structured Clinical Examination (OSCE)[11] and conducting group discussions on incidents and videos viewed. This time, five themes were implemented in 90 minutes × three sessions, so it was difficult to prepare enough time for a discussion. We believe it is necessary to increase the training time and to devise better methods for pruning and selecting training content.

Conclusion

We planned effective training even at treatment facilities that did not have radiotherapy equipment and examined the educational effects through a questionnaire survey.

Based on the educational curriculum for radiological technologists, we were able to build practical training with a high degree of student satisfaction by incorporating the principles of particle beam therapy and the measurement and evaluation of the absorbed dose.

In an effort to achieve more participatory training, it is necessary to aim for further training improvement centered around the keystones of "active participation" and "discussion."

Acknowledgments

I would like to express my deep gratitude to all of the students who cooperated with the questionnaire survey in advancing this research.

References

1) UNSCEAR ANNEX A.: Evaluation of medical exposure to ionizing radiation. UNSCEAR 2020/2021 Report Volume I, 2022.
2) ICRP.: Prevention of Accidents to Patients Undergoing Radiation Therapy. Publication 86. Annals of the ICRP, 2000.
3) Terashita T, et al.: Problem-based learning for radiological technologists: a comparison of student attitudes toward plain radiography. BMC Med Educ, 16, Article number 236, 2016.
4) Izewska J, et al.: Improving the quality of radiation oncology: 10 years' experience of QUATRO audits in the IAEA Europe Region. Radiother Oncol, 126, 183-190, 2018.
5) Eriksen JG, et al.: The updated ESTRO core curricula 2011 for clinicians, medical physicists and RTTs in radiotherapy/radiation oncology. Radiother Oncol, 103, 103-108, 2012.
6) Kelly PA, et al.: A comparison of in-class learner engagement across lecture, problem-based learning, and team learning using the STROBE classroom observation tool. Teach Learn Med, 17, 112-118, 2005.
7) Sangestani G, et al.: Comparison of problem-based learning and lecture-based learning in midwifery. Nurse Educ Today, 33, 791-795, 2013.
8) Wijnen M, et al.: Comparing problem-based learning students to students in a lecture-based curriculum: learning strategies and the relation with self-study time. Eur J Psychol Educ, 32, 431-447, 2017.
9) Li Q, et al.: Pre-training Evaluation and Feedback Improve Medical Students' Skills in Basic Life Support. Med Teach, 33, e549-555, 2011.
10) Alamrani MH, et al.: Comparing the Effects of Simulation-Based and Traditional Teaching Methods on the Critical Thinking Abilities and Self-Confidence of Nursing Students. J Nurs Res, 26, 152-157, 2018.
11) Harden RM, et al.: Assessment of Clinical Competence using Objective Structured Examination. Br Med J, 5955, 447-451, 1975.

Received November 20, 2023; accepted December 17, 2023

Detection of colitis using artificial intelligence with fat stranding in computed tomography images as a feature value

ETO Yoshihiro, M.S[1, 2)]*, ETANI Reo, Ph.D[3)], SHINAGAWA Yoshimitsu, Ph.D[4)], OJIMA Mitsuaki, Ph.D[5)]

1) Medical corporation Jikeikai Nishida hospital
2) Doctral Program, Health Sciences Graduate School, Oita University of Nursing and Health Sciences
3) Laboratory of Environmental Health Science, Department of Health Sciences, Oita University of Nursing and Health Sciences
4) Laboratory of Health Informatics and Biostatistics, Department of Health Sciences, Oita University of Nursing and Health Sciences
5) Laboratory of Environmental Health Science, Department of Health Sciences, Oita University of Nursing and Health Sciences

* E-mail: ethiro1967@gmail.com

Note: This paper is secondary publication, the first paper was published in the JART, vol. 71 no. 859: 24-33, 2024.

Key words: computed tomography images, SVM classification model, colitis detection, fat stranding

【Abstract】

Previous studies on the use of artificial intelligence to assist in the diagnosis of colitis on CT images have used the thickness of the colon wall after the use of digestive tract contrast media as a feature, but the diagnostic accuracy was not always high.

In this study, we verified that the CT value of fat stranding of colitis (HU) is a useful feature in the colitis detection model.

From non-contrast colitis CT images of 187 cases, we created an original image in which the affected area was cut into a 128 × 128 matrix, a mask image in which structures other than the fat stranding were erased, and a threshold image in which only the fat stranding was displayed.

The SVM classifier output the classification accuracy of the original image, mask image, and threshold image, and the results showed that the accuracy of the mask image and threshold image improved over the original image.

This indicates that fat stranding is a feature for higher accuracy classification.

1 INTRODUCTION

The number of computed tomography (CT) scans performed has increased exponentially in Japan over the last few decades because of the ability of CT scans to enable rapid acquisition of specific information.[1)]

However, despite the increase in the number of CT examinations, the number of radiologists is decreasing year by year,[2)] which is placing a heavy burden on current radiologists.[3, 4)]

Especially in emergency rooms (ERs), where radiologists are absent, diagnostic imaging is often performed by non-specialized ER physicians, and this has been reported to lead to a higher prevalence of misdiagnosis.[5, 6)]

Acute abdomen, the main target disease in the ER, has a high prevalence in patients of all age groups.[7, 8)] Ebina et al.[9)] reported that compared with radiologists, ER physicians have a higher misdiagnosis rate in diagnostic imaging of acute abdomen than in intracranial diseases.

This is largely attributed to the meticulous examination of vascular system, free air, and presence of ascites in addition to parenchymal and luminal organs required by CT imaging in the ER.

If an artificial intelligence (AI) system could achieve radiologist-level accuracy in interpretation of CT images in the detection of acute abdomen in abdominal CT imaging, it would improve work efficiency, such as by helping to prevent lesions from being overlooked and improving image interpretation. It would also

support diagnostic imaging by doctors other than radiologists, and could be a useful tool to compensate for the current shortage of radiologists.[6)]

However, in a literature review on the detection of acute abdominal disease using AI, Eto et al.[10)] reported that CT diagnostic imaging support for acute abdominal disease using AI has not been a primary focus of active research because the accurate identification of specific abnormalities or lesions within the abdominal organs poses challenges to AI owing to their complex and variable characteristics.

Among acute abdominal diseases, few studies have been conducted on AI diagnosis of colitis in particular.[11–14)]

Furthermore, existing studies have concluded that the accuracy of lesion detection is lower than that for other acute abdominal diseases such as renal and ureteral stones and gallstones. This is primarily because the thickness of the colon wall, identified as a feature, often leads to misclassification as an intra-abdominal organ, and false-negative results are likely to occur when the thickening of the colon wall is mild. In addition, to measure the thickness of the colon wall, previous reports have used oral or transvenous contrast agents, which is risky, necessitates expertise, and has the disadvantage of the inability to identify colitis if contrast agents are not available.

Other than morphological changes of the colon in colitis, other characteristics include fat stranding caused by inflammatory spillover to adipose tissue surrounding the colitis,[15–17)] as shown in Figure 1.

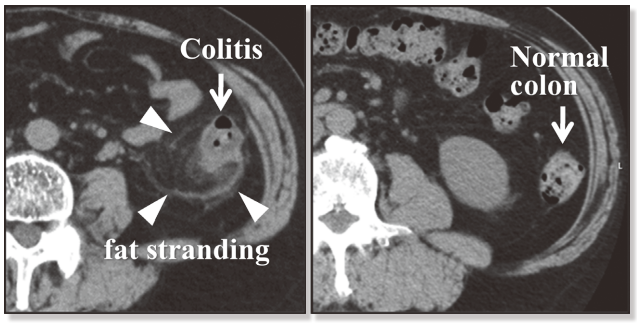

(a) Colitis (b) Normal colon

Fig. 1 CT image of fat stranding

Fat stranding increases CT values of adipose tissue around the colon.

This region of fat stranding has higher CT values than the surrounding normal fat. In other words, if the fat stranding can be detected with high accuracy by AI in non-contrast simple CT scans, the presence or absence of colitis can be diagnosed, thereby complementing the diagnosis of colitis by non-specialists in emergency medicine.

In the present study, with a focus on the CT value of fat stranding around colitis and how it differs from those of normal adipose tissue and the surrounding organs, we aimed to clarify whether fat stranding is an effective feature for colitis detection by machine learning (ML) models.

2 METHODS

In this study, colitis was defined as a general term for diseases that cause inflammation of the colon, including diverticulitis, infectious colitis, ischemic colitis, and ulcerative colitis.[18)]

1) Image collection for colitis analysis

From January 2013 to December 2021, 345 patients presented with abdominal pain as a primary symptom at the emergency or general outpatient clinic and were diagnosed with colitis. Of these cases, 211 diagnoses were confirmed through non-contrast abdominal CT images by two experienced radiologists with 35 and 13 years of expertise, respectively. After excluding patients without any discernible fat layer around the colon, those with conditions associated with generalized edema, and those exhibiting pronounced image artifacts due to movement or foreign bodies, 187 CT images were analyzed.

A single representative image from the colitis-affected region was chosen for each of the 187 patients. Images already linked to the

radiologist's colitis report were primarily selected. For cases where no image was linked, a radiological technologist with 18 years of experience in CT examinations chose an image displaying characteristic fat stranding indicative of colitis based on the radiologist's observations. All images were extracted from the imaging server in bitmap (bmp) format, with all patient-identifying information removed to protect privacy.

The demographic characteristics of the 187 patients with colitis are shown in Table 1. Notably, males were marginally more prevalent, and a significant portion, approximately 60%, were aged between 40 and 60 years. Most patients (about 89%) had been diagnosed with colonic diverticulitis, with the most common onset locations being the cecum and ascending colon (about 55%) and the descending colon (about 32%). The high prevalence of colonic diverticulitis is attributed to its standing as a common cause for gastrointestinal hospitalization,[19] its increasing incidence rate,[20, 21] and a rise in diagnoses in recent years.[22]

The device used was A: Activion 16 (Canon Medical Systems Corp., Otawara, Japan, between January 2013 and March 2019) and B: Fuji Supria Grande 64-row multi-helical CT system (Fuji film Healthcare Corp. (Currently Fuji film Medical Corp.), Tokyo, Japan, March 2019 and the end of December 2021) .

Of the 187 patients, 112 were examined using the equipment A. The remaining 75 patients were examined using the equipment B. The normal images were arbitrarily extracted so that the device, year, and number of affected sites were the same as those for the colitis images, and the total number of colitis and normal images was 374.

This study was approved by the ethics review committees of Medical Corporation Jikeikai Nishida Hospital (No. 202202-1) and the Oita University of Nursing and Health Science (No. 21-72).

Table 1 Breakdown of the 187 patients with colitis

Total number	187								
Sex	Male 102 / Female 85								
Age, years	10 ~	20 ~	30 ~	40 ~	50 ~	60 ~	70 ~	8 ~	90 ~
	2	8	27	39	37	35	25	12	2
Disease	Diverticulitis		Infectious colitis			Ischemic colitis			Other
	166		7			10			4
Site of inflammation	Ascending Cecum		Transverse		Descending		Sigmoid		Rectum
	102		6		60		18		1

Males were marginally more prevalent, and a significant portion, approximately 60%, were aged between 40 and 60 years. Most patients (about 89%) had been diagnosed with colonic diverticulitis, with the most common onset locations being the cecum and ascending colon (about 55%) and the descending colon (about 32%).

2) CT scanner imaging conditions

Both imaging systems utilized a tube voltage of 120 kV with automatic exposure control for the CT dosage. Output images maintained consistent noise levels across body shapes, set to standard deviation values of 8 for the Canon Activion 16 and 10 for the Fuji Supria Grande. Both systems had a 5-mm slice reconstruction interval with standard reconstruction functions applied. No image filtering was implemented post-scan. The window width and level were consistently set to 300 and 15, respectively, regardless of the equipment or imaging period.

3) Overview of the ML model development

An overview of the ML model development is shown in Figure 2. To verify that fat stranding around colitis was a feature, an original image was created by extracting the affected area of the original image into a 128 × 128 matrix. Normal images were also created in the same way. Histograms of these images were then developed, and through a combination of histogram bins, luminance thresholds, and hyperparameters, the SVM classifier was optimized for maximum classification accuracy. The accuracies of the mask and threshold images were compared with the original image to verify whether fat stranding had been captured as a feature.

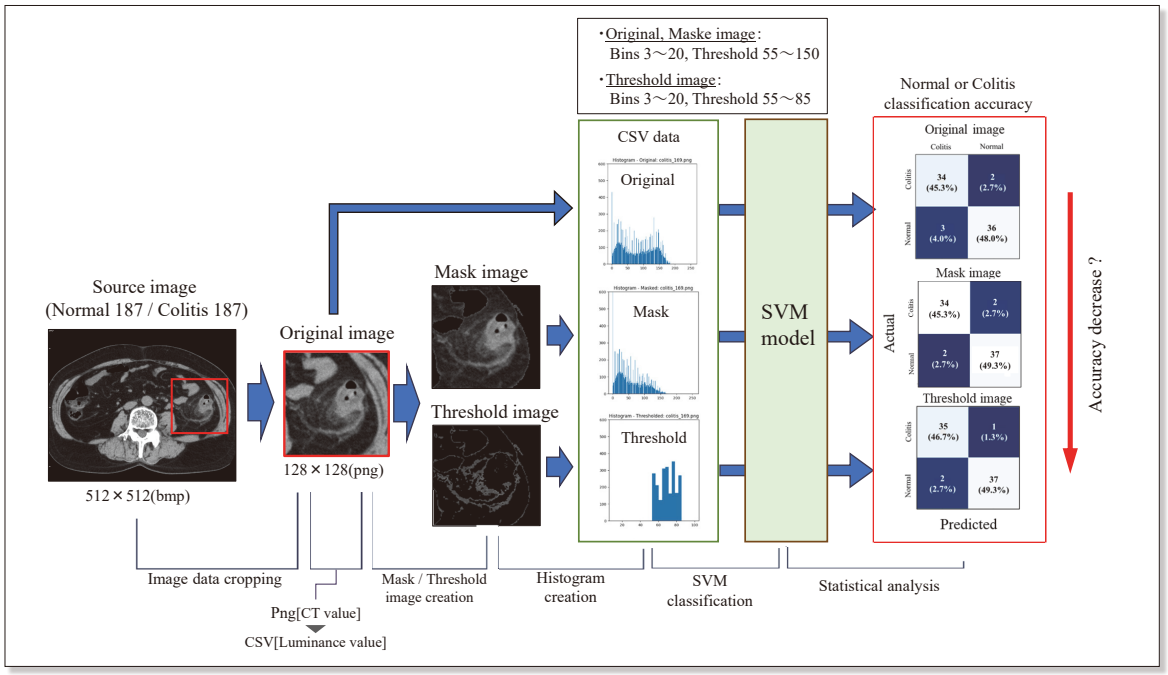

Fig. 2　Overview of the process for the construction of a machine learning model

To verify that fat stranding around colitis was a feature, an original image was created by extracting the affected area of the original image into a 128×128 matrix. Normal images were also created in the same way. In addition, the original images were converted to csv data, and a total of three types of images were created: a mask image in which structures other than fat stranding were deleted from the original image, and a threshold image in which only the luminance of fat stranding was displayed. Histograms of these images were then developed, and through a combination of histogram bins, luminance thresholds, and hyperparameters, the SVM classifier was optimized for maximum classification accuracy. The accuracies of the mask and threshold images were compared with the original image to verify whether fat stranding had been captured as a feature.

4) Dataset creation

①Image cropping

For the purpose of evaluating whether fat stranding is useful for detecting colitis using ML, the image data were cropped to an image size where the colon and fat stranding could fit together. The original image set was cropped as demonstrated in Figure 3 using image processing software. The format was also converted from "bmp" to "png" to minimize the file size and improve the handling efficiency. Normal images were also collected by cropping around the colon and converting the image file format in the same way.

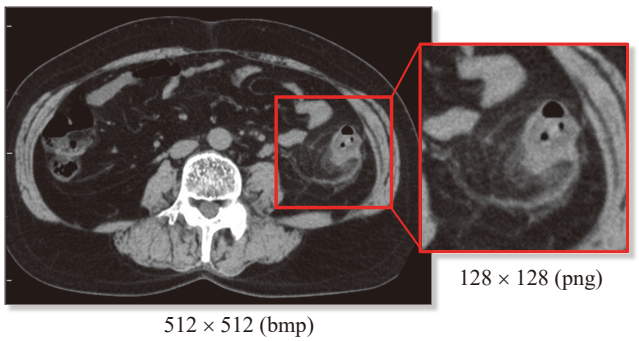

Fig. 3　Image cropping

The minimum area where the colon and fat stranding areas fit was determined to be a matrix size of 128 x 128, and all source images were cropped to create the original image. In addition, the image file format was converted from "bmp" to "png" for collection.

②Conversion of CT values to CSV luminance values

A Python script was utilized to convert CT values from the original images (both normal and colitis) into luminance values. This conversion rendered the images into a comma-separated value (CSV) format with an 8-bit 256 grayscale 128 × 128 matrix, as illustrated in Figure 4.

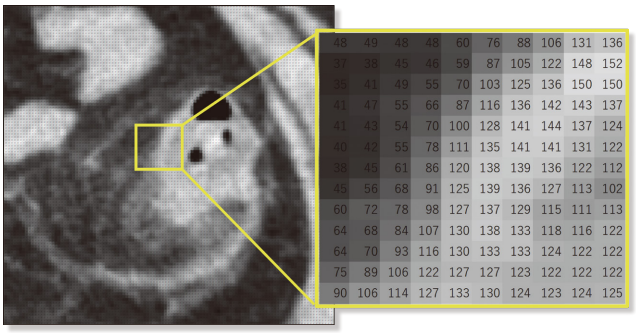

Fig. 4 Convert CT values to csv

For all original images of normal and colitis, CT values in 128 x 128 matrix, 8-bit 256 gray scale were converted to luminance values in csv file format.

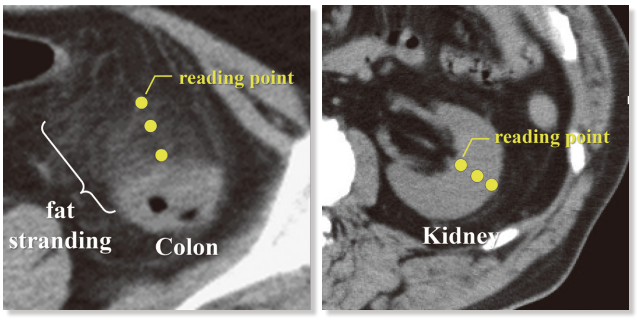

(a) (b)

Fig. 5 Fat stranding and organ luminance value measurements

(a) Luminance value of fat stranding: The luminance values of fat stranding at three points in the distal direction from the proximity of the colon wall were read, and the range of luminance values was determined from the average of these readings.
(b) Luminance values of organs: The luminance values of three points (inside, center, and outside of the organ) were read, and the range of luminance values was determined from the average values.

③Measurement of fat stranding, organ and tissue luminance values and CT values

To determine the fat stranding CSV luminance values, the range of luminance values was obtained from the original images of colitis in which fat stranding was relatively extensive. A total of 20 images were used: 10 images with fat stranding in the ascending colon, 6 in the descending colon, 2 in the transverse colon, and 2 in the sigmoid colon. The range of luminance values was determined from the average of the three luminance values read from the colon wall in the distal direction, as shown in Figure 5. For the colon wall, normal fat, bone, muscle, and kidney, 10 arbitrary images were selected, and the range was determined from the average of the luminance values read at three arbitrary points (outside, center, and inside) of each organ and other organs. The luminance value reading was the average of the nine matrices surrounding each point.

CT values were obtained using the measurement function of picture archiving and communication systems (PACS).

CT values were averaged by setting arbitrarily sized ROIs according to the organ geometry at the same locations as the measurement points in the csv. The fat measurement points were arbitrary sites without blood vessels or connective tissues.

Table 2 shows CT value and luminance value range for each tissue, organs, and fat stranding. Since the luminance values for each matrix varied, the measured values were displayed in units of 5.

The measurement results showed that the luminance values and CT values of fat stranding showed characteristic values that were clearly different from those of fat and organs.

④Generation of the mask and threshold images and histograms

To confirm that the SVM classifier could classify fat stranding as a feature, two types of images were created by eliminating structures other than fat stranding from the original image.

Table 2 CT and luminance values for fat stranding and each tissue and organ

	CT value (HU)	CSV luminance range
Bone	200 - 900	200 - 255
Muscle	40 - 80	140 - 160
Colon	15 - 50	120 - 150
Kidney	15 - 50	120 - 150
Fat stranding	−30 - 5	55 - 85
Fat	−70 - 120	0 - 10

CT and luminance values of fat stranding are separated from those of fat and organs.

Histograms were created using python functions for all normal and colitis csv datasets in the original images. Using OpenCV (https://opencv.org), an image processing library, we created a "mask image" in which the intra-abdominal organs were eliminated by performing mask processing based on a combination of image binarization using Otsu's method [23] and area filtering. In addition, a "threshold image" was created to display only the fat stranding luminance values in the range of "55–85" in the original image. Histograms were also created for all normal and colitis CSV datasets of the original, mask, and threshold images.

5) Classification by SVM classifier

The training and test data for the SVM classifier were split randomly using a Python function. Regarding the hyperparameters of the SVM classifier, those with the highest accuracy for the original image were determined, and using these hyperparameters, the highest accuracies for the mask and threshold images were determined for comparison with the original image.

To determine the hyperparameters with the highest accuracy for the original image classification, the accuracy was calculated by changing the combination of the histogram bins, luminance thresholds, and hyperparameter "kernel," "C," and "gamma" candidates. The histogram bins were set to "3, 5, 8, 10, 12, 15, 18, and 20" to balance the fineness of the features and computational load. The luminance threshold was set to "55–150" from the lower limit of fat stranding to the upper limit of real organs shown in Table 2. For each candidate hyperparameter, the kernel was set to "linear, poly, and rbf", C was set to "0.1, 1, and 10", and gamma was set to "0.001, 0.01, 0.1, 1, 10, and 100". The hyperparameters that output the highest accuracy were determined from the accuracy output for each bin using grid search in Scikit-learn (https://scikit-learn.org), a hyperparameter search method. The luminance threshold of the mask image was set to the same as that of the original image, and for the threshold image, the luminance range "55–85" of fat stranding in Table 2 was used.

6) Statistical analysis

Statistical evaluations were conducted using the Python library. Confusion matrices were then created for the highest accuracies of the original, mask, and threshold images. From these matrices, metrics such as accuracy, sensitivity, and specificity were derived.

7) Evaluation of misclassified image features

All 187 normal and colitis images in the original and threshold images were classified by the trained SVM classifier, and the images output as misclassified were extracted and evaluated for common features.

3 RESULTS

1) Histograms of the original, mask, and threshold images

Examples of histograms of the original, mask, and threshold images along with the CSV data are shown in Figure 6. Both the original and mask images showed a bimodal morphology, with the luminance range centered on the fat region and parenchymal organs.

In the masked image, the elimination of parenchyma reduced the brightness range of the parenchyma. Among the 187 normal and colitis images from the mask images, the target structures were completely erased in 24 normal and 84 colitis images; only the colon was evident in the remaining images. The histogram of the threshold images, which exclusively displayed the luminance range of fat stranding (55–85), indicated that the frequency of colitis images was higher than that of normal images.

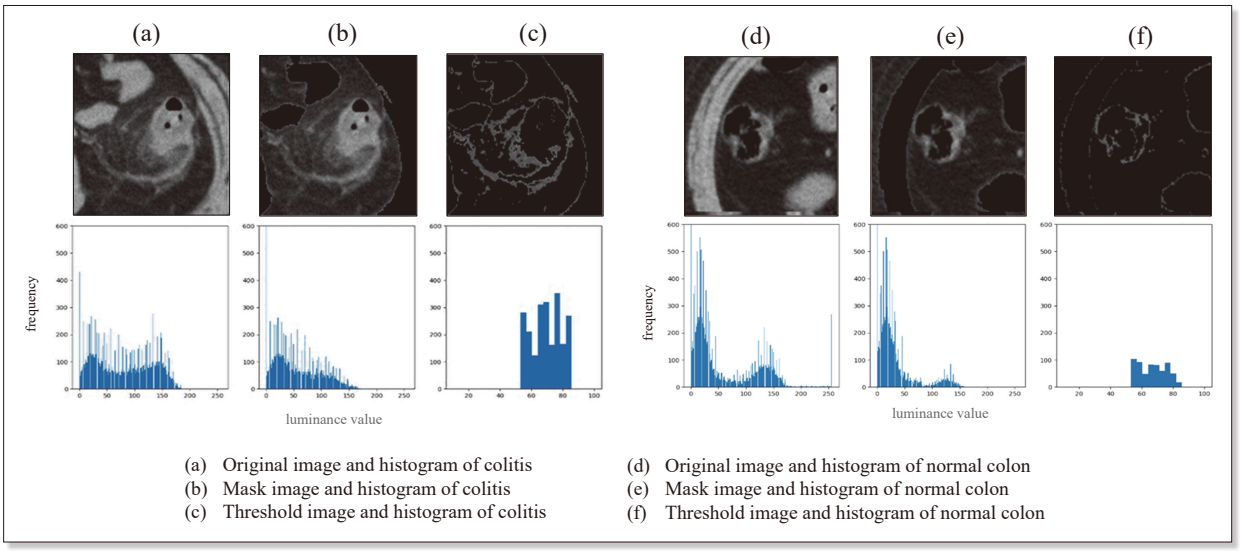

Fig. 6 Histograms of the original, mask, and threshold images for colitis and normal

Both the original and masked images showed a bimodal morphology, with luminance centered on the fat region and luminance centered on the parenchymal organs. Histograms of the threshold images showed a trend toward higher frequencies for colitis images than for normal images.

2) Classification by the SVM classifier

Of the 374 images (original, mask, and threshold), 299 (approximately 80%) (comprising 148 normal and 151 colitis) were randomly chosen for training. The remaining 75 images (approximately 20%) (39 normal and 36 colitis) were set aside for testing utilizing a Python function. In terms of classification accuracy for the original images, bins of 10 and 12 were chosen. After a grid search, the hyperparameters selected were: kernel (linear), C (1), and gamma (0.01). This configuration yielded a maximum accuracy of 93.3%. For the mask and threshold images, the hyperparameters were determined based on the original images: kernel (linear) and C (1). Table 3 shows the accuracy for each bin across the three image datasets. The mask image achieved a peak accuracy of 94.7% with 8 bins, while the threshold image reached 96.0% accuracy with 15 bins.

Table 3 Comparison of the accuracy of the original, mask, and threshold images

		Original image	Masked image	Threshold image
Image		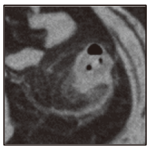	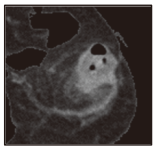	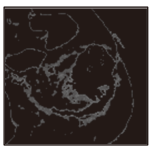
Hyper parameter		kernel : linear C : 1 gamma : 0.01	kernel : linear C : 1 gamma : scale	kernel : linear C : 1 gamma : scale
Luminance range		55~150	55~150	55~85
Bins	3	0.906	0.920	0.880
	5	0.906	0.920	0.920
	8	0.920	**0.947**	0.906
	10	**0.933**	0.933	0.920
	12	**0.933**	0.906	0.933
	15	0.906	0.880	**0.960**
	18	0.920	0.933	0.933
	20	0.890	0.866	0.920

After a grid search, the hyperparameters selected were: kernel (linear), C (1), and gamma (0.01). This configuration yielded a maximum accuracy of 93.3%. For the mask and threshold images, the hyperparameters were determined based on the original images. The mask image achieved a peak accuracy of 94.7% with 8 bins, while the threshold image reached 96.0% accuracy with 15 bins.

3) Statistical analysis

The confusion matrices in the bins and hyperparameters showing the highest accuracy for the original, mask, and threshold images are shown in Figure 7. For the original images, the recorded sensitivity and specificity were 94.4% and 92.3%, respectively. The mask images displayed values of 94.4% and 94.9%, respectively, while the threshold images posted values of 97.2% and 94.9%, respectively. The SVM classification model designed in this study showcased an impressive classification accuracy of 93.3% for the original images. Furthermore, the accuracies for the mask and

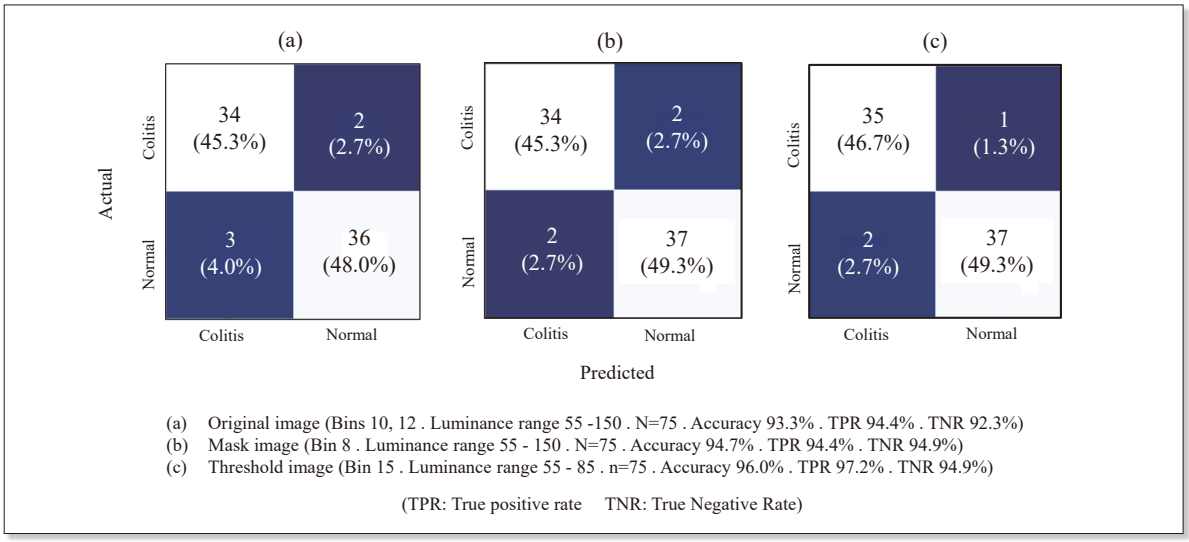

Fig. 7 Confusion matrices in showing the highest accuracy in the original, mask, and threshold images

The sensitivity and specificity of the original images were 94.4% and 92.3%, mask images 94.4% and 94.9%, and threshold images 97.2% and 94.9%.The original image also showed a high accuracy of 93.3%, while the accuracy of the mask and threshold images increased by an additional 1.4% and 2.7%.

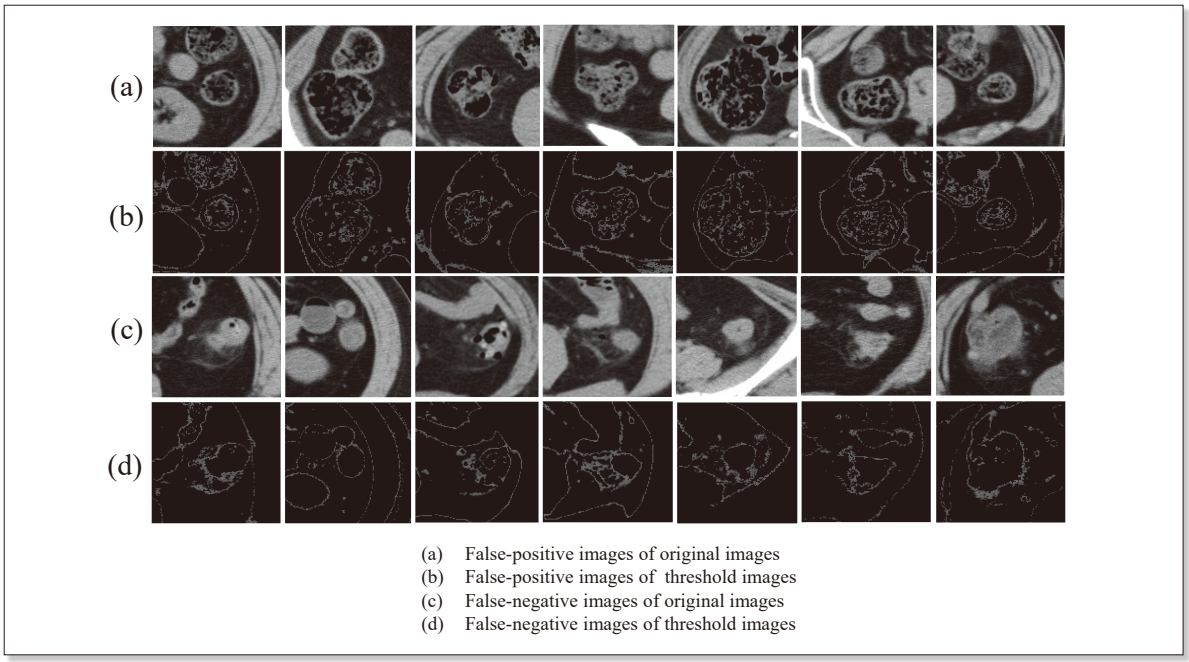

Fig. 8 Characteristics of false-positive and false-negative images

In cases where normal images were misidentified as colitis, the colon was dilated and there were many fecal masses with the same luminance as the fat stranding. The images in which colitis was misidentified as normal were characterized by small fat stranding areas.

threshold images surpassed the original by 1.4% and 2.7%, respectively. These findings indicate that the exclusion of structures other than fat stranding from the original image did not degrade the accuracy.

4) Feature evaluation of misclassified images

A trained SVM classifier was used to classify 187 normal and colitis images each in the original and threshold images. Figure 8 shows the seven images that were consistently misclassified in both the original and threshold datasets. Those images erroneously labeled as abnormal predominantly showcased a dilated colon, with fecal masses in the lumen reflecting the luminance of fat stranding. Conversely, the image that mistakenly labeled colitis as normal was characterized by a minimal fat stranding area.

4 DISCUSSION

Previous studies on colitis detection by AI have used gastrointestinal contrast agents and classified colitis based on deep learning, using the thickness of the colon wall as a feature. The accuracy, sensitivity, and specificity reported in those studies were not always high, ranging from 0.7 to 0.73, 0.73 to 0.94, and 0.73 to 0.95, respectively.[11–14)]

Previous studies have highlighted several challenges, including the difficulty of detecting inflamed regions due to variations in colonic morphology and individual differences, the need for strategies to prevent false positives from organs other than the colon, the influence of image slice thickness on detection accuracy, the risk of false negatives when wall thickening is not clearly defined or when lesions are small, and the potential misclassification of feces-containing colon segments as colitis. In this study, histograms of each CSV dataset of the original, mask, and threshold images were classified as colitis or normal using the SVM classification model constructed with fat stranding as a feature value, and all were able to detect colitis with a high accuracy of over 90%.

In addition, while previous studies have used complex algorithms to localize the colon from the source image and then measure the thickness of the colon wall, in the present study, the use of manually cropped images of colitis-affected areas and a simple classification algorithm based on histograms of image brightness were considered to be the reasons for the high accuracy. Moreover, the SVM classifier used in this study is a supervised classification algorithm introduced in 1992, which has been widely utilized for classification and regression tasks and is considered a powerful classifier in fields such as medical image processing.[24–26)] It is capable of providing higher classification accuracy than other commonly used pattern recognition methods, such as random forests[27)] and multilayer perceptron classifiers,[28)] and is particularly advantageous in environments with limited training data.[25)]

These characteristics of the SVM classifier are presumed to have contributed to the results obtained in this study.

In this study, the original images achieved an accuracy of 93.3% on the test data. The classification accuracy of the mask and threshold images, in which the colon and other organs were eliminated, did not decrease from the accuracy of the original image, but rather, increased by 1.4% and 2.7%, respectively. The reason why the mask and threshold images showed higher accuracy than the original images is thought to be that these processes clarified the fat stranding features and reduced the noise. In other words, the performance of the SVM classification model was improved as a result of the removal of less relevant background information by the mask processing and the enhancement of the fat stranding luminance by the process. This result confirms that the SVM classification model constructed in this study can capture fat stranding as a main

feature, and thus, we conclude that it is possible to classify colitis by fat stranding. The findings of this study, which focus on fat stranding, are expected to be beneficial for future research on AI-assisted CT diagnosis of colitis. Furthermore, since fat stranding is observed in diseases beyond colitis,[29–31] the approach using fat stranding as a feature may also be applicable to the detection of inflammatory diseases in abdominal organs other than the colon, as well as certain types of cancer.[32–34]

This study did have some limitations. First, fat stranding cannot be detected in patients without a fat layer around the colon. Second, accuracy may be reduced in patients with elevated soft tissue CT values because of diseases associated with generalized edema. To address these issues, it will be necessary to use a dataset that includes a variety of cases or to improve the fat stranding detection method. On the other hand, this study aims to detect colitis; however, fat stranding can present in various patterns, such as ischemic changes in the omentum or inflammation of adjacent organs.[16] Therefore, while inflammation can be detected, it may result in false positives for colitis.

It was also inferred that the reason for the false-positive results for colitis was the relatively large area occupied by fecal masses corresponding to the luminosity of the fat stranding. Although it is easy to classify the fat stranding in the area affected by colitis because the colon lumen is collapsed,[35] false-positives may occur when there is a colon with retained fecal mass in the vicinity of a normal colon with a collapsed lumen. In addition, false-negatives may occur when the area of fat stranding is mild. Methods to solve these problems and improve the classification algorithm itself could include the development of more advanced preprocessing and feature extraction methods, as well as the use of datasets containing a wider variety of cases. For example, an approach that combines feature extraction using CNNs and SVM classification technology may be able to achieve high performance classification accuracy for a wider variety of cases.[25]

In this study, an SVM classification model was trained and tested on a 128×128 matrix cutout of the affected area of a colitis CT scan images (no artifacts, specific noise level, constant Window Width/Level (WW/WL) diagnosed by two radiologists. However, to enhance clinical applicability, it is necessary to validate the accuracy with respect to noise levels and variations in WW/WL. Furthermore, further research is required to develop algorithms capable of automatically localizing and classifying fat stranding from original CT images.

5 CONCLUSION

This study highlights the efficacy of fat stranding as a pivotal feature in an SVM classification model to aid the AI-based diagnosis of colitis using CT scans. Such advancements may enable the highly accurate classification of colitis from CT scans without the need for gastrointestinal contrast agents, which could potentially expedite the diagnosis of colitis by doctors other than radiologists.

Future studies should aim to develop a model with enhanced precision and adaptability catering to a myriad of cases.

CONFLICTS OF INTEREST

The first author and all co-authors have no conflicts of interest to disclose.

ACKNOWLEDGMENTS

We thank the radiologists and radiology technicians at Nishida Hospital for their cooperation in this study.

References

1) Yasuo Nakajima, et al.: Radiologist supply and workload: international comparison. Radiation medicine, 26(8), 455-465, 2008.
2) Masatoshi Matsumoto, et al.: geographic distribution of radiologists and utilization of teleradiology in Japan: a longitudinal analysis based on National Census Data. PLoS One, 10(9), 2015.
3) Seiichi Kawamoto: Radiology and Artificial Intelligence [in Japanese]. Medical Journal of Osaka General Medical Center, 41(1), 3-19, 2019.
4) Hiroshi Fujita: AI-powered Diagnostic Medical Imaging Changes the Medical Field: Overview and Future Prospects for AI-based Image Diagnosis: "Third Eye" to Help Doctors [in Japanese]. Transactions of Information Processing Society of Japan, 62(2), 1-8, 2021.
5) Seiya Takamoto, et al.: The effect of the critical findings reporting by radiological technician in after-hours emergency CT. Journal of Japanese Society for Emergency Medicine, 22(5), 703-708, 2019.
6) Jin Joo Park, et al.: Convolutional-neural-network-based diagnosis of appendicitis via CT scans in patients with acute abdominal pain presenting in the emergency department. Scientific Reports, 10, 9556, 2020.
7) Hidetaka Onda: Current Status of Medical Care for the Elderly at Our Advanced Emergency Medical Center [in Japanese]. Journal of Nippon Medical School, 9(2), 129-134, 2013.
8) Hiroyuki Kato: Emergency diseases common in the elderly [in Japanese]. Japanese journal of geriatrics, 48(4) , 312-316, 2011.
9) Masatomo ebina, et al.: Diagnostic precision of emergency room CT and efforts to improve its quality. Journal of Japanese Society for Emergency Medicine, 18(1), 1-4, 2015.
10) Yoshihiro Eto, et al.: Literature review on the current status and issues of abdominal CT imaging diagnosis support using AI in emergency medicine [in Japanese]. The journal of the Japanese Association of Radiological Technicians, 70(9), 21-29, 2023.
11) Liu, J., et al.: Detection and diagnosis of colitis on computed tomography using deep convolutional neural networks. Medical physics, 44(9), 4630-4642, 2017.
12) Liu, J., et al.: Colitis detection on abdominal CT scans by rich feature hierarchies. In Medical Imaging 2016: Computer-Aided Diagnosis, March, 9785, 423-429. SPIE, 2016.
13) Liu, J., et al.: Colitis detection on computed tomography using regional convolutional neural networks. In 2016 IEEE 13th International Symposium on Biomedical Imaging (ISBI), April, 863-866. IEEE, 2016.
14) Wei, Z., et al.: Computer-aided detection of colitis on computed tomography using a visual codebook. In 2013 IEEE 10th International Symposium on Biomedical Imaging, April, 141-144. IEEE, 2013.
15) Thorisson, A., et al.: Diagnostic accuracy of acute diverticulitis with unenhanced low-dose CT. BJS open, 4(4), 659-665, 2020.
16) Thornton, E., et al.: Patterns of fat stranding. AJR. American journal of roentgenology, 197(1), W1-W14, 2011.
17) Lin, H. A., et al.: Periappendiceal fat-stranding models for discriminating between complicated and uncomplicated acute appendicitis: a diagnostic and validation study. World journal of emergency surgery: WJES, 16(1), 52, 2021.
18) Thoeni, R. F., et al.: CT imaging of colitis. Radiology, 240(3), 623-638, 2006.
19) Deery, S. E., et al.: Management of Diverticulitis in 2017. Journal of gastrointestinal surgery: official journal of the Society for Surgery of the Alimentary Tract, 21(10), 1732-1741, 2017.
20) Warner, E., et al.: Fourteen-year study of hospital admissions for diverticular disease in Ontario. Canadian journal of gastroenterology = Journal canadien de gastroenterologie, 21(2), 97-99, 2007.
21) Etzioni, D. A., et al.: Diverticulitis in California from 1995 to 2006: increased rates of treatment for younger patients. The American surgeon, 75(10), 981-985, 2009.
22) Strate, L. L., et al.: Epidemiology, Pathophysiology, and Treatment of Diverticulitis. Gastroenterology, 156(5), 1282-1298.e1, 2019.
23) Nobuyuki Otsu: A threshold selection method from gray-level histograms. IEEE transactions on systems, man, and cybernetics, 9(1), 62-66, 1979.
24) Boser BE, et al.: A training algorithm for optimal margin classifiers. Proceedings of the fifth annual workshop on Computational learning theory, 144-152, 1992.
25) Melaku BH, et al.: Detection and classification of gastrointestinal disease using convolutional neural network and SVM. Cogent Engineering, 9(1), 2084878, 2022.
26) Paoletti ME, et al.: A new GPU implementation of support vector machines for fast hyperspectral image classification. Remote Sensing, 12(8), 1257, 2020.
27) Belgiu M, et al.: Random forest in remote sensing: A review of applications and future directions. ISPRS journal of photogrammetry and remote sensing, 114, 24-31, 2016.
28) Noriega L: Multilayer perceptron tutorial. School of Computing. Staffordshire University, 4.5, 444, 2005.
29) Song, X., et al.: Relative CT number of periappendiceal fat stranding may be an applicable index for estimating the severity of acute appendicitis. The British journal of radiology, 94(1120), 20200437, 2021.
30) Mehta, P., et al.: A Case Report of Mesenteric Panniculitis. Cureus, 12(1), e6764, 2020.
31) Das, J. P., et al.: Imaging findings of immune checkpoint inhibitor associated pancreatitis. European journal of radiology, 131, 109250, 2020.
32) Bai, X, et al.: Rim Enhancement and Peripancreatic Fat Stranding in Preoperative MDCT as Predictors for Occult Metastasis in PDAC Patients. Academic radiology, S1076-6332(23)00119-8. Advance online publication, 2023.
33) Chung, J. W., et al.: Prognostic impact of perirenal fat stranding on oncologic outcomes in ureteral urothelial carcinoma. Investigative and clinical urology, 62(1), 23-31, 2021.
34) Damgaci, L., et al.: Diagnostic value of MDCT in determining the perinephric fat tissue and renal sinus invasion in patients with clear cell renal cell carcinoma. Nigerian journal of clinical practice, 24(4), 489-495, 2021.
35) Horsthuis, K., et al.: Detection of inflammatory bowel disease: diagnostic performance of cross-sectional imaging modalities. Abdominal imaging, 33(4), 407-416, 2008.

Received June 22, 2023; accepted January 29, 2024

Detection of the pulmonary migration of the iodine-125 brachytherapy seeds using chest X-ray energy subtraction images

IWAMURA Kohei, M.A.[1), 2)]*, WATANABE Tomoya[3)], KASAHARA Daiho[4)], ISHIDA Hideki, Ph.D.[3), 5)], NAKASHIMA Junya, M.A.[3), 6)], SAI Syogo, M.A.[6), 7)], SATO Hisaya, Ph.D.[4), 8)], KATO Kyoichi, Ph.D.[9), 10)]

1) Showa Medical University Koto Toyosu Hospital Radiological Technology Department
2) Showa Medical University, School of Nursing & Rehabilitation Sciences, Graduate School of Health Sciences
3) Showa Medical University Koto Toyosu Hospital Radiological Technology Department
4) Showa Medical University Hospital Radiological Technology Department
5) Showa Medical University, School of Nursing & Rehabilitation Sciences, Graduate School of Health Sciences
6) Showa Medical University, School of Nursing & Rehabilitation Sciences, Graduate School of Health Sciences
7) Showa Medical University Northern Yokohama Hospital Radiological Technology Department
8) Showa Medical University, School of Nursing & Rehabilitation Sciences, Graduate School of Health Sciences
9) Showa Medical University, School of Nursing & Rehabilitation Sciences, Graduate School of Health Sciences
10) Showa Medical University, Department of Radiological Technology

* E-mail: iwamura@cmed.showa-u.ac.jp

Note: This paper is secondary publication, the first paper was published in the JART, vol. 71 no. 863: 23-29, 2024.

Key words: brachytherapy, prostate cancer, chest X-ray, image processing, energy subtraction

【Abstract】
The migration of radioactive seeds into the lungs is a complication after iodine-125 (^{125}I) brachytherapy. In this study, the effects of two types of ^{125}I brachytherapy sources (AgX100 and STM1251) on the pixel values of the images were evaluated. Furthermore, receiver operating characteristic (ROC) analysis was used to assess the degree of detection of ^{125}I brachytherapy sources based on the energy subtraction images (soft and bone conditions) obtained from the chest X-ray images. The results showed that the pixel values did not differ between radiation sources. The difference in tube voltage was up to 35.67% and 24.66% for the AgX100 and STM1251 seeds, respectively. The area under the curve (AUC) in the ROC analysis was highest for the bone condition images, at 0.924 and 0.894 for AgX100 and STM1251, respectively.

1. Introduction

Prostate cancer is the second leading cause of cancer-related deaths among men in the United States. The mortality risk is high depending on the incidence rate and stage of progression [1)]. In Japan, the steadily increasing incidence of prostate cancer has attracted attention. Prostate cancer is classified into localized, locally advanced, and metastatic stages, and the treatment strategies are determined accordingly. Currently, various therapeutic options are available, making it possible to select the most appropriate treatment depending on the stage of the disease.

Iodine-125 (^{125}I) brachytherapy is an effective treatment for prostate cancer and is performed in patients with localized or locally advanced disease, including those at low, intermediate, and high risk. Approximately 50–100 titanium capsules (0.8 mm in diameter and 4.5 mm in length) containing ^{125}I are implanted in the prostate for irradiation. The treatment outcomes of brachytherapy are comparable to that after surgery in low-risk patients, and it is expected to provide a high quality of life. However, radioactive seeds tend to migrate into the lungs during brachytherapy, resulting in complications [2, 3)]. Reports have shown that pulmonary embolism may occur due to seed migration [4)].

At our institution, a chest X-ray is performed on the first postoperative day to differentially

diagnose seed migration. However, the visibility of the migrated seeds in the lungs using chest X-ray images may be compromised depending on their position and orientation. Stone et al. reported that among a total of 21,654 implanted ^{125}I brachytherapy seeds, pulmonary embolism due to seed migration was observed in 1.7% of the cases [5]. This suggests that at least 1.7% of seed migration cases may be overlooked in clinical practice, potentially leading to pulmonary embolism. Furthermore, studies on improving the visibility of ^{125}I brachytherapy seeds to prevent oversight remain limited.

Due to recent advancements in digital image processing technologies, energy subtraction images can be generated by computationally processing multiple images. Chest X-ray images obtained using energy subtraction can produce soft tissue images that exclude bony structures such as the ribs. Observing these images in combination with the original images can be effective in detecting abnormal opacities, such as pathological shadows [6-8].

As the ^{125}I brachytherapy seeds are chemically bonded to a silver-coated short wire and sealed in a cylindrical capsule made of pure titanium, we hypothesized that energy subtraction imaging might help detect shadows caused by the ^{125}I brachytherapy seed migration. Based on this principle, we evaluated the effectiveness of energy subtraction processing in chest X-ray images to detect the pulmonary migration of ^{125}I brachytherapy seeds using a chest phantom.

2. Methods

2-1 Equipment and Materials

This study used the BENEO high-voltage generator (Fujifilm, Tokyo, Japan), the 0.6/1.2P 324DK-125 X-ray tube unit (Shimadzu Corporation, Kyoto, Japan), and the DR-ID 600 flat panel detector (FPD) (Fujifilm). The ^{125}I brachytherapy seeds included AgX100 from Theragenics (Buford, GA, USA) and STM1251 from Bard Brachytherapy (Carol Stream, IL, USA) (Fig. 1).

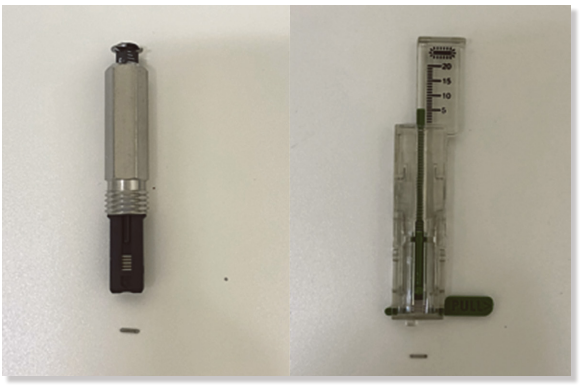

(a) (b)

Fig. 1 Two types of iodine-125 brachytherapy sources.
(a) AgX100 and (b) STM1251

Furthermore, the following tissue-equivalent phantoms were used: the Tough Water Phantom WD type (TWP) (Kyoto Kagaku, Kyoto, Japan), the Tough Bone Phantom BE type (TBP) (Kyoto Kagaku), and the Tough Lung Phantom LP type (TLP) (Kyoto Kagaku). The Chest Phantom N-1 (Kyoto Kagaku) was used. The acquired images were evaluated using a laptop monitor (Microsoft, Redmond, WA, USA), as this is how radiation oncologists typically review images in actual clinical practice. To replicate this environment, a regular laptop monitor was employed instead of a high-resolution monitor. Image analysis was performed using ImageJ (National Institutes of Health, Bethesda, MD, USA). Statistical analysis was conducted using JMP Pro 16 (SAS Institute, Cary, NC, USA).

2-2 Evaluation of the Effect of ^{125}I Brachytherapy Seeds on Pixel Values

The TWP, TLP, and TBP phantoms were stacked on the FPD. The AgX100 and STM1251 seeds were placed at the center of the TWP at a depth of 11 cm from the surface (Fig. 2). Images were acquired with a source-to-image receptor distance (SID) of 100 cm and an irradiation field size of 12 × 12 cm at the detector surface. The ^{125}I brachytherapy seed images were obtained under a constant tube current-time product of 2.5 mAs, and the tube voltage varied from 60 to 150 kV in 10 kV increments

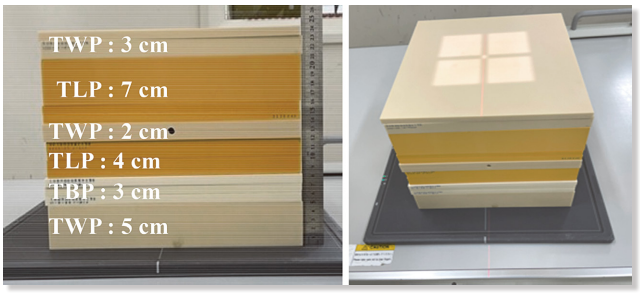

(a) (b)

Fig. 2 Representation of the photography geometry used in this study.
(a) The source was inserted 11 cm from the surface, (b) The field size was 12 × 12 cm on the photosensitive surface

Table 1 Radiographic conditions used to obtain the pixel values.

Tube Voltage [kV]	mAs	Field Size [cm]	SID [cm]
60 70 80 90 100 110 120 130 140 150	2.5	10 × 10	100

(Table 1). The acquired images were analyzed using ImageJ, where regions of interest (ROIs) were defined, and pixel values within the ROIs were measured. The ROI was set as a square with a fixed size of 300 × 300 pixels (Fig. 3), and its mean pixel value was recorded. The statistical significance of the differences in the effect of both types of ^{125}I brachytherapy seeds on the pixel values was evaluated using a t-test. A $p < 0.05$ was considered statistically significant.

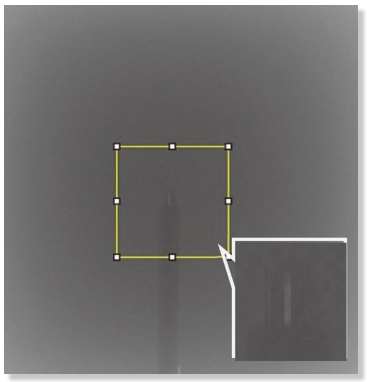

Fig. 3 Analysis of the pixel values of the radiation source using ImageJ.

2-3 Acquisition of the Energy Subtraction Images

The AgX100 and STM1251 seeds were randomly placed and fixed on the surface of the upper, middle, and lower lung fields of both sides of the chest phantom. The ^{125}I brachytherapy seeds were positioned in two orientations: perpendicular and parallel to the X-ray beam. Then, the seeds were randomly distributed throughout the lungs in each orientation. The geometric arrangement is shown in Fig. 4. Imaging was performed at 120 kV and 3.2 mAs.

(a) (b)

Fig. 4 Images showing the geometric arrangement of the radiography setup. The imaging conditions were set to frontal chest (120 kV, 3.2 mAs), and low-tube-voltage (60 kV, 3.2 mAs) images were also acquired for energy subtraction images.
(a) The distance was set at 200 cm, (b) The direct view from the back

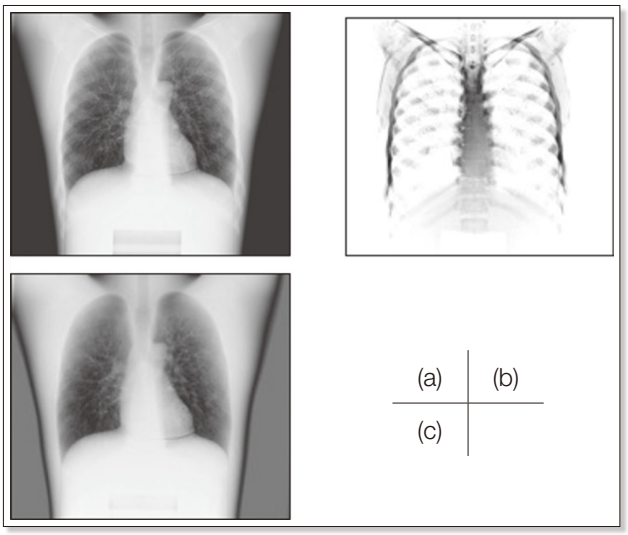

Fig. 5 The acquired images of the phantoms.
(a) The original, (b) the bone condition, and (c) soft tissue condition images

A low-tube-voltage condition of 60 kV and 3.2 mAs was used for energy subtraction imaging. Using the theoretical equation (1), bone and soft tissue energy subtraction images were generated in ImageJ by adjusting the weighting coefficients.

$$ES = \omega HQH - \omega LQL \quad \cdots (1)$$

where ES is the desired energy subtraction image, ωH and ωL are the weighting coefficients, and QH and QL are the high- and low-energy images, respectively. The bone condition image was created with ωH = 1.0 and ωL = 1.0, while the soft tissue condition image was created with ωH = 1.4 and ωL = 1.2 (Fig. 5).

2-4 Evaluation of the Energy Subtraction Images

To evaluate the detectability of ^{125}I brachytherapy seeds using the generated energy subtraction images, a total of 40 images were visually assessed on the laptop monitor: 20 images without ^{125}I brachytherapy seeds and 20 images simulating seed migration. These images were evaluated using a five-point confidence rating method. Images without the migrated ^{125}I brachytherapy seeds were classified as "normal," while those with migrated seeds were classified as "abnormal." Herein, migration refers to the displacement of the seeds into the lungs. Receiver operating characteristic (ROC) analysis was performed to assess the detectability of each type of ^{125}I brachytherapy seed, and the area under the curve (AUC) was calculated. Statistical significance was assessed using a t-test to compare the AUC of the energy subtraction images with that of the original images. $p < 0.05$ considered statistically significant. The evaluation was performed by ten radiologic technologists with 1 to 13 years of experience in diagnostic X-ray imaging (mean: 6.5 ± 2.9 years). Before conducting the visual assessment, the evaluators were provided with an explanation of the original images as training data. Each image was evaluated for 30 s, and the original, bone condition, and soft tissue condition images were visually assessed.

3. Results

3-1 Evaluation of the Pixel Values of the ^{125}I Brachytherapy Seeds

The TWP, TLP, and TBP phantoms were stacked on the FPD. Then, the AgX100 and STM1251 seeds were placed at the center of the TWP at a depth of 11 cm from the surface. Fig. 6 shows the relationship between the tube voltage and pixel values for both types of ^{125}I brachytherapy seeds. The maximum difference in the pixel values between both ^{125}I brachytherapy seeds was 8.1%, but this difference was not statistically significant ($p = 0.6997$). Additionally, the maximum difference in pixel values due to variations in tube voltage were 35.67% and 24.66% for the AgX100 and STM1251 seeds, respectively.

3-2 Evaluation of the Energy Subtraction Images

Figs. 7–9 show the ROC analysis results for detecting the ^{125}I brachytherapy seeds. The ROC analysis indicated that the detection capability, as measured by the AUC, did not depend on the type of ^{125}I brachytherapy seed.

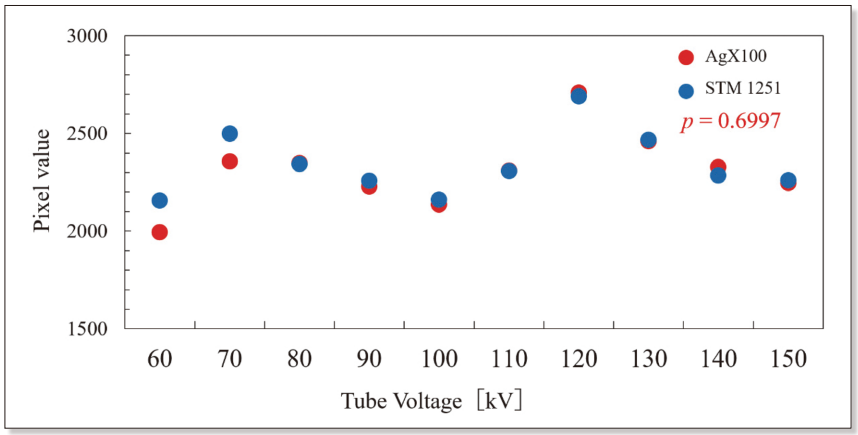

Fig. 6 The relationship between tube voltage and pixel value based on the brachytherapy source.

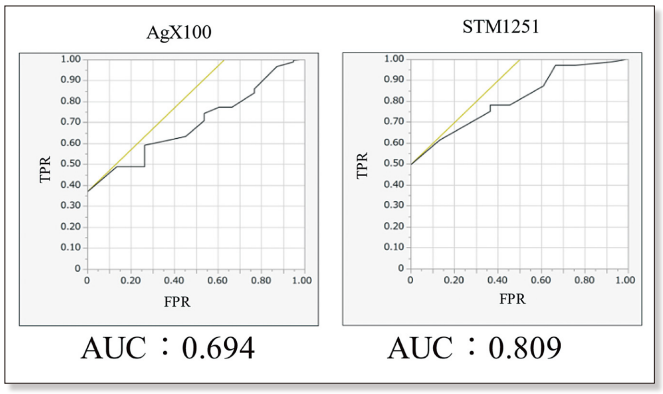

(a) AgX100 (b) STM1251

Fig. 7 Receiver operating characteristic analysis results of the original images.

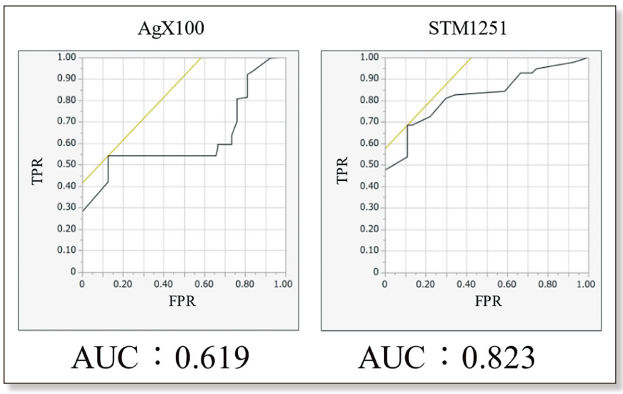

(a) AgX100 (b) STM1251

Fig. 9 Receiver operating characteristic analysis results of the tissue images.

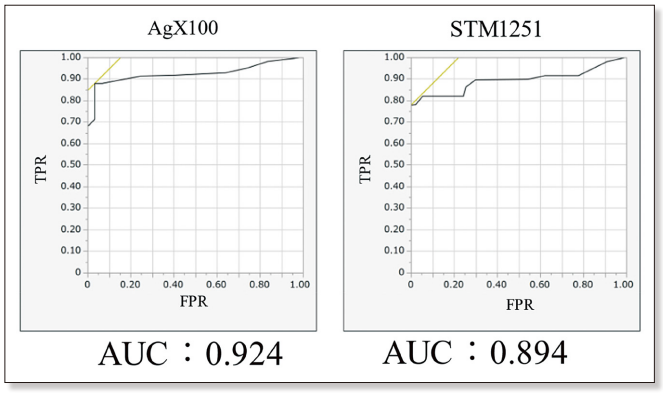

(a) AgX100 (b) STM1251

Fig. 8 Receiver operating characteristic analysis results of the bone images.

Table 2 Summary of the significance test results.

	p<0.05	
Type of brachysources	AgX100	STM1251
Original-Bone condition	< 0.001	< 0.001
Original-Tissue condition	< 0.001	0.5411
Bone-Tissue condition	< 0.001	< 0.001

Additionally, the AUC values for the bone condition images were 0.924 and 0.894 for the AgX100 and STM1251 seeds, respectively, making it the highest among all images. As shown in Table 2, the t-test results showed statistically significant differences in the AUC of the energy subtraction images compared with the original images for all comparisons, except that between the original and soft tissue condition images of the STM1251 seeds.

4. Discussion

In this study, the detectability of the migrated

^{125}I brachytherapy seeds was evaluated by applying energy subtraction to chest X-ray images obtained using a chest phantom. Gregory et al. reported that in patients who underwent prostate ^{125}I brachytherapy, the seeds migrated at least 2 mm after implantation in the prostate [9]. Additionally, since seed migration is relatively common during the treatment period, the position of the ^{125}I brachytherapy seeds should be monitored to minimize their movement [10-14]. During ^{125}I brachytherapy for prostate cancer, the seeds are often implanted near the prostate margin. Pulmonary migration occurs when the seeds travel through the bloodstream near the prostate, reaching the inferior vena cava and right heart system and eventually embolizing in the peripheral pulmonary vasculature [2]. This study focused on chest X-ray imaging to screen seed migration, particularly in the chest, the most common migration site. The effectiveness of energy subtraction processing in enhancing the detectability of ^{125}I brachytherapy seeds was examined.

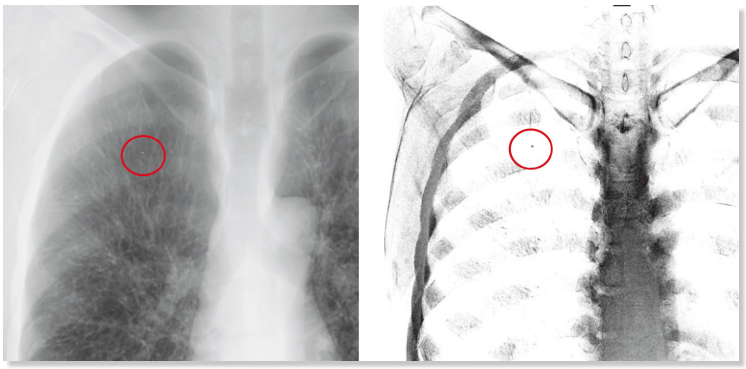

(a) original image (b) bone condition image

Fig. 10 A comparison of the original and bone condition images.

First, the changes in the pixel values of the X-ray images captured using the Theragenics AgX100 and STM1251 ^{125}I brachytherapy seeds were evaluated. These seeds differ in shape and size: AgX100 are 4.5 mm long and have a diameter of 0.8 mm, whereas the STM1251 has a total length of 4.55 mm and a diameter of 0.81 mm [15]. However, both seeds showed minimal variation in the pixel values with changes in the tube voltage. Despite the difference in their shape, the small size of both seeds likely contributed to the lack of statistically significant differences. Vimoj et al. evaluated the pixel values using magnetic resonance (MR) and X-ray images obtained with CyberKnife ®, a type of linear accelerator used in radiation therapy, to assess the migration of platinum and gold fiducial markers into various organs [16]. They reported no significant differences in the pixel values between MR and X-ray images, regardless of the organ where migration was simulated. Although their study focused on MR and high-energy X-ray imaging, as the ^{125}I brachytherapy seeds used in this study were made of titanium, a similar outcome was expected. In the diagnostic imaging range, interactions between X-rays and materials are primarily influenced by the photoelectric effect, making it less likely for scattered radiation to occur between the source and incident X-rays. These findings suggest that the tube voltage used in the diagnostic imaging range does not cause significant variations in pixel values, aligning with previous studies.

Next, ^{125}I brachytherapy seeds were randomly placed in the upper, middle, and lower fields on both sides of the lung area in the chest phantom. X-ray images were acquired, and energy subtraction images were generated from the original images. Visual assessment of the obtained images showed that detectability improved significantly in the bone condition images compared to the original images. This improvement is likely due to the removal of non-bone noise, enhancing the detectability of the ^{125}I brachytherapy seeds and increasing the visual assessment scores (Fig. 10). Notably, detectability improved as the seeds were placed closer to the center rather than at the peripheral lung regions, which suggests that the presence of rib structures overlapping the lung field in the chest X-ray images might influence

seed detectability. Conversely, no significant difference in detectability was observed between the soft tissue condition and original images. This might be because, in the soft tissue condition images, the enhancement of the peripheral areas of the lung markings reduced the visibility of the ^{125}I brachytherapy seeds. Regarding the placement angle and position of the ^{125}I brachytherapy seeds, both perpendicular and parallel orientations to the X-ray beam were considered. Since ^{125}I brachytherapy seeds are encased in titanium, they appear as high-absorption objects in the energy subtraction images. Consequently, their visibility improved when positioned parallel to the X-ray beam, as this orientation resulted in a larger visible surface area.

In summary, the detectability of the migrated ^{125}I brachytherapy seeds improved when they were positioned perpendicular to the X-ray beam and in the bone condition images. In a similar study, Kiguchi et al. used the dual-energy subtraction method to show that the detectability of diffuse lung diseases (simulated lesions, micronodular opacities, reticular opacities, and honeycomb patterns) improved when the subtraction images were used along with the original images [17]. Based on the results of this study and previous research, we believe that performing additional chest X-ray imaging after ^{125}I brachytherapy is beneficial. In Japan, ^{125}I brachytherapy has been performed since 2003. At our institution, 901 cases of ^{125}I brachytherapy have been performed since 2014 (as of February 2023). Approximately 32 instances of seed migration to the lungs were observed, accounting for 3.5% of all cases. Because seed migration to the lungs may lead to pulmonary embolism, it is crucial to detect such occurrences. At our institution, chest X-ray imaging is routinely performed for all patients following ^{125}I brachytherapy. As the number of prostate cancer cases is expected to increase, detecting ^{125}I brachytherapy seed migration to the lungs is imperative. Furthermore, this study has demonstrated that the energy subtraction processing of chest X-ray images enhances the detectability of ^{125}I brachytherapy seeds. Our results highlight the need for regular follow-up examinations after ^{125}I brachytherapy to prevent seed migration-induced pulmonary embolism. As chest X-ray imaging after ^{125}I brachytherapy is a simple procedure, the proposed method, which improves the detectability of the radioactive seeds, might be of significant value.

5. Conclusion

Energy subtraction processing of chest X-ray images using a chest phantom was particularly effective in the bone condition images, enhancing the visibility of ^{125}I brachytherapy seed migration into the lungs.

Conflict of Interest

The first author and all co-authors declare no conflicts of interest.

References

1) Saiga Kumiko, et al.: Future Estimations of Cancer Incidence in Japan. Cancer Statistics White Paper 2012—For Cancer Control Based on Data. Shinohara Publishing, 63-81, 2012.
2) Itami Jun, et al.: Examination of factors Affecting Seed Migration in Transperineal Prostate I-125 Brachytherapy. Jpn J Radiat Oncol, 17, 109-113, 2005.
3) Hemanth Boppana, et al.: A Case Report of Foreign Body Embolization. Cureus, 11(6), 4917, 2019.
4) Kunos CA, et al.: Migration of Implanted Free Radioactive Seeds for Adenocarcinoma of the Prostate Using a Mick Applicator. Brachytherapy, 3(2), 71-77, 2004.
5) Stone NN, et al.: Reduction of Pulmonary Migration of Permanent Interstitial Sources in Patients Undergoing Prostate Brachytherapy. Urology, 66(1), 119-123, 2005.
6) Sanada Shigeru, et al.: Temporal Subtraction Technique for Detection of Subtle Anomalies on Temporally Sequential Bone-subtracted Chest Radiographs by Energy Subtraction. Jpn J Radiol Tech, 56(3), 428-435, 2000.
7) Uemura Ryoichi, et al.: Application of CR in Lung Cancer Screening, Especially the Utility of Single-Shot Energy Subtraction Method. Lung Cancer, 30(3), 319-326, 1990.
8) Kido S, et al.: Clinical Evaluation of Pulmonary Nodules with Single-Exposure Dual-Energy Subtraction Chest Radiography with an Iterative Noise-Reduction Algorithm. Radiology, 194(2), 407-412, 1995.
9) Kobayashi Ken: Detection of Calcification in Lung Nodules Using Digital Radiography (Fuji Computed Radiography): Using Chest Single-Energy Subtraction Bone Images. Jpn J Med Radiol, 55(9), 638-645, 1995.
10) Gregory R, et al.: Reduction of Seed Motion Using a Bio-Absorbable Polymer Coating During Permanent Prostate Brachytherapy using a Mick Applicator Technique. Med Phys, 19(3), 44-51, 2018.
11) Badwan HO, et al.: AnchorSeed for the Reduction of Source Movement in Prostate Brachytherapy with the Mick Applicator Implant Technique. Brachytherapy, 9(1), 23-26, 2010.
12) Sugawara A, et al.: Incidence of Seed Migration to the Chest, Abdomen, and Pelvis After Transperineal Interstitial Prostate Brachytherapy with Loose ^{125}I Seeds. Radiat Oncol, 6, 130, 2011.
13) Chen WC, et al.: Radioactive Seed Migration After Transperineal Interstitial Prostate Brachytherapy and Associated Development of Small-Cell Lung Cancer. Brachytherapy, 11(5), 354-358, 2012.
14) Zhu AX, et al.: Prostate Brachytherapy Seed Migration to the Right Coronary Artery Associated with an Acute Myocardial Infarction. Brachytherapy, 5(4), 262-265, 2006.
15) Zhe Chen, et al.: Experimental Characterization of the Dosimetric Properties of a Newly Designed I-Seed Model AgX100 ^{125}I Interstitial Brachytherapy Source. Brachytherapy, 11(6), 476-482, 2012.
16) Vimoj J. Nair, et al.: Feasibility, Detectability and Clinical Experience with Platinum Fiducial Seeds for MRI/CT Fusion and Real-Time Tumor Tracking During CyberKnife® Stereotactic Ablative Radiotherapy. J Radiosurg SBRT, 3(4), 315-323, 2015.
17) Kiguchi Masao, et al.: Evaluation of Improvement of the Detection of Interstitial Lung Diseases by Using the Dual-Energy Subtraction Radiography Method of a Flat-Panel Detector System. Jpn J Radiol Tech, 63(12), 1362-1369, 2007.

Received August 22, 2023; accepted February 19, 2024

Cost calculation of peripheral venous catheterization for radiological technologists by Time-Driven Activity-Based Costing — Comparison in contrast CT examination before and after task shift —

SAKANO Daiki, MBA[1)], NISHIZAWA Yuka[2)], TANI Yuji, MBA, Ph.D.[3)], OGASAWARA Katsuhiko, MBA, Ph.D.[4)]*

1) Department of Care Work and Management, Faculty of Comprehensive Social Work, Japan Healthcare University
2) Department of Health Sciences, School of Medicine, Hokkaido University
3) Department of Medical Informatics and Hospital Management, Asahikawa Medical University / Department of Health Sciences, School of Medicine, Hokkaido University
4) Faculty of Health Sciences, Hokkaido University

* E-mail: oga@hs.hokudai.ac.jp

Note: This paper is secondary publication, the first paper was published in the JART, vol. 71 no. 866: 27-35, 2024.

Key words: Task shift, Cost Calculation, Vein Securement, Radiological Technologists, Contrast CT examination

【Abstract】
The 2021 revision of the Radiological Technologists Act has enabled radiological technologists to perform peripheral venous catheterization and needle removal. However, there are currently no reports on the economic efficiency of these tasks. Hence, trial calculation by cost accounting using Time-Driven Activity-Based Costing was attempted to evaluate the economic efficiency of radiological technologists performing these tasks in contrast CT examinations. The labor cost of contrast CT examinations was calculated based on the following criteria: 1) one radiological technologist and one nurse, 2) one radiological technologist, 3) one radiological technologist and one nurse stationed in the CT examination room, and 4) two radiological technologists. Results revealed that the labor cost per contrast CT examination was as follows: 1) 870 yen, 2) 578 yen, 3) 970 yen, and 4) 955 yen.

1. Introduction

Japan is currently reforming its medical care delivery system, including community healthcare visits. However, it is also facing new issues, such as the declining birthrate and aging population, shortage of medical personnel because of the declining population, and work-style reforms for healthcare professionals.

In this situation, with a view to the medical care delivery system in 2040, we are promoting not only the realization of the regional medical vision but also work-style reforms for doctors and medical personnel and effective measures to address the uneven distribution of doctors in a three-pronged approach. [1)] The "Act to amend the Medical Care Act, etc. to promote the assurance of a system for the efficient provision of high-quality and appropriate medical care" — enacted on May 21, 2021— lists "utilizing the expertise of each medical profession" as one of its goals; it recommends promoting task shifting/task sharing to reduce the burden on doctors and expand the scope of work for each profession so that medical professionals can better utilize their expertise and includes amendments to the Radiological Technologist Act.

On October 1, 2021, the new Radiological Technologist Act came into effect. Through task shifting, radiological technologists can now perform some duties of nurses under certain training conditions and can now perform the following six actions. [2)]

1) Inserting peripheral venous catheter for examinations using a contrast agent or ra-

dioisotope examinations, removing needles, and stopping bleeding
2) Connecting a device for injecting radioisotope drugs for RI diagnostic and operating said device
3) Connecting a contrast agent injection device to an arterial line (excluding those for arterial catheterization) and operating a contrast agent injection device to administer a contrast agent to an artery
4) Aspirating injected contrast agents or air during lower gastrointestinal examinations
5) Injecting a contrast agent through an inserted nasal catheter during an upper gastrointestinal examination and then removing the nasal catheter after examination of the contrast agent is completed
6) Ultrasound examinations of patients examined by a doctor or dentist, conducted at a location other than a hospital or clinic under the direction of that doctor or dentist

Before the task shift in conventional contrast CT examinations, the nurse had to accompany the patient in the CT examination room from peripheral venous catheterization until the needle was removed, and the radiological technologist had to call the nurse each time a contrast examination was performed. That is, each time a contrast CT examination was performed, there was a waiting time between calling the nurse for peripheral venous catheterization and their arrival, and there was a workload burden on the nurses involved in the series of tasks related to contrast CT examination.

In this study, we aimed to propose an economic evaluation model based on task shifts by radiological technologists that can be applied at each medical institution and to evaluate the economic efficiency of "task shifting and task sharing," the item promoting workstyle reform for doctors and medical professionals, by focusing on contrast CT examinations. To evaluate the impact on labor costs and examination times of having radiological technologists take over tasks related to contrast CT examinations, such as peripheral venous catheterization and removing, which were previously performed by nurses, through task shifting and task sharing, we estimated the time required by both to perform a series of examination-related tasks, such as peripheral venous catheterization, for each contrast CT examination and attempted to grasp the costs using Time-Driven Activity-Based Costing (TD-ABC).

2. Method

The methods used in this study are as follows.

1) Identify the processes and activities required for a contrast CT examination and organize the movement of people (radiological technologists, nurses, and patients) and information
2) Next, set the time required for each activity and the staff required to conduct it and consider four assumed scenarios based on different conditions
3) Calculate the working hours and costs of each staff member for four assumed scenarios
4) Conduct a sensitivity analysis for the four Assumed scenarios
5) Confirm the changes in labor costs and inspection times before and after the task shift

The costs associated with each assumed scenario were calculated using TD-ABC. The time required for the process and each activity in the contrast CT examination was set based on the examination flow at four hospitals in Hokkaido, and the unit salary of staff was calculated using the results of the Basic Survey on Salary Structure conducted by the Ministry of Health, Labor and Welfare, which aims to obtain a detailed understanding of the actual salary structure in Japan. [3)]

In this study, we used TD-ABC as a cost calculation method for contrast CT examinations. The cost calculation is done by dividing the cost to "direct costs" and "indirect costs." [4] Direct costs are directly recognized for the object of cost accounting (cost object). In this study, these are the personnel costs of radiological technologists and nurses. In contrast, indirect costs are not directly recognized in relation to the cost object, such as the purchase and maintenance costs of equipment and systems used across multiple products and services, utility bills, and the salaries of employees such as managers and office staff who are indirectly involved with the cost object products. TD-ABC is one of the cost-accounting methods devised by Kaplan and Anderson (2004) to relate indirect costs to products. In TD-ABC, the activities required to provide a product or service that is the subject of cost accounting are first identified, and the cost [yen] for each activity is calculated by multiplying the Capacity Cost Rate (CCR) [yen/min] of the relevant department by the time required for each activity. The CCR can be calculated using the following formula. [5]

CCR [yen/min]
= Cost of the department [yen] / Actual production capacity of the department's resources [minutes] ····· (1)

The time required for each activity was estimated by interviewing employees or direct observation by managers. Temporal accuracy is not important and is sufficient if approximately correct. The denominator, actual production capacity, is the theoretical production capacity (hours) minus the time not spent on work (breaks, training time, etc.) and has been reported to be approximately 80% of the theoretical production capacity. [5] TD-ABC reduces analysis costs compared to conventional cost-accounting methods, making it possible to calculate costs more simply.

To date, many studies have been conducted using TD-ABC in the field of radiology date, [6, 7, 8, 9] but few have targeted radiological technologists. [10]

In this study, the CCR is the salary per minute of radiological technologists and nurses.

2.1 Condition setting and assumed scenarios for contrast CT examination

In this study, we set up two scenarios with different operations of the CT examination room for contrast CT examinations. Furthermore, we set two scenarios after each task shift for a total of four.

Scenarios 1 and 2 are assumed scenarios before and after a work shift in cases where nurses are not always present in the CT examination room because of the low volume of contrast CT examinations. They are based on the staffing and operations of two hospitals with 200–300 beds in Hokkaido.

Scenarios 3 and 4 are assumed scenarios before and after a task shift in a case where a nurse in charge of peripheral venous catheterization in the front room (including the waiting room and treatment room) and a nurse who is always present in the CT examination room and responsible for tasks related to contrast CT examinations are assigned. They are based on the staffing and operations of 2 hospitals in Hokkaido with over 500 beds. At these hospitals, contrast CT examinations account for approximately half of the total number of examinations, and they operate multiple CT examination rooms, with each room performing 30–40 examinations per day. In Scenarios 3 and 4, procedures such as explaining the examination to the patient and peripheral venous catheterization were conducted outside the CT examination room; while a patient was getting changed and undergoing peripheral venous catheterization prior to being examined, another patient was being examined.

The assumed scenarios set up this time are as follows.

1) Before the task shift, when a contrast CT examination was performed by a radiological technologist, a request was made to a nurse at the nursing station.
2) After the task shift, when one radiological technologist is performing all tasks
3) Before the task shift, the examination was performed by one radiological technologist and one nurse stationed in the CT examination room, and peripheral venous catheterization was conducted in the front room.
4) After the task shift, the examination was performed by two radiological technologists, and peripheral venous catheterization was conducted in the front room.

The major categories were "Process with preprocessing in the front room," "(Patient) Identification," "Pre-processing," "Examination," "Post-processing," and "Inspection." Next, the specific activities of each process are defined as activities, and the time required for each activity is defined as the amount of time required for each activity. In addition, to understand the work structure during the examination, we divided the areas where radiological technologists, nurses, and patients stay during their respective activities into the waiting room, examination room, control room, and nurse station and attempted to visualize the movements between activities. Similarly, the information was visualized using arrows to show where it moved from.

Each scenario was developed in consultation with collaborators with 10–30 years of experience as radiological technologists and was reviewed by those at the model hospital.

2.1.1 Setting activity times - Scenario 1: 1 radiological technologist, 1 nurse (before task shift)

The work structure for Scenario 1 is shown in Table 1. As this scenario involves an accompanying nurse during the examination from peripheral venous catheterization to removing the needle, time is required to request the

Table 1 Scenario 1: One radiological technologist and One nurse (before task shift)

Process	Activity	No	Waiting room	Examination room	Control room				Nurse station	Time (min)	Time(min) (Radiological technologist)	Time(min) (nurse)	Cost (yen)
					CT	RIS	Inspection system	PACS					
Identification	Patient information / Examination method	1	□							0			
		2	□		⇦	⇦○				1	1		
Pre-processing	Request to nurse	3	□		○⇨				⇨△	0.5	0.5		
	Patient guidance	4	□←	←	←○					0.2	0.2		
		5	□☞○→	☞→						1	1		
	Inspection explanation / Change instructions	6		□○						4	4		
	Set up	7		□○						1.5	1.5		
		8		□○→	→					0.2	0.2		
Examination	Patient confirmation and vein securing	9		□⇐	○				⇐△	(2)		2	
		10		□△						3	3	3	
		11		□△⇒	⇒○					0.2	0.2	0.2	
	Start position / Condition selection	12		□	△○					1	1	1	
	Inspection	13		□	△○					5	5	5	
Post-processing	State confirmation / Needle removal	14		□⇐←	⇐△←○					0.2	0.2	0.2	
		15		□△○						1	1	1	
		16		□○△⇒					⇒	(2)		2	
	Guiding patients / Changing clothes / Tidying up	17	☜←	☜□←○						1	1		
		18	○→	→						0.5	0.5		
		19		○						2	2		
		20		○→	→					0.2	0.2		
Inspection	Transfer to inspection system	21			○⇨	⇨	⇨			(2)	(2)		
	Transfer to PACS	22					○⇨	⇨		(1)	(1)		
									Total	22.5min	22.5min	14.4min	870yen

○ : Radiological technologist △ : Nurse □ : Patient
→ : Movement of radiological technologist ⇒ : Movement of nurse ☞ : Movement of patient ⇨ : Transfer of information

nurse to perform the task and travel from the nurse station to the CT examination room. Following the model hospital's operations, the travel time of a nurse for No.s 9 and 16 was not counted in the examination time but only in the calculation of the nurses' labor costs because the radiological technologist simultaneously explained things to the patient and provided post-examination guidance. Additionally, image inspection (No. 21) and data transfer to the PACS (No. 22) were conducted in parallel with the time that the nurse was taking care of steps such as peripheral venous catheterization and, therefore, were not counted in the examination time.

2.1.2 Setting activity time - Scenario 2: 1 radiological technologist (after task shift)

Table 2 shows the business structure for Scenario 2. As the radiological technologist performs every step from peripheral venous catheterization to removing the needle, nurses no longer need to be involved in contrast CT examinations.

2.1.3 Setting activity times - Scenario 3: 1 radiological technologist, 1 nurse stationed in the CT examination room (before task shift)

The work structure for Scenario 3 is presented in Table 3. One radiological technologist and one nurse who was stationed in the CT examination room were involved in tasks related to contrast CT examinations, and peripheral venous catheterization was performed by a nurse stationed in the front room or another location before entering the CT examination room. Notably, nurses stationed in front rooms and so on refer to all nurses who take blood samples and performed peripheral venous catheterization on patients undergoing contrast CT examinations in front rooms before CT examinations, waiting rooms, and treatment rooms throughout the hospital and do not refer

Table 2 Scenario 2: One radiological technologist (after task shift)

Process	Activity	No	Waiting room	Examination room	Control room				Nurse station	Time (min)	Cost (yen)
					CT	RIS	inspection system	PACS			
Identification	Patient information / Examination method	1	□							0	
		2	□		⇦	⇦○				1	
Pre-processing	patient guidance	3	□←	←	←○					0.2	
		4	□☞○→	☞→						1	
	Inspection explanation / Change instructions	5		□○						4	
	Set up	6		□○						1.5	
Examination	Patient confirmation and vein securing	7		□○						3	
		8		□○→	→					0.2	
	Start position / Condition selection	9		□	○					1	
	Inspection	10		□	○					5	
Post-processing	State confirmation / Needle removal	11		□←	←○					0.2	
		12		□○						1	
	Guiding patients / Changing clothes / Tidying up	13	☜←	☜□←○						1	
		14	○→	→						0.5	
		15		○						2	
		16		○→	→					0.2	
Inspection	Transfer to inspection system	17			○⇨	⇨	⇨			2	
	Transfer to PACS	18					○⇨	⇨		1	
									Total	24.8min	578yen

○ : Radiological technologist □ : Patient
→ : Movement of radiological technologist ☞ : Movement of patient ⇨ : Transfer of information

Table 3 Scenario 3: One radiological technologist and one nurse stationed in the CT examination room (before task shift)

Process	Activity	No	Waiting room	Examination room	Control room				Nurse station	Time (min)	Time(min) (Radiological technologist)	Time(min) (nurse)	Cost (yen)
					CT	RIS	Inspection system	PACS					
Pre-processing in the front room	Inspection explanation / Change instructions	1	□◆							0.2	0.2	0.2	
		2	□◆							4	4	4	
	Patient confirmation and vein securing	3	□▲							3	3	3	
Identification	Patient information / Examination method	4	□		△←⇦	←⇦○				0	0.3	0.3	
Pre-processing	Patient guidance	5	□←	←	←○△					0.2	0.2	0.2	
		6	□☞○→	☞→	⇐△					1	1	1	
	Set up	7		□○△						1	1	1	
		8		□○→△⇒	→⇒					0.2	0.2	0.2	
Examination	Start position / Condition selection	9		□	△○					1	1	1	
	Inspection	10		□	△○					5	5	5	
Post-processing	State confirmation / Needle removal	11		□⇐←	⇐△←○					0.2	0.2	0.2	
		12		□△○						1	1	1	
	Guiding patients / Changing clothes / Tidying up	13	☜←	☜□←○△⇒						1	1	1	
		14	○→	→	△					0.2	0.2	0.2	
		15		○	△					2	2	2	
		16		○→	→△					0.2	0.2	0.2	
Inspection	Transfer to inspection system	17			△○⇨	⇨	⇨			(2)	(2)	(2)	
	Transfer to PACS	18			△		○⇨	⇨		(1)	(1)	(1)	
									Total	20.5min	20.5min	20.5min	970yen

○ : Radiological technologist △ : Nurse □ : Patient ▲ : Nurse in the front room ◆ : Front room reception staff
→ : Movement of radiological technologist ⇒ : Movement of nurse ☞ : Movement of patient ⇨ : Transfer of information

to a specific nurse; therefore, they are not subject to task shift in this study. Radiological technologists are involved in a series of tasks related to CT examinations, such as guiding patients, positioning them, taking pictures, cleaning, and image inspection. Nurses stationed in the CT examination room were responsible for injecting contrast agents during contrast CT scans and removing the needle after the scan. Following the operations of the model hospital in this study, the nurses, in general, did not guide the patients around or raise or lower the examination table. Additionally, reception staff perform tasks such as accepting patients and providing instructions on how to change clothes in the front room; however, because this does not affect the task shift of the radiological technologists and nurses in this study, the labor costs of the reception staff are not considered in the examination costs.

In addition, image inspection (No. 17) and the image data transfer to the PACS (No. 18) are not counted in the examination time because, following the operations of the model hospital, the radiological technologist handles these tasks in parallel while the nurse is attending to the patient.

2.1.4 Setting activity times - Scenario 4: 2 radiological technologists (after task shift)

Table 4 shows the work structure of Scenario 4, in which the work of the nurses stationed in the CT examination room in Scenario 3 is a task shift to radiological technologist. The examination was assumed to be performed by two radiological technologists sharing the work. Radiological Technologist A was primarily responsible for patient care tasks such as guiding patients from the front room to the CT examination room, positioning them, removing needles, and cleaning up, while Radiological Technologist B operated the CT, confirmed patient information and examination methods, and performed examinations and image review.

As with Scenario 3, No.s 17 and 18 are not counted as examination time, as Radiological Technologist B is handling these tasks in paral-

Table 4　Scenario 4: Two radiological technologists (after task shift)

Process	Activity	No	Waiting room	Examination room	Control room				Nurse station	Time (min)	Time(min) (Radiological technologist)	Time(min) (nurse)	Cost (yen)
					CT	RIS	Inspection system	PACS					
Pre-processing in the front room	Inspection explanation / Change instructions	1	□◆							0.2	0.2	0.2	
		2	□◆							4	4	4	
	Patient confirmation and vein securing	3	□▲							3	3	3	
Identification	Patient information / Examination method	4	□		●←⇦	←⇦○				0.3	0.3	0.3	
Pre-processing	Patient guidance	5	□←	←	←○●					0.2	0.2	0.2	
		6	□☞○→	☞→	⇦●					1	1	1	
	Set up	7		□○●						1	1	1	
		8		□○→●⇒	→⇒					0.2	0.2	0.2	
Examination	Start position / Condition selection	9		□	●○					1	1	1	
	Inspection	10		□	●○					5	5	5	
Post-processing	State confirmation / Needle removal	11		□⇐←	⇐●←○					0.2	0.2	0.2	
		12		□●○						1	1	1	
	Guiding patients / Changing clothes / Tidying up	13	☜←	☜□←○●⇒						1	1	1	
		14	○→	→	●					0.2	0.2	0.2	
		15		○	●					2	2	2	
		16		○→	→●					0.2	0.2	0.2	
Inspection	Transfer to inspection system	17			●○⇨	⇨	⇨			(2)	(2)	(2)	
	Transfer to PACS	18			●		○⇨	⇨		(1)	(1)	(1)	
									Total	20.5min	20.5min	20.5min	955yen

○ : Radiological technologist A　● : Radiological technologist B　□ : Patient　▲ : Nurse in the front room　◆ : Front room reception staff
→ : Movement of radiological technologist A　⇒ : Movement of radiological technologist B　☞ : Movement of patient　⇨ : Transfer of information

lel with Radiological Technologist A, who is primarily responsible for patient care, guiding the patient, and peripheral venous catheterization.

2.2 Cost setting and sensitivity analysis for staff engaged in contrast CT examinations

The hourly salary (yen) and CCR (salary per minute (yen)) for each job type are shown in Table 5, citing the average salary (hourly salary equivalent) by job type from the 2022 Basic Survey on Salary Structures. [3] The standard values were 23.3 yen/min for radiological technologists and 24.0 yen/min for nurses.

In addition, because staff salaries, which are a factor that significantly affects costs, are thought to vary depending on place of employment, ability, position, and years of service, a sensitivity analysis was conducted using salaries as a variable. Sensitivity analysis is used when making plans or forecasts to determine the extent to which a different number that moves in tandem changes when a certain number deviates from a predicted value. Sensitivity analysis makes it possible to clarify the stability, risk, and flexibility of a plan or model. In this study, the range of change in salary for radiological technologists and nurses was examined as the amount of change between 1 and 20 years, calculated as the standard salary

Table 5　Cost setting for each occupation and Capacity Cost Rate (CCR)

Occupation	Type	Standard valu (0 years)	Value obtained by multiplying the standard value by the ability/experience adjustment index					
			1 year	2 years	3 years	5 years	10 years	20 years
Radiological technologist	Hourly wage [yen]	1,397	1,608	1,763	1,790	1,885	2,054	2,558
	CCR=Salary per minute [yen]	23.3	26.8	29.4	29.8	31.4	34.2	42.6
Nurse	Hourly wage [yen]	1,438	1,655	1,815	1,842	1,940	2,114	2,633
	CCR=Salary per minute [yen]	24.0	27.6	30.3	30.7	32.3	35.2	43.9
Ratio when Standard valu is 100%		100%	115%	126%	128%	135%	147%	183%

Table 6 Staff labor costs, examination time, and sensitivity analysis

Scenario No	examination time(minutes)			Labor cost (Standard value)[yen]			Sensitivity analysis (100~183%)[yen]
	Radiological technologist	Nurse	Total	Radiological technologist	Nurse	Total	
Scenario 1 One radiological technologist and One nurse(before task shift)	22.5	14.4	22.5	524	346	870	870 ~ 1,591
Scenario 2 One radiological technologist (After task shif)	24.8		24.8	578		578	578 ~ 1,057
Scenario 3 One radiological technologist and One nurse stationed in the CT examination room (before task shift)	20.5	20.5	20.5	478	492	970	970 ~ 1,774
Scenario 4 Two radiological technologists (after task shift)	20.5		20.5	955		955	955 ~ 1,748

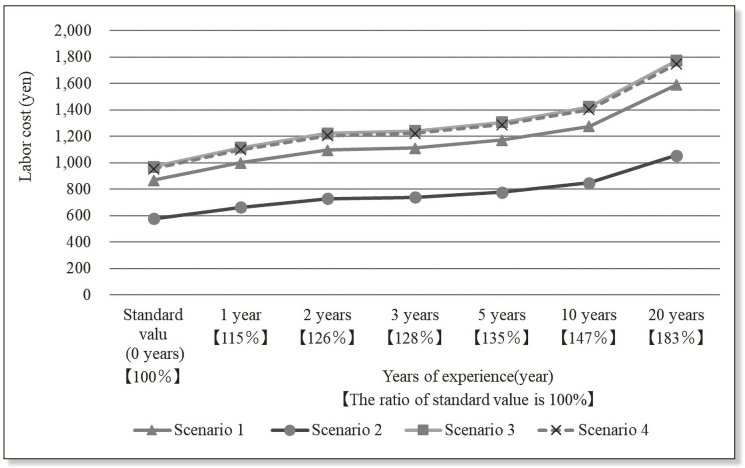

Fig. 1 Cost changes because of salary

value multiplied by the ability and experience adjustment index. The range of fluctuation follows the range of fluctuation in the average salary (hourly salary equivalent) data by occupation from the 2022 Basic Survey on Salary Structure [3], with the base value (0 years = 0 years of service) set at 100% in 0 years to 183% in 20 years.

3. Results

3.1 Cost and examination time for contrast CT examination

Table 6 shows the calculation results of the labor costs required for contrast CT examinations. In terms of the standard value amounts, in Scenario 1, the calculated labor costs were 524 yen per radiological technologist and 346 yen per nurse, for a total of 870 yen. In Scenario 2, the calculated labor cost was 578 yen per radiological technologist. In Scenario 3, the calculated labor costs were 478 yen per radiological technologist and 492 yen per nurse, for a total of 970 yen. In Scenario 4, the calculated labor cost was 955 yen in total for 2 radiological technologists. The examination time was 22.5 minutes for Scenario 1, 24.8 minutes in Scenario 2, and 20.5 minutes in Scenarios 3 and 4, respectively.

3.2 Sensitivity analysis using salary as a variable

The range of change in labor costs when salary is used as a variable is shown in Table 6 and Figure 1. The salaries of radiological technologists and nurses were calculated with a range of 100–183% depending on changes in experience. In Scenario 1 (one radiological technologist and one nurse), the range was 870–1,591 yen; in Scenario 2 (one radiological technologist), the range was 578–1,057 yen; in Scenario 3 (one radiological technologist and one nurse stationed in the CT examination room), the range was 970–1,774 yen; in Scenario 4 (two radiological technologists), the range was 955–1,748 yen. Unsurprisingly, the

results suggest that labor costs are higher when the personnel assigned to a facility have many years of experience.

4. Consideration

4.1 Usefulness of evaluating task shift using TD-ABC analysis

In this study, we referred to previous research [6-10] and used TD-ABC to organize the labor costs and time required for the Process and Activity, in contrast to CT examinations, by dividing them into those four radiological technologists and nurses (Scenarios 1 and 3). Based on this, we created Scenarios 2 and 4, which assumed that the work currently performed by nurses was a task shift to radiological technologists.

In contrast to CT examinations, peripheral venous catheterization, which was previously performed by nurses, has been shifted to radiological technologists. Using the TD-ABC method to analyze and evaluate this, the Process and Activity involving radiological technologists and nurses became clear, and the changes in labor costs and time during the task shift could be easily identified. Therefore, using the TD-ABC to analyze and evaluate task shifts during contrast CT examinations is highly useful.

Furthermore, because previous case studies mentioned the use of TD-ABC to evaluate other radiology tasks, similar methods could be used to analyze and evaluate task shifts, not only in contrast CT examinations but also in other tasks performed by radiological technologists.

4.2 Comparison before and after task shift

This study clarified the work structure and costs involved in contrast CT examinations before and after a task shift. Comparing Scenarios 1 and 2, the costs are reduced by 292 yen, or approximately 34%. This is because radiological technologists now perform the work that was previously done by nurses, thus, reducing labor costs for nurses. Additionally, the examination time was 2.3 minutes longer in Scenario 2 than in Scenario 1. This may be because, although the time for requesting contrast from the nurse and moving around in Scenario 1 is reduced, the radiological technologist alone now perform other activities in sequence, which were performed in parallel while the nurse was moving around and peripheral venous catheterization was being performed. The time required to request a nurse is assumed to be 0.5 minutes, with the nurse traveling for 2 minutes; however, in the field, this duration is often significantly longer depending on the work situation of the nurse in charge of the contrast CT examination. By having a single radiological technologist perform the work, there is no possibility of fluctuations in examination time, and nursing labor costs can be reduced. In addition, because nurses do not need to accompany patients during examinations, they should be able to free up that time to perform other tasks.

Next, comparing Scenarios 3 and 4, the costs were 970 yen in Scenario 3 and 955 yen in Scenario 4 (i.e., a reduction of 15 yen or approximately 1.5%), while the examination time remained unchanged because there was no change in the operations within the CT examination room. The change in cost was because of the difference in capacity cost rates between radiological technicians and nurses. The change in examination time might have occurred because in both scenarios, the staff in the front room performed peripheral venous catheterization; thus, there was no effect from the task shift by the CT examination room staff.

In conclusion, the comparison of Scenarios 1 and 2 before and after the task shift suggests the possibility of reducing costs and extending examination times by allowing a single radiological technologist to perform contrast CT examinations through the task shift. A comparison of Scenarios 3 and 4 suggested that there was no impact on costs or examination times,

even if the staff involved in contrast CT examinations were changed from nurses to radiological technologists.

4.3 Limitations of this study and prospects

In this study, the time required for each Process and Activity in contrast CT examinations was set based on the examination conditions at the four hospitals and by interviewing the radiological technologists at those hospitals. However, the detailed content, flow, and time of work vary from facility to facility, and the actual work is more complex, with a variety of tasks being performed in parallel and succession depending on the situation, making it difficult to generalize the results. In the future, by investigating the situation at each medical institution, it will be possible to create more precise scenarios and work structures and analyze the cost-effectiveness of radiological technologists' efforts regarding peripheral venous catheterization and needle removal.

In addition to the cost and time involved, we also found that for hospitals operating as described in Scenario 3, the cost and time required would be almost the same, even if radiological technologists were to handle the tasks of peripheral venous catheterization and needle removal. This is believed to contribute to greater freedom in personnel allocation. As the working population is expected to continue to decline in the future, when it becomes difficult to hire nurses or when nurses in charge of peripheral venous catheterization and needle removal suddenly cannot be secured because of infectious diseases that require patients to stay at home, such as influenza or COVID-19, radiological technologists can take their place. We believe that this will lead to the establishment of a stable system for performing contrast CT examinations, and we would like to make this issue a future research topic.

However, in addition to peripheral venous catheterization and needle removal during contrast CT examinations, nurses play a role in responding to any side effects that may occur because of contrast injection. Most side effects of contrast agents are acute and occur within a few minutes of administration, with a probability of less than 3% being mild and 0.004% being severe, such as low blood pressure, difficulty breathing, or loss of consciousness. [11, 12] Therefore, nurses are stationed in the CT examination room to monitor the patient's condition for a few minutes after the examination. For radiological technologists to perform contrast CT examinations alone after the task shift, in addition to training them in their new duties, it will be necessary to raise their awareness of safety management, establish safety education and systems such as rapid first aid and means of contacting doctors and nurses, and implement risk management for emergency situations by conducting simulations.

In addition, the time taken for peripheral venous catheterization depends greatly on factors such as the skill of the staff and the patient's condition. However, as this study did not fully take these points into account, this will be an area of future research.

5. Conclusion

In this study, we aimed to clarify the impact on examination costs and examination times when radiological technologists perform tasks such as establishing intravenous access and removing needles, which had previously been performed by nurses. We clarified the work structure when radiological technologists and nurses performed a series of tasks, such as peripheral venous catheterization, during contrast CT examinations, and calculated costs using TD-ABC. Regarding contrast CT examinations, the following four scenarios were assumed: (1) one radiological technologist and one nurse, (2) one radiological technologist, (3) one radiological technologist and one nurse who is always in the CT examination room, and (4) two radiological technologists. The labor costs

were calculated based on the assumed work structure for each scenario. The results were 1) 870 yen, 2) 578 yen, 3) 970 yen, and 4) 955 yen, and the examination times were 1) 22.5 minutes, 2) 24.8 minutes, 3) 20.5 minutes, and 4) 20.5 minutes, respectively. Comparing Scenarios 1 and 2, in which there was no nurse stationed in the CT examination room, when a contrast CT examination, including peripheral venous catheterization and needle removal, was performed by a single radiological technologist after the task shift, the labor cost per examination was reduced by 292 yen (approximately 34%) compared to before the task shift, and the examination time was extended by 2.3 minutes (approximately 10%) compared to when a nurse was present. In medical institutions that do not have nurses stationed in the CT examination room, examination times will increase by approximately 10%, but labor costs are expected to decrease by approximately 34% per contrast CT examination.

Furthermore, when comparing Scenarios 3 and 4, in which peripheral venous catheterization was performed in the front room or a similar location, and a nurse was always present in the CT examination room, having two radiological technologists perform the examination, including peripheral venous catheterization and needle removal after the task shift, the labor cost per examination was reduced by 15 yen, or approximately 1.5%, while the examination time did not change. This suggests that the employment status of radiological technologists and nurses may have little impact on labor costs and examination times, regardless of the professional assigned to the CT examination room.

Conflict of interest

All authors and co-authors have no conflicts of interest to disclose.

Acknowledgments

We would like to thank the radiological technologists at four hospitals in Hokkaido for their cooperation.

References

1) 66th Social Security Council Medical Subcommittee: Document 1-1 Reform of the medical care delivery system, 2019. https://www.mhlw.go.jp/content/12601000/000504323.pdf (accessed on January 10, 2023)
2) Japan Society of Radiological Technologists (Public Interest Incorporated Association): Resource site regarding the amendment of the Radiological Technologists Act, 2021. http://www2.jart.jp/activity/kokujikousyuu_siryou_2021.html (accessed on December 12, 2022)
3) Ministry of Health, Labor and Welfare: Average salary by occupation based on the Basic Survey on Salary Structure in 2022, 2023. https://www.mhlw.go.jp/content/000980675.pdf (accessed on November 21, 2023)
4) Susumu Ueno et al.: Fundamentals of Management Accounting: Theory and Practice, 4th ed., pp. 62-64, Tax Accounting Association, 2010.
5) Tadashi Shimura: How is TDABC different from ABC? IT Newsletter, Vol. 8, 1-2, Bunkyo University Graduate School of Informatics, 2012.
6) Prasad R Shankar, et al.: Time-Driven Activity-Based Costing in Radiology: An Overview. J Am Coll Radiol, Vol 17, 125-130, 2020.
7) Mohammad Ghasemi Rad, et al.: Time-Driven, Activity-Based Costing to Reduce Interventional Radiology Suite Idle Time. Cureus, 14(11), 2022.
8) Sadia Choudhery, et al.: Basics of time-driven activity-based costing (TDABC) and applications in breast imaging. 2020. Br J Radiol, DOI: https://doi.org/10.1259/bjr.20201138
9) H L Nisenbaum, et al.: The costs of CT procedures in an academic radiology department determined by an activity-based costing (ABC) method. J Comput Assist Tomogr, 24(5), 813-823, 2000.
10) Hiroshi Muto, et al.: Filmless versus film-based systems in radiographic examination costs: an activity-based costing method. BMC Health Serv Res, 11(246), 2011.
11) JA Niigata Kouseiren Ojiya General Hospital: For those undergoing CT, MRI, and other examinations using contrast agents, 2019. https://www.ojiya-ghp.jp/img/m_personnel/a04.pdf (accessed on December 12, 2022)
12) Ryohei Kuwazuru: Revised Edition: Super Practical Handbook of Side Effects of Contrast Media You Should Know. 14-20, PILAR PRESS, 2016.

Received October 5, 2023; accepted March 27, 2024

Calibration curves for radiochromic films using enhanced dynamic wedge dose gradients

SHIMA Katsumi, Ph.D.*, ABE Tadanori, Ph.D.

Faculty of Health Sciences, Department of radiology science, Japan Healthcare University

* E-mail: katsumi-shima@jhu.ac.jp

Note: This paper is secondary publication, the first paper was published in the JART, vol. 71 no. 866: 36-46, 2024.

Key words: Radiochromic film dosimetry, calibration curve, VMAT/IMRT Patient specific QA, Wedge filter

【Abstract】
In this study, we propose a method to generate a calibration curve for relative dose verification using radiochromic film (RCF) in a single irradiation. The calibration curve was generated using the dose profile calculated with wedges on the treatment planning system and the density profile of the RCF image. Our method using the dose profile of the 60-degree EDW dose image and the density profile of the RCF image took one-tenth the time of the conventional method, and by limiting the range of profiles used, it was possible to generate a calibration curve with the same accuracy as the conventional method.

1. Introduction

Intensity Modulated Radiation Therapy (IMRT) and Volumetric Modulated Arc Therapy (VMAT) are currently the primary techniques used for radiation therapy, with a rising number of patients receiving these treatments [1]. These treatment techniques modulate the intensity of the beam. Therefore, the dose and other parameters must be verified in advance before the beam from the radiation therapy device is delivered to the patient. Dose distribution verification assesses the spatial spread of the dose for verification before the actual irradiation of the patient. The dose distribution determined by the treatment planning system (TPS) is compared with the dose distribution during actual irradiation to verify TPS calculation accuracy. Radiochromic films (RCF) containing small photosensitive nuclei are employed to verify dose distribution in conjunction with a flatbed scanner to read the exposed RCF. Using the appropriate combination of scan resolutions allows the acquisition of near-continuous dose distributions. In addition, the RCF components consist of human tissue equivalents, exhibiting favorable energy response characteristics for photons with a continuous energy spectrum emitted from a linear accelerator. Therefore, the RCFs are effective tools for dose distribution verification [2]. The RCF exposed to the dose requiring verification is converted using a calibration curve, which plots known doses against the density of the irradiated RCF. Calibration curves are created by plotting several different combinations of known doses against irradiated RCF densities using a consistent radiation intensity. The graphic represents the density on the horizontal axis and the dose on the vertical axis. The quality of the calibration curve depends on the number of dose levels, with a minimum of 12 recommended calibration points [3].

The dose used in the calibration curve is selected using two methods. One involves utilizing the water-absorbed dose determined via actual measurements (absolute dose verification), while the other employs the dose calculated by the TPS (relative dose verification) [4]. The dose employed for absolute dose verification is influenced by variations in the accelerator output. Therefore, deviations are controlled

according to the quality control policy of each treatment facility. In addition, it is recommended to use a 2% accelerator X-ray output constancy for patients undergoing IMRT [5]. Conversely, the dose employed for relative dose verification corresponds to the moment the beam characteristics of the accelerator are registered in the TPS. Therefore, the accelerator output fluctuation cannot be ascertained in real-time. However, a precisely regulated X-ray output exhibits a small deviation between the dose calculated by the TPS and the actual dose delivered.

Using RCF for dose verification presents two challenges. The first involves the time and effort required to generate accurate calibration curves. The recommended method for constructing accurate calibration curves requires a total of 12 RCFs: 11 RCFs irradiated at different doses and one non-irradiated RCF. This process is highly time- and labor-intensive. The second issue pertains to the variation in the dose delivered from the accelerator. To minimize this effect, it is imperative that accelerators are subject to a continuous maintenance program [4].

S. Pecić, et al. proposed the use of dose gradients with physical wedge filters to generate calibration curves using RCF [6]. This method eliminated the need for multiple irradiations with different doses, allowing calibration curve generation using the dose gradient obtained from a single irradiation cycle. The doses in the present study are determined via continuous measurements using an ionization chamber dosimeter with a three-dimensional water phantom system. Therefore, the calibration curves in previous studies represent absolute dose verifications.

The calibration curves generated in this study denote relative dose verifications after RCF irradiation using an enhanced dynamic wedge (EDW) and doses calculated by the TPS. The EDW modulates the dose intensity and creates a dose gradient by moving the Y JAW during irradiation. Furthermore, EDWs are less likely to increase scattered radiation or change energy than filter-type wedges [7]. This study aims to propose a simple, accurate method to generate calibration curves for relative dose verification using RCF.

2. Material and methods

2-1 Dose and RCF images creation

ECLIPS version 15.1 (Varian Medical Systems, Palo Alto, CA, USA) was employed for RCF irradiation treatment planning. This process involved a water-equivalent solid phantom (400 mm × 400 mm × 215 mm Tough Water Phantom, Type WE: Kyoto Kagaku Co. Ltd., Kyoto, Japan) while an image CT scanner was employed for actual RCF irradiation. The CT value of the water-equivalent solid phantom was set to -10 Hounsfield units (HU), with a mass density of 0.9955 g/cm^3 and a relative electron density of 0.9903 [8]. The accelerator (True Beam STx, Varian Medical Systems) parameters included gantry and collimator angles of 0 degrees, X-rays as the radiation type, an energy level of 6 MV, and a dose rate of 600 MU/min. The dose gradient used to generate the calibration curve must adequately address the dose range necessary for dose distribution verification using RCF. Therefore, the RCF irradiation depth was established as the maximum dose depth (15 mm from the phantom surface) for 6 MV X-rays, characterized by a significant dose gradient. The analytical anisotropic algorithm (AAA) was used for dose calculation, while a 2 mm dose grid was selected.

Irradiating a single RCF using a consistent arbitrary dose produced an RCF with a film density that corresponded to that dosage. The RCFs for calibration curve creation were generated via irradiation from a low to a high dose for dose distribution verification. Multiple RCFs with film densities that responded to the irradiated doses were used to create the calibration curves (hereafter referred to as the convention-

al method). The treatment plan for this method involved positioning the isocenter in the center of the water-equivalent solid phantom surface at a depth of 15 mm from the surface. The irradiation field on this plane measured 100 mm × 100 mm. Eleven treatment plans were created with delivery doses of 30, 50, 70, 100, 120, 140, 170, 200, 230, 250, and 300 cGy, respectively. The isocenter represented the dose prescription point for all the treatment plans. The TPS calculation yielded MU values of 30.0, 50.1, 70.1, 100.1, 120.2, 140.2, 170.2, 200.3, 230.3, 250.4, and 300.4, respectively. This study utilized RCFs irradiated using conventional methods were used as the reference.

A single RCF with a film density that responded to a range of doses was produced via dosage irradiation at a dose gradient established via EDW. The isocenters employed for the treatment planning using the calibration curve generated via this method (hereafter referred to as the wedge method) were identical to those utilized by the conventional method. The irradiation field in the isocenter plane was 100 mm × 200 mm (Y1: 100 mm, Y2: 100 mm), while EDW60-IN was used to establish the dose gradient. Irradiation of 120 cGy was scheduled for delivery to the isocenter, while the MU value was 281.1.

The conventional method used the dose prescribed by the TPS. The doses used in the wedge method were calculated in the coronal plane of the water-equivalent solid phantom at a depth of 15 mm in the TPS. The dose distribution was converted to a dose image in DICOM format in 32-bit grayscale, with a pixel size of 1 mm × 1 mm, a pixel value (PV) ranging from 860 to 998844, and a PV-to-dose conversion factor of 2.7372249×10^{-6}. The dose D_{plan} derived from the dose image was determined using Equation (1) and the dose conversion coefficients mentioned above. The PV (PV_{image}) was determined via a rectangular ROI, oriented with its long side aligned to the dosage gradient, using ImageJ version 1.54d (National Institutes of Health, Bethesda, MD, USA), and placed in the geometric position as that of the ROI used to read the actual irradiated RCF.

$$D_{plan} = PV_{\text{image}} \times 2.7372249 \times 10^{-6}\,[\text{Gy}] \qquad (1)$$

This study utilized Gafchromic EBT3® film (8 × 10 inches) as the RCF. One RCF was cut into 254 mm × 125 mm pieces for irradiation using the wedge method and 40 mm × 40 mm pieces for conventional method irradiation. The cut RCFs were irradiated according to the treatment plan of each technique. The accelerator output on the day of RCF irradiation was 100.373%.

After 24 hours, the irradiated RCFs were read [9] using an ES-10000G flatbed scanner (Seiko Epson Corporation, Nagano Japan) and Epson Scan software (Version 3.04J: Seiko Epson Corporation). Before reading the RCF, five blank scans were performed as a warm-up. The RCF was placed with the long axis of the active component crystal parallel to the reading direction of the flatbed scanner. A transparent glass was placed over the RCF to prevent curvature relative to the flatbed scanner during reading. The scanned images were saved in TIFF format at a resolution of 150 dpi in transparent mode and 48-bit color. An RCF was read three times on a flatbed scanner, each time saving a TIFF image. Three RCF images are thus created from one RCF. The red image was extracted from the three images and averaged, while a median filter was applied at five-pixel intervals to generate the RCF image.

2-2 Region of interest (ROI) Considerations

The AAPM Task Group 235 recommends that the ROIs for reading RCFs should be irradiated at a consistent dosage, with a dose profile variation not exceeding 3% on the calibration film, and that the PV histograms should exhibit normal distribution [2]. In this study, square ROIs (10 mm × 10 mm) were used when employing

the conventional method [2] and rectangular ROIs when utilizing the wedge method. Since the rectangular ROIs had to be large enough to include the entire dose gradient in the longitudinal direction, the long side was 210 mm to accommodate the penumbra of the irradiated field (200 mm).

The RCF and dose images were used to examine the short sides of the rectangular ROI. Furthermore, the RCF images were employed for the PV histogram analysis. Due to the absence of a dose gradient in the short-side direction, the width of the normally distributed PV histogram in the ROI was considered. The long side of the ROI in this study in the dose gradient direction was 1 mm, while the width of the short side perpendicular to the dose gradient varied between 1 mm and 10 mm in 1 mm increments. The histogram analysis was performed by acquiring the PVs of the RCF images using rectangular ROIs with long sides of 1 mm and short sides ranging from 1 mm to 10 mm at 1 mm increments. The dose images were employed to obtain the dosage profiles using the line tool and rectangular ROIs for dose comparison at arbitrary locations. The reference was the dose profile of the line tool. The horizontal dose gradient direction (long side) of the rectangular ROI was 210 mm. The direction perpendicular to the dose gradient (short side) was expanded equally to the left and right while the center position remained unchanged. Therefore, the rectangular ROIs from which the dose profiles were acquired were 210 mm on the long side, 2 mm and 5 mm on the short sides, and extended every 10 mm from 10 mm to 100 mm. The dose profile was analyzed by extracting PVs from the dose images for each rectangular ROI.

The pixels in the dose images were converted to mm at 1 [pixel] = 1 [mm], while those in the RCF images were calculated as follows:

$$1\ [\text{pixel}] = 25.4\ [\text{mm}] / 150\ [\text{dpi}] = 0.169\ [\text{mm}] \quad (2)$$

2-3 Calibration Curve Generation

The ImageJ software was employed to analyze the RCF images obtained via the flatbed scanner. After color separation, a red image was extracted from the three RCFs and averaged:

$$PV_{ave} = (PV_1 + PV_2 + PV_3) / 3 \quad (3)$$

where PV_{ave} is the PV of the averaged red image and PV_1, PV_2, and PV_3 indicate the PVs of each red image. A median filter was applied to the red image at five-pixel intervals to remove noise. The 11 conventionally irradiated reference RCF images and one unirradiated image were read as the average of the PVs using a square ROI (10 mm × 10 mm) [2]. The calibration curves for the conventional method were generated using 12 reference RCF images (one unirradiated). The calibration curves for the wedge method were created using RCF images irradiated with EDW. The dimensions of the ROI used to read the RCF corresponded with those delineated in Sections 2-2. The PV values obtained via each method were converted to a net optical density (netOD) using Equation (4) [2]:

$$netOD = OD_{exp} - OD_{unexp} = \log_{10}(PV_{\text{unexp}}/PV_{\text{exp}}) \quad (4)$$

where PV_{exp} is the PV of the irradiated RCF and PV_{unexp} is the PV of the unirradiated RCF. Since the red image was extracted from a 48-bit color image, and the PV was scaled from 0 to 65535 (2^{16}-1), a 16-bit RCF image was used for analysis.

2-4 Calibration curve evaluation

Approximate functions were obtained from the calibration curves generated via the conventional and the wedge methods, which were used to convert an arbitrary *netOD* to a dose. The cubic polynomial with the highest coefficient of determination was selected as the approximation function for dose conversion.

The netOD was converted to a dose using the following equation:

$$D = a \cdot netOD^3 + b \cdot netOD^2 + c \cdot netOD \quad (5)$$

where a, b, and c are constants. The calibration function utilizing netOD consistently passes through the origin (0, 0). The calibration curves were evaluated by converting the arbitrary netOD to a dose using the conventional and wedge methods, after which the results were compared. In addition, this evaluation examined the dose gradient range used for the calibration curves generated via the wedge method. The calibration curve was generated by limiting the dose range to that of the dose gradients (netOD profile in RCF images and dose profile in dose images), which included 10 mm increments from ±40 mm (dose range 85.7-179.2 cGy) to ±90 mm (dose range 59.0-271.7 cGy) centered on the isocenter. The dose profile contained dose data at 1 mm intervals, making it possible to plot the dose versus the netOD at 81 points for the smallest ±40 mm and at 181 points for the largest ±90 mm. Excel (Microsoft Corporation, Redmond, WA, USA) was used for all analyses.

2-5 Calibration curve generation time consideration

To examine the temporal impact of the wedge method, the time required to generate the calibration curves using both the conventional and wedge techniques was quantified. The time necessary for RCF irradiation and subsequent image analysis was determined.

The actual RCF irradiation duration was defined as the total time from the initiation of start X-ray exposure to its conclusion, including the RCF exchange period. The time required for RCF exchange included the following procedures: The time necessary to press the switch of an automatic door on the control console; the time required for the automatic door to open wide enough for a person to enter; the time from entry to the treatment couch; the time necessary to retrieve the RCF from within the phantom, install a new RCF, and load the phantom; the time from the treatment couch to exit; the time required for the automatic door to close; and the time necessary to return to the operating console for the next irradiation. However, the time required to install and remove the water-equivalent solid phantom was excluded from the measurement of the time necessary for RCF irradiation since phantom installation and removal duration were the same for both methods.

The actual time necessary for RCF image analysis included the installation of the RCF on the scanner, three readings, color separation via the analysis software, averaging, and median filter application. However, the time required for the empty scan, which was a common item in both cases, was excluded.

3. Results

3-1 Generating the dose and RCF images

Figure 1 depicts the dose and RCF.

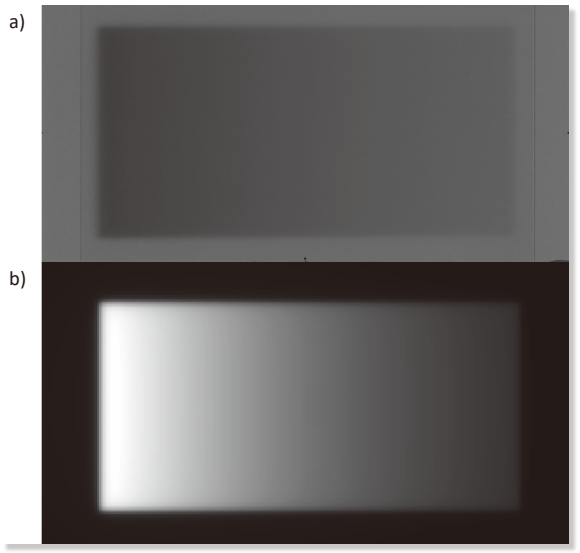

Fig. 1 (a) shows the RCF averaged over three scans and the averaged RCF median-filtered every 5 pixels. (b) shows the dose distribution at 60 degrees EDW at the peak depth of the water-equivalent solid phantom output from the treatment planning system.

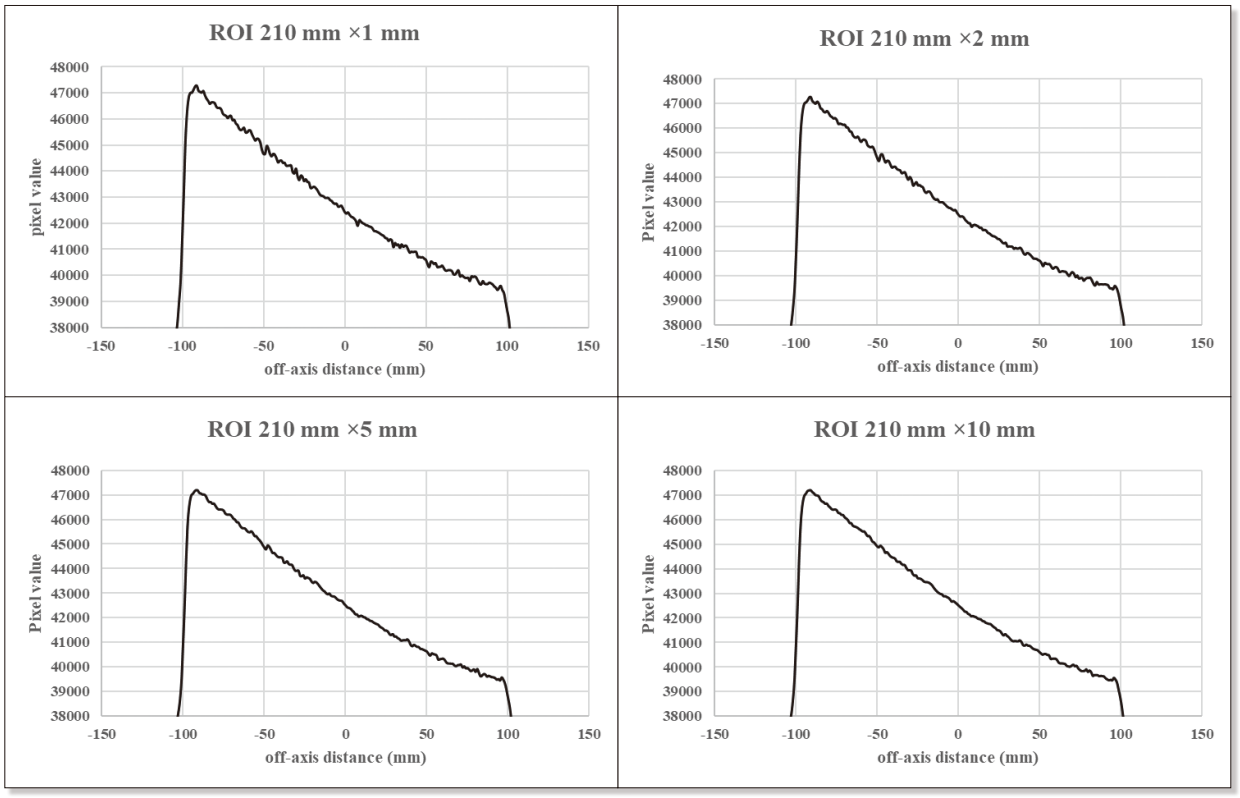

Fig. 2 The graph shows profiles of pixel values obtained from RCF images. The profiles are obtained by changing the short side of the rectangular ROI.

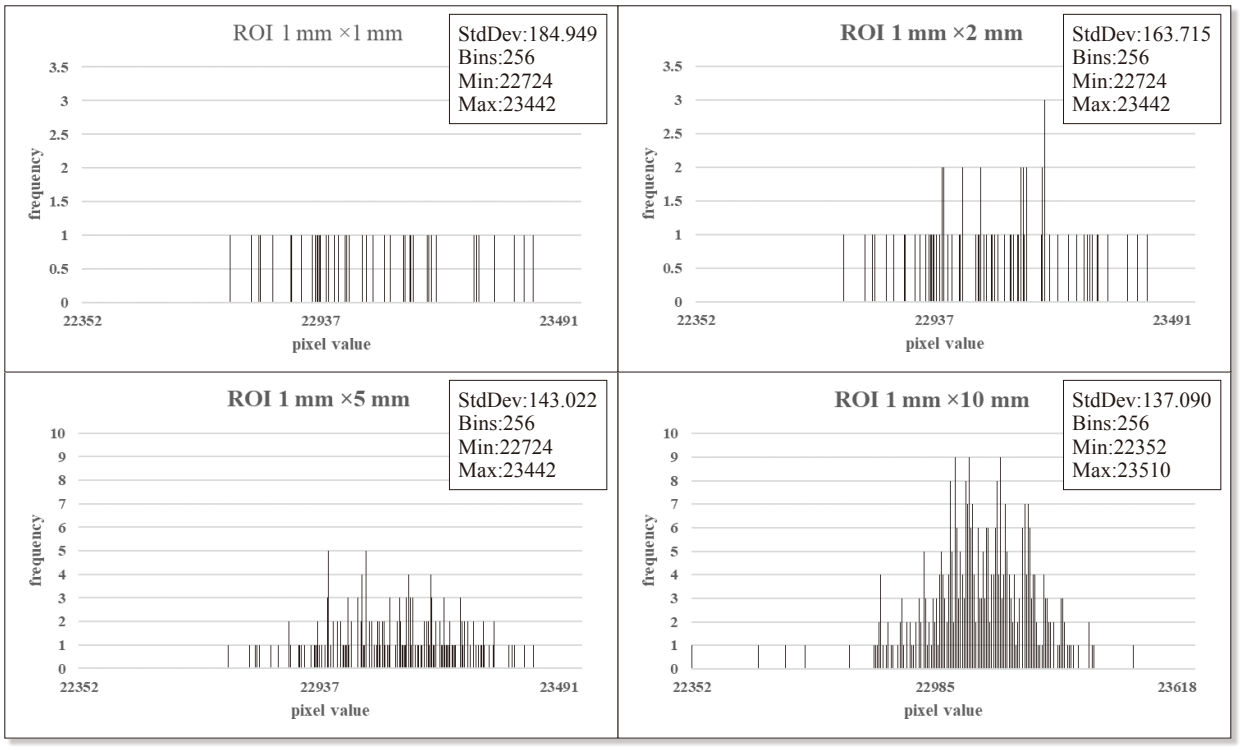

Fig. 3 The graph shows histograms of pixel values obtained from RCF images acquired by changing the short side of the rectangular ROI.

3-2 Rectangular ROI evaluation

Figures 2 and 3 show the PV graph and histogram, respectively, after analysis of the rectangular ROI in the short-side direction using the RCF image obtained via the wedge method. The results showed that the standard PV deviation tended to decrease as the width of the short edge increased. The PV histogram showed a normal distribution pattern when the short-edge width exceeded 5 mm.

Table 1 shows the rectangular ROI dose differences relative to the line tool after evaluating the dose images of the rectangular ROI short-side direction. The dosage deviation from the reference dose profile at a specified location was 0.1% for the rectangular ROIs with short edges of 20 mm or larger. A rectangular ROI of 210 mm × 10 mm was defined for the RCF analysis based on the results of these two evaluations.

3-3 Calibration Curve

Figure 4 displays the calibration curves generated using the conventional and wedge methods (±80 mm: dose range 0-252.7 cGy). The profile penumbra was employed as a reference for the registration of the dose and RCF images used in the wedge method. The use of

Table 1 Difference between the dose profile created by the rectangular ROI and the reference dose profile created by the line tool. The short side of the rectangular ROI was varied from 2 mm to 100 mm to obtain dose profiles.

Dose difference relative to reference profile (%)										
Short Side of rectangular ROI (mm)	Off-axis distance in long axis direction (mm)									
	-90 mm	-70 mm	-50 mm	-30 mm	-10 mm	10 mm	30 mm	50 mm	70 mm	90 mm
2	0.0%	0.0%	0.0%	0.0%	0.0%	0.0%	0.0%	0.0%	0.0%	0.0%
5	0.0%	0.0%	0.0%	0.0%	0.0%	0.0%	0.0%	0.0%	0.0%	0.0%
10	0.0%	0.0%	0.0%	0.0%	0.0%	0.0%	0.0%	0.0%	0.0%	0.0%
20	-0.1%	-0.1%	-0.1%	-0.1%	0.0%	-0.1%	-0.1%	-0.1%	-0.1%	-0.1%
30	-0.2%	-0.2%	-0.2%	-0.1%	-0.1%	-0.1%	-0.1%	-0.2%	-0.2%	-0.2%
40	-0.3%	-0.2%	-0.2%	-0.2%	-0.1%	-0.1%	-0.2%	-0.3%	-0.3%	-0.3%
50	-0.3%	-0.3%	-0.3%	-0.2%	-0.1%	-0.1%	-0.3%	-0.3%	-0.4%	-0.4%
60	-0.4%	-0.3%	-0.4%	-0.3%	-0.1%	-0.1%	-0.3%	-0.4%	-0.5%	-0.5%
70	-0.5%	-0.4%	-0.4%	-0.3%	-0.1%	-0.1%	-0.3%	-0.5%	-0.5%	-0.7%
80	-0.5%	-0.4%	-0.4%	-0.3%	-0.1%	-0.2%	-0.4%	-0.5%	-0.6%	-0.8%
90	-0.5%	-0.4%	-0.4%	-0.3%	-0.1%	-0.2%	-0.4%	-0.6%	-0.7%	-0.8%
100	-0.5%	-0.5%	-0.5%	-0.3%	-0.1%	-0.2%	-0.4%	-0.6%	-0.8%	-0.9%

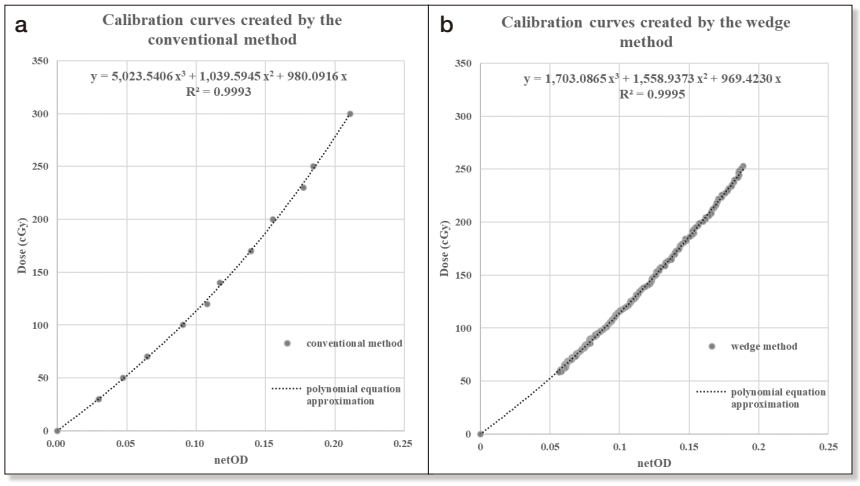

Fig. 4 Calibration curves generated by the conventional method (a) and the wedge method (b). The conventional method was created with 11 doses. The wedge method was generated with 161 doses. The wavy lines are approximate curves of cubic functions, and the dots are known doses corresponding to the netOD read from the RCF.

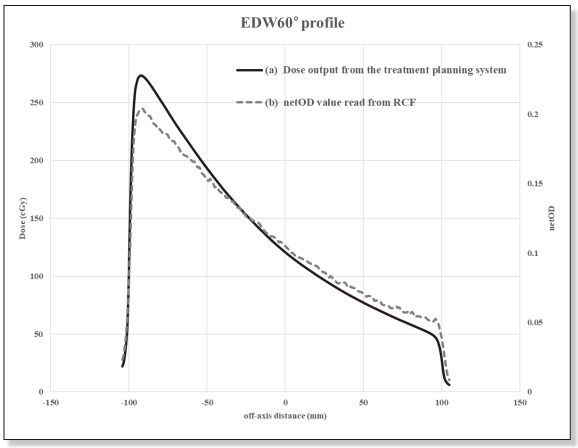

Fig. 5 EDW60° profiles are shown. (a) Dose profile obtained from dose images. (b) netOD profile calculated from the PV of the RCF image. In (a) and (b), the penumbra was visually adjusted to establish its position, respectively.

ImageJ as the analysis software prevented the typical marker registration procedure of the RCF. Therefore, the penumbra locations of the profiles in both images were carefully adjusted to determine the center positions (Figure 5).

The calibration curves using the conventional method were generated by plotting the netOD obtained from the unirradiated and 11 irradiated RCFs against the dose delivered to each. The calibration curves using the wedge method (±80 mm: dose range 0-252.7 cGy) were produced by plotting the netOD versus the dose at 161 points. The coefficients of determination for both approximate functions were almost identical at 0.9993 and 0.9995.

3-4 Calibration curve evaluation

The range of dose profiles used to generate the calibration curves was examined to evaluate the accuracy of those produced via the wedge method. The calibration curves were generated from ±40 mm (dose range 85.7-179.2 cGy) to ±90 mm (dose range 59.0-271.7 cGy), centered on the isocenter. Figure 6 shows the calibration curves for ±40 mm, ±60 mm, ±80 mm, and ±90 mm. Since the dose profile range used to generate the calibration curve was expanded, the coefficient of determination R^2 tended to be closer to 1.

Arbitrary netODs were converted to doses using the calibration curves generated via the conventional and wedge methods, after which the results were compared. Approximate functions obtained from the results of the calibration curves were used for dose conversion, with that derived via the conventional method designated as D_{conv} and that obtained using the wedge method denoted as D_{40}-D_{90}, where D represented the dose. The subscripts indicate the distance from the isocenter (= dose range). The dose conversion equation by the approximate function is as follows:

$$D_{conv} = 5023.54 \cdot netOD^3 + 1039.59 \cdot netOD^2 + 980.09 \cdot netOD \quad (6)$$

$$D_{40} = 9254.93 \cdot netOD^3 - 299.76 \cdot netOD^2 + 1081.56 \cdot netOD \quad (7)$$

$$D_{50} = 5024.37 \cdot netOD^3 + 728.51 \cdot netOD^2 + 1020.64 \cdot netOD \quad (8)$$

$$D_{60} = 507.39 \cdot netOD^3 + 1745.06 \cdot netOD^2 + 965.75 \cdot netOD \quad (9)$$

$$D_{70} = 1920.74 \cdot netOD^3 + 1436.31 \cdot netOD^2 + 981.61 \cdot netOD \quad (10)$$

$$D_{80} = 1703.09 \cdot netOD^3 + 1558.94 \cdot netOD^2 + 969.42 \cdot netOD \quad (11)$$

$$D_{90} = 715.80 \cdot netOD^3 + 1869.73 \cdot netOD^2 + 946.61 \cdot netOD \quad (12)$$

Table 2 shows the dose conversion from an arbitrary netOD using the approximate formula above, which is presented as conventional conversions. The wedge method conversion shows the netOD profile range used for the calibration curves, as well as the deviation (%) between the dose converted by each calibration curve and the dose converted via the conventional method. The dose deviation was calculated using the following equation, where the x subscript indicates the dose range.

$$\text{Dose deviation} = (D_x - D_{conv}) / D_{conv} \times 100 \ [\%] \quad (13)$$

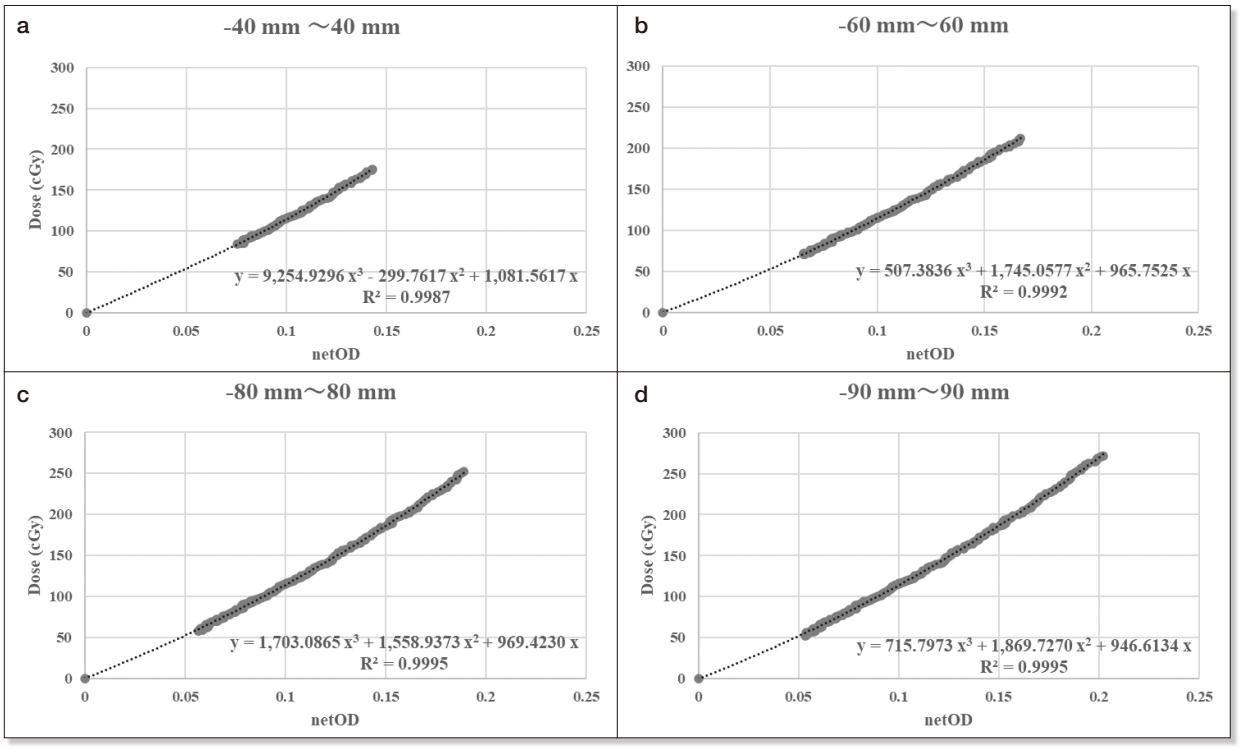

Fig. 6 Dots indicate netOD values corresponding to doses. The dashed line indicates the approximate curve. The dose gradients used to create the calibration curves range from (a) ±40 mm (0 to 175.8 cGy), (b) ±60 mm (0 to 211.9 cGy), (c) ±80 mm (0 to 252.7 cGy), and (d) ±90 mm (0 to 271.7 cGy).

Table 2 Dose conversion results for an arbitrary netOD using approximate functions obtained by the conventional and wedge methods. The conventional method shows the dose. The wedge method shows the error between the dose for the range of profiles used and the dose from the conventional method. Gray text indicates results from extrapolation.

Arbitrary netOD	conventional method	wedge method					
		Arbitrary netOD that can be dose-converted by approximate formulas					
		0～0.143	0～0.153	0～0.167	0～0.178	0～0.189	0～0.202
	Convert dose (cGy)	± 40 mm	± 50 mm	± 60 mm	± 70 mm	± 80 mm	± 90 mm
0	0	0.0%	0.0%	0.0%	0.0%	0.0%	0.0%
0.01	9.9	8.9%	3.8%	-0.8%	0.5%	-1.1%	-2.6%
0.02	20.1	7.6%	3.4%	-0.2%	0.8%	-0.6%	-1.9%
0.03	30.5	6.4%	3.1%	0.3%	1.0%	-0.3%	-1.2%
0.04	41.2	5.3%	2.7%	0.6%	1.2%	0.0%	-0.7%
0.05	52.2	4.3%	2.4%	0.9%	1.3%	0.2%	-0.3%
0.06	63.6	3.4%	2.1%	1.1%	1.3%	0.3%	0.1%
0.07	75.4	2.6%	1.7%	1.2%	1.3%	0.4%	0.3%
0.08	87.6	2.0%	1.4%	1.2%	1.2%	0.4%	0.5%
0.09	100.3	1.4%	1.1%	1.1%	1.1%	0.3%	0.6%
0.1	113.4	0.9%	0.8%	1.0%	0.9%	0.2%	0.6%
0.11	127.1	0.5%	0.5%	0.7%	0.7%	0.1%	0.5%
0.12	141.3	0.1%	0.3%	0.4%	0.4%	-0.2%	0.3%
0.13	156.0	-0.1%	0.0%	0.1%	0.1%	-0.4%	0.1%
0.14	171.4	-0.3%	-0.2%	-0.3%	-0.3%	-0.7%	-0.1%
0.15	187.4	-0.3%	-0.5%	-0.8%	-0.7%	-1.1%	-0.5%
0.16	204.0	-0.4%	-0.7%	-1.3%	-1.1%	-1.5%	-0.9%
0.17	221.3	-0.3%	-0.9%	-1.9%	-1.6%	-1.9%	-1.3%
0.18	239.4	-0.2%	-1.2%	-2.5%	-2.1%	-2.3%	-1.8%
0.19	258.2	0.0%	-1.4%	-3.2%	-2.6%	-2.8%	-2.3%
0.2	277.8	0.2%	-1.6%	-3.9%	-3.1%	-3.3%	-2.9%
0.21	298.2	0.5%	-1.7%	-4.6%	-3.7%	-3.8%	-3.5%

Table 3 The table shows the series of time required to irradiate RCF and the series of time required to analyze RCF images.

Time required for irradiation of RCF		
	conventional method Time taken (sec.)	wedge method Time taken (sec.)
1st Irradiation	3.0	29.0
RCF exchange	85.0	0.0
2nd irradiation	5.0	0.0
RCF exchange	85.0	0.0
3rd irradiation	7.0	0.0
RCF exchange	85.0	0.0
4th irradiation	10.0	0.0
RCF exchange	85.0	0.0
5th irradiation	12.0	0.0
RCF exchange	85.0	0.0
6th irradiation	14.0	0.0
RCF exchange	85.0	0.0
7th irradiation	17.0	0.0
RCF exchange	85.0	0.0
8th irradiation	20.0	0.0
RCF exchange	85.0	0.0
9th irradiation	23.0	0.0
RCF exchange	85.0	0.0
10th irradiation	25.0	0.0
RCF exchange	85.0	0.0
11th irradiation	30.0	0.0
Collecting	50.0	50.0
total	1,066.0	79.0

Time required for RCF image analysis		
	conventional method Time taken (sec.)	wedge method Time taken (sec.)
reading (e.g. by a scanner)	106	243
analysis	208	208
RCF exchange	6	0
total (per sheet)	320	451
total (per 12 sheets)	3,840	

The dose-convertible netOD varied depending on the range of netOD profiles used. Table 2 shows the netOD range that can be dose-converted. The black numbers representing the deviation from the reference indicate the dose deviation converted from the netOD within the range of the calibration curve, while the gray letters indicate the dose deviation by extrapolation since it is outside the calibration curve range. The results showed that the dose conversion using the approximate function created for ±60 mm and ±70 mm yielded a dose difference below 2% compared to the conventional method.

3-5 The time required to create the calibration curve consideration

Table 3 shows the time required to generate calibration curves using the conventional and wedge methods. In the facility used for irradiation, the distance from the operating console to the treatment couch in the treatment room was approximately 25 m. After completing the irradiation of one RCF, it was replaced with a new one, and irradiation continued. This process was completed in approximately 85 seconds. With the conventional method, the irradiation time increased at a higher dose since it relied on the MU value. The MU value of the wedge method was 281, and the time for its irradiation was 29 seconds. The total time required for the series of irradiations was 1,066 seconds (17 minutes) for the conventional method and 79 seconds (1.3 minutes) for the wedge method. The wedge method reduced irradiation time by 92.6% compared to the conventional method.

The reading time of the three RCFs, including the first preview display, was approximately 106 seconds for the conventional method and 243 seconds for the wedge method. The image analysis duration was about 208 seconds for both methods and was independent of the RCF size. The total time required to analyze the RCF images was 3,840 seconds (64 minutes) for the conventional method and 451 seconds (7.5 minutes) for the wedge method. The wedge method reduced the required analysis time of the RCF images by 88.3% compared to the conventional method.

4. Discussion

This study proposed a method for generating a calibration curve based on the dose (image) output by the TPS and the corresponding

irradiated RCF (image). The maximum dose depth, at which a larger dose gradient could be obtained, was chosen as the depth in the phantom at which the RCF was irradiated. At an irradiation field in the EDW wedge direction of 200 mm, the dose gradient of 60° EDW yielded doses ranging between approximately 50 cGy and 270 cGy. This facilitated the generation of calibration curves that included 200 cGy, representing the dose for one fraction commonly used in radiation therapy. However, we believe that the measurement at the maximum dose depth should be avoided because it may include scattered radiation from the HEAD structure of the accelerator. However, the scattered radiation is taken into account when calculating the dose distribution via TPS. In addition, no corrections are made for the accelerator output in the measurements since this method involves relative dose verification using accelerator outputs registered in the TPS. Therefore, it is necessary to ensure that the accelerators used comply with each facility's quality control policy and that the dose and geometric accuracy of the accelerators are guaranteed.

The positional error between the dose and RCF images affected the accuracy of the calibration curve since the calibration curve generated via the wedge method in this study relied on the steep dose gradient resulting from 60° EDW. The geometry of the two images had to be precisely matched to accurately plot the dose and density. The dose image output from the TPS identified the exact center location according to the coordinates. During typical dose analysis using an RCF, a laser pointer installed in the treatment room is used as a guide to set a marker indicating the center position of the RCF when it is installed in the phantom. Although dedicated film analysis software has a function to align the center positions of both images, the dosimetry software used in this study did not have this ability and could consequently not reference the markers set in the RCF. Therefore, we have developed a method for the visual adjustment of the penumbra, which is considered the limiting factor of the positioning in this study. Therefore, the results of this study may exhibit a small dose bias due to positioning errors.

AAPM TG 235 suggests that the ROI follows a normal distribution with a standard deviation of an appropriate size for the histogram of all PVs [2]. This study used a rectangular ROI for the wedge method. Increasing the short edge of the ROI during the analysis of the RCF images resulted in normal distribution in the PV histogram, which was statistically similar to that suggested by AAPM TG 235. The dose image evaluation showed a slight dose difference when the short side was enlarged (Table 1). This was considered an effect of the flattening filter since the depth at which the image was acquired represented the maximum dose depth. Figure 7 shows the dose profile in the short-sided direction obtained from the dose image using the line tool. This study used a short edge size of 10 mm, resulting in a dose difference of up to 0.09%. Sizes larger than 10 mm exhibited dose differences exceeding 0.10%, possibly because the dose difference between the isocenter and off-axis limited the expansion in the short side direction.

The dose profiles derived from the 210 mm long ROI were examined to determine a specific range, instead of using the entire range obtained. Chełmiński K et al. compared TPS-calculated EDW dose profiles with the measured results and found errors for large angular wedges at low energies [10]. In addition to the impact of the accelerator, we believe that the problem also includes the flatbed scanner used to read the irradiated RCF [2]. In the dose profile range examined in this study, the dose discrepancy at lower doses tended to be more pronounced in a dose range of ±50 mm or less. Although increasing the utilized range improved the fitting of the approximate function derived from the calibration curve, the dose difference

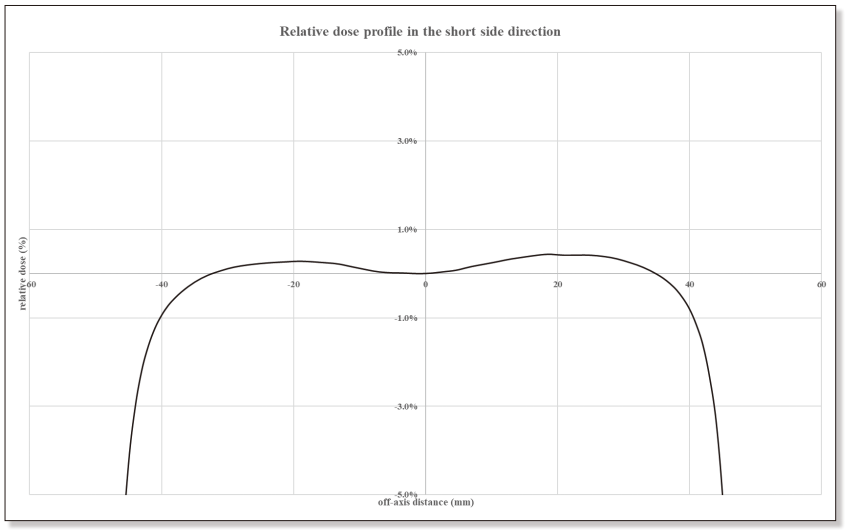

Fig. 7 Dose profiles in the short side direction obtained from dose images with the line tool. Doses are normalized by isocenter (%).

tended to be more significant in the low- and high-dose regions in a range exceeding ±80 mm. Due to the higher dose and lack of netOD plots, the narrower dose range used may affect the slope of the calibration curve. In addition, the flatness of the flatbed scanner and the accuracy of the RCF installation are considered influencing factors across a broad dose range.

We expected the calibration curves to be more accurate by plotting the calculated dose and density at a more significant TPS than the conventional method. However, the results of this study were comparable to the conventional method, and we believe that there may not be a proportional relationship between the number of plots and the accuracy of the calibration curves. In general, the RCF problem causes PV variation, while the flatness of the scanner used to read the RCF density and the accuracy of the RCF placement affect accurate dose and concentration plots. Therefore, we believe it is important to perform film analysis using a method that can resolve these issues.

Approximation functions enable the calculation of projected doses beyond the plotted ranges of the density and dose. Calculating the extrapolated dose using the approximation function generated in a range of ±50 mm allowed a dose evaluation within 2%. However, due to the significant differences at low doses, we recommend exercising caution when assessing extrapolated doses. Although some reports have suggested the possibility of extrapolated dose conversion [6], we believe that our results are inconclusive because the deviations of extrapolated doses vary randomly over the range of dose profiles used in this study.

Lewis D et al.[11] suggest that approximation using a rational function can accurately produce a calibration curve with only a few plots of the dose versus the PV. They describe a reconstruction method that simultaneously reads three RCFs per film analysis: an unirradiated RCF, an RCF irradiated at a known dose, and a dose-verified RCF, as well as a technique for correcting the calibration curve using a one-scan protocol. We also considered approximate curves with rational functions similar to theirs, but the polynomial approximation was used because it offered a superior fit.

We compared the time required to generate calibration curves, showing a potential overall time reduction of 89.2%. The wedge method in this study showed promise for obtaining calibration curves with the same accuracy as the conventional method within only 10 min-

utes after RCF irradiation. However, we believe that the time required for image evaluation depends on the software used to analyze the irradiated RCFs and may differ from the results shown in this study.

This study introduces a method that decreases the time required for producing a calibration curve using RCF by approximately 90%, compared to conventional techniques. This reduced duration indicates the feasibility of generating a new calibration curve for each dose analysis utilizing an RCF. The results of this study show that dose conversion by the approximate function generated in the ±60 mm and ±70 mm dose profile ranges differ by less than 2% from the dose obtained via the conventional method, indicating that the dose conversion can achieve accuracy comparable to the conventional approach. However, the dose profile range in this study is affected by the dose gradient resulting from EDW, the flatness of the scanner during RCF reading, and the RCF installation error. Therefore, it is necessary to confirm the range of dose profiles used at each facility.

5. Conclusion

This study presents a simple method involving relative dosimetry using the relationship between the dose output from the TPS and the actual irradiated RCF density. Our method using the dose profiles from the EDW 60° dose images and the density profiles from the RCF images requires only one-tenth the time of the conventional method. Limiting the profile range used enables the generation of calibration curves with an accuracy equivalent to the conventional method.

Conflict of interest disclosure

First author and co-authors have no conflicts of interest to disclose.

Acknowledgments

We would like to thank Dr. Seiji Tomori, Department of Radiology, National Hospital Organization Sendai Medical Center, for his great help in writing the paper.

References

1) Numasaki Hodaka, et al.: Report on the 2019 Periodic Structural Survey of Radiotherapy Facilities Nationwide (Report 1). Japanese Society of Radiation Oncology, 2022.
2) Niroomand-Rad A, et al.: Report of AAPM Task Group 235 Radiochromic film dosimetry: An Update to TG-55. Med Phys, 47(12), 5986-6025, 2020.
3) Bouchard H, et al.: On the characterization and uncertainty analysis of radiochromic film dosimetry. Med Phys, 36(6), 1931-1946, 2009.
4) Kawauchi Toru, et al.: Dose Verification Methods for Intensity Modulated Radiation Therapy. Japan Society of Medical Physics, 2013.
5) Klein E, et al.: Task Group 142 report: Quality assurance of medical accelerators. Med Phys, 36(9), 4197-4212, 2009.
6) Pecić S, et al.: Physical wedge as a tool for radiochromic film calibration. Z Med Phys, S0939-3889 (23) 00077-6, 2023.
7) Liu C, et al.: Characterizing output for the Varian enhanced dynamic wedge field. Med Phys, 25(1), 64-70, 1998.
8) Japan Society of Medical Physics, ed.: Standard Methods of Measuring Water Absorbed Dose in External Radiotherapy. 197, Tushosangyousha, 2012.
9) Shima K, et al.: Analysis of post-exposure density growth in radiochromic film with respect to the radiation dose. J Radiat Res, 53, 301-305, 2012.
10) Chełmiński K, et al.: Dynamic wedges – dosimetry and quality control. Rep Pract Oncol Radiother, 11(2), 67-75, 2006.
11) Lewis D, et al.: An efficient protocol for radiochromic film dosimetry combining calibration and measurement in a single scan. Med Phys, 39(10), 6339-6350, 2012.

Received April 16, 2024; accepted May 13, 2024

Characteristic evaluation of water-based pigment skin marker for radiation therapy

MIYAZAKI Naoto[1], SAKAI Yusuke[2]*, KUBO Kazuki[2], KOSAKA Hiroyuki[2], NAKAYAMA Shinichi[3], HIROSE Mizuki[4], KAWAMATA Hiroaki[1], MONZEN Hajime[2]

1) Department of Radiology, Hyogo Prefectural Awaji Medical Center
2) Department of Medical Physics, Graduate School of Medical Sciences, Kindai University
3) Division of Clinical Radiology Service, Okayama Central Hospital
4) Department of Radiation Oncology, Okayama Central Hospital

* E-mail: ysakai.kmsyo@gmail.com

Note: This paper is secondary publication, the first paper was published in the JART, vol. 71 no. 867: 28-33, 2024.

Key words: Skin marking, Water-based pigment marker, Radiation therapy, Safety material, Moisturizer

【Abstract】
Purpose: Skin markers are widely used in external radiation therapy to ensure the accuracy of the irradiation position. While some conventional skin markers contain harmful substances, the HM skin marker has fully disclosed components, ensuring safety. The purpose of this study is to evaluate the characteristics and performance attributes of the HM skin marker through animal experiments.
Methods: Using miniature pig, we investigated the characteristics of the HM skin marker such as writable distance, resistance to moisturizers, and removal method without damaging the skin after treatment or when misdrawn. Additionally, we evaluated the visibility of HM skin marker in five colors when illuminated with in-room lasers used for patient positioning.
Results: The total writable distance was approximately 17-18 m. When rubbed with a finger over moisturizer, the markings only slightly faded. Using baby oil, the markings could be easily removed. The black and dark brown markers showed excellent visibility when illuminated with the in-room lasers in even a darkened room.
Conclusion: The HM skin marker, which is disclosed its components, has excellent clinical characteristics including sufficient writable distance, high resistance to moisturizer, and ease of removal without damaging the skin. Therefore, the HM skin marker is suggested to be highly practical skin marker in the field of radiotherapy.

Introduction

In external radiation therapy, skin markers are commonly used to accurately position patients at the correct irradiation site during each treatment session. Traditionally, oil-based markers, compounded skin markers made with fuchsine-based ink in the hospital's pharmacy, and marker pens containing methylrosaniline chloride have been widely used both in Japan and internationally. Since skin markers come into direct contact with the patient's skin, high safety is required [1]. However, fuchsine-based skin markers contain highly irritating solvents, such as resorcinol and liquid phenol, which may cause allergic reactions and skin rashes. Furthermore, pharmaceuticals containing methylrosaniline chloride have been reported to pose genetic toxicity and carcinogenic risks [2], and as a result, the manufacture and sale of such products was halted in Japan in 2022. Additionally, skin markers require high durability to remain visible for a long period, as their fading during the treatment period can lead to reduced accuracy of irradiation positioning and increase the burden on medical staff due to the need for reapplication [3, 4]. The typical duration of radiation therapy ranges from one week to about one month, whereas the average durability of an oil-based marker is approximately three days. Given this background, the use of alternative skin markers such as water transfer decals and temporary tattoos has been increasing in recent years [5-7]. However, there are issues such as skin irritation and the lack of disclosure regarding the substances and additives

contained. In response, Nakayama et al.'s research group developed a new water-based pigment marker (HM Skin Marker, Hayakawa Rubber Co., Ltd, Hiroshima, Japan), made from cosmetic ingredients and edible materials with clearly defined safe components [8]. HM Skin Marker offers high safety along with superior durability compared to oil-based pens, and it also has reduced ink transfer to clothing. Therefore, it is anticipated to be a valuable alternative in clinical radiation therapy settings, replacing traditional skin markers. In radiation therapy, there are several key characteristics that skin markers should possess for practical use. In radiation therapy, moisturizers may be applied to the skin during the treatment period [9], so resistance to moisturizers is an important characteristic for markers. Furthermore, at the completion of the treatment period or in the case of marking errors, it is preferable for the marker to be easily removed. Additionally, during treatment, skin markings are compared with alignment lasers in the treatment room, and patient positioning is performed. However, the color of the lasers and the conditions during alignment vary by facility, and as a result, the suitable marker color may differ. The ease of visibility of markings relative to the laser is crucial for ensuring the precision of the irradiation position. The purpose of this study is to elucidate the characteristics of the HM skin marker anticipated for clinical use and to demonstrate whether it satisfies the essential requirements for a marker. Such characteristics in skin markers for radiation therapy have not been reported previously. In this study, we conducted investigations and experiments by utilizing minipigs [10-12], which have a high correlation with human skin in terms of histological similarity and permeability.

1. Methods

1-1 HM Skin Marker

The ink of the HM skin marker (Fig. 1) is composed of water, film-forming agents, coloring agents, and other ingredients, and does not contain toxic substances. The composition of these components is shown in Table 1. All the included components are approved as 'Quasi-Drug Ingredients 2022' in Japan [13].

Fig. 1 HM skin marker
The ink used is composed of cosmetic materials with confirmed safety.

Table 1 Composition of the HM skin marker ink

Component	Material	Mass composition ratio (%)
Solvent	Water	58.5
Film former	Styrene/acrylates copolymer	20
Coloring agent	Pigment dispersion	20
Thickener	Xanthan gum	0.2
Moisturizing and antibacterial agent	1,3-butyleneglycol	1
Preservative agent	Methylparaben Ethylparaben Phenoxyethanol	0.3

1-2 Ink Characteristics Evaluation

The animals used were 18-month-old Göttingen minipigs (Hamaguchi Lab Plus Inc., Osaka, Japan). Pig's skin is widely used as an alternative to human skin due to its histological similarity and high correlation in permeability [10-12]. A mixed anesthetic (medetomidine 0.04 mg/kg and midazolam 0.3 mg/kg) was intramuscularly injected in the cage. Throughout the experiment, isoflurane 2% was continuously inhaled.

1-2-1 Writing Performance

To evaluate the writable distance per marker, a straight line approximately 20 cm long was

drawn on the pig's torso using a ruler. The process continued without exerting pressure until the ink faded and could not be completely drawn, after which the distance was measured.

1-2-2 Resistance to Moisturizers

During radiation therapy, patients may apply moisturizers to prevent dryness and irritation around the treatment area. To assess the resistance of the HM skin marker to moisturizers, a moisturizer (HEPATREAT, NIPPON ZETTOC Co., Ltd, Tokyo, Japan) was applied to the straight lines drawn on the pig's torso in the previous section. After applying the moisturizer, friction was applied using a finger to observe changes such as reduction in intensity, fading, and smudging.

1-2-3 Ease of Removal

Unnecessary markings after the completion of radiation therapy and the markings that were drawn mistakenly should be promptly removed from the skin without causing irritation. The straight lines drawn on the pig's torso in the previous section were each treated with alcohol disinfectant (hereafter referred to as disinfectant), cleansing oil (COVERMARK, Osaka, Japan), and baby oil (Pigeon, Tokyo, Japan) to assess their ease of removal. Using gauze soaked with each liquid, the straight lines that were drawn were wiped off, and the remaining lines were visually inspected.

1-3 Visibility

1-3-1 Alignment Laser

The visibility of the markings when superimposed with the laser was assessed. Straight lines in yellow, orange, dark brown, black, and navy blue were drawn on the forearms of one male and one female volunteer. The markers of each color consist of the same materials, excluding the color components. In general, the laser projectors are installed in the treatment room along with the treatment equipment. The laser colors used were red, blue, and green. The red (APOLLO cross red, LAP LASER, Lüneburg, Germany) and blue (Halcyon, Varian Medical Systems, CA, USA) lasers were provided by projectors installed in the treatment room, while the green laser (SANWA SUPPLY INC., Okayama, Japan) was provided by a laser pointer. Observations were conducted visually in each treatment room. The assessment of the green laser was conducted in the same room as the red laser. The illumination level in the room was varied in three stages: fully lit, half lit, and off. The illumination was measured using a lux meter (TM-209M, TENMARS ELECTRONICS, Taiwan). The illumination levels in the room for each lighting condition were as follows.

Red and green lasers:
Fully lit: 247.0 lux, Half lit: 74.7 lux,
Off: 12.7 lux.

Blue laser:
Fully lit: 340.1 lux, Half lit: 101.3 lux,
Off: 7.9 lux.

The distances from the markings to the observers were set at 1 m and 40 cm. Three observers assessed the visibility of the markings under each condition using a 5-point scale. The scores were assigned as follows: 1 = 'Not distinguishable,' 5 = 'Completely distinguishable from the laser,' with values assigned between 1 and 5 accordingly. Furthermore, the assessments of all other test items were also conducted by the same observers.

1-3-2 Bolus

The visibility of the markings (yellow, orange, dark brown, black, and navy blue straight lines) drawn on the forearm of the volunteer was assessed through the bolus (Bolus material, MEDTEC, CIVCO Radiotherapy, IA, USA).

1-4 Ethical Considerations

All animal experimental procedures in this study were conducted in accordance with the guidelines for the management and use of laboratory animals, following the animal experi-

ment regulations of Hamaguchi Lab Plus Co., Ltd. The study was approved by the Ethical Review Committee of Okayama Central Hospital (Approval No. 20230107). All volunteers and observers provided informed consent prior to participation in the study and participated voluntarily.

2. Results

2-1 Ink Characteristics Evaluation

2-1-1 Writing Performance

Fig. 2 shows the markers drawn on the body of the pig. The total distance that could be marked with a single marker was approximately 17 to 18 meters. Additionally, during the continuous use of the markers, the pen tip dried several times, causing skipping; however, re-capping the marker and allowing it to stand temporarily made it possible to draw again.

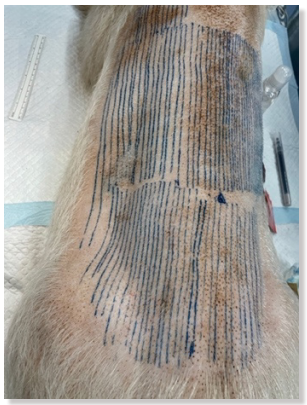

Fig. 2 Markings drawn by the HM skin marker on the pig's body

Approximately 20 cm-long markings were repeatedly drawn until the ink ran out.

2-1-2 Resistance to Moisturizers

Fig. 3 shows the result of rubbing the markings with a finger over the moisturizer. The marking at the center, where friction occurred, showed slight smearing but did not completely disappear, only becoming slightly faded.

Fig. 3 Markings after rubbed with a finger over moisturizer, 10 minutes after they were drawn.

2-1-3 Ease of Removal

Fig. 4 shows the markings after being wiped off with disinfectant, cleansing oil, and baby oil, respectively. Baby oil was the most effective at removing the marking, followed by disinfectant. On the other hand, when cleansing oil was applied with a finger, it spread to the surrounding area, and even after being wiped off with gauze, it was unable to completely remove the marking. Furthermore, by mixing with ultrasound gel, each solution was able to remain in place on the marked area without flowing off.

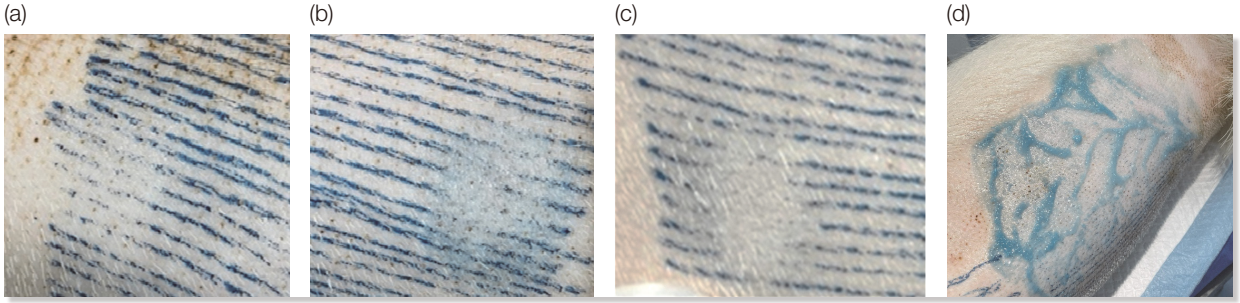

Fig. 4 Markings after wiped with each solution

(a) Disinfectant (b) Cleansing oil (c) Baby oil (d) Echo gel mixed with baby oil

Fig. 5 Visibility of skin markings drawn with a five-color marker under various conditions: Room light and illuminated laser
(a) Fully lit (247.0 lux) (b) Half lit (74.7 lux); Green laser (c) Off (12.7 lux); Red laser

2-2 Compatibility with Laser Colors

Fig. 5 shows straight lines drawn with markers in yellow, orange, dark brown, black, and navy blue on a volunteer's forearm. All the colored straight lines were clearly visible under normal lighting conditions. Currently available HM skin markers in navy blue exhibited high visibility (score of 4 or higher) under all conditions, except for the blue laser under no lighting (5-point scale: 1). Additionally, both dark brown and black markers exhibited high visibility (score of 4 or higher) under all conditions. On the other hand, both yellow and orange markers exhibited low visibility (score of 3 or lower) under almost all conditions.

Fig. 6 shows the markings made with different colors under bolus overlay, where all colors except yellow exhibited high visibility.

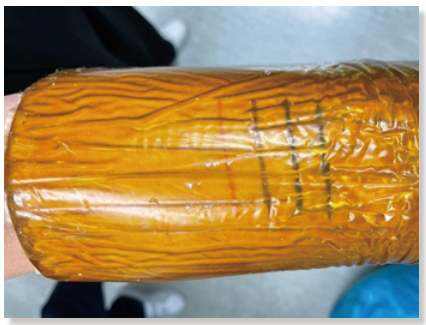

Fig. 6 Visibility of skin lines drawn with a five-color marker through a gel bolus

3. Discussion

Over the long history of radiation therapy, skin markers have played an important role [7]. In recent years, markerless systems have gained attention for reducing patient burden and improving treatment efficiency [14-16]. Given that only 2.4% of facilities do not use markers, skin markers remain important [1]. Currently, oil-based markers are the most commonly used (84.2%) due to their ease of handling and availability [1]. However, oil-based markers contain harmful components such as xylene, raising concerns about safety [1]. Against this background, skin markers that combine safety, durability, and practicality have been in demand for many years. HM skin markers are made from skin-friendly ingredients, primarily based on cosmetic-grade materials. Furthermore, it has been reported that HM skin markers have about twice the durability of oil-based markers when tested on the upper arm of a volunteer [8]. This study conducted a detailed examination of the practical properties of HM skin markers, including writing performance, resistance to moisturizers, and removal characteristics through animal experiments. Additionally, visibility under alignment lasers in treatment rooms was assessed with five different color markers under various conditions. The results showed that black and dark brown markers exhibited high visibility under all conditions with the alignment laser. Regarding marker color variations, it is generally necessary to have about two colors in clinical settings, considering patient preferences (e.g., for less noticeable colors) and functional purposes (e.g., distinguishing multiple isocenters) [17]. Currently, only navy blue

markers are commercially available, but dark brown markers blend well with skin tones and are less noticeable in daily life, making them particularly useful. In terms of writing performance, the continuous use of the pen caused some smudging due to the drying of the ink tip in this capillary-based system. However, clinical markings typically involve drawing several short lines (a few centimeters to 20 cm), so the writing performance is considered sufficient for clinical use. The retention of markings during the treatment period is crucial for ensuring treatment accuracy. However, many patients want the markings removed early after treatment [17]. In this study, baby oil was found to be the most effective at removing the ink. The ink used in HM skin markers is specifically formulated to be resistant to natural skin oils (sebum) and sweat, which explains why cleansers containing similar lipid substances were less effective at removing the markings. The cleansing oil contained squalane and other unsaturated fatty acids (lipids), which may explain its limited removal effectiveness. The faintness of the marking when rubbed hard was likely due to the pigment ink in the HM skin marker forming a film on the skin, which was partially removed by friction. However, in clinical settings, it is unlikely that such strong friction would occur on the marked area, so this is not considered a major concern. In contrast, mineral oil-based products like baby oil demonstrated superior removal effectiveness. Baby oil is designed to be gentle on infants' skin, making it suitable for removing markings from skin weakened by radiation therapy without causing irritation. Radiation therapy often leads to dry skin and inflammation, and moisturizers are recommended during treatment [9]. Typically, markings are applied near the irradiated areas, and applying moisturizers to these areas can lead to the markings fading. However, HM skin markers showed mild smudging but did not completely fade when exposed to moisturizers, making re-marking possible. Caution is needed with moisturizers containing high amounts of mineral oil, as they may affect the removal of HM skin markers.

4. Conclusion

HM skin markers are made from fully disclosed, skin-safe ingredients and possess excellent writing performance, resistance to moisturizers, and easy removal without skin irritation. Additionally, the black and dark brown markers, which are not commercially available, exhibited high visibility under treatment lasers used for patient positioning. These properties suggest that HM skin markers are highly practical for use in radiation therapy settings.

Conflict of Interest

Author Hajime Monzen has received a research grant from Hayakawa Rubber Co., Ltd. He also received funding from the 2023 Scientific Research Fund (23K07194). No other authors have any conflicts of interest to disclose.

Acknowledgments

The authors would like to express their gratitude to Hiromi Murakami of Hayakawa Rubber Co., Ltd. and Nobuyuki Mizuguchi, Deputy Director of the Technical Department at the Kindai University School of Medicine Animal Experimentation Joint Research Center, for their cooperation in this research.

References

1) Radiotherapy Kataroukai: Working Group Report on the Standardization of Marking. 2021.
2) Health Canada: 2019. Important Safety Information. https://recalls-rappels.canada.ca/en/alert-recall/health-canada-warns-canadians-potential-cancer-risk-associated-gentian-violet (07 April, 2024, date last accessed)
3) Morgan-Fletcher SL.: Prescribing, recording and reporting photon beam therapy (supplement to ICRU report 50), ICRU report 62. Br J Radiol, 74, 294, 2001.
4) American Association of Physicists in Medicine: physical aspects of quality assurance in radiation therapy. AAPM Report 13, 1984.
5) Yabutani T, et al.: Verification of the portal skin mark for radiotherapy. Jpn. J. Radiol. Technol, 59, 1295-302, 2003.
6) Wurstbauer K, et al.: Skin markings in external radiotherapy by temporary tattooing with henna: improvement of accuracy and increased patient comfort. Int J Radiat Oncol Biol Phys, 50, 179-81, 2001.
7) Rathod S, et al.: Skin markings methods and guidelines: a reality in image guidance radiotherapy era. South Asian J Cancer, 1(1), 27-9, 2012.
8) Nakayama S, et al.: Development and evaluation of a novel water-based pigment marker for radiation therapy skin marking. Radiol Phys Technol, 16(4), 543-551, 2023.
9) Sekiguchi K, et al.: The effectiveness of moisturizer on acute radiation-induced dermatitis in breast cancer patients: a systematic review and meta-analysis. Breast Cancer, 30(1):2-12, 2023.
10) Todo Hiroaki: On the skin permeability of drugs via animal skin. Drug Delivery Systems, 32(5), 411-417, 2017.
11) Gray GM, et al.: Lipid compositions of cells isolated from pig, human, and rat epidermis. J Lipid Res, 16(6), 434-40, 1975.
12) Wester RC, et al.: Percutaneous absorption of salicylic acid, theophylline, 2, 4-dimethylamine, diethyl hexyl phthalic acid, and p-aminobenzoic acid in the isolated perfused porcine skin flap compared to man in vivo. Toxicol Appl Pharmacol, 151(1), 159-65, 1998.
13) Pharmaceutical Safety and Environmental Health Bureau of Health, Labour and Welfare.: 2021. Standards for Quasi-drug Ingredients. https://www.mhlw.go.jp/content/000839905.pdf (07 April, 2024, date last accessed).
14) Heinzerling JH, et al.: Use of surface-guided radiation therapy in combination with IGRT for setup and intrafraction motion monitoring during stereotactic body radiation therapy treatments of the lung and abdomen. J Appl Clin Med Phys, 21(5), 48-55, 2020.
15) Batista V, et al.: Surface guided radiation therapy: An international survey on current clinical practice. Tech Innov Patient Support Radiat Oncol, 22, 1-8, 2022.
16) Svestad JG, et al.: Surface-guided positioning eliminates the need for skin markers in radiotherapy of right sided breast cancer: A single center randomized crossover trial. Radiother Oncol, 177, 46-52, 2022.
17) Asada H, et al.: Emotional experiences of skin markings among patients undergoing radiotherapy and related factors: a questionnaire-based cross-sectional study. Patient Prefer Adherence, 16, 1359-69, 2022.

Received October 5, 2023; accepted January 17, 2024

A Study of Reducing Imaging Time Using Deep Learning Reconstruction in Pituitary MRI Examination

MORI Ryutaro[1)]*, UENO Masayuki[1)], KANEKO Akihiro[1)], SEKITO Yuichi[1)], ONO Hidetoshi[2)]

1) Department of Diagnostic Radiology, Nakamura Memorial Hospital
(Currently, Department of Radiation Science, Hirosaki University (First author only))
2) Department of Radiation, Nakamura Memorial Hospital

* E-mail: d.forest@hirosaki-u.ac.jp

Note: This paper is secondary publication, the first paper was published in the JART, vol. 71 no. 862: 14-21, 2024.

Key words: Deep Learning Reconstruction, Pituitary, Time Reduction

【Abstract】
We investigated the possibility of using Deep Learning Reconstruction (DLR) to maintain image quality and reduce imaging time in pituitary MRI examinations. We evaluated images of phantoms and healthy volunteers and confirmed that DLR improved SNR and spatial resolution. The objective evaluation showed that PSNR and SSIM were decreased, but DLR was suggested to improve image quality and ensure visibility. In this study, the imaging time was reduced from 3 minutes 12 seconds to 1 minute 37 seconds for T_1WI and from 2 minutes 51 seconds to 1 minute 28 seconds for T_2WI under the imaging conditions using DLR, suggesting a reduction of approximately 50% while maintaining image quality. Further validation is needed for clinical use.

1. Introduction

In the examination of the pituitary gland, MRI, which provides excellent soft tissue contrast, is useful due to its ability to delineate anatomical structures and their relationship with surrounding tissues. In particular, MRI is known to be superior to CT in depicting tumor structures, the optic chiasm, and the parasellar region [1)]. Furthermore, for microscopic lesions, 3.0T MRI is known to be superior to 1.5T MRI in depiction [2-5)]. Thus, when evaluating the boundary between normal and abnormal tissues, the high spatial resolution of high-magnetic-field MRI is considered useful for depicting fine structures and assessing the degree of lesion infiltration [3, 4, 6)]. Therefore, one of the challenges has been the prolonged scan time required to achieve sufficient SNR for diagnosis and high spatial resolution [6)]. At our institution, the routine pituitary gland MRI protocol utilizes a 3.0T MRI system with 2D turbo spin echo (TSE) T_1- and T_2-weighted imaging at a slice thickness of 2 mm in three planes, with an acquisition averaging factor of 2. The total scan time was approximately 20 minutes.

Deep learning (DL) is increasingly being adopted in the medical imaging field and is widely used for lesion detection and segmentation [7-8)]. Deep learning reconstruction (DLR), a reconstruction method using DL to enhance MRI image quality, has been developed [9)]. In recent years, the number of MRI systems equipped with DLR applications has been increasing [10-13)].

Various methods have been developed for DLR. Among them, Deep Resolve (DR), developed by Siemens Healthineers (Erlangen, Germany), is a technology for noise reduction and high-resolution processing. DR enables the acquisition of higher-quality images than conventional methods [12-13)].

Therefore, in pituitary gland MRI, the use of DR, a DLR technology integrated into the system, is considered a potential approach to re-

ducing scan time while maintaining conventional image quality. In this study, we first clarified the impact of DR on MRI image quality through image evaluation using phantom experiments. Second, we evaluated the image quality of accelerated pituitary gland imaging using DR in a study with healthy volunteers. This study aimed to investigate whether DR can reduce scan time while maintaining the image quality of pituitary gland examinations.

2. Study Conditions

2-1. Participants

We provided a thorough explanation of the study's purpose and the volunteers' right to refuse or withdraw participation at any time, both in writing and orally. The study included 15 healthy volunteers, aged 24 to 58 years, who provided informed consent (12 males, 3 females; mean age, 36.6±9.1 years).

Furthermore, this study was reviewed and approved by our institution's ethics committee. (Approval No.: 202307-03).

2-2. Equipment Used

The MRI scanner used was the MAGNETOM Vida 3.0T (Siemens Healthineers), and the Head-Neck 20-channel coil was used. The phantoms used were a 5300 mL plastic bottle phantom provided with the MRI system (solute per 1000 g of distilled H_2O: 3.75 g $NiSO_4 \cdot 6H_2O$ + 5 g NaCl), and a 90-401 MRI phantom (acrylic/PVA gel, Motohashi Kasei Kogyo Co., Chiba, Japan). Image analysis was performed using ImageJ 1.53a (National Institutes of Health, Bethesda, MD, USA).

2-3. Deep Learning Reconstruction (DLR)

The DLR technology used in this study was Deep Resolve (DR). DR is divided into Deep Resolve Gain (DRG) and Deep Resolve Sharp (DRS). DRG is a denoising technology that enables high-precision noise reduction without extending scan time by using a noise map generated from raw data [13]. DRS is a technology for enhancing image resolution, trained on both low-resolution and high-resolution datasets [13]. In addition, DRG can be used independently, and the denoising factor can be adjusted from 1 to 8. DRS can be toggled ON or OFF, but when DRS is ON, it must be used in conjunction with DRG.

2-4. Imaging Conditions

A 2D TSE sequence was used for imaging. The fixed imaging conditions are as follows:

- FOV: 160 mm, Slice thickness: 2.0 mm, Number of slices: 15, Flip angle: 150°, Average (AVE): 2, Interpolate: ON
- T_1WI: TR/TE = 520 ms/9.5 ms, Base matrix: 256 × 256, Bandwidth: 391 Hz/pixel, Voxel size: 0.31 × 0.31 × 2 mm
- T_2WI: TR/TE = 3600 ms/86 ms, Base matrix: 320 × 320, Bandwidth: 260 Hz/pixel, Voxel size: 0.25 × 0.25 × 2 mm

Imaging conditions were modified according to each evaluation item. From this point onward, both T_1WI and T_2WI with AVE: 2 and DLR: OFF were defined as the conventional conditions. Furthermore, the scan times were as follows: [AVE1] T_1WI: 1 min 37 sec, T_2WI: 1 min 28 sec; [AVE2] T_1WI: 3 min 12 sec, T_2WI: 2 min 51 sec; [AVE3] T_1WI: 4 min 46 sec, T_2WI: 4 min 14 sec.

3. Methods

3-1. Image Quality Evaluation with DR

Signal-to-noise ratio (SNR) was measured to evaluate the image quality of DRG, while mean amplitude was used to assess the spatial resolution of DRS. All scans were performed five times, and the average value was calculated.

3-1-1. SNR Evaluation

The bottle phantom provided with the MRI system was used. The imaging conditions for T_2WI were modified by varying AVE from 1 to 3 and the denoising strength of DRG from 1 to

8. Therefore, SNR was calculated using the subtraction method based on Equation (1) and compared. The imaging plane was set to axial. In calculating SNR, a circular region of interest (ROI) covering 75% of the imaging plane was set, and the signal value and standard deviation (SD) were measured.

$$SNR = \frac{SI_{ave}\sqrt{2}}{SD_{sub}} \quad \cdots (1)$$

SI_{ave}: The average signal value of the ROI in two scans, SD_{sub}: The standard deviation of the subtraction image.

Statistical analysis was performed using Modified R Commander 4.3.1 [14], and Dunnett's multiple comparison test was conducted. The significance level was set at 95% ($p < 0.05$).

3-1-2. Spatial Resolution Evaluation

A profile curve was obtained from the 1 mm pin-pattern section of the 90-401 MRI phantom. The amplitude of the profile curve represents the contrast response of the 1 mm pin-pattern section and indicates the spatial resolution at a frequency of 0.125 cycles/mm [15]. Thus, spatial resolution was comparatively evaluated based on the profile curve and its amplitude [15]. Imaging was performed with the base matrix varied at 224, 240, 256, 272, 288, 304, and 320, and comparisons were made between DRS ON and OFF. The profile curve was measured using ImageJ. The amplitude was calculated as the difference between the average of four maximum values and the average of five minimum values, and then normalized by the average value of the phantom background.

3-2. Objective Evaluation

The bottle phantom was scanned using T_1WI and T_2WI. As imaging conditions, conventional conditions (AVE2) and experimental conditions (AVE1) were set, with the denoising strength varied from 1 to 8 in the experimental conditions. All scans were performed five times, and the average value was calculated. Peak Signal-to-Noise Ratio (PSNR) and Structural Similarity (SSIM) were calculated based on the conventional conditions to compare the image quality of both methods.

PSNR is defined by Equation (2) and is a mathematical measure of image quality based on the pixel differences between two images [16].

$$PSNR = 10\,log\,\frac{L^2}{MSE} \quad \cdots (2)$$

PSNR equals SNR when all pixel values are equal to the maximum possible pixel value. L represents the maximum possible pixel value, which is 255 for an 8-bit image. Mean Squared Error (MSE) is defined as the average of the squared differences in pixel intensity between two images. A higher PSNR value indicates less degradation [17-18].

Furthermore, SSIM is considered an objective metric that aligns more closely with human visual perception and is defined by Equation (3) [19].

$$SSIM(x,y) = \frac{(2\mu_x\mu_y+C_1)(2\sigma_{xy}+C_2)}{(\mu_x^2+\mu_y^2+C_1)(\sigma_x^2+\sigma_y^2+C_2)} \quad \cdots (3)$$

Here, μ_x and μ_y represent the average pixel values, σ_x and σ_y denote the standard deviation of the images, and σ_{xy} is the covariance of the images. C_1 and C_2 are correction factors calculated using the following equations.

$$C_1 = (K_1L)^2, \quad C_2 = (K_2L)^2$$

In this study, SSIM was calculated using K_1 = 0.01 and K_2 = 0.03, as determined from previous literature [19]. SSIM takes values ranging from 0 to 1. Statistical analysis was performed using Modified R Commander 4.3.1 [14], and the Steel-Dwass multiple comparison test was conducted. The significance level was set at 95% ($p<0.05$).

3-3. Visual Evaluation Using Images from Healthy Volunteers

T_1WI and T_2WI were acquired from healthy volunteers who provided informed consent

under both conventional and experimental conditions. The conventional condition was set to AVE2 with DR OFF, while the experimental condition was set to AVE1 with denoising strength 8 and DRS ON. Visual evaluation was performed for each image by one radiologist (27 years of experience) and two radiological technologists (22 and 15 years of experience).

The evaluation items included the visibility of the pituitary structure (anterior pituitary lobe, optic chiasm, and pituitary stalk) and image noise. Subjective evaluation was performed using the following five-point scale.

Visibility of the structure: 5. The signal is uniform, and the contour is clear. 4. The signal is slightly uneven, and the contour is slightly blurred. 3. The structure is visible, but some parts are unclear. 2. The overall image is blurred or almost invisible. 1. The structure is not identifiable.

Image noise: 5. Almost no noise. 4. Inconspicuous noise. 3. Noise is present but acceptable. 2. Noticeable noise, but diagnosis is still possible. 1. Unacceptable noise.

All statistical analyses were performed using Modified R Commander 4.3.1 [14]. Image evaluation between DLR ON and OFF was compared using the Wilcoxon test, and inter-rater agreement was calculated using Fleiss' kappa coefficient. For both tests, the significance level was set at 95% ($p < 0.05$).

4. Results

4-1. SNR Evaluation

The relationship between AVE, denoising strength, and SNR is shown in Fig. 1. The relationship between SNR and the imaging conditions — AVE2 with DRG OFF (conventional) and AVE1 with DRG OFF to 8 — is shown in Fig. 2. An increase in the denoising strength of DRG resulted in a corresponding increase in SNR. For all AVE settings, a denoising strength of 8 yielded the highest SNR. Furthermore, compared to the conventional condition (AVE2 with DRG OFF), AVE1 with a denoising strength of 6 or higher showed a significantly higher SNR.

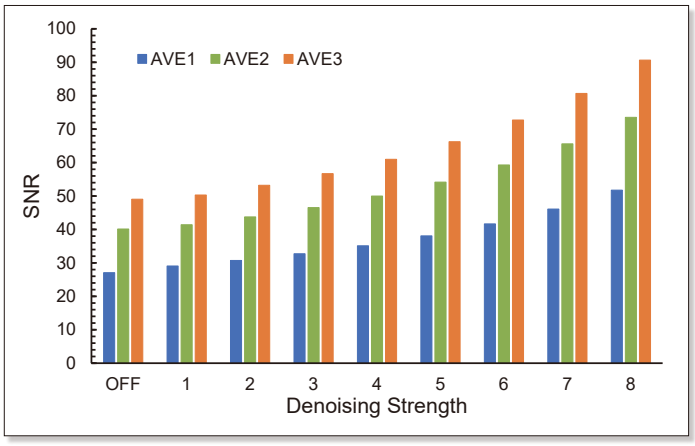

Fig. 1 SNR with varying denoising strength and number of AVE.

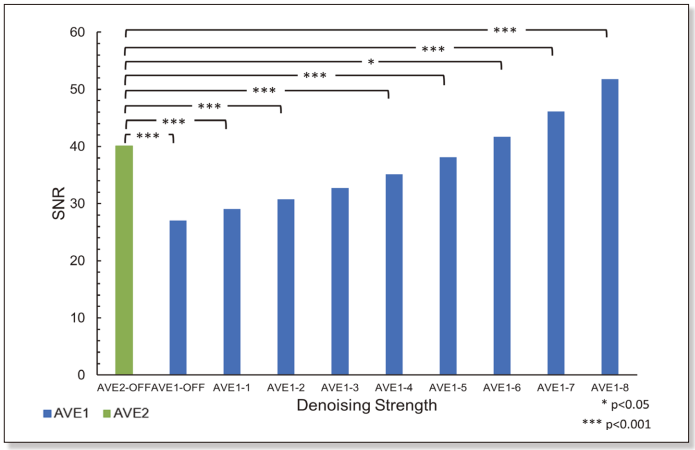

Fig. 2 SNR under conventional conditions (AVE2, DRG OFF) and AVE1 with DRG OFF to 8.

4-2. Spatial Resolution Evaluation

The profile curves with varying base matrix sizes are shown in Fig. 3, and the relationship between DRS and mean amplitude is shown in Fig. 4. For matrix size 224, the mean amplitude was calculated using the identifiable maximum and minimum values, as the profile curve with DRS OFF could not be clearly distinguished. In

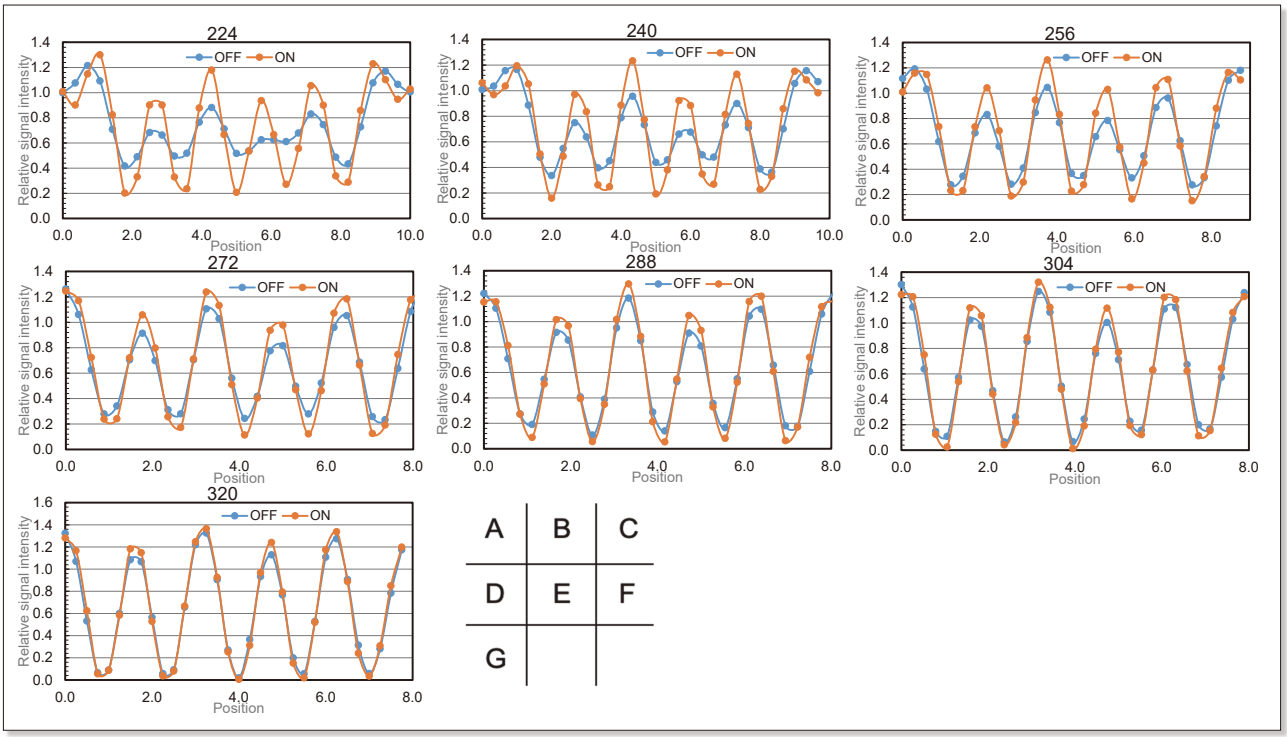

Fig. 3 Profile curves with DRS ON and OFF (A: matrix 224 × 224, B: 240 × 240, C: 256 × 256, D: 272 × 272, E: 288 × 288, F: 304 × 304, G: 320 × 320).

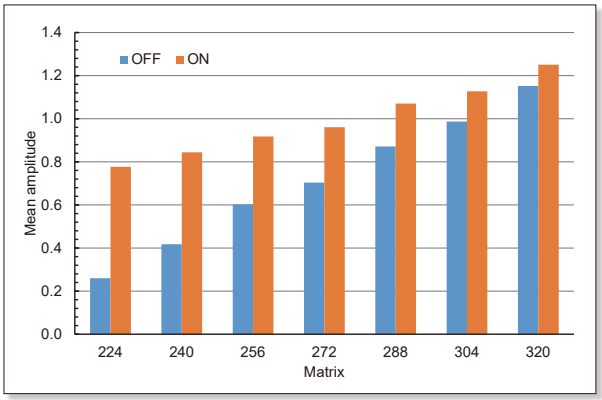

Fig. 4 Mean amplitude with varying base matrix.

all matrix sizes, enabling DRS ON increased the mean amplitude. However, the increase rate of mean amplitude when switching from DRS OFF to ON was as follows: 224: 199%, 240: 102%, 256: 52%, 272: 37%, 288: 23%, 304: 14%, and 320: 9%. As the matrix size increased, the improvement rate of mean amplitude decreased, indicating that the effect of DRS ON on the profile curve diminished. The mean amplitude was approximately equal between base matrix 288 with DRS OFF and base matrix 240 with DRS ON. Moreover, the mean amplitude for base matrix 224 with DRS ON was higher than that for base matrix 272 with DRS OFF.

4-3. Objective Evaluation of Image Quality

The calculated PSNR and SSIM are shown in Fig. 5 and Fig. 6. Furthermore, the Steel-Dwass multiple comparison test showed significant differences between groups with different symbols ($p < 0.05$). PSNR increased with higher denoising strength; however, no significant differences were observed in T_1WI. In T_2WI, PSNR was highest at denoising strength 8 and was significantly higher than those at strengths 1 through 5. The overall average PSNR was 29.94 dB for T_1WI and 27.45 dB for T_2WI, with T_1WI showing a higher value than T_2WI.

Similarly, SSIM increased with higher denoising strength. The highest SSIM value was observed at denoising strength 8 for both T_1WI and T_2WI, and it was significantly higher than those at strengths 1 through 6. The overall average SSIM was 0.92 for T_1WI and 0.78 for T_2WI, with T_1WI showing a higher value, similar to the PSNR results.

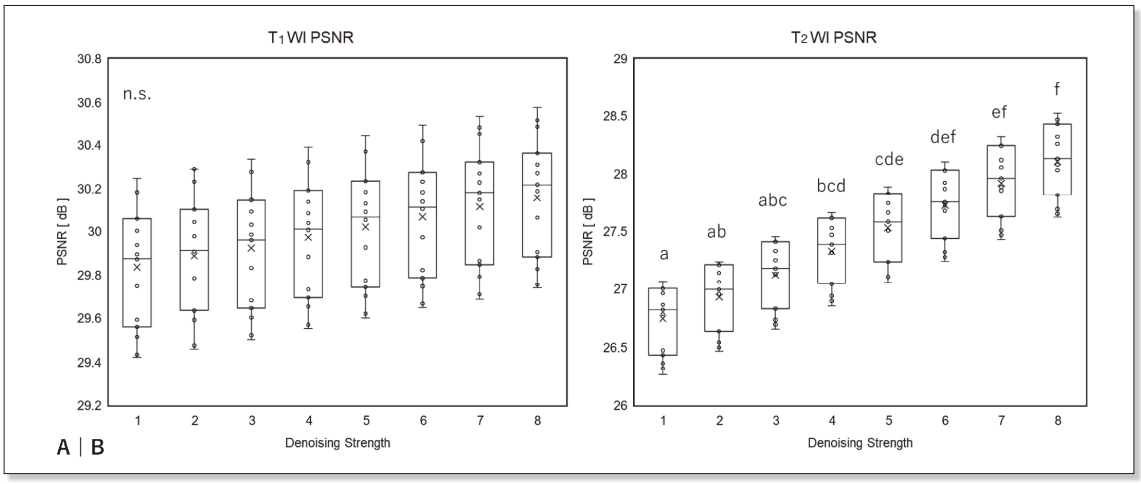

Fig. 5 PSNR with DLR ON and OFF for varying denoising strengths (A: T_1WI, B: T_2WI). Significant differences were observed between groups with different symbols ($p < 0.05$).

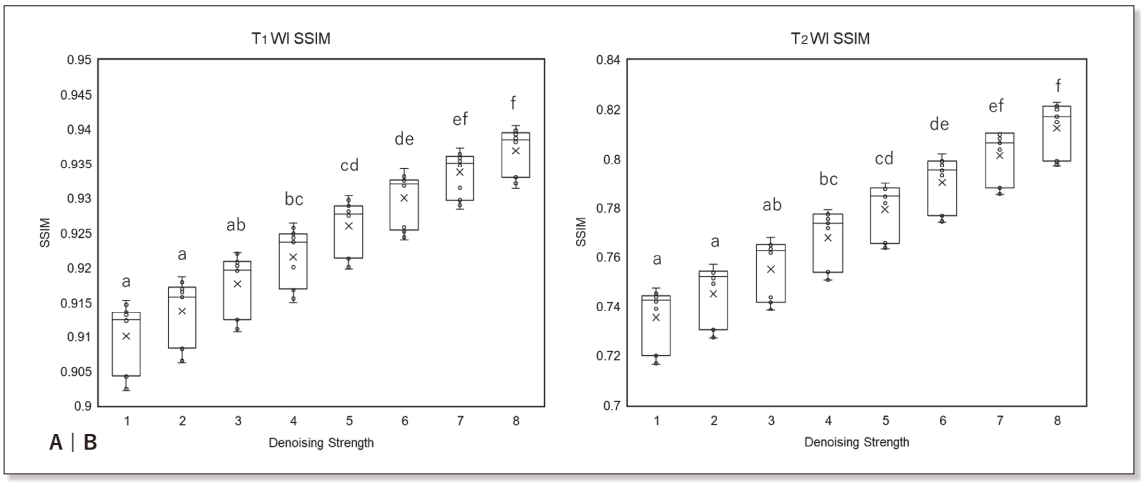

Fig. 6 SSIM with DLR ON and OFF for varying denoising strengths (A: T_1WI, B: T_2WI). Significant differences were observed between groups with different symbols ($p < 0.05$).

4-4. Visual Evaluation Using Images from Healthy Volunteers

The results of the visual evaluation of the pituitary in healthy volunteers under AVE2 with DLR OFF and AVE1 with DLR ON are shown in Table 1. An example of the images used for evaluation is shown in Fig. 7. As a result of the kappa analysis, the inter-rater agreement scores for structural visibility were 0.564 for the anterior pituitary lobe, 0.442 for the optic chiasm, and 0.335 for the pituitary stalk. The score for image noise was 0.393. For the anterior pituitary lobe and image noise, there were no significant differences in scores between DLR ON and OFF for Readers 1 and 3 in both T_1WI and T_2WI, while Reader 2 showed significantly lower scores with DLR ON. For the pituitary stalk and optic chiasm, the evaluations differed between T_1WI and T_2WI. In T_1WI, all evaluators gave equal or lower scores with DLR ON compared to DLR OFF. However, in T_2WI, higher scores were obtained with DLR ON for the pituitary stalk by Readers 1 and 3, and for the optic chiasm by Reader 2.

5. Discussion

In this study, we hypothesized that the use of DLR in pituitary MRI examinations could enable scan time reduction while maintaining conventional image quality. Thus, we investigated the impact of DR on MRI image quality

Table 1 Result of visual evaluation and Wilcoxon rank-sign sum test for T_1WI and T_2WI with DLR ON/OFF in three readers.

	Anterior Pituitary	Pituitary Stalk	Optic Chiasm	Noise
Reader1				
T_1WI (mean ± SD)	4.69 ± 0.46	3.81 ± 0.81	3.38 ± 0.60	3.63 ± 0.60
T_1WI DLR (mean ± SD)	4.44 ± 0.50	3.56 ± 0.70	2.88 ± 0.60	3.44 ± 0.50
p-value	n.s	n.s	n.s	n.s
T_2WI (mean ± SD)	4.94 ± 0.24	4.00 ± 0.79	5.00 ± 0.00	4.00 ± 0.35
T_2WI DLR (mean ± SD)	4.88 ± 0.33	4.56 ± 0.50	5.00 ± 0.00	3.94 ± 0.24
p-value	n.s	n.s	n.s	n.s
Reader2				
T_1WI (mean ± SD)	4.50 ± 0.61	4.94 ± 0.24	4.81 ± 0.39	4.19 ± 0.39
T_1WI DLR (mean ± SD)	4.25 ± 0.43	4.75 ± 0.43	4.50 ± 0.61	3.69 ± 0.46
p-value	n.s	n.s	n.s	0.0156
T_2WI (mean ± SD)	4.75 ± 0.43	4.63 ± 0.78	4.81 ± 0.39	4.69 ± 0.46
T_2WI DLR (mean ± SD)	4.44 ± 0.48	4.19 ± 0.60	4.94 ± 0.43	3.13 ± 0.66
p-value	0.0312	n.s	n.s	0.0273
Reader3				
T_1WI (mean ± SD)	4.56 ± 0.50	3.81 ± 0.81	3.81 ± 0.73	3.50 ± 0.50
T_1WI DLR (mean ± SD)	4.00 ± 0.61	3.50 ± 0.87	3.81 ± 0.88	3.50 ± 0.61
p-value	0.0312	n.s	n.s	n.s
T_2WI (mean ± SD)	4.88 ± 0.33	3.75 ± 0.75	5.00 ± 0.00	3.94 ± 0.43
T_2WI DLR (mean ± SD)	4.75 ± 0.43	3.94 ± 0.56	4.94 ± 0.24	3.75 ± 0.43
p-value	n.s	n.s	n.s	n.s

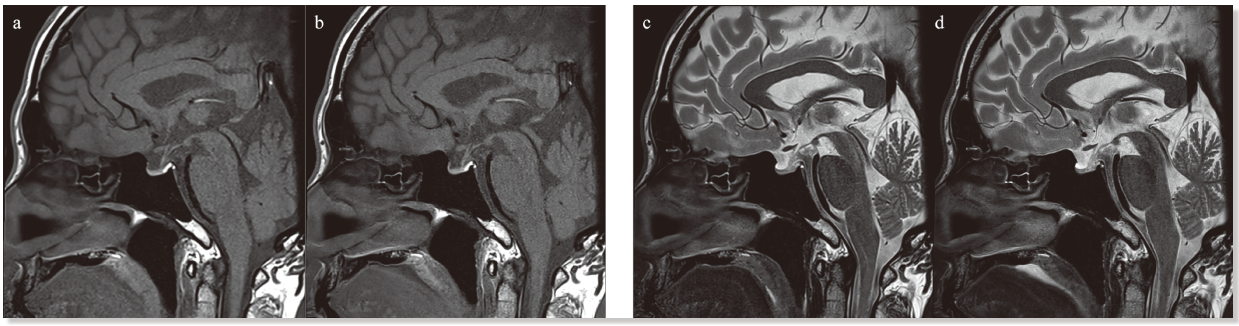

Fig. 7 Representative MR images from a 51-year-old healthy male volunteer.

(a) T_1WI without DLR, (b) T_1WI with DLR, (c) T_2WI without DLR, (d) T_2WI with DLR. For the optic chiasm, all readers gave a score of 5 on T_2WI (c, d). On T_1WI, one reader gave a score of 5 and two readers gave a score of 4 for image (a), while two readers gave a score of 5 and one reader gave a score of 4 for image (b).

through phantom experiments and evaluated the image quality of accelerated pituitary imaging using DR in healthy volunteers.

In the SNR evaluation using phantom experiments, significantly higher SNR values were obtained under the conditions of AVE1 with a denoising strength of 6 or higher compared to the conventional setting (AVE2 with DRG OFF). Thus, the use of DLR may allow for equal or higher SNR compared to conventional settings, even when the number of AVE is reduced.

Similarly, in the spatial resolution evaluation using phantom experiments, the mean amplitude increased with the use of DRS. Based on the results, the mean amplitude was approximately equal between base matrix 288 with DRS OFF and base matrix 240 with DRS ON. The mean amplitude with base matrix 224 and DRS ON was higher than that with base matrix 272 and DRS OFF. Even with base matrix 224

and 240, mean amplitude values equivalent to those of base matrix 272 and 288 were obtained. Thus, the use of DRS suggests an improvement in spatial resolution, and comparable or even higher spatial resolution may be achieved even with a reduced base matrix.

In the objective evaluation using phantom experiments, PSNR and SSIM values were lower for T_2WI than for T_1WI. This suggests image quality degradation and decreased similarity in T_2WI due to the reduced number of AVE. PSNR is an indicator where higher values indicate less image degradation, with typical values ranging from 30 to 50 dB in lossy compressed images [17-18]. Furthermore, SSIM is an indicator where values closer to 1 indicate higher similarity to the reference image, with values above 0.90 generally considered the standard threshold [18-19]. The average PSNR across denoising strengths 1 to 8 was 29.94 dB for T_1WI and 27.45 dB for T_2WI. The average SSIM over the same range was 0.92 for T_1WI and 0.78 for T_2WI. These results indicate that T_2WI showed greater image degradation and lower similarity compared to T_1WI. Thus, in objective evaluation, reducing the number of AVE in T_1WI was considered to have minimal impact on image degradation and similarity due to the effect of DLR. In contrast, the lower average PSNR and SSIM values in T_2WI indicated image quality degradation and decreased similarity. However, increasing the denoising strength resulted in higher PSNR and SSIM values in both T_1WI and T_2WI, suggesting that DRG is effective in reducing image degradation and improving similarity. Therefore, in both T_1WI and T_2WI, using a high denoising strength when the number of AVE is reduced may allow image quality comparable to that of conventional conditions to be achieved.

In the visual evaluation of the pituitary in healthy volunteers, DLR ON resulted in significantly lower scores for the anterior pituitary lobe and image noise as assessed by Reader 2. This is likely due to the reduced number of AVE, which diminished the artifact-suppression effects provided by signal summation and noise smoothing [20]. Furthermore, a potential disadvantage of using DRS is that it may accentuate artifacts. The pituitary structure is located near the center of the field of view, and flow artifacts overlapping the structure reduce image contrast. These artifacts may have been accentuated by DRS, resulting in increased image noise and lower scores for the anterior pituitary lobe and image noise. However, no significant differences were observed among all evaluators for the optic chiasm and pituitary stalk, and increased scores with DLR ON were observed in T_2WI. This is likely because, in anatomically well-defined structures with clear edges, the impact of artifacts was reduced by DRG, allowing the benefits of improved spatial resolution provided by DRS to be realized. Based on the above, DLR may help maintain or improve the visibility of the optic chiasm and pituitary stalk. Furthermore, since the reduction in visibility of the anterior pituitary lobe was minimal, the reduction in the number of AVE may have been adequately compensated for by DLR.

In this study, phantom experiments demonstrated that using DRG with a denoising strength 6 or higher, along with DRS ON, resulted in SNR and spatial resolution exceeding those of the conventional condition, even when the number of AVE was reduced. In the visual evaluation, DLR was suggested to help maintain visibility. These findings suggest that DLR may enable the maintenance of image quality while reducing scan time by approximately 50% in pituitary imaging.

6. Conclusion

In this study, we hypothesized that DLR could reduce scan time while maintaining image quality, and conducted an image quality evaluation. In the phantom experiments, the increase in noise due to the reduced number

of AVE was considered to be compensable by DLR. However, in the objective evaluation, decreases in PSNR and SSIM were observed. On the other hand, the use of high denoising strength led to improved similarity, and the results of the visual evaluation suggested that DLR helped maintain visibility. Taken together, these findings suggest that reducing the number of AVE to shorten scan time while compensating for the resulting image degradation with DLR may be an effective approach. This study investigated 2D TSE. The scan times under baseline conditions were 3 minutes 12 seconds for T_1WI and 2 minutes 51 seconds for T_2WI, while under DLR-based experimental conditions, they were 1 minute 37 seconds for T_1WI and 1 minute 28 seconds for T_2WI. Thus, in this study, it is considered that DLR enables approximately a 50% reduction in scan time for pituitary MRI examinations. Furthermore, the results of the visual evaluation indicated that image quality was affected by physiological factors. Therefore, future studies should examine imaging conditions that also consider the impact of artifacts by using clinical images.

Conflict of Interest

The authors declare no conflicts of interest related to this study.

References

1) R. L. GUY, et al.: A comparison of CT and MRI in the Assessment of the Pituitary and Parasellar Region. Clinical Radiology, 43, 156-161, 1991.
2) Louis J. Kim, et al.: Preliminary Experience with 3-Tesla MRI and Cushing's Disease. Skull Base, 17, 273-277, 2007.
3) Marco Varrassi, et al.: High-resolution magnetic resonance imaging at 3T of pituitary gland: advantages and pitfalls. Gland Surgery, 8, 208-215, 2019.
4) Hisato Nakazawa, et al.: Efficacy of magnetic resonance imaging at 3T compared with 1.5T in small pituitary tumors for stereotactic radiosurgery planning. Jpn J Radiol, 32, 22-29, 2014.
5) David B. Stobo, et al.: Initial experience of 3 Tesla versus conventional field strength magnetic resonance imaging of small functioning pituitary tumours. Clinical Endocrinology, 75, 673-677, 2011.
6) K. Pinker, et al.: The value of high-field MRI (3T) in the assessment of sellar lesions. Europian Journal of Radiolory, 54, 327-334, 2005.
7) Kai Zhang, et al.: Beyond a Gaussian Denoiser: Residual Learning of Deep CNN for Image Denoising. IEEE Trans Image Process, 26(7), 3142-3155, 2017.
8) Kaiming He, et al.: Deep Residual Learning for Image Recognition. IEEE in CVPR, 770-778, 2016.
9) Chang Min Hyun, et al.: Deep learning for undersampled MRI reconstruction. Phys.Med.Biol, 63, 135007 (15pp), 2018.
10) Masafumi Kidoh, et al.: Deep Learning Based Noise Reduction for Brain MR imaging: Tests on Phantoms and Healthy Volunteers. Magn Reson Med Sci, 19, 195-206, 2019.
11) Hiroyuki Akai, et al.: Commercially Available Deep-learning-reconstruction of MR Imaging of the Knee at 1.5T Has Higher Image Quality Than Conventionally-reconstructed Imaging at 3T: A Normal Volunteer Study. Magn Reson Med Sci, 22, 353-360, 2023.
12) R. Marc Label: Performance characterization of a novel deep learning-based MR image reconstruction pipeline. arXiv.06559, 2008.
13) Nicolas Behl.: Deep Resolve – Mobilizing the Power of Networks. MAGNETOM Flash, 78, 1-6, 2021.
14) Eiki Tsushima.: Modified R Commander 4.3.1. https://home.hirosaki-u.ac.jp/pteiki/r/ (Accessed 2025-03-30).
15) Kazunori YAMAKOSHI, et al.: High Spatial Resolution Head and Neck 2-point DIXON Method 3D-GRE Imaging at 3T. Japanese Journal of Magnetic Resonance in Medicine, 36(2), 73-84, 2016.
16) Yusra A, et al.: Comparison of Image Quality Assessment: PSNR, HVS, SSIM, UIQI. International Journal of Scientific & Engineering Research, 3(8), 2012.
17) Anitha S, et al.: Quality Assessment of Resultant Images after Processing. Computer Engineering and Intelligent Systems, 3(7), 105-112, 2012.
18) Masahiko Kobako.: Toward Standardization – Standardization Committee Report (3): Image Compression Guidelines for Digitized Documents. Journal of image & information management 50(5), 21-24, 2011.
19) Zhou Wang, et al.: Image Quality Assessment: From Error Visibility to Structural Similarity. IEEE transactions on image processing, 13(4), 2004.
20) Masaki Terada, et al.: Examination of Upper Abdominal Region in High Spatial Resolution Diffusion- weighted Imaging Using 3-Tesla MRI. Japanese Journal of Radiological Technology, 65(3), 312-322, 2009.

Received September 25, 2022; accepted November 1, 2023

Efforts to promote patient safety in pediatric sedation MRI examinations:The role of radiological technologists

SAITO Tomomi[1)]*, NAGAHAMA Koei[1)], TANAHASHI Yosuke[1)], MURA Miwa[1)], KURAHASHI Sena[1)], OKADA Shuhei[1)], ITO Sadanori[1)], TERASHITA Shintaro[2)]

1) Department of Radiology, Toyama University Hospital
2) Department of Pediatrics, Toyama University School of Medicine

* E-mail: r062012@med.u-toyama.ac.jp

Note: This paper is secondary publication, the first paper was published in the JART, vol. 71 no. 857: 20-25, 2024.

Key words: MRI, pediatric, sedation, patient safety, interprofessional collaboration

【Abstract】
Pediatric patients are often unable to remain still during Magnetic resonance imaging (MRI) examinations, and sedation is often warranted. However, guidelines for pediatric sedation examinations were unclear. Using "Recommendations on pediatric sedation for MRI examination," we evaluated and reviewed the current system in our hospital. The results revealed that the equipment and emergency medical system in the MRI examination room were inadequate. Radiological technologists must take responsibility for ensuring that the equipment provides safe examinations and for safety management during MRI examinations, including emergencies. Emergency simulation-based learning with various professional staff will lead to the creation of a consensus for enhancing patient safety during sedation through interprofessional collaboration, and it is hoped that this will continue.

1. Introduction

MRI developed rapidly in the late 1980s. Today, computed tomography (CT) and MRI are responsible for most diagnostic imaging. MRI is widely employed in pediatric patients because it has no radiation exposure and superior contrast resolution compared with CT. However, pediatric patients are often unable to remain still during MRI examinations and sedation is often warranted. A 2010 survey conducted by the Medical Safety Committee of the Japan Pediatric Society on the management of sedation in pediatric patients undergoing MRI examinations revealed that 147 of 416 facilities (35%) experienced adverse events, some of which were serious complications such as cardiac or respiratory arrest [1)]. Against this background, the Japan Pediatric Society, the Japanese Society of Pediatric Anesthesiology, and the Japanese Society of Pediatric Radiology published "Recommendations on Pediatric Sedation for MRI Examination" (hereinafter referred to as the "The Recommendations") in May 2013 and proposed standards to render sedation for MRI examinations in pediatric patients safer. The revised edition was published in February 2020 and more emphasis was placed on safety management during MRI examinations, such as patient monitoring and emergency backup. Alternatives to sedation have been presented [2)].

Our hospital is a core pediatric hospital with 28 of the 612 beds in the pediatric ward. It provides treatment for a wide range of pediatric conditions, including neurological diseases, malignant tumors, hematological diseases, cardiovascular diseases, and premature infants and newborns. Approximately 300 MRI examinations are conducted annually for pediatric patients under 10 years of age, with approximately 200 examinations requiring sedation. These patients may be outpatients, inpatients, or newborns admitted to the neonatal intensive care unit. The method of sedation also

Table 1 Special environment for MRI examinations

1. Normal medical equipment cannot be brought into the MRI examination room due to the strong magnetic field.
2. The gantry structure of the MRI machine makes it difficult to monitor the patient.
3. The gantry structure of the MRI machine makes it difficult to access the airway.
4. It is difficult to monitor the patient because the MRI examination room is dim.
5. Deep sedation is warranted during the examination due to the long period of immobility and noise.
6. Physicians are held for long periods of time for MRI examinations.
7. Lack of staff with pediatric expertise during the MRI examination.

varies from patient to patient. For example, some patients may visit the MRI examination room after being sedated orally, whereas others may be administered intravenously after entering the MRI examination room. Pediatric sedation during MRI examinations is a procedure in a special environment with various possible risks [3] (Table 1); therefore, we believe it is necessary for healthcare professionals involved in MRI examinations to acquire knowledge to perform safe examinations. The examination procedure and response to sudden changes in a patient should be clarified and shared among various professionals. However, the radiological technologists and nurses in charge of MRI at our hospital are rotators who are also in charge of other departments; therefore, many lack knowledge and experience in pediatric sedation and are anxious about it. Although pediatric sedation MRI examinations are treated as special examinations with limited appointment times, the actual examination procedure is left to the physician in charge at the time because sedation is conducted by the pediatric outpatient physician on duty, which changes daily.

In this study, we evaluated and reviewed the current system based on The Recommendations to perform safer pediatric sedation MRI examinations. Furthermore, we conducted a joint interprofessional training seminar on pediatric sedation MRI examinations to unify and improve safety management awareness.

2. Method

2-1. Evaluation and review based on The Recommendations

Using The Recommendations, we evaluated the achievement of the recommended items in our current system when performing pediatric MRI examinations under sedation. The evaluation sheet accompanying The Recommendations [2] was used for evaluation. The items for the test-ordering physician, sedation physician, and person dedicated to patient monitoring were evaluated by a pediatrician, whereas the items for the facility concerned were evaluated by a pediatrician and a radiological technologist. The recommendation level was divided into three levels: (A) must, (B) strongly recommended, and (C) desired. Pediatricians and radiological technologists shared items judged as unachievable on the evaluation sheet and reviewed the current system.

2-2. Training seminar

Pediatricians provided lectures on pediatric sedation to radiological technologists and nurses. After collecting opinions from radiological technologists and nurses on anxieties and questions about pediatric sedation MRI examinations in advance, the lecture included the content of these opinions.

On the same day, we performed a simulation of a sudden change in a patient during a pediatric sedation MRI examination (hereafter referred to as “simulation”). The goal was to be able to respond to a patient in case of a sud-

Table 2 Simulation scenarios

	Case1	Case2
Patient	7-year-old boy	3-year-old boy
Region	Brain	Brain
Purpose	Epilepsy	Brain tumor
Sedative type	Thiopental sodium intravenous administration	Thiopental sodium intravenous administration
Situation	During positioning, SpO2 dropped, and breathing stopped.	1 minute into the examination, SpO2 dropped, and breathing stopped.

den change during the examination by dividing the roles among different professionals and collaborating with each other. The entire group was divided into two groups to ensure that all participants could role play. Each group was divided into the first and second halves to simulate the case 1 and case 2 scenarios, respectively (Table 2), which were grouped to ensure an even distribution of various professionals. Group members discussed and decided who would be responsible for which role. Each group was assigned two pediatricians, who acted as facilitators. Participants performed the simulation while checking their roles using a patient emergency response chart. The participants were debriefed after each scenario. Based on the results of a questionnaire answered by the participants after the training seminar, we evaluated their anxiety regarding pediatric sedation MRI examinations before and after the simulation on a 5-point scale (very anxious, slightly anxious, fair, not very anxious, and not at all anxious). The questionnaire also included an open-ended space for impressions and opinions regarding the training seminars. Informed consent for the questionnaire responses was documented and consent for the study was obtained by submitting the questionnaire.

3. Results

3-1. Evaluation and review based on The Recommendations

As a result of the evaluation, the number of the recommended items achieved in The Recommendations was 40/45 for recommendation level (A), 9/10 for recommendation level (B), and 5/7 for recommendation level (C).

Based on our review, we improved and achieved the following three items at the recommendation level (A). 1) "To record the details of monitoring during sedation on the recording form"; this was achieved by revising the existing recording form used in the pediatric department for sedation MRI examinations. 2) "Assigning personnel to respond to emergencies and sharing the emergency medical system among them," we performed a simulation and shared it among various professionals. 3) "To develop procedures, such as where to place items used in emergencies," we did a simulation and developed a manual.

Prior to the simulation, we reviewed existing patient emergency response charts and created a new chart for pediatric sedation. In the existing response chart, the radiological technologist in charge of the examination confirmed the sudden change in the patient, rings the call buzzer to request assistance, and transports the patient to the treatment room, accompanied by assembled nurses and radiologists. Emergency treatment was performed in the treatment room using an emergency cart. The assistant radiological technologist requests Code Blue, the hospital's emergency broadcast, contacts the attending physician, and guides the emergency department physicians. The changes are as follows: [1] The pediatrician is present from the beginning of the examination and monitors

the patient's condition so that the pediatrician and radiological technologist confirm the sudden change concurrently; [2] use a pediatric emergency box brought by the pediatrician, not an emergency cart; and [3] as a first option, request assistance from the backup pediatrician, not a Code Blue (Fig. 1).

The two items of recommendation level (A) that have not been achieved or will be achieved in the future are as follows: 1) "To establish in advance a backup system for times when human resources are stretched thin (nights and holidays)," and (2) "When the MRI machine is updated, monitor cameras from two or more directions and a multi-functional monitor including an MRI-safe capnometer should be equipped." The items that have not been achieved or that will not be improved soon are as follows: recommendation level (B) "To prepare MRI-safe capnometers," recommendation level (C) "To prepare MRI-safe automatic blood pressure monitors and ECG monitors for patients who need them," and "To place a monitoring area until awakening in locations that are easily accessible from the MRI examination room and located near the examination room."

Recommendation level (A) "To establish in advance a backup system for times when human resources are stretched thin (nights and holidays)," which was judged to be not achieved at the time of evaluation, was subsequently achieved with the new operation of the Pediatric Code Blue. It was decided that the emergency department physicians would assemble with a pediatric response set.

Thus, 44/45 items in recommendation level (A), 4 items improved, while 9/10 items in recommendation level (B) and 5/7 items in recommendation level (C) were finally achieved (Fig. 2).

3-2. Training seminar

Eight pediatricians (including senior pediatric residents), nine radiological technologists, and 12 nurses from the radiology department participated in the training seminar. Some radiological technologists and nurses are in charge of MRI examinations during both the day and night shifts, while others are in charge only during the night shift. However, because pediatric sedation MRI examinations are conducted infrequently during the night shift, some staff have no prior experience of pediatric sedation MRI examinations. Four pediatricians participated as facilitators in the training seminars.

<table>
<tr><th>The radiological technologist in charge of the examination</th><th>The nurse in the MRI room</th><th>The nurse in the treatment room</th><th>The pediatrician</th><th>The assistant radiological technologist</th></tr>
<tr><td>Confirm the sudden change in the patient.</td><td rowspan="2"></td><td rowspan="2"></td><td>Confirm the sudden change in the patient.</td><td></td></tr>
<tr><td rowspan="2">Communicate the sudden change in the patient.
Ring the call buzzer to request assistance.
Remove the coil.</td><td rowspan="2">Examine the patient.</td><td rowspan="2">Turn off the call buzzer.
Request assistance from nurses.</td></tr>
<tr><td>Assemble for assistance.</td><td>Detect the sudden change in the patient.</td></tr>
<tr><td>Prepare for transfer to MRI-safe stretcher.</td><td>Assist the pediatrician.</td><td>Prepare the treatment room.
Move waiting patients.</td><td>Request assistance from the backup pediatrician as needed.</td><td>MRI-safe stretcher into the examination room.</td></tr>
<tr><td rowspan="2">Transport the patient to the treatment room.
Close the examination room.</td><td rowspan="2">Transport the patient to the treatment room.</td><td rowspan="2">Transport the patient to the treatment room.</td><td rowspan="2">Transport the patient to the treatment room.</td><td>Contact the backup pediatrician if requested by the pediatrician.</td></tr>
<tr><td>Contact the emergency department for assistance as needed.</td></tr>
<tr><td>Prepare patient files.</td><td>Prepare the pediatric emergency box.</td><td>Prepare the biological information monitor.</td><td rowspan="2">Perform emergency treatment.</td><td rowspan="2">Guide the backup pediatricians and the emergency department physicians.
Guide other patients.</td></tr>
<tr><td colspan="2">Measure and record vitals.
Prepare oxygen and suction.</td></tr>
<tr><td>Communicate the situation to physicians.</td><td colspan="2">Assist physicians.</td><td>Communicate the patient's condition to the backup pediatricians and the emergency department physicians.</td></tr>
<tr><td colspan="5">Exit the patient from the treatment room.</td></tr>
<tr><td>Record the occurrence of the sudden change in the Radiology Information System.</td><td>Record the occurrence of the sudden change in the Hospital Information System.</td><td></td><td>Record the occurrence of the sudden change in the Hospital Information System.</td><td></td></tr>
</table>

Fig. 1 The patient emergency response chart during pediatric sedation MRI examinations
Bold text changed for pediatric sedation.

Recommendation level		Number of Items	Contents
A	Achieved	40	
	Review	4	1) To record the details of monitoring during sedation on the recording form 2) Assigning personnel to respond to emergencies and sharing the emergency medical system among them 3) To develop procedures, such as where to place items used in emergencies 4) To establish in advance a backup system for times when human resources are stretched thin (nights and holidays)
	Not achieved	1	1) When the MRI machine is updated, monitor cameras from two or more directions and a multi-functional monitor including an MRI-safe capnometer should be equipped
B	Achieved	9	
	Review	-	
	Not achieved	1	1) To prepare MRI-safe capnometers
C	Achieved	5	
	Review	-	
	Not achieved	2	1) To prepare MRI-safe automatic blood pressure monitors and ECG monitors for patients who need them 2) To place a monitoring area until awakening in locations that are easily accessible from the MRI examination room and located near the examination room

Fig. 2 Results of the evaluation and review of the current system in our hospital

Pediatricians provided lectures on the types and procedures of sedatives and the complications associated with sedation, including actual accidents, to acquire and share knowledge of pediatric sedation among the participants.

In the simulation-based learning, the emergency contact for the backup pediatrician was posted in each examination room, and the emergency contact system was shared among the participants. The location of the pediatric emergency box brought by the pediatrician was decided to be on the emergency cart in the center of the control room. The two items of recommendation level (A) were achieved. Using an actual examination room, each participant was able to play the role of a concrete image, and everyone could simulate the role while talking to each other. During the debriefing after the simulation, participants were able to comment freely on their impressions and opinions, regardless of their job position. The pediatricians reaffirmed the dimness of the examination room and the narrowness of the bore and commented that monitoring (visually) the movement of the thorax for early detection of hypoventilation in a sedated patient is not easy in this environment. Although monitor cameras from two directions were placed in the examination room for monitoring, the examination room did not contain a capnometer. As a remedial measure, we decided to use a pulse oximeter and a respiration cushion for respiratory synchronization accessory to the MRI machine, depending on the patient's unstable respiratory status and the position of the coil used (Fig. 3).

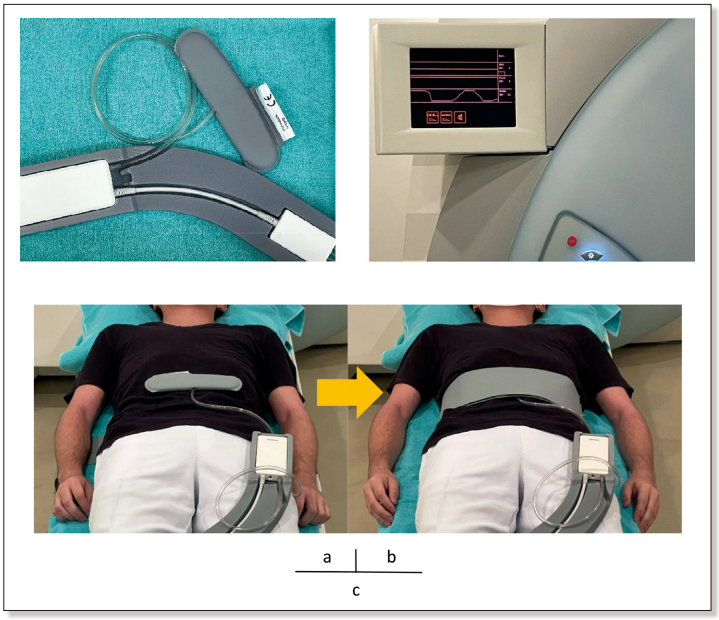

Fig. 3 Example of how to use the respiration cushion

a) The respiration cushion.
b) The respiratory pattern is displayed on a monitor in the MRI examination room.
c) The respiration cushion is placed in a location where there is a large movement due to breathing, and the belt is wrapped around the cushion.

Nurses commented on the need to secure flow lines for transporting patients in the sudden change, to prepare space for treatment, and to respond to parents.

In the questionnaire survey, 70% of the respondents were very anxious or slightly anxious before the simulation; however, this percentage decreased to 30% after the simulation. In the open-ended space, participants gave their impressions and opinions, such as "The simulation gave me a better image of what to expect in case of an emergency," "It was good to be able to confirm what I was anxious about," and "I hope the training seminar will be held regularly."

4. Discussion

The Recommendations are divided into three main phases: 1) Establishment of Management System: Chapter I "Explanation and Consent" and Chapter III "Backup System for Emergencies," 2) Advance Preparation: Chapter II "Patient Assessment" and Chapter IV "Restriction of Oral Intake Before Sedation," 3) Early Detection and Response to Abnormalities: Chapter V "Patient Monitoring," and Chapter VI "Care and Confirmation of Patient Awakening After the Examination." [4] Pre- and post- examination items are performed in pediatric outpatient and inpatient wards, and it is difficult for radiological technologists to be present; thus, pediatricians and nurses are inevitably tasked with these items. In pediatric sedation MRI examinations, what we radiological technologists can do as a team with interprofessional collaboration is to monitor the patient during the examination and respond to emergencies in case of abnormalities. Safety management during examinations is a more important item in the revised version. In the safety management of patients during examinations, we believe that radiological technologists should assist busy physicians with their tasks. The physician is responsible for the safety of the patient under sedation, and the radiological technologist is responsible for ensuring that the patient can safely undergo an examination in the MRI examination room.

Monitoring during the examination is described as monitoring oxygenation with a pulse oximeter and visual monitoring of the respiratory status (including visual monitoring of the monitor). In addition, monitoring end-tidal carbon dioxide tension with capnometers and monitoring with cameras from two or more directions is strongly recommended [2]. In this study, we decided to use a pulse oximeter and a respiration cushion as alternative measures because we did not have a capnometer. However, this is not the method recommended as an alternative in The Recommendations, but rather a rule within our hospital. For other hospitals, the results suggest that the purchase of expensive capnometers remains a hurdle, although there was a slight increase in 2016 to 84% and 7%, respectively [5], compared to 74% for pulse oximeters and 1% for capnometers in the 2010 survey [1]. In 2014, "Particular requirements for the safety of installations of magnetic resonance equipment for medical diagnosis," the Japanese Engineering Standards of Radiological Apparatus was revised requiring MRI equipment used to image pediatric patients to be equipped with monitor cameras to check respiration from two directions, the head side and the leg side [4]. In a 2016 survey, after the revision of safety requirements, only 34% of hospitals satisfied this requirement [5]. It is unrealistic to ask the hospital for a one-off request for major construction and budgets to provide the required equipment, and not all hospitals will respond immediately. Currently, MRI examination rooms are not designed for anesthesia, including sedation. The MRI system itself should be enhanced, and the environment should be safe for anesthesia from the design stage, including the layout, piping, monitoring system, sealing, and light dimming. The concept of "MRI for anesthesia" is desired to be

popularized [6]. We believe that the role of the radiological technologist is to explain the need for these considerations to the hospital at the time of MRI machine renewal or renovation. Radiological technologists are responsible for ensuring that patients can safely undergo examination in the MRI examination room; therefore, they should take the initiative to encourage hospitals to have the necessary equipment and supplies to provide safe examinations. The MRI building is scheduled to be renovated within 5 years at our hospital, and we hope to realize all the unachieved items: a multi-functional monitor including an MRI-safe capnometer, MRI-safe automatic blood pressure monitors, and ECG monitors, and an area for monitoring patients until awakening in the MRI building.

However, there were no clear rules or shared information among various professionals regarding the assignment and maintenance of personnel, supplies, and medicines in emergencies or the backup team. To create a consensus for improving sedation patient safety through interprofessional collaboration, it is effective to perform joint interprofessional training seminars in off-the-job locations, where there is no tension in clinical work [7], and we sought to make improvements by performing a joint interprofessional training seminar. Feedback and debriefing are important in simulation-based learning. Listening to various professional opinions not only deepens individual awareness but can also lead to an improvement in patient safety by recognizing and discussing common problems among various professionals [8]. From the radiological technologists' point of view, it was a great achievement to have a common recognition that the most important thing is to transport the patient out of the MRI examination room quickly in case of a sudden change. We are not allowed to bring normal medical equipment into the MRI examination room, which prevents us from providing adequate emergency treatment, and we must prevent secondary accidents caused by accidentally bringing metallic equipment into the examination room in the haste of a sudden change. Various professional roles must be shared to transport patients quickly from the examination room (to the treatment room). Radiological technologists in charge of safety control should strongly inform various professional staff that magnetic metal equipment is not allowed in the MRI examination room, owing to the strong magnetic field that is constantly generated. We hope that various professionals will acquire and share knowledge regarding the safe management of MRI examinations.

In this study, the training was conducted within the hospital; therefore, opinions and agreements were exchanged between acquaintances working in the same office. The Sedation Essence in Children Under Restricted Environment (SECURE) course provides the opportunity to gather information from other hospitals. The SECURE course is a hands-on course sponsored by the Medical Safety Committee of the Japan Pediatric Society and is open to physicians, nurses, and radiological technologists from a variety of hospital sizes. In addition to classroom lectures and roleplay, participants will hear specific measures of how other hospitals respond to sedation. Although we did not participate in this course, it will be held 14 times by 2022. We would like to participate in the SECURE course because it is an opportunity for us to hear how other hospitals are responding to the opinions raised in this study, such as alternative measures in the case of not having a capnometer and how to respond to parents in the case of a sudden change in a patient.

The results of the questionnaire after the training seminar suggested the need to continue the training seminar to further promote sedation patient safety and to create a consensus for improving sedation patient safety through interprofessional collaboration. We believe that

the participation of more professionals, such as emergency department physicians, nurses, and anesthesiologists, will be necessary in the future. In this study, pediatricians took the lead in lecturing, creating simulation scenarios, and acting as facilitators. We hope that training seminars will continue under the initiative of the physicians, nurses, and radiological technologists who participated in the SECURE course. It is easy to return the common awareness among various professionals gained through hands-on learning to clinical practice; therefore, we, radiological technologists, and various other professionals are expected to play a role as providers of pediatric sedation MRI examinations [7]. We believe that creating a consensus for improving sedation patient safety through interprofessional collaboration will be easier by having various professionals take on the role of the provider.

5. Conclusion

We evaluated and reviewed the current system based on The Recommendations with the purpose of providing safer pediatric sedation MRI examinations. Sharing knowledge about pediatric sedation and safety management of MRI examinations among various professionals and strengthening the collaboration system through simulation-based learning will lead to the creation of a consensus for improving sedation patient safety through interprofessional collaboration and is expected to promote patient safety.

I presented some parts of this paper at the 13th Academic Workshop for Radiological Technologists in three Prefectures in Hokuriku on March 7, 2021.

Conflict of Interest

The authors declare no conflicts of interest regarding this study.

References

1) Katsumori H, et al.: Survey on the management of sedation in pediatric patients undergoing MRI examinations. J Jpn Pediatr Soc, 117(7), 1167-1171, 2013.
2) the Japan Pediatric Society, the Japanese Society of Pediatric Anesthesiology, the Japanese Society of Pediatric Radiology published: Recommendations on Pediatric Sedation for MRI Examination. J Jpn Pediatr Soc, 124(4), 771-805, 2020.
3) Kusakawa I: Recommendations on pediatric sedation for MRI examinations: now & future. J Jpn Soc Pediatr Radiol, 33(2), 46-50, 2017.
4) Otake H: Anesthesiologist Perspective on "Recommendations on Pediatric Sedation for MRI Examination". The Journal of Pediatric Practice, 83(12), 1701-1706, 2020.
5) Yamanaka G, et al.: Current Status of Sedation during MRI Examination at Pediatric Specialty Training Facilities. J Jpn Pediatr Soc, 121(11), 1920-1929, 2017.
6) Kasuya S: Procedural Sedation and Analgesia for Children. Ped Cardiol Card Surg, 30(6), 612-623, 2014.
7) Komasawa N, et al.: Need for In-hospital Simulation-based Sedation Training Course: Significance of Interprofessional Training for Medical Safety Improvement. JJSCA, 39(2), 216-221, 2019.
8) Komasawa N, et al.: Significance of Medical Simulation Training for Improving Patient Safety in Critical Care. JJSCA, 34(2), 214-221, 2014.
9) Terashita S, et al.: Efforts to promote patient safety using recommendations on pediatric sedation for MRI examinations. J Jpn Pediatr Soc, 125(11), 1591-1597, 2021.

Received July 7, 2023 ; accepted December 12, 2023

Survey on Female radiological technologists Attitudes toward the Working Environment

NAKAMURA Masami[1)], NAKAI Yuichi[1), 2)], SAKIYAMA Kohshi[1)], OZAKI Michio[3)], SAI Shogo[2), 4)], SATO Hisaya[2), 5)], TAKAHASHI Toshiyuki[1), 2)], WATANABE Hiroyuki[2)], KATO Kyoichi[2), 6)]

1) Department of Radiological Technology, Showa University Northern Yokohama Hospital
2) Department of Radiological Medicine, Graduate School of Health Sciences, Faculty of Health Sciences, Showa University
3) Department of Radiological Technology, Showa University Hospital
4) Department of Radiological Technology, Showa University Koto-Toyosu Hospital
5) Department of Radiological Technology, Showa University Fujigaoka Hospital
6) Department of Radiological Technology, Showa University

∗ E-mail: nakami@cmed.showa-u.ac.jp

Note: This paper is secondary publication, the first paper was published in the JART, vol. 71 no. 858: 30-40, 2024.

Key words: Female Engineer, Working Environment, Awareness Survey

【Abstract】
We conducted a questionnaire survey on work styles and gender disparities among radiological technologists across eight hospitals and one clinic affiliated with Showa University. The survey also examined the attitudes of female radiological technologists regarding their work styles. The results indicated that female engineers in all groups expressed a desire to continue working after marriage and childbirth; however, there were notable differences between the perspectives of female engineers and those of managers concerning work styles. Furthermore, many female engineers were reluctant to pursue managerial positions, citing concerns that childbirth, childcare, and eldercare would hinder their opportunities for advancement. It is essential to cultivate a workplace environment that supports flexible work arrangements and to establish systems and a culture that enable female engineers to pursue their long-term careers while balancing their life plans.

Introduction

The Japanese government has established a policy to promote women's participation in the workforce as a key pillar of the country's growth strategy. In light of the rapid population decline, decreasing birthrate, and aging population, the inclusion of women in the workforce is essential for revitalizing both society and the economy [1)]. According to the "2020 Edition of The Reality of Working Women" published by the Ministry of Health, Labour and Welfare (MHLW), women comprise 44.3% of the total labor force. Furthermore, the labor force participation rate of women, analyzed by age group (in 5-year increments), has reached its highest level since comparable data became available in 1968 [2)]. Additionally, the MHLW is promoting a proactive approach called "Positive Actions" to address disparities between male and female workers, such as the underrepresentation of women in staff positions and the predominance of male managers. Specifically, these actions involve setting specific numerical goals for the number of women in leadership roles, establishing targets to be achieved, and determining a timeframe for accomplishing these objectives [3)].

Regarding women's healthcare, there is an increasing number of women's clinics and advancements in women's health services, particularly in the area of mammography, where our radiological mammography technologists play a crucial role. Mammography, a specialized testing method, can be uncomfortable, and many female patients report feelings of

embarrassment during the procedure[4]. Enhancing the breast cancer screening rate is essential for developing cost-effective health policies. Currently, mammography is primarily performed by female technologists, with a growing demand for female radiological technologists in this field. One factor contributing to lower screening rates is the presence of male radiological technologists[4]. The number of women enrolling in 3-to4-year radiologic technology programs is on the rise, with over 50% of students being women in each institution. According to the 2010 census data, the ratio of female radiographers was 18.9%, which increased to 22.8% in 2017 [5]. In a male-dominated work environment, the average length of employment for female radiographers is relatively short, indicating that improvements are still needed to create an environment where female technologists can thrive. Although the proportion of women in managerial positions across various industries has been increasing annually, it remains below 20%, significantly short of the government's goal of having 30% of women in managerial roles by 2020 [6]. A similar trend is anticipated for female radiographers.

In this study, we conducted a questionnaire survey regarding working conditions and the gender gap among radiological technologists from eight hospitals and one clinic affiliated with Showa University. The study aims to analyze current and future trends and explore their perspectives on the working conditions of female radiographers.

1. Methods

1-1. Research subjects and methods

The survey included 169 clinical radiologists from eight hospitals and one clinic affiliated with Showa University. Information regarding the questionnaire was disseminated via email, and the survey was conducted using a web-based anonymous questionnaire developed through Google Forms. The questionnaire comprised single-select questions (①-⑪) and multiple-select questions (⑫-⑭). The survey period spanned 15 days, from November 1, 2021, to November 15, 2021. Responses were collected online.

1-2. Survey contents

The survey consisted of a total of 14 questions, encompassing the working conditions of female technologists, work environment, personal circumstances, motivations for promotions, and challenges in the workplace. The details of the questions and options are provided below. Some terms were modified without altering the content of the survey responses. The questionnaire was conducted anonymously to guarantee confidentiality. The data obtained will be used solely for the purposes of this study.

About the working conditions of female radiographers

Question 1: What are your views on working after marriage and childbirth? (If you are male, what do you think of your female colleagues' work practices?)

Options: I want to work after marriage and childbirth / I want to work after taking maternity leave / I want to work reduced hours after taking childcare leave / I want to resign after getting married / I want to resign after becoming pregnant

Question 2: What are your thoughts on your desire to work while raising children? (If you are male, what do you think of your female colleagues' work preferences?)

Options: I want to work full-time / I want to work reduced hours / I want to stop working while the child is young but eventually return to full-time work / I want to resign

Question 3: Do you believe you can handle night shifts after maternity and childcare leave? (If you are male, what do you think of your female colleagues' ability to work night shifts?)

Question 4: Should female radiographers actively take childcare leave?

Question 5: Should female radiographers in training work shorter hours?

About the workplace environment

Question 6: Do you think childbirth, childcare, or nursing care affects your promotion opportunities?

Question 7: Is the workplace an environment conducive to taking childbirth leave and childcare leave?

Question 8: Do you think men and women are treated equally in the workplace?

Question 9: Do you believe men and women receive equal opportunities for promotion?

About your environment and motivation for promotion

Question 10: Are you able to balance work with family, childcare, and nursing care at your current workplace?

Question 11: Do you aspire to become an executive (assistant chief or higher)?

Options for 3-11: Agree/Somewhat agree / Neither agree nor disagree / Somewhat disagree / Disagree

About the challenges in the work environment

Question 12: What do you perceive as the challenges for female radiographers in maintaining employment? (Multiple answers allowed)

Options: Nothing in particular / Research activity / Night shifts / Irregular work hours / Work environment where women face advancement barriers / Sexual and power harassment / Few female executives / Personal health management / Returning to work after pregnancy and childbirth / Lack of support from family members living with you / Balancing care of your parents / Balancing work and family life after marriage / Balancing parenting responsibilities

Question 13: What measures do you believe are necessary for women to continue working in the same workplace after giving birth, both at home and in society? (Multiple answers allowed)

Options: Introduction of reduced working hours and work-from-home systems / Work style reform to include improvement of long working hours for both men and women / Prohibition of unfavorable treatment regarding promotions due to parenting and nursing care responsibilities / Changing women's mindset about continuing to work / Fostering understanding from others and changing perceptions about women continuing to work / Enhancing support systems for balancing parenting and nursing care in the workplace / Changing men's understanding and mindset towards participating in household chores / Enhancing housekeeping and parenting support services / Enhancing nursing care support services / Creating an environment where children can be cared for, such as through childcare and after-school care services

Question 14: What do you identify as obstacles for female radiographers to achieve success? (Multiple answers allowed)

Options: Nothing in particular / Relationships among women at work / Women's perceived lack of professionalism / Shorter average length of employment compared to men / Challenges of night shifts / Challenges of overtime / Lack of awareness and understanding from supervisors and male coworkers / Lack of societal awareness and understanding / Heavier family responsibilities compared to men

1-3. Ethical consideration

In conjunction with the questionnaire survey, an online consent form was distributed to participants. This form included a statement clarifying that participants would not face any disadvantageous treatment should they choose not to consent to the implementation or continuation of the study or if they opted to withdraw their consent at any time. Consent was obtained from participants upon completion of the survey.

This study received approval from the Ethical Committee of Showa University (Approval number 21-071-A).

1-4. Evaluation of the questionnaire results

Based on the collected responses, the survey results were tabulated and analyzed by categorizing them into groups: men, women, executives, and non-executives. Department managers, division managers, and assistant managers were classified as executives, while senior staff and radiographers were categorized as non-executives.

2. Results

2-1. Breakdown of the number of responses and respondents

The number of respondents was 154, resulting in a response rate of 91%.

The length of employment by gender is displayed in Fig. 1.

Among the respondents, there were 113 male radiographers (73%) and 41 female radiographers (27%).

The following summarizes the number of respondents by length of service: 0-10 years: 59 male radiographers and 33 female radiographers; 11-20 years: 27 male and 4 female; 21-30 years: 10 male and 3 female; ≥31 years: 14 male and 0 female (four participants did not respond to the question).

The average length of service was 13.4 years for male radiographers and 7.3 years for female radiographers (four participants did not

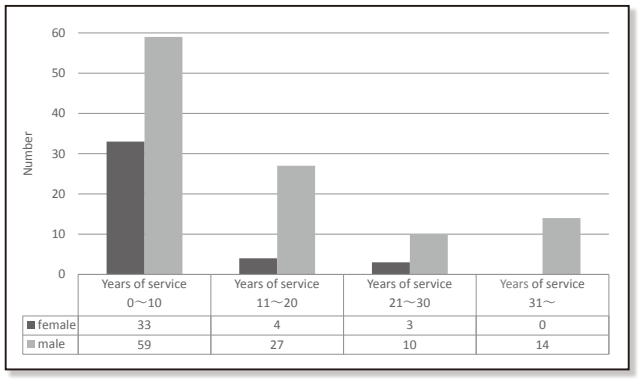

Fig. 1 Years of service by gender

Table 1 Marriage and presence of children

		female		male	
		subsection chief or above	Less than a subsection chief	subsection chief or above	Less than a subsection chief
unmarried	With children	0	0	0	0
	No children	1	31	3	57
married	With children	1	5	16	19
	No children	0	3	7	10
Total		2	39	26	86

respond to the question).

Regarding the participants' positions, there were 26 male executives, 2 female executives, 86 male non-executives, and 39 female non-executives (one participant did not respond to the question).

Table 1 presents the marital status of the participants and whether they have children.

There were 60 unmarried males, 32 unmarried females, 52 married males, and 9 married females.

Additionally, there were 35 males and 6 females with children, while 77 males and 35 females did not have children.

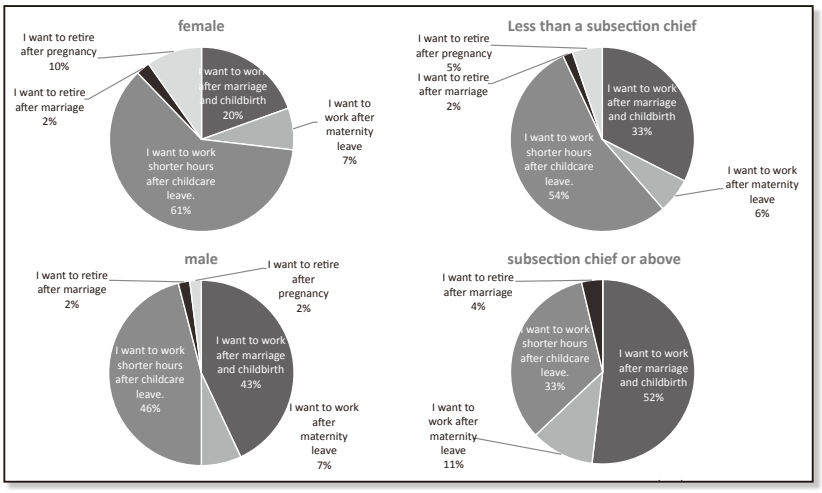

Fig. 2 What do you think about how to work after marriage and childbirth? (Q1)

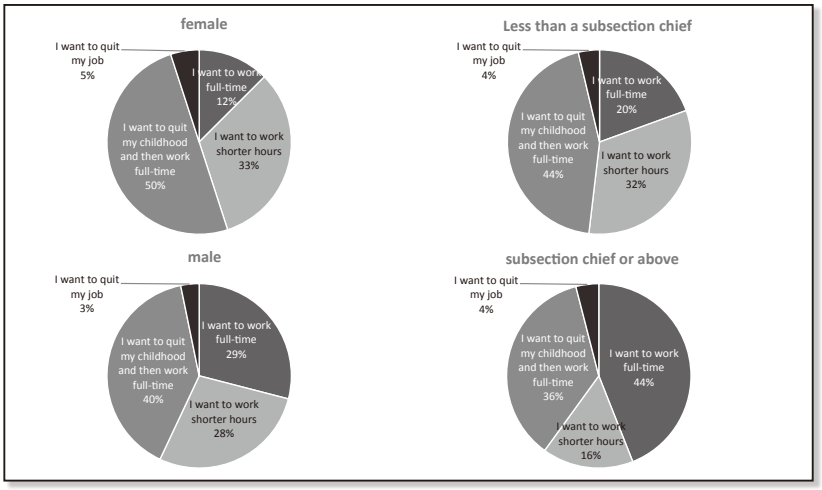

Fig. 3 What are your thoughts on your desire to work while raising children? (Q2)

2-2. About the working conditions of female radiographers

Figure 2 presents the responses to the question "① What are your thoughts on working after marriage, pregnancy, and childbirth? (If you are male, what are your thoughts on your female colleagues' work arrangements?)"

In all groups, approximately 90% responded with, "I want (them) to work after getting married and following childbirth."

Those who indicated, "I want (them) to work reduced hours after taking childcare leave," comprised 46% of males, 61% of females, 33% of executives, and 54% of non-executives. This suggests higher proportions of males compared to females, as well as executives compared to non-executives.

Responses to the statement, "I want (them) to resign after getting married", were 4% for males, 12% for females, 4% for executives, and 7% for non-executives, indicating that a majority of those who wish for resignation are women.

Figure 3 illustrates the responses to the question, "②What are your thoughts on working while raising children? (If you are male, what do you think of your female colleagues' work preferences?)" Among the respondents, 29% of males, 12% of females, 44% of executives, and 20% of non-executives expressed a desire for full-time work, revealing higher proportions among males and executives compared to their female and non-executive counterparts.

Regarding the option, "I want (them) to work reduced hours," the responses were 28% for males, 33% for females, 16% for executives,

and 32% for non-executives, indicating a smaller percentage among executives.

For the statement, "I want to stop working while the child is young but eventually return to full-time work," the responses were 40% for males, 50% for females, 36% for executives, and 44% for non-executives, indicating a lower percentage among executives.

Finally, regarding the statement, "I want to resign," the responses were 3% for males, 5% for females, 4% for executives, and 4% for non-executives, showing no significant differences among the groups.

Figure 4 depicts the responses to the question, "③Do you believe you can manage night shifts after maternity and childcare leave? (If you are male, what do you think of your female colleagues' ability to handle night shifts?)" The combined responses of "Agree" and "Somewhat agree" were 30% for males, 25% for females, 22% for executives, and 29% for non-executives, revealing no significant differences among the groups.

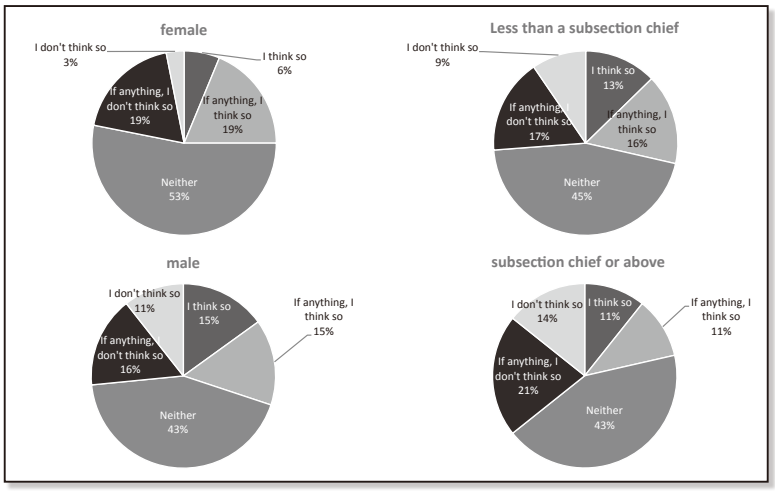

Fig. 4 Do you think you can handle night shifts after maternity and childcare leave? (Q3)

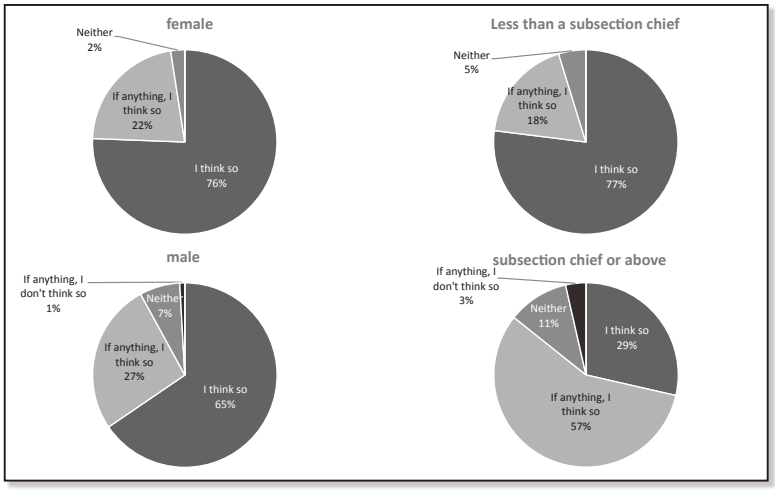

Fig. 5 Do you think female engineers should actively take childcare leave (Q4)

Those who responded "Somewhat disagree" and "Disagree" included 27% males, 22% females, 35% executives, and 26% non-executives, indicating that executives represented the highest proportion of individuals who felt they could not manage night shifts.

Figure 5 illustrates the responses to the question, "④Do you think female radiographers should actively take childcare leave?" Among the respondents, 92% of males, 98% of females, 86% of executives, and 95% of non-executives expressed agreement or somewhat agreement, suggesting that approximately 90% across all groups believe female radiographers should actively take childcare leave.

In response to

The statement "Agree" shows the distribution as follows: 65% males, 76% females, 29% executives, and 77% non-executives, which highlights a lower percentage among executives.

Those who responded "Somewhat disagree" and "Disagree" comprised 1% males, 0% females, 3% executives, and 0% non-executives.

Figure 6 presents the responses to the question, "⑤Do you think female radiographers in training should actively work shorter hours?" The agreements included 78% males, 84% females, 74% executives, and 82% non-executives, indicating that approximately 70% or more across all groups believe female ra-

diographers should actively work shorter hours.

Regarding the "Agree" responses, the breakdown was as follows: 50% males, 57% females, 26% executives, and 58% non-executives, again reflecting a smaller percentage among executives.

Those who responded "Somewhat disagree" and "Disagree" were composed of 6% males, 3% females, 11% executives, and 3% non-executives, demonstrating a higher percentage among executives.

2-3. About the work environment

Figure 7 presents the responses to the question, "⑥Do you think childbirth, childcare, or nursing care affects your promotion?" The respondents who answered "Agree" and "Somewhat agree" included 44% of males and 56% of females, with 58% of executives and 46% of non-executives. This indicates a higher percentage of agreement among females compared to males, as well as among executives compared to non-executives.

The respondents who answered "Somewhat disagree" and "Disagree" comprised 13% of males, 10% of females, 8% of executives, and 12% of non-executives, demonstrating no significant differences among the groups.

Figure 8 illustrates the responses to the question, "⑦Is the workplace an environment where it is easy to take childbirth leave and childcare leave?" Among those who answered "Agree" and "Somewhat agree," 43% were males, 41%

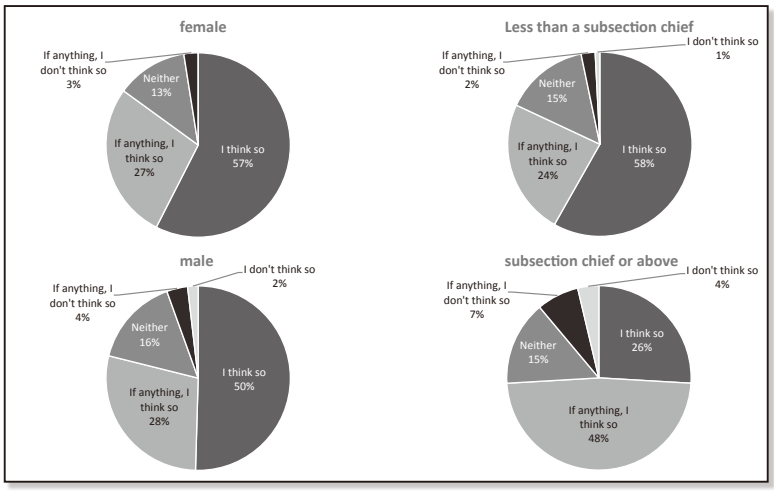

Fig. 6 Do you think female engineers in training should actively work shorter hours (Q5)

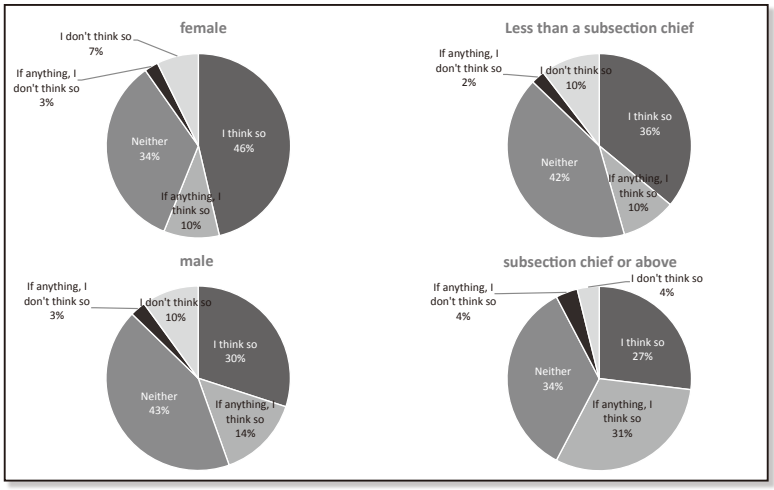

Fig. 7 Do you think childbirth, childcare, or nursing care affect your promotion or promotion? (Q6)

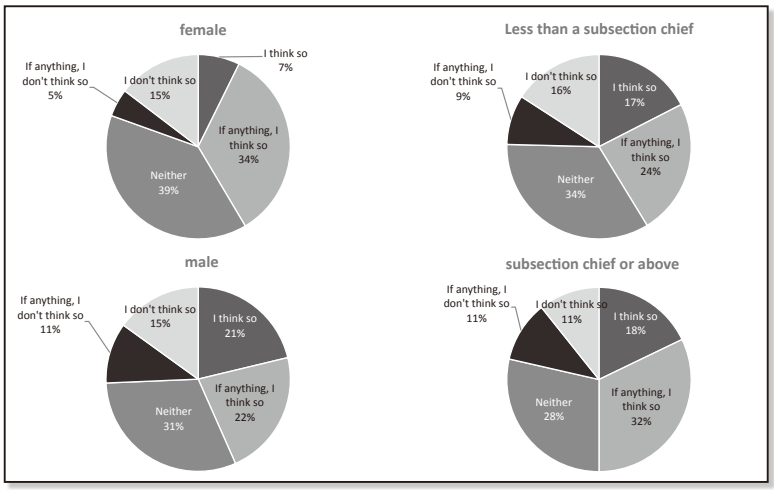

Fig. 8 Is the workplace an environment where it is easy to take childbirth leave and childcare leave? (Q7)

were females, 50% were executives, and 41% were non-executives, indicating a slightly higher percentage among executives.

The respondents who answered "Somewhat disagree" and "Disagree" included 26% of males, 20% of females, 22% of executives, and 25% of non-executives, again showing no significant differences among the groups.

Figure 9 displays the responses to the question, "⑧Do you think men and women are equal in their work?" The respondents who answered "Agree" and "Somewhat agree" included 51% of males, 61% of females, 64% of executives, and 51% of non-executives, indicating a higher percentage of agreement among females compared to males, as well as among executives compared to non-executives.

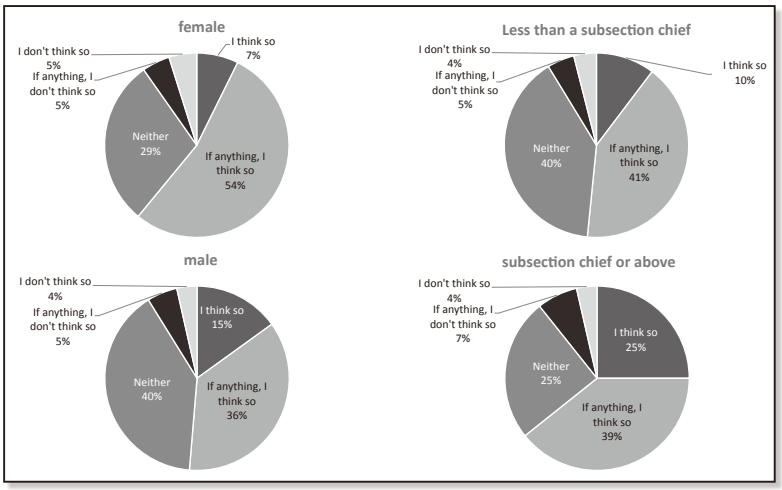

Fig. 9 Do you think men and women are equal in their work? (Q8)

The respondents who answered "Somewhat disagree" and "Disagree" comprised 9% of males, 10% of females, 11% of executives, and 9% of non-executives, showing no significant differences among the groups.

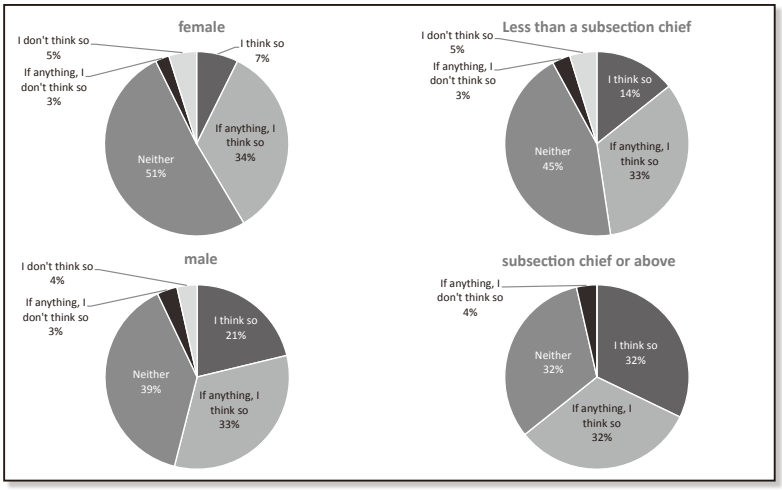

Fig. 10 Do you think men and women are equal in terms of promotion? (Q9)

Figure 10 presents the responses to the question, "⑨Do you think men and women are equal in terms of promotion?" The respondents who answered "Agree" and "Somewhat agree" included 54% of males, 41% of females, 64% of executives, and 47% of non-executives, indicating a higher percentage of agreement among males compared to females, as well as among executives compared to non-executives.

The respondents who answered "Somewhat disagree" and "Disagree" comprised 7% of males, 8% of females, 4% of executives, and 8% of non-executives, again showing no significant differences among the groups.

2-4. About your environment and motivation for promotion

Figure 11 illustrates the responses to the question, "⑩Are you able to balance work with family, childcare, and nursing care at your current workplace?" The results indicate that among those who responded "Agree" and "Somewhat agree," the percentages were as follows: males: 35%, females: 22%, executives: 29%, and non-executives: 32%. This data highlights a lower percentage of female respondents who feel they can achieve this balance.

In contrast, for those who answered "Somewhat disagree" and "Disagree," the distribution was: males: 13%, females: 10%, executives:

25%, and non-executives: 10%. This indicates a higher percentage of executives expressing difficulty in achieving work-life balance.

Figure 12 presents the responses to the question, "⑪Do you want to become an executive (assistant chief or higher)?" Among those who answered "Agree" and "Somewhat agree," the breakdown was: males: 35%, females: 12%, executives: 64%, and non-executives: 21%. This demonstrates that a smaller proportion of female respondents expressed interest in pursuing executive positions, while a significant majority of executives indicated a desire for advancement.

For those who answered "Somewhat disagree" and "Disagree," the distribution was as follows: males: 38%, females: 54%, executives: 12%, and non-executives: 49%. This reveals a higher percentage of female respondents who do not wish to pursue executive roles, contrasted with a lower percentage among executives.

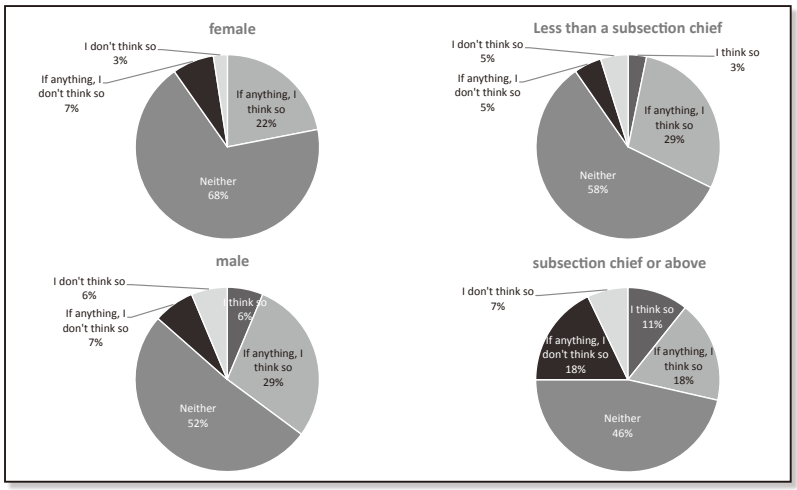

Fig. 11 Are you able to balance work with family, childcare, and nursing care at your current workplace? (Q10)

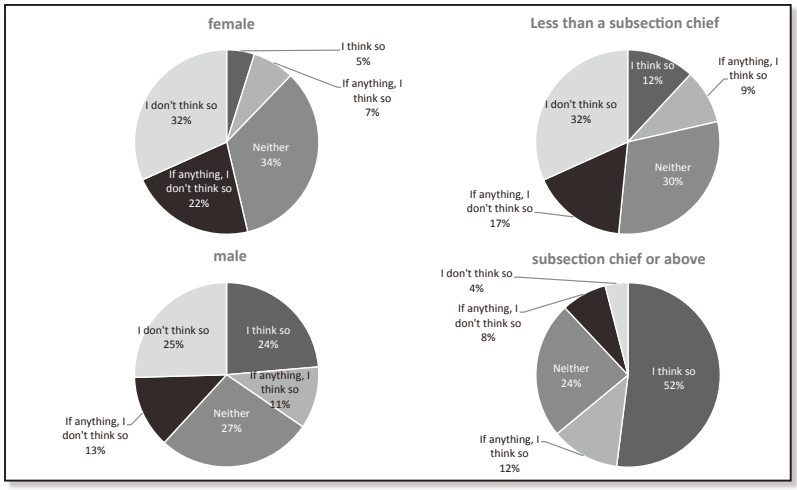

Fig. 12 Do you want to become an executive (assistant chief or higher)? (Q11)

2-5. About the challenges in the work environment

Figure 13 presents the responses to the question, "⑫What do you think are the challenges for female radiographers to remain employed?" All groups identified "balancing parenting and family responsibilities," "returning to work after pregnancy and childbirth," and "balancing work and family life after marriage" as significant challenges.

The female and executive groups cited "balancing parenting and family responsibilities," while the male and non-executive groups identified "balancing work and family life after marriage" as the most challenging factor.

Figure 14 illustrates the responses to the question, "⑬What do you think is necessary for women to continue working in the same workplace after giving birth at home, in society, and at work?" Across all groups, many respondents emphasized the need for "creating an environment that supports child care, such as childcare services and outside school hours care," "enhancing nursing care support services," "changing the understanding and mindset of men regarding participation in household chores," and "improving housekeeping and parenting support services."

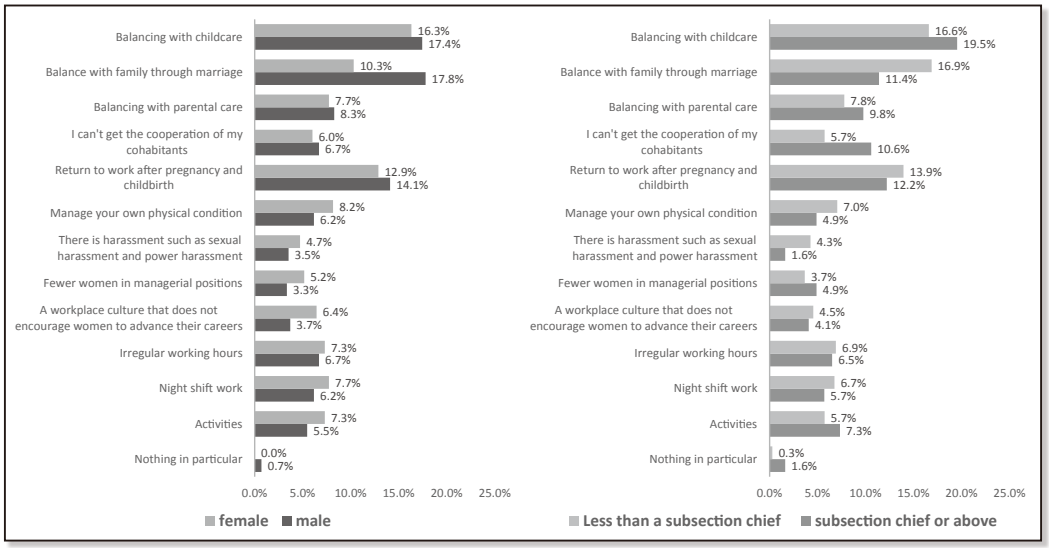

Fig. 13 What do you think are the challenges for female engineers to keep working? (Q12)

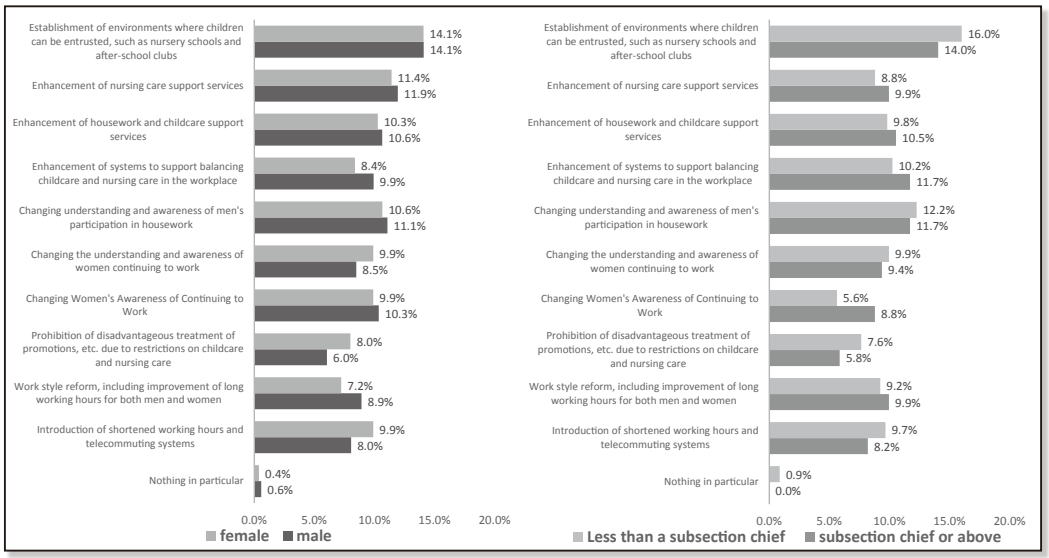

Fig. 14 What do you think is necessary for women to continue working in the same workplace after giving birth at home, in society, and at work? (Q13)

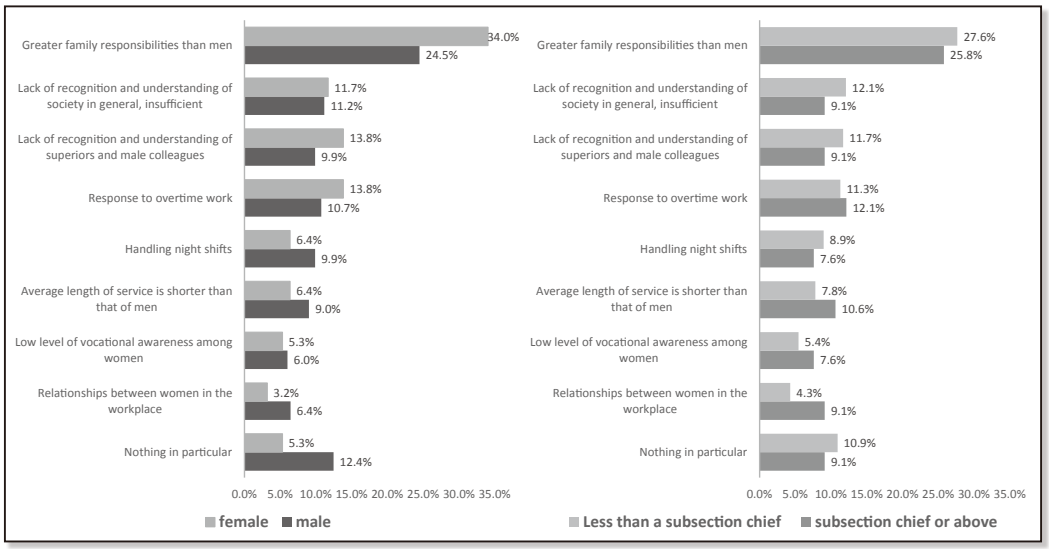

Fig. 15 What do you think are the obstacles for female engineers to succeed (Q14)

Figure 15 depicts the responses to the question, "What do you think are the obstacles for female radiographers to succeed?" All groups noted obstacles such as "lack of awareness and understanding from supervisors and male coworkers," "challenges of dealing with overtime," and "general societal lack of awareness and understanding" as significant barriers.

Across all groups, "greater family responsibilities compared to men" was identified as the primary obstacle.

Responses of "nothing in particular" and "shorter average length of employment compared to men" were most frequently selected by the male and executive groups, respectively.

In the female group, "lack of awareness and understanding from supervisors and male coworkers" and "challenges of dealing with overtime" were the most frequently noted obstacles.

3. Discussion

Approximately 90% of respondents expressed a desire for "I want (them) to work after getting married and childbirth" across all groups, while approximately 10% of female technologists indicated they wished to resign following marriage or childbirth.

According to the "Overview of the 1st Longitudinal Survey of Adults in the 21st Century (2012 Cohort) and the 11th Longitudinal Survey of Adults in the 21st Century (2002 Cohort)" [7], the willingness to continue working after marriage revealed that 18.4% of single women with permanent jobs in the 2002 Cohort stated, "I will quit my job after getting married," compared to 10.1% in the 2012 Cohort. This indicates a decrease in the percentage of those willing to resign from their jobs after marriage in the more recent cohort. Additionally, among individuals who were single (and employed prior to marriage) at the time of the first survey and subsequently married within the 9 years, the rates of those who left the workforce were 28.9% in the 2002 Cohort and 16.9% in the 2012 Cohort, again demonstrating a decline in the proportion of individuals leaving their jobs after marriage in the later cohort.

A similar trend can be observed in the results of our questionnaire, which indicates a high percentage of female radiographers who wish to continue working without quitting in the future.

However, few female technologists expressed a desire to work full-time while raising children. Instead, they prefer to take childcare leave or work reduced hours, seeking flexible work arrangements that prioritize child-rearing. Conversely, the study revealed a high proportion of executives who expressed the belief that "I want (them) to work full-time." While they acknowledge the need for women to take childcare leave and work reduced hours, their willingness to support these arrangements is lower than that of other groups, suggesting a gap in their understanding of desired working styles.

There were no significant differences in awareness of night shifts between men and women. However, the study indicated that executives were significantly more likely to perceive it as challenging for female technologists returning from childcare leave to manage night shifts.

Currently, employees in the Department of Radiological Technology at Showa University can take childcare leave and work reduced hours without complications. The reform of the Child Care and Family Care Leave Act in April 2022 has encouraged more men to take parental leave, and the number of male workers requesting this leave is expected to increase further in the future. In recent years, there has been a rise in unexpected vacancies due to COVID-19-related sick leave and close contact rules. Executives must consider rotations, workload allocation, handover processes, operational continuity, and staff leave arrange-

ments, especially when multiple employees take time off simultaneously. This situation may have contributed to a lack of enthusiasm for childcare leave and reduced hours, as indicated in the questionnaire survey.

Executives may also perceive that female employees cannot handle night shifts due to difficulties in maintaining work flexibility. To bridge the awareness gap between female technologists and their executives, we must continue promoting on-the-job training (OJT) technical education, which has been implemented in our hospital. Additionally, it is essential to analyze work allocation and workload by day of the week and time while also optimizing staffing and fostering active teamwork within each division. Furthermore, we may need to establish criteria for securing replacement personnel based on the number of vacancies.

Effective communication between female radiographers and their supervisors regarding their requests and circumstances is vital for making necessary operational adjustments. Support from the company and executives, alongside the individual efforts of female technologists, is crucial for their skill development and professional growth.

The results of the questionnaire regarding the work environment revealed that many radiographers felt it was easy to take childcare leave after childbirth. Similarly, concerning gender equality, numerous radiographers believed that gender equality in the workplace has been achieved.

However, over 50% of female technologists and executives indicated that childbirth, parenting, and nursing care adversely impact their promotional opportunities.

The reasons cited include the fact that taking time off, such as parental leave, can result in a discrepancy in years of service and hinder employees from engaging in research, obtaining certifications, or continuing their education. Additionally, female radiographers expressed concerns that the prevailing work culture may negatively influence their supervisors' perceptions. They feared that supervisors might doubt their ability to balance work and personal responsibilities. Within the Department of Radiological Technology at Showa University, there are internal regulations governing promotion qualifications, which are reviewed annually. As employees gain access to these regulations upon becoming eligible for promotions, a lack of understanding regarding evaluation criteria may have contributed to the negative sentiments expressed.

To alleviate anxiety and uncertainty surrounding promotion evaluations, it is essential to communicate clearly the evaluation criteria outlined in the internal regulations. This should include specific evaluation items and expectations, assisting each radiographer in comprehending their individual evaluation criteria. Furthermore, providing education and follow-up on these items may enhance transparency in the promotion process and evaluation criteria.

Regarding the environment and motivation for promotion, 35% of males felt they could effectively balance work, family, parenting, and caregiving responsibilities, while only 22% of females reported the same. Additionally, a significant 54% of female technologists expressed a lack of desire to ascend to executive positions. The reasons cited for this reluctance include challenges in balancing work and family, increased responsibilities, and heightened overtime and workload. Questionnaire results indicate that female radiographers are apprehensive about maintaining a work-life balance if they transition into executive roles that demand greater responsibility and time commitment. Given that female technologists often bear primary responsibility for childbirth, parenting, and caregiving, their career advancement may be deprioritized. Currently, there are only two female executives, suggesting that the benefits and opportunities associated with

these roles have not been effectively communicated.

To enhance motivation for promotion, it is essential to encourage women by gradually delegating rewarding tasks, such as leadership roles, while clearly articulating the advantages of executive positions. Furthermore, providing support for maintaining work-life balance is crucial so that women can perceive managerial roles positively. Creating an environment where female technologists feel motivated to pursue promotions and actively seek careers in executive positions is vital.

Regarding the challenges in the work environment, the group of female technologists identified "balancing parenting and family responsibilities," the need for "enhanced social environments and support services," and the necessity for a "shift in men's understanding and engagement in household chores" as critical factors for their continued employment.

The issues of "heavier family responsibilities compared to men" and the "absence or lack of awareness and understanding from supervisors and male colleagues" were highlighted as significant obstacles to the success of female radiographers. These findings indicate that female workers seek environments that enable them to balance work and family life effectively; thus, it is essential to address their concerns regarding work-life balance. While improving their family environments is vital, it is important to recognize that individual perspectives and approaches within the home can vary significantly, complicating generalizations. Therefore, it is crucial to cultivate a workplace environment that accommodates flexible work arrangements and fosters a culture where female technologists can pursue long-term career plans aligned with their life goals.

Supporting female technologists in maintaining their careers and fostering a fair and comprehensive work environment requires ongoing efforts. These efforts should include the rationalization of working hours, implementation of work-life balance support initiatives, creation of environments and programs that actively promote career advancement, increased transparency in promotion processes and evaluation criteria, and the provision of education and training on gender bias to cultivate understanding and respect for a fair work environment.

4. Study limitations

In this study, the percentage of female radiographers was notably low, which may have resulted in the opinions and perspectives of male participants being disproportionately represented in the questionnaire results. Furthermore, the findings of this study do not accurately reflect the views of radiographers nationwide, as the participants were restricted to facilities of the same affiliation. The generalizability of the study's results must be assessed by collecting data from additional facilities in future research.

5. Conclusion

We have identified the current status and challenges regarding the working conditions of female radiological technologists, as well as the gender gap within the Department of Radiological Technology at Showa University, through a questionnaire survey.

Our intention is to utilize this information to foster an improved work environment in the future.

Acknowledgement

We would like to express our sincere gratitude to all those who have contributed to this research in the Department of Radiological Technology, Showa University.

Conflicts of Interest

The lead authors and all co-authors have no conflicts of interest to declare.

References

1) Mari Nakagawa: Policy Issues for Expansion of Women's Participation in Policy and Decision-making Processes and Work-life Balance for Men and Women in Japan. Japanese Journal of Family Relations, 35 (0), 75-83, 2016.
2) Employment Environment and Equal Employment Bureau, Ministry of Health, Labour and Welfare. 2020 Edition The Reality of Working Women. https://www.mhlw.go.jp/bunya/koyoukintou/josei-jitsujo/dl/20-01.pdf (accessed on Mar 31st, 2023)
3) Council for Promoting Women's Empowerment: What are positive actions? https://www.mhlw.go.jp/positive-action.sengen/about.html (accessed on Mar 31st, 2023)
4) Shizuko Kobayashi, et al.: Study on Promotional Factors and Obstructive Factor to Breast Cancer Screening Behavior among Japanese Women. Journal of Japan Association of Breast Cancer Screening, 15 (1), 69-74, 2006.
5) Ministry of Health, Labour and Welfare: (2015) Vital Statistics. 2016.
6) Gender Equality Bureau of the Cabinet Office: Basic Plan for Gender Equality – For the Society Where All Women Can Shine in Reiwa Era –. https://www.gender.go.jp/about_danjo/basic_plans/5th/pdf/detail.pdf (accessed on Mar 31st, 2023)
7) Overview of the 1st Longitudinal Survey of Adults in the 21st Century (2012 Cohort) and the 11th Longitudinal Survey of Adults in the 21st Century (2002 Cohort) . https://www.mhlw.go.jp/toukei/saikin/hw/judan/seinen14/dl/gaiyou.pdf (accessed on Mar 31st, 2023)

Received March 3, 2023 ; accepted December 14, 2023

Image quality test using phantom and evaluation of clinical images with two different FDG calibration times on a SiPM-based PET/CT scanner

NAGASE Tomoaki

Kanagawa Cancer Center, Department of Radiological Diagnosis Technology

＊ E-mail: nagase.04007@kanagawa-pho.jp

Note: This paper is secondary publication, the first paper was published in the JART, vol. 71 no. 859: 34-39, 2024.

Key words: image quality test, evaluation of clinical images, two different FDG calibration times, SiPM-based PET/CT scanner

【Abstract】

Many SiPM-based PET-CT scanners are in operation across Japan, including in our hospital. In this hospital, established in 2021 we perform 16 examinations per day, utilizing FDG calibration times of 10:00 and 12:30. In this study, we aimed to demonstrate that clinical images can be obtained reliably under these operational conditions. First, we conducted an image quality test using a phantom to evaluate the performance of the SiPM-based PET scanner. The results indicated that the quality standards were not met for low-dose and short-duration imaging. Subsequently, we evaluated clinical images from 489 patients, using evaluation indices such as $NEC_{patient}$, $NEC_{density}$, and Liver SNR. More than 99% of patients met the threshold for all evaluation criteria when the acquisition time was set to the default of 2 minutes at 2.1 MBq/kg.

Introduction

As of January 1, 2012, there are 587 positron emission tomography-computed tomography (PET-CT) scanners in operation in Japan, including PET/MR, MRPET, and breast PET systems[1]. Notably, the adoption of PET-CT scanners utilizing semiconductor detectors (SiPM-based PET) is steadily increasing[2]. Unlike conventional photomultiplier tube detectors, SiPM-based PET uses semiconductor detectors (SiPMs), enabling high-resolution imaging with short scanning times[3]. Since January 2021, our hospital has been utilizing a SiPM-based PET system (Discovery™ MI, GE Healthcare) and conducting tests using the standard radiopharmaceutical Fluorodeoxyglucose Injection (FDGscan® Injection, hereafter, FDG, Nihon Medi-Physics).

Sixteen patients were examined daily at our hospital, with FDG calibration times set at 10:00 and 12:30. The first patient received the FDG injection at 8:50, and the injection interval between patients was 10–15 min. Imaging was performed 60 min after the start of the injection. The acquisition time per bed (acquisition time) was adjusted for each patient using a calculation formula.

However, all radiopharmaceuticals, including FDG, exhibit radioactive decay over time. Consequently, when using the two calibration times mentioned above, there is a possibility that the radioactivity may be insufficient in some patients. In addition, with an injection interval of 10–15 min, the examination time per patient is reduced, resulting in a shorter acquisition time.

Therefore, in this study, we aimed to ensure stable clinical image quality for 16 patients undergoing PET-CT scans under these operational conditions. To achieve this, we first conducted image quality testing using a phantom. The default values for the acquisition time in clinical practice were determined based on the values and phantom images obtained from this test. Subsequently, we evaluated the clinical

images obtained to assess the efficacy of these acquisition times in maintaining image quality.

1. Methods

1.0 Image reconstruction method and equipment performance

The image reconstruction method used for the SiPM-based PET scanner was the Block Sequential Regularized Expectation Maximization (BSREM) method (Q.Clear, GE Healthcare). This Q.Clear method incorporates penalized maximum likelihood estimation, where noise is controlled by the penalty parameter (β value, GE Healthcare). Therefore, there is no need to set Iteration or Subset parameters, and the only parameter that requires adjustment is the β value. This β value ranges 1–10,000, and in this study, the β value was set to 400 for both the image quality test and evaluation of clinical images. We selected this value because in whole-body ^{18}F-FDG scans, a β value of 400 to 500 is used,[4] and in the evaluation of pulmonary nodules, a β value of 400 or 600 is used[5, 6]. The other performance is shown in Table.

1.1 Image quality test using phantom

The phantom used in this study was the NEMA Body phantom (phantom). Following the "Phantom Test Protocol for Whole-Body PET Imaging Using ^{18}F-FDG, 3rd Edition"[7] (protocol), FDG was introduced into the phantom to achieve a sphere-to-background (BG) ratio of 4:1. Phantom imaging was conducted at three different radioactivity concentrations in the BG region: 4.22 kBq/mL, 2.11 kBq/mL, and 1.45 kBq/mL. These concentrations were selected based on the assumption that 370 MBq and 185 MBq of FDG would be injected to a patient weighing 60 kg (370/60=6.2 MBq/kg, 185/60=3.2 MBq/kg), as outlined in the protocol. In addition, this is consistent with the lower limit of the recommended dose range of 2-5 MBq/kg body weight, as per the "FDG PET and PET/CT Clinical Practice Guidelines 2020"[8]. The acquisition time was set to 30 min, and image reconstruction was performed for each minute of acquisition.

In this phantom test, we evaluated the QN ratio of the 10 mm sphere ($Q/N_{10\,mm}$) and relative recovery coefficient (recovery coefficient) of the phantom. According to the "Guidelines for FDG-PET/CT Imaging of Cancer, 2nd Edition"[9] (Guidelines), the reference value for $Q/N_{10\,mm}$ is 2.8%, whereas the target value for the recovery coefficient in the protocol is 0.38.

1.2 Evaluation of clinical images

The participants were 489 patients who underwent PET-CT examinations between February 8 and April 2, 2021. A breakdown of the requesting departments is shown in Fig. 1. The formula for calculating the acquisition time is

Table Discovery™ MI performance

PET-CT characteristics	
Detector material	LBS（Lutetium Based Scintillator）
Coincidence window width（ns）	5.25
Detector ring diameter（mm）	744
Crystal size（mm^3）	3.95（trans axial）×5.3（axial）×25（radial）
Trans axial field of view（mm）	700
Axial field of view（mm）	250
Axial sampling interval（mm）	2.78
Number of imaging plane	89
Number of crystals/ ring	544

as follows:

Concentration at phantom imaging:

$$\frac{1}{\text{Acquisition time at phantom imaging (sec)}} = \frac{\text{Dose (MBq)}}{\text{Weight (kg)}} : \frac{1}{\text{Acquisition time (sec)}} \quad (1)$$

The three evaluation metrics used in this study were the Noise Equivalent Count (NEC) per patient ($NEC_{patient}$), NEC density ($NEC_{density}$), and Signal to Noise Ratio (SNR) of the liver (Liver SNR), as outlined in the guidelines. $NEC_{patient}$ was normalized by the axial length of the measurement range, whereas $NEC_{density}$ was divided by the body volume of the measurement range. The guidelines specify evaluation criteria for these clinical image evaluation items, with target values for $NEC_{patient}$, $NEC_{density}$, and Liver SNR set at 13, 0.2, and 10, respectively. The nuclear medicine work support system (ONTi®, PDRadio pharma) was used to calculate both $NEC_{patient}$ and $NEC_{density}$, whereas the calculation of Liver SNR was based on the established guidelines.

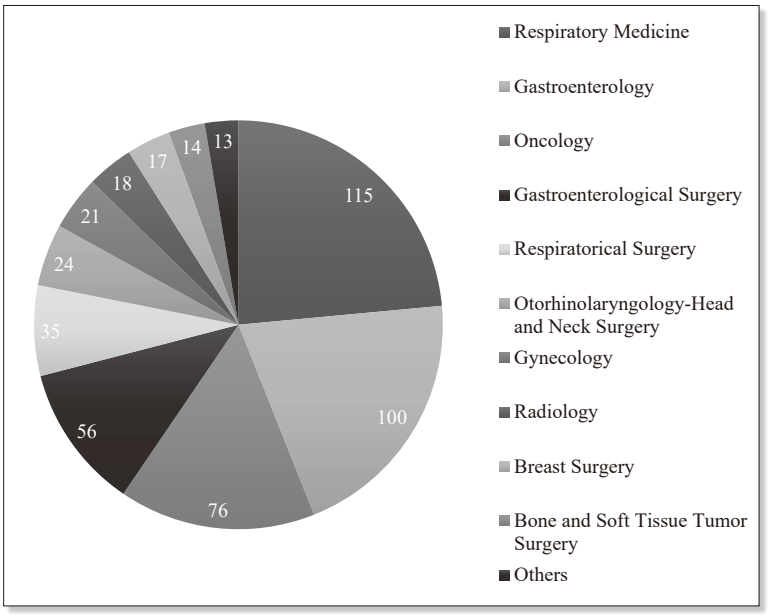

Fig. 1 Distribution of the 489 patients by department

1.3 Ethical considerations

This study was approved by our hospital's Clinical Review Committee (approval number: 2021eki24). Since the 489 patients whose clinical images were evaluated, did not undergo any invasive procedures or interventions, an opt-out approach was used, and informed consent was not required.

2. Results

2.1 Image quality test using phantom

The $Q/N_{10\,mm}$ exceeded the reference value of 2.8% in all cases, except for the 1-minute acquisition at 1.45 kBq/mL (Fig. 2). As reference, phantom images were collected at radioactivity concentrations of 4.22 kBq/mL, 2.11 kBq/mL, and 1.45 kBq/mL, with acquisition times of 1, 2, 3, 4, and 30 minutes (Fig. 3). The recovery coefficients were approximately 1.0 for all spheres, except for the 10 mm sphere. For the 10 mm sphere, the recovery coefficients were 0.69 at 4.22 kBq/mL, 0.68 at 2.11 kBq/mL, and 0.74 at 1.45 kBq/mL (Figs. 4-5). Based

		Acquisition Time (min)									
		1	2	3	4	5	6	7	8	9	10
Concentration (kBq/mL)	4.22	5.39	7.78	9.30	9.92	10.27	10.99	11.71	12.38	12.80	12.95
	2.11	3.02	5.04	6.55	7.40	8.03	8.16	8.34	8.48	8.64	8.86
	1.45	2.64	3.98	4.82	5.69	6.66	7.46	8.00	8.29	8.46	8.82

Fig. 2 QH ratio of 10 mm spheres at each acquisition time for each radioactivity concentration

on these results, a 2-minute acquisition at 2.1 MBq/kg (equivalent to 1.45 kBq/mL) was selected as the default value in the formula. Subsequently, this value was used to calculate the acquisition time in a clinical setting.

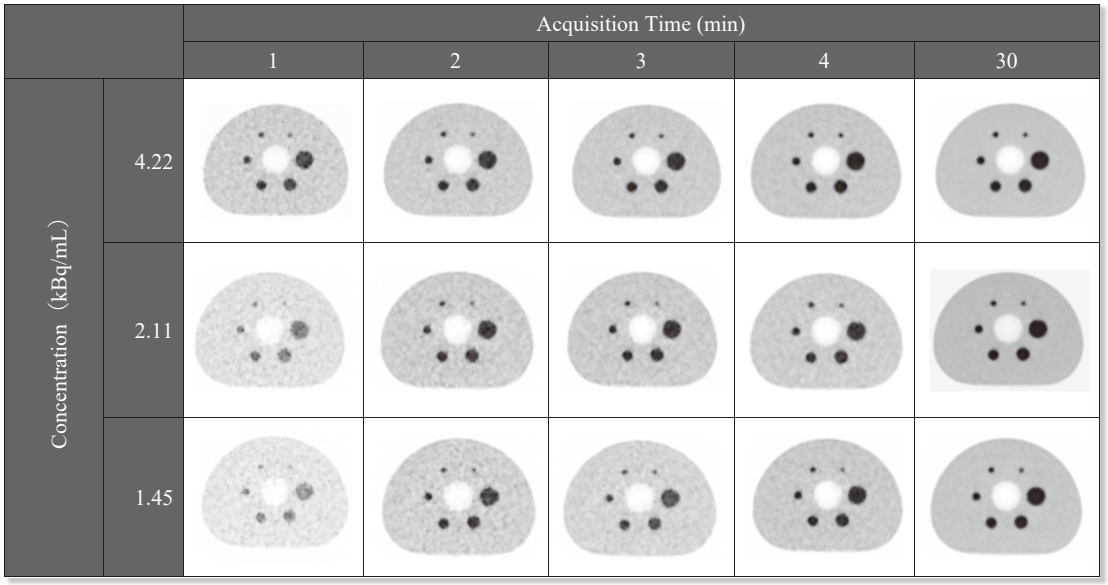

Fig. 3　Phantom images at each acquisition time for each radioactivity concentration

Concentration（kBq/mL）	Sphere size（mm）					
	10	13	17	22	28	37
4.22	0.69	1.03	1.07	1.05	1.03	1.00
2.11	0.68	0.99	1.05	1.03	1.03	1.00
1.45	0.74	1.01	1.02	1.03	0.97	1.00

Fig. 4　Recovery coefficients for each sphere size at each radioactivity concentration

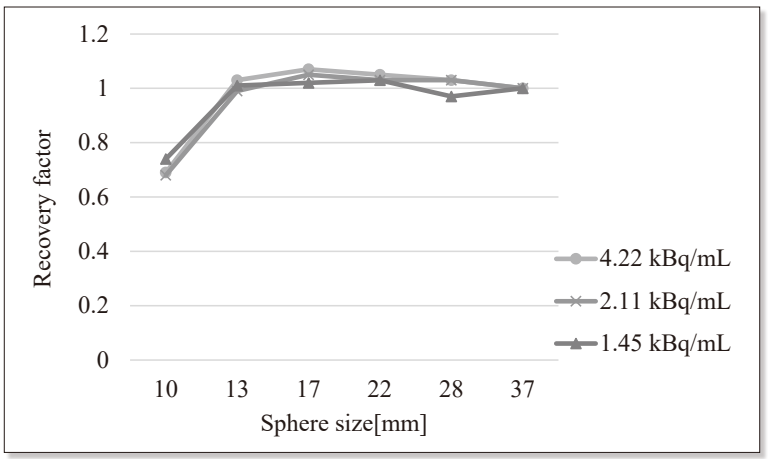

Fig. 5　Recovery coefficients for each sphere size at each radioactivity concentration

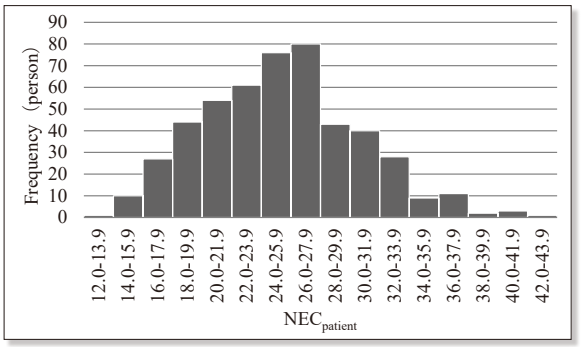

Fig. 6 Histogram of $NEC_{patient}$

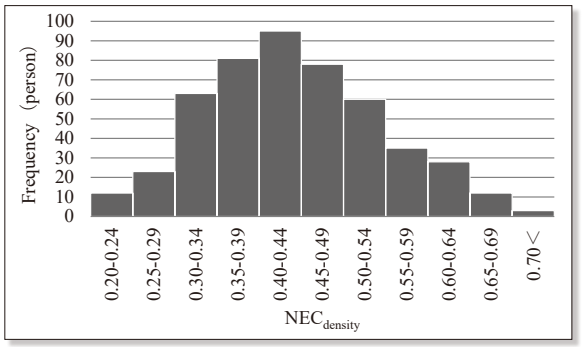

Fig. 7 Histogram of $NEC_{density}$

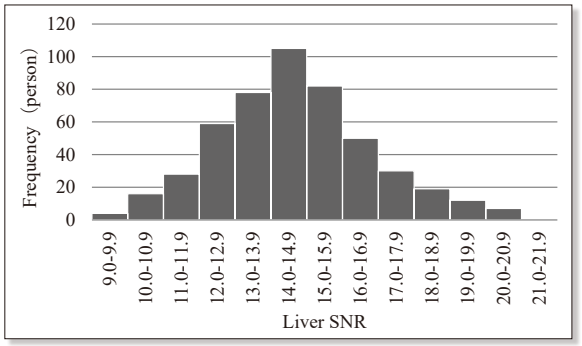

Fig. 8 Histogram of Liver SNR

2.2 Evaluation of clinical images

The acquisition time was calculated using the following formula:

$$\text{2.1 (MBq/kg)}: \frac{1}{120\ (\text{sec})} = \frac{\text{Dose (MBq)}}{\text{Weight (kg)}} : \frac{1}{\text{Acquisition time (sec)}} \quad (2)$$

The $NEC_{patient}$ was 13 or higher in 488 of the 489 patients (99.8%) (Fig. 6), and the $NEC_{density}$ was 0.2 or higher in all 489 patients (100%) (Fig. 7). The Liver SNR was 10 or higher in 486 of 489 patients (99.3%) (Fig. 8). The average weight of the 489 patients was 58.2 kg; the average dose per kilogram body weight was 4.3 MBq/kg, with a maximum dose of 8.9 MBq/kg and a minimum dose of 1.6 MBq/kg. The average uptake time was 62.5 minutes.

3. Discussion

In this study, we investigated the performance of SiPM-based PET and evaluated clinical images based on the acquisition time derived from this performance. In the image-quality test using the phantom, we examined the $Q/N_{10\,mm}$ and the recovery coefficient. For $Q/N_{10\,mm}$, when the radioactivity concentration in the BG region was 4.22 kBq/mL or 2.11 kBq/mL, the standard value was met with an acquisition time of 1 minute. However, when the radioactivity concentration was 1.45 kBq/mL, the standard value could not be achieved with an acquisition time of 1 minute (Fig. 2). Despite the high sensitivity of SiPM-based PET, it is evident that the standard values cannot be met when the radioactivity concentration is too low or the acquisition time is too short. As shown in the phantom images, the 1-minute acquisition at 1.45 kBq/mL contained significant noise, making it almost impossible to visually evaluate the 10 mm sphere (Fig. 3). Considering that the $Q/N_{10\,mm}$ for a 2-minute acquisition at 1.45 kBq/mL is better than that for a 1-minute acquisition at 2.11 kBq/mL, and the 10 mm sphere could be evaluated more accurately in the phantom image, we determined that a default value of 2.1 MBq/kg for a 2-minute acquisition is preferable for clinical use. Furthermore, the dose per body weight could be lower than 2.1 MBq/kg depending on the appointment time. If the acquisition time is too short, the examination may be completed too quickly. The recovery coefficients for the 10 mm spheres ranged from 0.68 to 0.74, while for the spheres of 13 mm or more, they con-

verged to almost 1.0 at all radioactivity concentrations (Fig. 4-5).

The target value for the relative recovery coefficient in the protocol was 0.38, which indicates a high cross-sectional resolution of the SiPM-based PET. In addition, the best result for the recovery coefficient of the 10 mm sphere was 1.45 kBq/mL for each radioactivity concentration. Since radiation measurements can be irregular, multiple measurements are required for accuracy[10]. However, the image quality test using the phantom was performed only once, and it is possible that the results could have varied if the test had been repeated multiple times.

In the evaluation of clinical images, most cases met the evaluation criteria for each of the $NEC_{patient}$, $NEC_{density}$, and Liver SNR (Fig. 6-8). The acquisition time calculation formulas ((1) and (2)) used in this study were developed by our team. These formulae incorporate the ratio of the dose per body weight and the reciprocal of the acquisition time. The approach is based on reports suggesting that when the dose per body weight is high (or low), the Liver SNR remains equivalent, regardless of whether acquisition time is short (or long)[11].

Additionally, the 489 patients were selected through continuous sampling without selection bias, and the departments requesting scans were diverse (Fig. 1), which likely resulted in a range of FDG accumulation. Furthermore, the default value of 2.1 MBq/kg in the calculation formula, derived from the phantom image quality test results, differs slightly from the radioactivity concentration observed at the time of imaging during clinical imaging due to factors such as urine excretion between injection and imaging. However, almost all the cases met the evaluation criteria for the three assessment parameters. Therefore, it can be concluded that there were no issues with the calculation formula for the acquisition time used in clinical practice. In addition, as the average uptake time was 62.5 minutes, the long acquisition time did not impact other patients, and the examination could be performed within the allotted time for each patient and scheduled timeslot at our hospital. As a result, we can confidently say that the default value of 2.1 MBq/kg and the 2-minute acquisition time used in clinical practice were appropriate. However, some clinical images did not meet the evaluation criteria. For these cases, we determined that there was no significant issue, as there were no discrepancies between the two evaluation items that did not meet the evaluation criteria and the evaluation items that met the criteria.

A limitation of the study is that, during the image quality test, the actual clinical dose per body weight could not be predicted. The average weight of the 489 patients in this study was 58.2 kg, and the average dose per kilogram of body weight was 4.3 MBq/kg, with a maximum of 8.9 MBq/kg and a minimum of 1.6 MBq/kg. In the phantom study, we assumed doses of 6.2 MBq/kg, 3.2 MBq/kg, and 2.1 MBq/kg, with 2.1 MBq/kg as the default value for calculating the acquisition time in clinical practice. In clinical settings, where FDG dosages can vary among individuals, it is important to note that the results from the phantom image quality test, which assumed a lower dose of 2.1 MBq/kg, were evaluated based on this assumption. Despite this, the results demonstrated that $NEC_{patient}$, $NEC_{density}$, and Liver SNR could be calculated for the 489 patients in this study.

Conclusion

In the image quality test using the phantom, the $Q/N_{10\,mm}$ exceeded the guideline reference value when the radioactivity concentration in the background region of the phantom was 4.22 kBq/mL, 2.11 kBq/mL (1-minute acquisition), or 1.45 kBq/mL (2-minute acquisition). In addition, the recovery coefficient for the 10 mm sphere was less than 1 at all radioactiv-

ity concentrations, while it was almost 1 for the 13 mm sphere.

In the evaluation of clinical images, the guidelines were met in almost 100% of patients for $NEC_{patient}$, 100% for $NEC_{density}$, and 99.3% for Liver SNR, when the acquisition time was set to the default of 2 minutes at 2.1 MBq/kg.

Conflict of Interest

There are no conflicts of interest to disclose.

References

1) Igaku Chuo Zasshi Kankokai: List of facilities with PET, PET/CT, cyclotron, etc. Gekkan Shin-Iryo, Vol. 48, No. 3, 2021.
2) Igaku Chuo Zasshi Kankokai: List of facilities with PET, PET/CT, cyclotron, etc. Gekkan Shin-Iryo, Vol. 45, No. 3, 2018.
3) Kaneda, T: Advances in PET equipment -with a focus on semiconductor PET/CT-. Clinical Imaging, 35(8), 890-898, 2019.
4) Teoh EJ, et al.: Phantom and Clinical Evaluation of the Bayesian Penalized Likelihood Reconstruction Algorithm Q.Clear on an LYSO PET/CT System. J Nucl Med, 56(9), 1447-1452, 2015.
5) Teoh EJ, et al.: Novel penalized likelihood reconstruction of PET in the assessment of histologically verified small pulmonary nodules. Eur Radiol, 26(2), 576-584, 2016.
6) Messerli M, et al.: Impact of a Bayesian penalized likelihood reconstruction algorithm on image quality in novel digital PET/CT: clinical implications for the assessment of lung tumors. EJNMMI Physics, 5(1), 27, 2018.
7) Japanese Society of Nuclear Medicine, PET Nuclear Medicine Committee: Phantom Test Protocol for Whole-Body PET Imaging Using ^{18}F-FDG, 3rd Edition. 2018. http://www.jsnm.org/wp_jsnm/wp-content/themes/theme_jsnm/doc/FDG_WBscan_PhantomTest_20180117.pdf (2020.12.25)
8) Japanese Society of Nuclear Medicine: FDG PET, PET/CT Clinical Practice Guidelines 2020.
9) Fukuda H, et al.: Cancer FDG-PET/CT Imaging Method Guidelines, 2nd Edition. Nuclear Medicine Technology, 33, 377-420, 2013.
10) Japan Radioisotope Association: First Time Radiation Measurement. Maruzen Publishing, 2012.
11) Kangai Y, et al.: Evaluation of potentially influential factors for positron emission tomography image quality in liver signal-to-noise ratio utilizing a delivery ^{18}F-fluoro-2-deoxy-D-glucose study on $Bi_4Ge_3O_{12}$-positron emission tomography/computed tomography. Nihon Hoshasen Gijutsu Gakkai Zasshi, 70(8), 784-792, 2014.

Received August 7, 2023 ; accepted December 27, 2023

A retrospective study using the Gini coefficient to model failure of multiphase motorized contrast injectors in angiography

KAKUTA Kazuya[1, 3)*], MINAKAWA Takahiro[2)], NEMOTO Shumpei[3)], IKEDA Masamitsu[3)]

1) Department of Disaster Medicine, Fukushima Medical University Hospital
2) Department of Radiology, Takeda General Hospital
3) Department of Radiology, Fukushima Medical University Hospital

* E-mail: kakuta-k@fmu.ac.jp

Note: This paper is secondary publication, the first paper was published in the JART, vol. 71 no. 859: 40-44, 2024.

Key words: angiography, injector, Gini coefficient, failure, Lorenz curve

【Abstract】
Multiphase contrast injectors are used for diagnosis and treatment in angiography. Maintenance and inspection of multiphase contrast injectors must be performed without exception. In this study, we retrospectively examined injector failures that occurred between one regular inspection and the next regular inspection, and we evaluated the non-uniformity of the occurrence of injector failures. A retrospective histogram analysis was performed on the number of days from the periodic inspection date to the repair date of multiphase contrast injectors, and the Gini coefficient was calculated from the Lorenz curve. Although the timing of repairs was uneven, increasing failure rate-type failures in the failure rate function increased when injectors were used beyond their useful life. Combining daily inspections and periodic inspections with operational checks can be expected to prevent failures of multiphase contrast injectors.

Introduction

Multiphase motorized contrast media injectors used for angiography (hereinafter referred to as "injector") fall under the category of specially-designated medical devices requiring maintenance as defined in Article 2, Paragraph 8 of the Act on Securing Quality, Efficacy and Safety of Products Including Pharmaceuticals and Medical Devices[1)]. The term "specially-designated medical devices requiring maintenance" as used in this Act refers to medical devices designated by the Minister of Health, Labour and Welfare (MHLW) after seeking the opinion of the Pharmaceutical Affairs and Food Sanitation Council as those requiring special knowledge and skills for their maintenance, inspection, repair, and other related work owing to the significant potential risk to the diagnosis, treatment, or prevention of disease in the event of failure to provide proper maintenance. In addition, the section on the maintenance and inspection of the injector's attachment states that maintenance and inspection should be performed to maintain the performance of the device and ensure safety[2, 3, 4)]. Maintenance and inspection include daily inspections by the user and periodic inspections by a contractor[5)]. These are called preventive maintenance. Daily inspections are performed by the persons associated with the medical equipment, and periodic inspections are performed at regular intervals. The purpose of these regular operations is to ensure the safety, performance, and reliability of medical devices.

Maintenance and inspection services in the laws and regulations are based on the statement in Article 15-3, Paragraph 2 of the Medical Care Act, which states, "Beyond what is provided for in the preceding paragraph,

when the administrator of a hospital, clinic, or birthing center wishes to entrust the operation of the hospital, clinic, or birthing center that are prescribed by Cabinet Order as having a significant influence on physicians' or dentists' diagnoses, on the services of midwives, or on the hospitalization or admission of patients, pregnant women, women in labor, or women resting after childbirth, the administrator must entrust the relevant operations to a party who meets the requirements prescribed by an Order of the MHLW as a party with the ability to properly undertake these operations according to the type of operation undertaken at the relevant hospital, clinic, or birthing center [6]." This structure is supplemented by the Order for Enforcement of the Medical Care Act and the Enforcement Regulations on the Medical Care Act. Article 4-7, item 4 of the Order for Enforcement of the Medical Care Act defines "maintenance and inspection services for medical devices specified by an Order of the MHLW",[7] and article 9-8-2 of the Enforcement Regulations on the Medical Care Act indicates that "Medical devices prescribed by Order of the MHLW" [8] are "specially-designated medical devices requiring maintenance" as defined in the aforementioned Act on Securing Quality, Efficacy and Safety of Products Including Pharmaceuticals and Medical Devices. The Medical Affairs Bureau of the MHLW has issued a regulation stating that "In using medical devices, the methods of use specified by the manufacturer and seller of the medical device should be observed". Therefore, the person responsible for the safety management of medical devices must organize and manage information on the safe use, maintenance, and inspection of medical devices, such as the accompanying documents and instruction manuals of medical devices [9, 10]. Moreover, the safe use of medical devices requires that medical personnel has a solid understanding of how to use medical devices and respond calmly and appropriately to any problems that may arise. The aim of maintenance and inspection is to decrease the probability of medical equipment malfunctions and other abnormalities, and to increase the probability that normal conditions will be maintained through early identification of abnormal conditions and detection of minor malfunctions. However, in our survey, we found no reports discussing the maintenance and inspection of injectors. The aim of this study was to evaluate the heterogeneity in the occurrence of injector failures by conducting a retrospective study of failures that occurred between one periodic inspection and the next periodic inspection.

1. Methods

1-1. Target of the survey

The survey targeted injectors used for arterial injection of contrast media in an angiography room, totaling six devices: three PRESSPRO® installed in February 2009, one PRESSPRO GEO-150® installed in February 2009, and two PRESS DUO Elite® installed in December 2020 (Nemoto Kyorindo, Tokyo, Japan). These injectors are inspected annually at the same time by a contractor (Nemoto Kyorindo) meeting the requirements stipulated in Article 9-12 of the Enforcement Regulations on the Medical Care Act[8]. During periodic inspections, the vendor replaces protective cases, keypads, key covers, flexible cables, and connectors. In addition, motor screws are retightened and ball screws are greased as necessary. The study period was from January 1, 2010 to March 31, 2022, and the dates of repairs and periodic inspections were recorded from the reports of periodic inspections and repairs during this period.

1-2. Calculation of the Gini coefficient

The number of repair reports was assumed to be the number of repairs. The approximate number of classes was obtained using the

Sturges formula (1):

$$\text{Number of classes} \approx 1 + \log_2 \text{number of repairs} \quad \cdots (1)$$

The period from the regular inspection date to the next regular inspection date was set as one year, and the classes were set to approximate the calculated number of classes. The class defined here is the number of days since the regular inspection date. The frequencies, relative frequencies, and cumulative relative frequencies for each class were determined, and Pareto charts were created. Cumulative relative frequencies were obtained for each class and number of repairs, and Lorenz curves were constructed. The Gini coefficient (GC) was calculated from the Lorenz curve and the line of equality using equation (2):

$$\mathrm{GC} = \frac{1}{2n^2\bar{y}} \sum_{i=1}^{n} \sum_{j=1}^{n} |y_i - y_j| \quad \cdots (2)$$

where GC is the Gini coefficient, n is the number of classes, y_i and y_j are the mean within the i, j [th] class from the bottom ($y_1 < y_2 < \ldots < y_n$), and $\bar{y}$ is the mean value.

By setting t as the number of days since installation and considering the failure rate as a function of time $\lambda(t)$, it is possible to draw a failure rate curve. The failure rate curve, also called the bathtub curve because it resembles the shape of a bathtub, models the failure rate of medical equipment [11, 12, 13].

Failure rate curves can contain three periods with a different change in the failure rate with time t. The first is an early period characterized by a decreasing failure rate (DFR), known as early failure. During this period, individual countermeasures are effective against early failures. The reasons for DFR include the use of defective materials, occurrence of defects during manufacturing, mismatch with the external operating environment, and inadequate handling during transportation. Debugging, such as screening to remove defective products in advance, aging for stabilization, and break-in operation, is effective in reducing initial failures. The second is a period characterized by a constant failure rate (CFR). During the CFR period, the failure rate has stabilized and countermeasures have been completed. The causes of failures during this period are unknown, and it is difficult to predict when failures will occur. Moreover, failures cannot be removed by debugging. The third is a period characterized by an increasing failure rate (IFR), known as wear failure. During this period, the failure rate increases owing to wear, fatigue, and deterioration of components. Therefore, preventive maintenance, such as replacing parts that have reached the end of their service life before failure occurs, is important[14]. The duration of the DFR, CFR, and IFR periods depends on the shape parameter m, which specifies the shape of a particular population distribution. In this case, the failure rate function $\lambda(t)$ can be described by equation (3):

$$\lambda_{(t)} = \frac{m}{\eta}\left(\frac{t-\gamma}{\eta}\right)^{m-1} e^{-\left(\frac{t-\gamma}{\eta}\right)^{m}} \quad \cdots (3)$$

where $\lambda(t)$ is the failure rate function, t is the number of days to repair, m is the shape parameter, γ is the position parameter, and η is the scale parameter. Scale parameter η determines the abscissa scale of $\lambda(t)$, and position parameter γ is related to the peak position of the distribution.

In equation (3), when η is set to 1 and γ to 0, the failure rate function $\lambda(t)$ depends only on the shape parameter m, as shown in equation (4):

$$\lambda_{(t)} = mt^{m-1}e^{-t^m} \quad \cdots (4)$$

Therefore, DFR occurs when $0 < m < 1$, while CFR occurs when $m = 1$, and IFR occurs when

$1 < m$.

2. Results

2-1. Survey results of periodic inspection dates and repair dates

The number of repairs was 11 during the study period. Table 1 shows the failure details. Among the six injectors surveyed, each of two injectors was repaired four times. The operation panel accounted for the highest percentage of malfunctions, which was 36.4%. Loose heads and partially damaged heads were next, accounting for 18.2% of malfunctions. Caster damage, syringe failure, and discrepancy between input and output volumes accounted for 9.1% of the failure cases.

2-2. Gini Coefficient

According to Equation (1), the number of classes was approximately 5. Therefore, the classes were set to 70 (repairs performed from 1 to 70 days after the maintenance inspection date), 140 (repairs performed from 71 to 140 days after the maintenance inspection date), 210 (repairs performed from 141 to 210 days after the maintenance inspection date), 280 (repairs performed from 211 to 280 days after the maintenance inspection date), and 365 (repairs performed from 281 to 365 days after the maintenance inspection date. Repair was performed from 365 days after the maintenance and inspection date. The frequency, relative frequency, cumulative frequency, and cumulative relative frequency against the number of days between the periodic inspection date and the repair date are shown in Table 2 and the Pareto chart in Fig. 1. The frequencies were higher for the 140 and 280 classes than the other classes, and the corresponding cumulative relative frequencies also changed steeply. The Lorenz curve is shown in Fig. 2. The GC, calculated using equation (2), was 0.33.

Table 2 Frequency, relative frequency, cumulative frequency, and cumulative relative frequency against the number of days between the periodic inspection date and repair date

Number of days	Frequency	Relative frequency	Cumulative frequency	Cumulative relative frequency
1 – 70	2	0.18	2	0.18
71 – 140	3	0.27	5	0.45
141 – 210	1	0.09	6	0.55
211 – 280	3	0.27	9	0.82
281 – 365	2	0.18	11	1

Table 1 Repair details for each multiphase motorized contrast media injector

Case	Injector	Number of days from the inspection date (days)	Failure content
1	PRESSPRO	111	Poor interlocking
2	PRESSPRO	116	Poor interlocking
3	PRESSPRO	331	Loose head
4	PRESSPRO	202	Caster damage
5	PRESSPRO GEO	262	Defective syringe
6	PRESSPRO	64	Poor interlocking
7	PRESSPRO	231	Mismatch between input and output values
8	PRESSPRO	347	Broken parts
9	PRESSPRO	229	Loose head
10	PRESS DUO Elite	3	Poor interlocking
11	PRESS DUO Elite	73	Broken parts

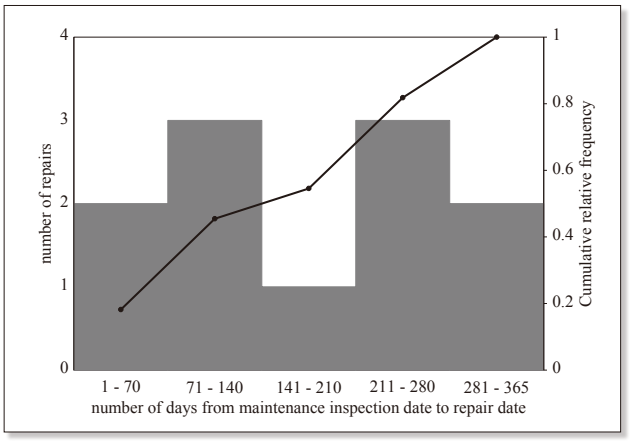

Fig. 1 Pareto chart

The repair frequency of each class is shown as a bar graph, and the cumulative relative frequency as a line graph.

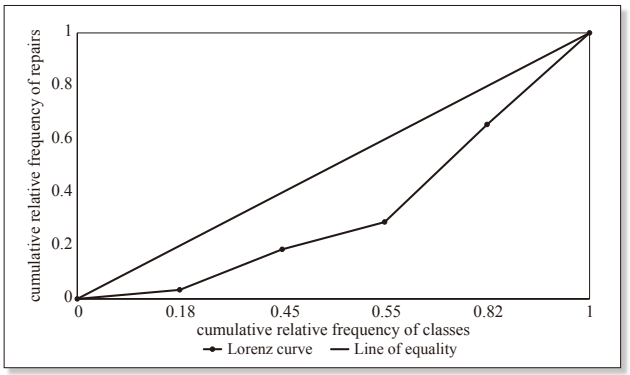

Fig. 2 Lorenz Curve

The upper straight line is the equal distribution line, and the lower solid line is the Lorenz curve obtained in this study.

3. Discussion

Table 1 shows that 8 of the 11 failures occurred in two PRESSPRO units installed in 2009. Because this is a retrospective study, it is assumed that failures arise from a mixture of normal use and human factors. In particular, caster damage, syringe defects, and partial damage may be attributed to human factors. The Pareto chart in Fig. 1 indicated that the relationship between the number of repairs and the number of days from the periodic inspection date to the repair date was represented by a bimodal histogram. Hence, failures requiring repair occurred within the periods of the 140 and 280 classes (days after the periodic inspection). GC represents the "heterogeneity" calculated from a Lorenz curve drawn using two cumulative relative frequencies, as used in economics[15] and in pattern recognition and machine learning[16]. The Lorenz curve was constructed with the cumulative relative frequency of repairs in each class on the horizontal axis and the cumulative relative frequency of repairs on the vertical axis. If the number of repairs occurs uniformly in each class, then the Lorenz curve coincides with a straight line with a slope of 45 degrees passing through the origin (line of equality). The more inhomogeneous it is, the further away from the equal distribution line it is. GC is one of the representative indicators for objectively analyzing and comparing inequality[17]. GC represents the evenness of distribution by the ratio of the area bounded by the Lorenz curve and the line of equality to the area of the triangle below the line of equality. GC takes values between 0 and 1. GC approaches 1 when the inter-sample difference is large and approaches 0 when it is small. It should be noted that even for the same GC, the inequality changes when the shape of the Lorenz curve differs[18]. As a practical guide, GC less than 0.2 indicates absolute uniformity, GC in the range of 0.2–0.3 indicates high uniformity, GC in the range of 0.3–0.4 indicates inhomogeneity, GC in the range of 0.4–0.6 indicates high inhomogeneity, and GC equal to 0.6 and above indicates absolute inhomogeneity[19, 20]. According to the Lorenz curve shown in Fig. 2, GC was 0.33, indicating that failures occurred inhomogeneously. Failures in the 70 and 140 classes were DFR-type failures because $\lambda(t)$ was observed in the range of $0 < m < 1$, while failures in the 210 class shifted to CFR-type failures because $\lambda(t)$ was observed when $m = 1$, and failures of the 280 and 365 classes were IFR-type failures because $\lambda(t)$ was observed when $1 < m$.

One of the two PRESS DUO Elite units installed in 2020 did not require repair during the study period. The other PRESS DUO Elite

unit required repair within a short time after its installation, and thus the failure likely occurred during the DFR period. The PRESS PRO units have been used for more than its service life, and thus failures of these units during the study period were likely IFR-type failures. Angiography and interventional radiology technologists are required to assure and control the quality of related equipment[21]. The largest proportion of interlocking failures in the results are failures that affect interventional radiology procedures. These malfunctions have a significant impact on patient examination and treatment, including difficulty in obtaining quantitative contrast images and interrupted examinations. Although detecting malfunctions before the procedure begins is desirable, it is difficult to achieve. Based on the above results, malfunction prevention and recurrence prevention are important when considering quality assurance of injectors in the future. Prevention of malfunctions refers to identifying potential problems that may occur with the use of the device before the procedure is performed and taking measures to prevent them from actually occurring. Prevention of recurrence is a measure to eliminate the cause of a problem that has already occurred or the influence of the cause so that it will not recur, including corrective measures. The items to be inspected, the period of time, and the evaluation criteria should be updated as guidelines are revised and new devices and treatment methods are introduced[22]. Daily inspections, including visual and operational inspections, by radiological technologists who use the injectors can prevent the occurrence of malfunctions during procedures. Early detection of malfunctions can prevent secondary and tertiary malfunctions and shorten downtime because the injector can be repaired before it becomes a malfunctioning equipment that requires a long time to repair. When secondary or tertiary failures occur, it is extremely difficult to identify the cause of the failure, and repair is time-consuming and economically expensive. Daily inspections are important to ensure that equipment is always maintained in the best possible condition[23].

The limitations of this study include the small sample population because only cases in which repair reports were generated were considered as failures, analysis was not conducted for each injector, and cases in which recovery was achieved by restarting the injector were excluded. Future research will focus on analyzing the logs of each injector to conduct more detailed failure analysis.

4. Conclusion

A backward histogram analysis was performed on the number of days from the injector's periodic inspection date to the repair date, and the GC was calculated. Repair dates were heterogeneous, although IFR-type failures increased when injectors were used beyond their service life. A combination of daily and periodic inspections, including operational checks, is expected to prevent injector failures.

Acknowledgments

A partial abstract of this study was presented at the 79th Annual Meeting of the Japanese Society of Radiological Technology held on April 16, 2023. We thank Edanz (https://jp.edanz.com/ac) for editing a draft of this manuscript.

Conflicts of Interest

The first author and all co-authors have no conflicts of interest to disclose.

References

1) Act on Securing Quality, Efficacy and Safety of Products Including Pharmaceuticals and Medical Devices. Act No. 145. [Accessed: 5 November, 2022]
2) PMDA: Contrast Injection System PRESSPRO GEO-150. https://www.info.pmda.go.jp/downfiles/md/PDF/610006/610006_227ABBZX00010000_A_01_01.pdf. [Accessed: 5 November, 2022]
3) PMDA: Contrast Injection System PRESS DUO elite. https://www.info.pmda.go.jp/downfiles/md/PDF/610006/610006_230ABBZX00059000_A_01_01.pdf. [Accessed: 5 November, 2022]
4) PMDA: Contrast Injection System Arcatena. https://www.info.pmda.go.jp/downfiles/md/PDF/610006/610006_301ABBZX00020Z00_A_01_01.pdf. [Accessed: 5 November, 2022]
5) Inomata H. Reasons why maintenance and upkeep are necessary, rationale for frequency, benefits, etc. https://www.mhlw.go.jp/shingi/2009/07/dl/s0710-8e.pdf. [Accessed: 5 November, 2022]
6) Medical Care Act. Act No. 205. [Accessed: 5 November, 2022]
7) Order for Enforcement of the Medical Care Act. [Accessed: 5 November, 2022]
8) Enforcement Regulations on the Medical Care Act. [Accessed: 5 November, 2022]
9) Director, Regional Medical Planning Division, Medical Policy Bureau, Ministry of Health, Labour and Welfare. Operational considerations for ensuring systems for safety management related to medical devices. Medical Affairs Bureau, No. 0612 No. 1, June 12, 2018.
10) Director-General of the Medical Policy Bureau, Ministry of Health, Labour and Welfare. Partial Enforcement of the Act for Partial Revision of the Medical Service Act, etc. for the Purpose of Establishing a System for Providing High-Quality Medical Care. Medical Policy Bulletin No. 0330010, March 30, 2007.
11) JCS. Guidelines for usage and maintenance of equipment in cardiovascular diagnosis and treatment. 2009.
12) Nakane S. Specific analysis methods for extending the service life of sewer pipes <Part 2>. Journal of sewerage monthly, Vol 32, No 13, 56-63, 2009.
13) Japanese society of radiological technology. Interventional Radiologic Technology. 132-140, 2015.
14) Hosoya K. Textbook for QC Certification Examination Level 1. JUSE Press, 404-13, 2021.
15) Kimura K. Decomposition of the Gini coefficient. Quarterly Journal of Economics, Hokkai-Gakuen University, Vol 68, No 3&4, 29-56, 2021.
16) Iiyama M. Usable! Statistical Tests and Machine Learning—IV: Pattern Recognition Using Random Forests. Systems/Control/Information, Vol 59, No 2, 71-6, 2015.
17) Ito N, et al. Evaluation of the Gini coefficient extended to the case of negative sample totals. Theory and Methods, Vol 27, No 1, 117-30, 2012.
18) Matsubara N, et al. Introduction to Statistics, 17-40, Tokyo University Press, 2009.
19) Fujiwara K, et al. Trends for the Geographic Distribution of Radiological Resources in Hokkaido, Japan: Data Analysis Using Gini Coefficient and Herfindahl-Hirschman Index. Japanese Journal of Radiological Technology, Vol 72, No 10, 970-7.
20) Ameryoun A, et al. The assessment of inequality on geographical distribution of Non-cardiac intensive care beds in Iran. Iranian J Public Health, 40, 25-33, 2011.
21) Japanese Society of Interventional Radiology. Recommendations on the Practice System for Performing IVR Procedures. https://www.jsir.or.jp/wp-content/uploads/2017/ 07/ivr_syugiteigen-20170708.pdf. [Accessed: 5 November, 2022]
22) Murakami S, et al. QA/QC for high-precision radiation therapy ~Safety and treatment accuracy upwards~. J Kyorin Med Soc, Vol 51, No 2, 139-49, 2020.
23) Oishi R, et al. Efficacy of maintenance service of dialyzer device carried out by clinical engineer. The Showa University Journal of Medical Sciences. Vol 80, No 1, 19-28, 2020.

Received October 5, 2023; accepted March 27, 2024

Effectiveness of pre-shots in general radiography as considered from the management of loss images

FUKUDA Tomoya[1)]*, ISHIMOTO Tomohiro[2)], NARUSE Noriyasu[1)], KOBAYASHI Katsunori[1)]

1) Department of Radiological Technology, Japan Organization of Occupational Health and Safety Asahi Rosai Hospital Radiological technologist
2) Department of Radiological Technology, Japan Organization of Occupational Health and Safety Chugoku Rosai Hospital Radiological technologist

* E-mail: staroh@yahoo.co.jp

Note: This paper is secondary publication, the first paper was published in the JART, vol. 71 no. 864: 28-34, 2024.

Key words: shot miss rate, lateral view of the knee joint, low-dose pre-shot, retake, reshot

【Abstract】
The introduction of software has made it easy to calculate the number of shots and the shot miss rate in general radiography.

In the data for 2021, the overall shot miss rate was 11.4%. By imaging menu, the highest shot miss rate overall was seen in the lateral view of the knee joint, exceeding 40% for the standing lateral view of the knee joint. We tried the method of taking a low-dose pre-shot on the lateral view of the knee joint, because of its high shot count and high miss rate, and then taking normal shots after confirming the position. After introducing the pre-shots, the shot miss rate decreased, but was still above zero even after taking pre-shots.

The success and failure of the first normal shot taken before introducing pre-shots and the first pre-shot image were compared as first shots. The results indicated that for situations in which the shot miss rate is high, pre-shots are effective and do not affect the imaging technique.

Introduction

The medium for general radiography, a type of radiological examination, has undergone a transition from analogue film screen systems to digital devices such as computed radiography (CR) and flat panel detectors (FPD). In recent years, advances in equipment have rendered it feasible to ascertain the status of device utilization and the number of shots per menu. In the context of the film screen system, if a film required re-shot, the film purchase cost was forfeited, and the term 'radiographic loss film' (henceforth referred to as 'x-ray image loss') was employed. In the contemporary era, with the advent of digital equipment, the medium of film has been superseded by data, Nevertheless, the term 'X-ray image loss' remains in current usage. In this paper, the term 'miss shot' is employed to denote the phenomenon of X-ray image loss.

As demonstrated in the findings of the 1992 survey on miss shot in film screen systems [1)], the predominant cause of miss shot was identified as an error in the shoting conditions. In other cases, there were also reports of loss of film due to equipment failure, with a miss shot rate of 4%. In the context of film, the miss shot can lead to an increase in the incident surface dose as the same image is repeatedly captured. Patient waiting times were longer and also needed to be as low as possible due to the loss of film purchase costs. Digital systems are filmless, which makes re-shoting easier than with film screens. Consequently, an increase in miss shots is to be expected.

The use of the pre-shot method was considered to reduce the miss shot rate of current digital systems. In this method, low-dose radiography is performed first, followed by adequate patient positioning before normal imaging begins. The low-dose radiography is hereafter referred to as 'pre-shot'.

Re-shot is also sometimes described as failed radiograph, re-radiograph or re-imaging, but in this paper, re-shot is used as a unifying term.

1. Preliminary investigation

ASSISTA Management (Fujifilm Medical, Tokyo, Japan) is a system designed for the management of FPDs. The uploading of various conditions during radiography to the data center results in the automatic organization and display of data in graphs and lists with various analysis axes. The number of miss shots, miss shot rate, and the respective site and engineer can also be extracted, so the data before and after the start of the pre-shot were compared.

The term 'pre-shot' refers to the process of acquiring a preliminary image under low-dose conditions once the body position for the area to be radiographed has been determined. This is followed by the acquisition of the normal shot once the body position is confirmed to be satisfactory. In the event that this proves to be inadequate, the subsequent step involves re-establishing the position. Following the completion of a pre-shot confirmation procedure, the process of normal shoting may be initiated once it has been ascertained that the position is adequate.

In order to ascertain the shooting menus to be pre-shot, miss shot rates for each menu were calculated using data from April to September 2021. As demonstrated in Figure 1, imaging of the knee joint was predominant, occupying the top one to four positions. However, it was determined that menus with a limited number of inspections and an elevated X-ray miss shot rate exerted negligible influence on the aggregate number of inspections. Consequently, these menus were excluded from the present survey, which was conducted with the number of shots taken into consideration.

Pre-shots were initiated on the standing lateral view of the right knee joint, standing lateral view of the left knee joint, lying lateral view of the right knee joint and lying lateral view of the left knee joint, which are the menu areas with the highest miss shot rate. The pre-shot images were judged to have too high an S-value, a measure of sensitivity used to stabilize image density, to be of a quality that could be used for diagnostic imaging. For this reason, the images are not stored on the server as reference images and are not treated as miss shot. A record of the dose is kept for both normal miss shot and pre-shot images.

2. Method

2-1 X-ray shoting conditions of the knee joint

The hospital uses an FPD system. Shoting conditions were a tube voltage of 55 kV, tube

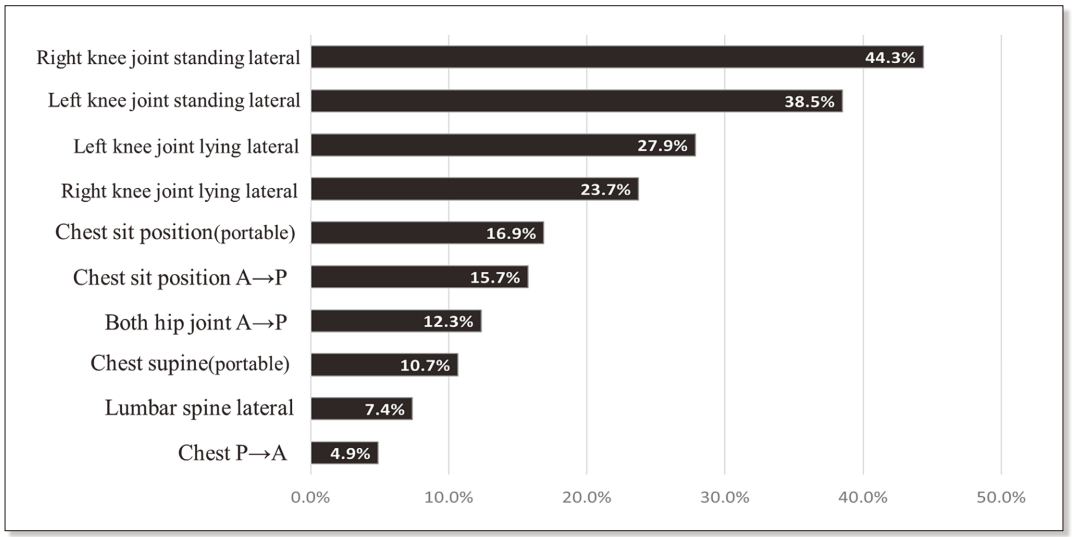

Fig. 1 Shot miss rate for each imaging menu

current time product of 6 mAs and a Cu 0.1 mm additive filter. The distance between the focus and receiver was 120 centimetres, and the incident surface dose was calculated by multiplying the incident surface air kerma, a value calculated by PCXMC [2], by the backscattering coefficient. The incident surface dose for the knee joint is thus 0.052 mGy. For pre-shot shoting conditions, the tube voltage is 55 kV, as in normal radiography. The tube current time product was set to 0.5 mAs, given that the minimum exposure time of the imaging system is 0.5 msec. The additional filter was also the same as for normal radiography. It was determined that the pre-shot images should have an incident surface dose as low as possible. Following a thorough visual evaluation by the technicians, it was determined that the dose should be set at approximately one-twelfth of the normal dose, in order to confirm the misalignment of the medial and lateral condyles.

The study was approved by the Ethics Committee of the hospital (reception number 05-07).

2-2 Definition of re-shot

Given that there are no technologists in the hospital who have been with the company for less than five years, the decision to re-shot is made by the radiological technologists themselves. In the majority of cases, multiple individuals are involved in an X-ray shot, and in such instances, re-shot may be conducted based on a consensus among the involved parties. The knee joint lateral view acceptance criteria are as follows: an acceptable misalignment of medial and lateral condyles is 7 mm [3].

2-3 Comparative period

The study design was that of a case-control study, and data were collected retrospectively. The period of no pre-shot was defined as the period from April 2021 to December 2021 ('2021') at this hospital, and the period from January 2022 to December 2022 ('2022') was defined as the pre-shot period.

2-4 Verification of changes in miss shot rate before and after the start of pre-shot

In the preliminary investigation depicted in Figure 1, the shoting menus that exhibited the highest miss shot rate were identified as the left and right standing lateral views of the knee joint, as well as the left and right lying lateral views of the knee joint. Consequently, a pre-shot was meticulously prepared for each shoting menu, and the miss shot rates before and after the initiation of the pre-shot were subjected to rigorous scrutiny.

The objective of this study is to reduce the miss shot rate. To this end, an investigation was conducted into how the pre-shot of the knee joint changed the overall miss shot rate in 2021 and 2022.

2-5 Comparative studies between groups with different numbers of shots

The relevance of miss shots was investigated as a group of three technicians who mainly perform general radiography (Group A) and a group of nine technicians who mainly perform modalities such as CT and MRI and take fewer general radiographs (Group B), although all 12 technicians are responsible for general radiography. In 2021, the mean number of knee joint lateral views obtained was 200 in Group A and 40 in Group B. There is no turnover of technicians between groups within the period under comparison.

2-6 Verification of pass criterion

In pass criterion for knee joint lateral views was also verified in images taken at the request of orthopedic surgeons and in images that had not been operated on, among the images stored on the server during the period indicated in 2-3. The displacement of the Medial and Lateral Condyles was measured using a 21.3-inch, 2-megapixel monitor, and the mean and standard deviation of the measurements were calculated.

Table 1 2021 and 2022 protocol design
Comparing of success and failure of the first normal shot and pre-shot

year	case	1st shot	2nd shot	3rd shot
2021	Success on the first shot	Normal shot success	-	-
	Success on the second shot	Normal shot mistake ⇨	Normal shot success	-
2022	Success on the first shot	Pre-shot success ⇨	Normal shot success	-
	Success on the second shot	Pre-shot mistake ⇨	pre-shot success ⇨	Normal shot success

2-7 First shot verification

By using a low-dose pre-shot, it was also necessary to verify whether the initial position setting was not inappropriate, as if the patient was just trying to take a shot at first. The first shot is referred to as the first shot (hereafter referred to as '1st shot'), and we examined how the ratio of successes and failures of the 1st shot changed between 2021 and 2022.

Table 1 shows the protocol for the sequence of shots in 2021 and 2022, where the 1st shot in 2021 is the normal shot; if the 1st shot is a miss (mistake), the normal shot is continued in the 2nd shot.

The 1st shot in 2022 refers to the pre-shot. Even if the pre-shot is successful (success), the normal shot of the 2nd shot is required. If the first shot fails, a pre-shot is taken on the second shot, followed by a normal shot.

A comparison was made between the successes and failures of the first shot in 2021 and 2022 in order to verify whether the position settings in the pre-shot were inappropriate.

The pre-shot data has not been registered as a miss shot. Consequently, verification was conducted using image data in the CR console, where patient information and other data pertaining to general radiography equipment is recorded and image confirmation is performed. This procedure was undertaken instead of during the specified period indicated in 2-3. Note that the data in the CR console is only stored for about two months. Consequently, the data preceding the initiation of the pre-shot was also designated for the same period, i.e. from October to December 2021. The data subsequent to the initiation of the pre-shot period was collected from October to December 2022.

2-8 Statistical analysis

Statistical analysis was conducted utilizing the College Analysis Ver. 8.6 software program developed by Fukui. [4] Due to the limited number of radiological technologist, miss shot rates were not subjected to statistical analysis for mean values. However, a chi-square test was employed for each group to ascertain the existence of an association between the differences in the aggregate results. Wilcoxon's rank sum test was utilized to assess the discrepancy between medial and lateral condyles, given the distribution's non-normal nature. The significance level was set at 1%, with $P < 0.01$ denoting a statistically significant difference.

3. Result

3-1 Variation in miss shot rate by menu in the knee joint lateral view

As illustrated in Table 2, the miss shot rates for different menus of the knee joint are shown for the comparison period. The miss shot rate prior to the pre-shot was 44.2% for the right knee joint standing lateral view, 25.0% for the right knee joint lying lateral view, 37.8% for the left knee joint standing lateral view and 27.9% for the left knee joint lying lateral view. After the pre-shot was started, the data showed that

Table 2 Before pre-shot (2021) and after pre-shot (2022) for shot miss rate (Only lateral view of the knee joint)

Year	site	Number of shots	Miss shots	Shot miss rate (%)
2021	Right - Standing lateral view	208	92	44.2
	Right - Lying lateral view	364	91	25.0
	Left - Standing lateral view	188	71	37.8
	Left - Lying lateral view	394	110	27.9
2022	Right - Standing lateral view	192	10	5.2
	Right - Lying lateral view	248	26	10.5
	Left - Standing lateral view	170	8	4.7
	Left - Lying lateral view	233	25	10.7

5.2% of the patients had a right knee joint standing lateral view, 10.5% had a right knee joint lying lateral view, 4.7% had a left knee joint standing lateral view and 10.7% had a left knee joint lying lateral view.

3-2 Changes in miss shot rates across the whole of general radiography

The overall miss shot rates for general radiography in 2021 and 2022 are shown in Table 3. The overall miss shot rate prior to the initiation of the pre-shot was 11.7%, however, by 2022, when the knee joint pre-shot was initiated, the miss shot rate had decreased to 7.3%.

Table 3 Before pre-shot (2021) and after pre-shot (2022) for shot miss rate

Year	Number of shots	Miss shots	Shot miss rate (%)
2021	11907	1395	11.7
2022	8087	589	7.3

Table 4 Shot miss rate of lateral view of the knee joint in 2021 and 2022

year		Success image	Failure image	Mean (%)
2021	Group A	523	242	31.6
	Group B	267	122	31.4
				P = 0.910
2022	Group A	581	40	6.4
	Group B	193	29	13.1
				P = 0.017

All technologist had been employed for at least five years, so lack of experience was not thought to be a factor

3-3 Compare the miss shot rate of the knee joint lateral view between groups with different numbers of shots

The results of the miss shot rates for the entire knee joint lateral view in 2021 and 2022 in Group A and Group B are shown in Table 4. In 2021, the miss-shot rate in Group A was 31.6% and in Group B 31.4%. The miss shot rate in 2022 after the start of pre-shot decreased to 6.4% in Group A and to 13.1% in Group B. The findings of the 2021 test yielded P = 0.910, and the 2022 results also demonstrated P = 0.017, indicating that there were no statistically significant differences between the groups

Table 5 Investigation of misalignment between the medial and lateral condyles

year	Standing position (mm)		Lying position (mm)	
	AV	SD	AV	SD
2021	3.78	2.60	3.90	2.71
2022	3.36	2.11	3.67	2.41
	P = 0.130		P = 0.483	

3-4 Verification of pass criteria

Table 5 shows the results of examining the pass criteria for medial and lateral condylar misalignment before and after the start of the pre-shot. A decrease was observed from 3.78 mm to 3.36 mm in the standing position and from 3.90 mm to 3.67 mm in the supine position, but no significant difference was detected.

Table 6　1st shot for knee joint lateral view

year	site	Success	Misstake	Shot miss rate (%)
2021 (Normal shot)	standing lateral view	69	62	47.3
2022 (Pre-shot)		32	39	54.9
				P = 0.302
2021 (Normal shot)	lying lateral view	202	83	29.1
2022 (Pre-shot)		84	91	52.0
				$P = 9.01 \times 10^{-7}$

3-5　Comparison of first shots

Table 6 shows the results of the 1st shot in the standing and lying positions.

In the standing position results, there were 69 successful and 62 unsuccessful first shots in 2021.

In 2022, the number of cases where the initial pre-shot was successful and proceeded to a normal shot was 32, while the number of cases where two or more pre-shots were made and a re-take was necessitated due to an error was 39. The respective successes and failures were then subjected to calculation using the chi-square test, P = 0.302, and it was established that no significant differences were found.

Similarly, in the lying position results, there were 202 successful first shots and 83 failures in 2021, and in 2022 there were 84 successful first pre-shots and 91 pre-shots that were re-worked and pre-shot two or more times. When testing whether there was an association between each success and failure, $P = 9.01 \times 10^{-7}$, $P < 0.01$, which was a significant difference and rejected the association. In other words, in the lying position, it was found that pre-shotting the first shot was associated with more miss shots.

4. Consideration

4-1　Miss shot rate of the lateral view of the knee joint in 2021

In a preliminary survey, the most frequently photographed areas were listed in order of frequency, and the lateral view of the knee joint was the top photographed area with the highest miss rate. In our hospital, we only have standing and lying lateral views and no other imaging methods, but in the previous hospital, in addition to the usual standing and lying lateral views, we also had gravity sag view imaging [5] and extensional lateral views, which sometimes resulted in multiple photographic losses in the same patient. Although there are no special radiographic techniques at this hospital, lateral radiographic techniques for total joint replacement [6)-8)] were performed with the same meticulous care as at the previous hospital, including the overlap of the two pegs of the femoral component. Increasingly, orthopedic surgeons requesting imaging are demanding accuracy and reproducibility of frontal and lateral views. The reason for this is that when checking the condition of the bone cement that holds the artificial joint in place, if the artificial joint is radiographed at an angle, the bonding area between the cement and the artificial joint may not be visible. Orthopedic surgeon ordered a re-shot, and the discrepancy in the image was checked and found to be 2.5 mm. This figure is smaller than the average value for displacement in knees without a history of artificial joint surgery presented in Table 5 and is thought to reflect the missed shot rate from the 2021 survey, as more reproducibility is required.

4-2 Knee miss shot rate in 2021 and 2022

The results for the missed shot rate in 2021 show a significant decrease in 2022 after the start of the pre-shot, but as the 2022 data in Table 2 shows, missed shots did not disappear completely. In the case of emergency radiography where the pre-shot was not used, or in the standing lateral view, the body was supported by placing the non-examined side on an aid and holding a grip stick with both hands, but in some cases the body could not be held in position after the pre-shot and moved, resulting in a re-shot. Human error was also a factor, with the pre-shot menu being mixed with the normal shot menu. The sequence of shots is frontal, lateral and axial, but in some cases the order of the shots was changed due to the patient's condition, which also changed the order of the pre-shot menu, leading to errors.

4-3 Effects of different numbers of shots on the miss shot rate

The results of the comparison of the missed shot rate between the high and low shot groups showed no significant differences in 2021 and 2022. The results suggest that the missed shot rate is high even for technicians with 7-8 years of experience, regardless of the number of shots taken, and even for technicians who take a lot of general radiographs. After the start of pre-shots, the number of missed shots was slightly higher in group B, although there was no significant difference in the missed shot rate between the groups. This was attributed to the fact that fewer emergency shots were taken at night or on holidays in group A, and more were taken in emergency situations in group B than in group A.The use of pre-shots for emergencies will be considered in the future, if necessary.

4-4 Views on the increase in the overall miss shot rate

It is indisputable that the lowest possible miss shot rate is desirable, but re-shots are increasing in practice. In 1992, the miss shot rate was 4% when the film screen was in use, but with the switch to a digital system, the miss shot rate in this hospital was 11% in 2021.

The fact that digital systems can be easily re-shot is considered to be a contributing factor to the increased miss shot rate. As demonstrated in Table 2, the 2021 study revealed a miss shot rate of 44.2% for the right knee joint in a standing lateral view, indicating that approximately one in two patients required re-shooting. Furthermore, the miss shot rate for the lying lateral view of the right knee joint was 25.0%, suggesting that approximately one in four patients experienced re-shoting. In short, it is an area where mistakes are made.

After the start of pre-shots in 2022, the proportion of re-shots was around 5% in the standing lateral view and 10% in the lying lateral view, thus reducing the proportion of re-shots. Furthermore, Table 3 shows that the overall miss shot rate in 2021 was 11.7%, which exceeded 10%, but as a result of changing the imaging system to pre-shot for the high miss shot rate sites, the overall miss shot rate fell to 7.3% in 2022, suggesting the effectiveness of pre-shot.

4-5 Effects of pre-shot in the knee joint

Pre-shot is also a matter of radiographic technique, and we understand that there are many different opinions. This is not to say that we neglect radiographic technology, but we believe that pre-shots have a raison d'être when it comes to radiography where greater precision is required. In the case of the standing lateral view, the results of the measurement of the displacement of the internal and external condyles in Table 5 showed no significant differences before and after the start of the pre-shot. Table 6 also shows the results of the first shot verification. It was assumed that there would be a significant difference if the setting was inappropriate. However, no significant differences emerged. In the case of normal shoting

and in the case of pre-shoting, the first mistakes made in the first shot were the same in both normal and pre-shot cases. It was therefore denied that improper positioning had taken place. The average miss shot ratio of the standing lateral view before the pre-shot was more than 40% on the left and right sides, and the miss shot rate after the pre-shot was 5%, which was a significant improvement, suggesting that pre-shot should be actively used.

Similarly, in the supine lateral view, no significant differences were found between the results of the endocondyle and exocondyle measurements (Table 5). Table 6 verified the results for the 1st shot and found significant differences. The number of 1st shot misses increased after the start of pre-shots. The reason for this is that the tendency to repeat the pre-shot is due to the awareness of the need to make more adjustments and submit a better image because of the low dose. This was considered to be one of the reasons for the low awareness of re-shot. The percentage of 1st shot miss shots in the standing lateral view shown in Table 6 was 54.9%, whereas the percentage of errors in the lying lateral view was 52.0%, which is the same as the standing lateral view.

In the lying lateral view, the average left-right miss shot rate was around 25% (right 25.0%, left 27.9%) in 2021 before the start of the pre-shot shown in Table 2. Miss shot rate after the start of the pre-shot was around 10%, which is not effectively lower than in the standing lateral view. In addition, the proportion of misses increased in the 1st shot, and it was judged that aggressive use of pre-shot was less effective. It was considered preferable for use by new technicians in their first 1-3 years of employment, or only when accuracy is required, such as when imaging prostheses.

4-6 Pre-shots reduce radiation dose

If re-shot is required during normal shot, the normal shot is repeated. If the first shot fails, the normal shot is taken twice, which is twice as much exposure as if first shot succeeded. If a pre-shot is performed, even if the first shot fails, the incident surface dose can be significantly reduced by a factor of 1.16 by performing the pre-shot again and then the normal shot. However, for patients without re-shot, this can result in extra exposure. A patient with no re-shot means that the 1st shot was successful, in which case the exposure dose is 1.08 times higher. In our case, this increases from 0.052 mSv to 0.06 mGy.Detection efficiency is the same for CR and FPD because the imaging tube voltage in our hospital is in low voltage range [9]. It is therefore also available for CR systems. The average number of pre-shots per person since pre-shotting started is 1.8 and including the increased exposure dose in error-prone imaging, pre-shotting is considered to be a necessary system.

5. Conclusion

The present study investigates the incidence of miss shots in general radiography and examines the effectiveness of pre-shots for radiography menus with high miss shot rate.

In instances where the imaging exhibited a miss shot rate of more than 40%, such as in the standing lateral view of the knee joint, the active utilization of pre-shots was deemed more efficacious. This approach served to reduce the miss shot rate and forestall an escalation in the incident surface dose, a consequence of multiple shots attributable to errors.

Conversely, in instances where the miss shot rate is approximately 25%, such as in the lying lateral view of the knee joint, the utilization of pre-shots may merely augment the number of shots, thereby obscuring the efficacy of pre-shots. Consequently, the utilization of pre-shots is deemed advantageous in scenarios where enhanced reproducibility is imperative. The concept of reimaging is directly linked to imaging technology and given the current state

of FPD penetration and dose optimization, the usefulness of pre-shots has been confirmed.

6. Acknowledgement

We would like to express our gratitude to Junji Shinotsu, Head of the Central Radiology Department of Chugoku Rosai Hospital, and all the members of the Central Radiology Department of Asahi Rosai Hospital for their cooperation in conducting this study.

7. Conflicts of interest

The first author and all co-authors have no conflicts of interest to declare.

References

1) Hara, Sinji., et al.: Causes and countermeasures for missed shot films. Chugoku Rosai Hospital Medical Journal, Vol. 1, No. 1, 1992.
2) Servomaa A, et al.: Organ dose calculation in medical x ray examinations by the program PCXMC. Radiat Prot Dosim, 80(1–3), 213-219, 1998. doi:10.1093/oxfordjournals.rpd.a032509.
3) Japanese Society of Radiological Technology Supervision: radiographic technique (9-4_Knee joint - lateral view 269). Ohmsha, 2014.
4) Fukui Masayasu: College Analysis. https://sites.google.com/view/fukuimasayasu (Accessed 16.12.2023).
5) Hidaka, Kuniyuki, et al.: Gravity Sag View of Lateral Radiography of the Knee. Journal of the Japanese Society of Radiological Technology, 63(4), 412-419, 2007.
6) Ando Eiji: Radiography of TKA for radiological technologists to know Part 1 (Difference between CR and PS type implants). INNERVISION, 31(10), 82-85, 2016.
7) Ando, Eiji.: Radiography for TKA that radiological technologists need to know, Part 2 (on TKA frontal view of load radiography in the standing position). INNERVISION, 31(11), 90-94, 2016.
8) Ando Eiji: Radiography of TKA that radiological technologists should know, Part 3 (on TKA lying lateral view of non-loaded radiography by supine position). INNERVISION, 31(12), 72-76, 2016.
9) Kunitomo, Hiroshi., et al.: Physical Image Properties of Digital Radiography Systems in Low Dose Range. Journal of the Japanese Society of Radiological Technology, 68(8), 961-969, 2012.

Received April 3, 2024 ; accepted August 4, 2024

A novel image processing method incorporating calcification information by combining fresh blood imaging-magnetic resonance (MR) angiography with MR bone imaging in patients with lower extremity artery disease

NAKAYAMA Hidetoshi[1)]*, MORIMOTO Ryota[1)], FUKUNAGA Aya[1)], OGINO Kazuhide, MD, PhD[2)], KOBAYASHI Masami, MD, PhD[3)], MUKUDA Naoko, MD, PhD[3)]

1) Japanese Red Cross Tottori Hospital, Division of Radiological Technology
2) Japanese Red Cross Tottori Hospital, Department of Cardiology
3) Japanese Red Cross Tottori Hospital, Department of Radiology

* E-mail: wptmy939@ybb.ne.jp

Note: This paper is secondary publication, the first paper was published in the JART, vol. 71 no. 867: 41-48, 2024.

Key words: lower extremity artery disease (LEAD), fresh blood imaging (FBI) MRA, MR bone imaging, calcification, addition

【Abstract】
In this study, by applying summation processing to fresh blood imaging (FBI)-magnetic resonance angiography (MRA) and MR bone imaging, we hypothesized that a novel MRA image incorporating calcification information could be generated for patients with lower extremity artery disease (LEAD). We analyzed the percentage of additive processing between FBI-MRA and MR bone imaging. The addition ratio was varied in six LEAD cases; the contrast-to-noise ratio (CNR) between the arterial wall calcification, nearby muscle, and arterial lumen was measured. Mean CNR values improved between the arterial lumen and arterial wall calcification sites in all additive images. The higher the addition percentage, the higher the value between the arterial lumen and the muscle. Between the muscle and arterial wall calcification sites, the lower the addition percentage, the higher the value. A novel MRA image processing method incorporating calcification information was successfully developed, and a FBI-MRA addition of 12.5–3.125% was recommended.

1. Introduction

Lower extremity artery disease (LEAD), a subset of peripheral artery disease, is a chronic occlusive disease of the major arteries of the lower limbs, and is caused by arteriosclerosis. This condition is synonymous with lower extremity occlusive arteriosclerosis, which has traditionally been used as the diagnostic term[1, 2)].

Patients with LEAD frequently have comorbid chronic kidney disease, and vascular calcification is a characteristic feature of this disease[3)]. Furthermore, in patients undergoing dialysis, the severity of lower limb arterial calcification correlates with the clinical severity of LEAD[4)]. In endovascular treatment, the choice of the balloon and approach varies depending on the location of calcification[5)].

Thus, obtaining information on the location, extent, and positional relationship of the calcification with the artery is crucial for the treatment of LEAD.

Angiography has traditionally been considered the gold standard for the diagnosis of LEAD. However, owing to its invasiveness, it is rarely performed solely for diagnostic purposes. In recent years, non-invasive imaging modalities such as computed tomography (CT) and magnetic resonance

imaging (MRI), which are both convenient and highly reproducible, have been increasingly utilized because of their non-invasiveness[6].

Although CT angiography (CTA) requires contrast agents, it offers advantages over other imaging techniques by allowing the assessment of calcification levels, intramural thrombi, and extravascular lesions. In contrast, MR angiography (MRA) can be performed without contrast agents, making it a viable option for patients with renal impairment. However, MRA does not provide information on vascular calcification[7-9].

Among MRA techniques, fresh blood imaging (FBI)-MRA provides visualization of arterial stenosis and occlusion in the pelvic and lower limb arteries comparable to CTA, while also providing a clear depiction of the collateral circulation[10]. This technique utilizes electrocardiogram gating to exploit differences in signal intensity based on the blood flow velocity. During diastole, arterial blood flow slows, resulting in high signal intensity in fast spin echo sequences. Conversely, during systole, rapid blood flow promotes spin dephasing, creating flow voids within arteries. As venous blood flow remains slow during both systole and diastole, veins consistently exhibit high signal intensity. Arterial signals can be selectively extracted by subtracting the systolic image from the diastolic image [6].

Although a limitation of MRA is its inability to provide information on calcifications, it has traditionally been difficult to evaluate structures such as cortical bone surfaces, ligaments, tendons, and calcifications on MRI because these tissues appear as low-signal areas in the images. This is because such tissues contain only small amounts of water molecules, which serve as the primary signal source in MRI. Moreover, the water molecules present are primarily bound water, which exhibits highly restricted motion and extremely short T_2 relaxation times. For instance, the T_2 relaxation time of cortical bone at 3.0T is approximately 390 μs.

With conventional pulse sequences, the available echo time (TE) is in the range of several milliseconds. This delay in signal acquisition is too long, causing the rapidly decaying signal after radiofrequency irradiation to become undetectable, thereby rendering these structures as low-signal regions. However, a new imaging technique, MR bone imaging, developed to obtain calcification information using MRI, has garnered significant attention.

One approach to obtain information on calcification involves the gradient-echo (GRE) method. Because the cortical bone appears as a low-signal area in GRE imaging, post-processing techniques have been applied to invert the signal contrast, thereby rendering the bone as a high-signal structure. However, this inversion process also enhances other low-signal regions in the image, making it difficult to distinguish the bone from other structures. To address this issue, artifacts that contribute to low signal intensities, such as those caused by chemical shift effects, must be minimized. Therefore, MR bone imaging uses in-phase imaging.

Furthermore, to enhance signal intensity, multi-echo GRE methods, which acquire and sum multiple echoes in a single scan, are advantageous [11, 12].

1.1. Overview

By applying summation processing to FBI-MRA and MR bone imaging, we hypothesized that a novel MRA image incorporating calcification information could be generated. This approach enables visualization of vascular structures and calcifications in a non-contrast, non-invasive manner, potentially serving as a new diagnostic option for LEAD.

Therefore, in this study, we aimed to determine the optimal summation ratio, which is a key element of this image-processing technique.

2. Methods

2.1. Ethical Considerations

This study was reviewed and approved by the ethics committee of our institution (approval no. Reiwa 5-126).

2.2. Study Participants

The participants of this study were all patients (six cases: three males and three females) who underwent lower limb MRA for suspected LEAD between June 2022 and August 2023. The mean patient age was 81.2 ± 8.07 years.

2.3. Equipment

Imaging was performed using a 1.5T superconducting whole-body MR scanner (Vantage Titan ver.4.0, Canon Medical Systems, Tochigi, Japan). A 32-channel spine coil and a 16-channel body coil were used as the receiving coils. Additionally, a workstation (Ziostation2 Plus, Ziosoft, Tokyo, Japan) was used to generate curved planar reconstruction images.

2.4. Imaging Parameters

For MR bone imaging, a field echo 3D sequence with multi-echo acquisition was used with the following parameters: repetition time, 18 ms; TE, 4.6/9.2/13.8 ms; flip angle (FA), 7°; fat suppression, off; field of view (FOV), 40/42 cm, matrix 256/256; slice thickness, 2 mm; and number of acquisitions (NAQs), 1.

For FBI-MRA, a fast advanced spin-echo 3D sequence combined with the short TI inversion recovery method was used with the following parameters: TR, 2908 ms; TE, 80 ms; FA/flop angle, 90/150;, inversion time (TI), 130 ms; black blood TI, off; FOV, 40/42 cm, matrix, 256/256; slice thickness, 3 mm; and NAQs, 1.

For summation processing, FBI-MRA images were reconstructed with a slice thickness of 2 mm to match the MR images.

2.5. Image Positioning

Summation processing was performed using MR bone imaging and FBI-MRA. For effective summation processing, obtaining arterial images with clear differentiation on FBI-MRA is essential. To achieve this, venous structures must also be stably visualized, allowing precise subtraction of veins from the combined arterial and venous images.

FBI-MRA is an imaging method that utilizes signal intensity differences between systole and diastole, where both arteries and veins appear as high-signal regions when blood flow is slow [13]. Therefore, to reduce the effects of decreased peripheral blood flow velocity in the target veins and to minimize flow void artifacts, mild compression fixation was applied to the epigastric and abdominal regions.

To reduce the number of imaging slices, cushions were used during positioning to maintain uniform lower limb height. However, to avoid compression of posterior running vessels, such as the popliteal vein, and ensure stable venous visualization across systole and diastole, care was taken to prevent excessive pressure on these structures.

Previous studies have reported that blood flow velocity is affected by the body position[14]. When the feet are internally rotated, tension in the thigh adductor muscles may increase, potentially compromising venous visualization stability. Therefore, the feet are positioned externally.

Additionally, to minimize motion artifacts caused by respiration, spacers were placed between the patient and coil, in addition to compression fixation, to ensure that the coil did not come into direct contact with the patient.

2.6. Measurement Method

The acquired MR bone and FBI-MRA images were processed using a built-in application to generate summation images based on the following equation:

Additional image = A + B/x ····· (1),

where A represents MR bone imaging and B represents FBI-MRA.

To evaluate the effect of the summation ratios, the value of x was varied, and the signal intensity of FBI-MRA was reduced to 100%, 50%, 25%, 12.5%, 6.25%, and 3.125% of the original intensity before summation (Fig. 1).

For the generated summation images, ImageJ (National Institutes of Health, Bethesda, MD) was used to analyze all 6 cases at 54 locations

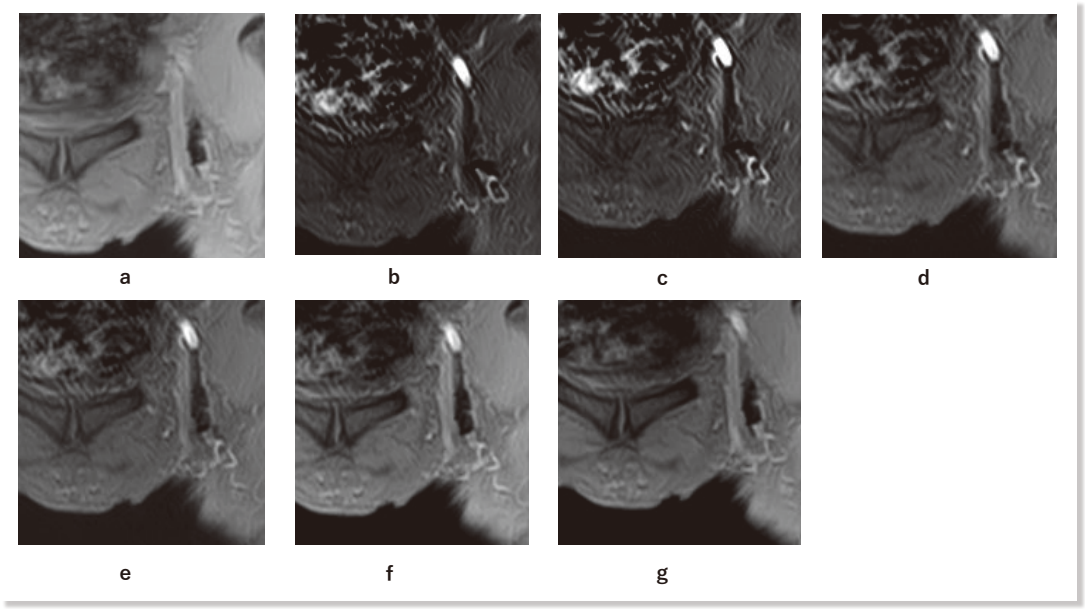

Fig. 1 MR bone imaging and FBI-MRA images with the ratio of addition varying from b-g.

a: No addition, b: 100% addition, c: 50% addition, d: 25% addition, e: 12.5% addition, f: 6.25% addition, and g: 3.125% addition.

FBI, fresh blood imaging
MRA, magnetic resonance angiography
MR, magnetic resonance

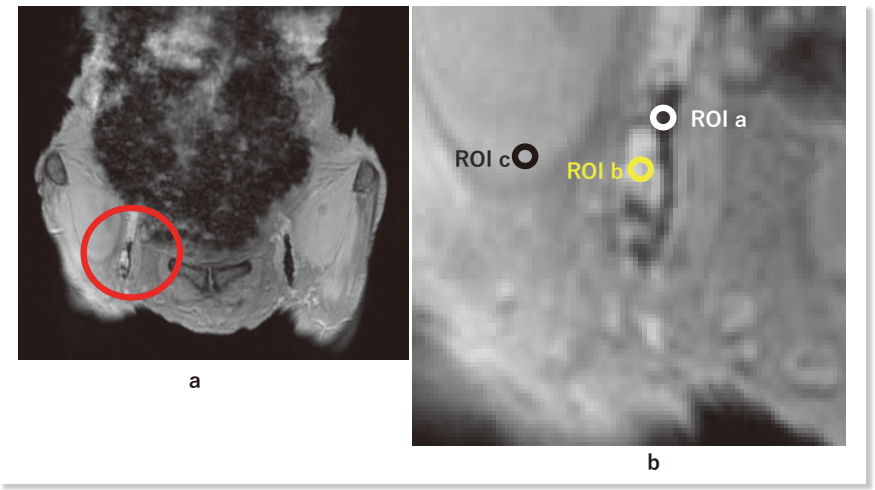

Fig. 2 CNR measurement points in the tissues.

a: Original additive image. b: Enlarged view of the measurement range.
ROI a: calcified area, ROI b: arterial lumen, and ROI c: muscle.

CNR, contrast-to-noise ratio
ROI, region of interest

(all within the superficial femoral artery). For each location, three regions of interest (ROIs) were defined: the arterial wall calcification site (a), adjacent muscle (b), and arterial lumen (c). The mean signal intensity and standard deviation were measured for each ROI. The measurement points for contrast-to-noise ratio (CNR) analysis are shown in Fig. 2.

Based on the measurement results, the CNR values were calculated for the following tissue comparisons.

1. Between the arterial lumen and arterial wall calcification site
2. Between the arterial lumen and muscle
3. Between the muscle and arterial wall calcification site

CNR evaluation was performed using the following equation: [15]

$$\text{CNR (root mean square)} = |S_A - S_B| / \{ (SD_A^2 + SD_B^2)/2 \}^{1/2} \quad \cdots\cdots\cdots (2),$$

where S_A and S_B represent the mean signal intensities of the two ROIs being compared, and SD_A and SD_B represent their respective standard deviations.

To assess whether significant changes occurred in each summation image compared with MR bone imaging alone, multiple comparison testing was performed using the Steel test. The significance level was set at $p < 0.05$.

2.7. Image Interpretation

Based on the study results, summation images with inversion processing were generated, and image interpretation was performed for one patient with LEAD (an 86-year-old female).

3. Results

A graph based on the CNR measurement results for the arterial lumen and arterial wall calcification site is shown in Fig. 3. Compared with MR bone imaging without summation, all FBI-MRA summation images showed improved CNR. The summation image with FBI-MRA at 6.25% yielded the best results. The mean CNR value of MR bone imaging without summation was 9.53 ± 4.74, whereas that of the FBI-MRA 6.25% summation image was 12.45 ±

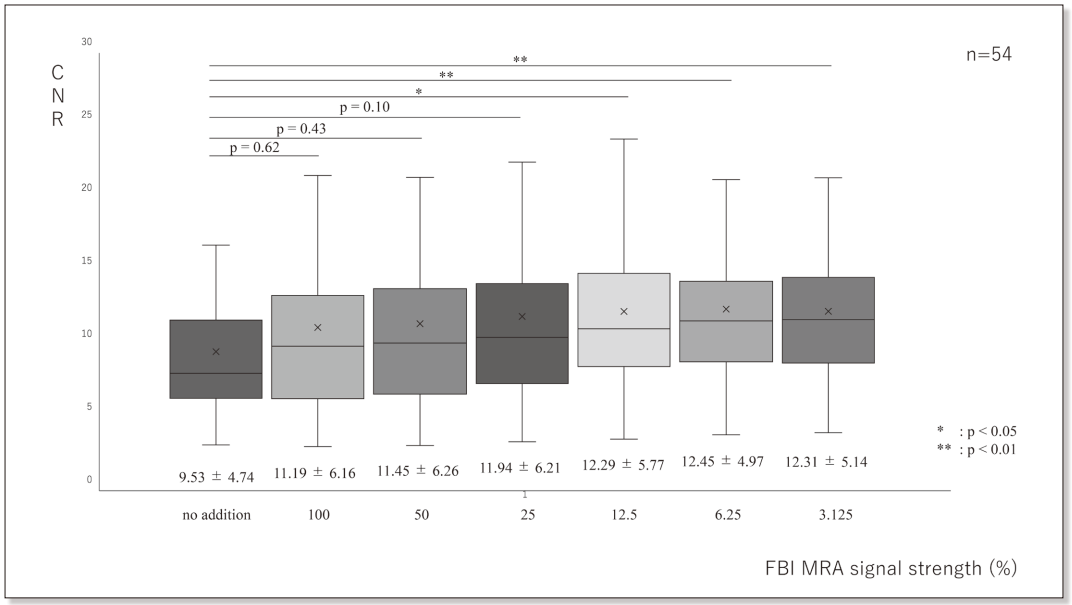

Fig. 3 CNR of the arterial lumen and arterial wall calcification.
CNR, contrast-to-noise ratio

4.97. Statistical testing revealed significant differences in summation images with FBI-MRA at 12.5% or lower.

A graph based on the CNR measurement results for the arterial lumen and muscle is shown in Fig. 4. The mean CNR value of MR bone imaging without summation was 3.59 ± 3.11, whereas all FBI-MRA summation images showed a substantial increase in the CNR. Higher summation ratios of FBI-MRA resulted in higher CNR values, with the FBI-MRA 100% summation image achieving the highest CNR (15.02 ± 11.80). However, statistical testing indicated significant differences among all the combinations.

A graph based on the CNR measurement results for the muscle and arterial wall calcification site is shown in Fig. 5. The

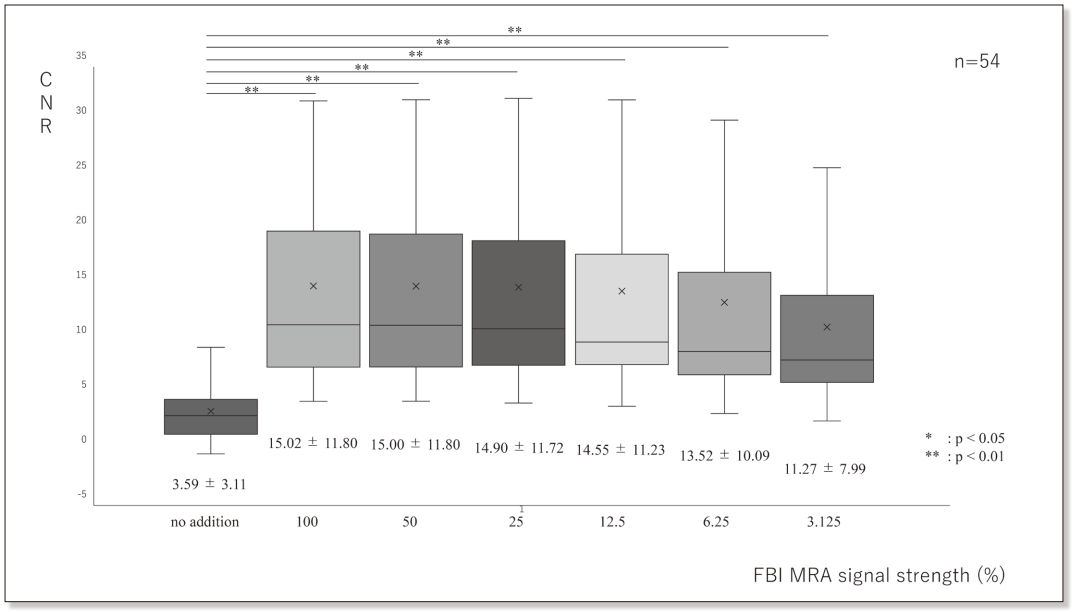

Fig. 4 CNR of the arterial lumen and muscle.

CNR, contrast-to-noise ratio

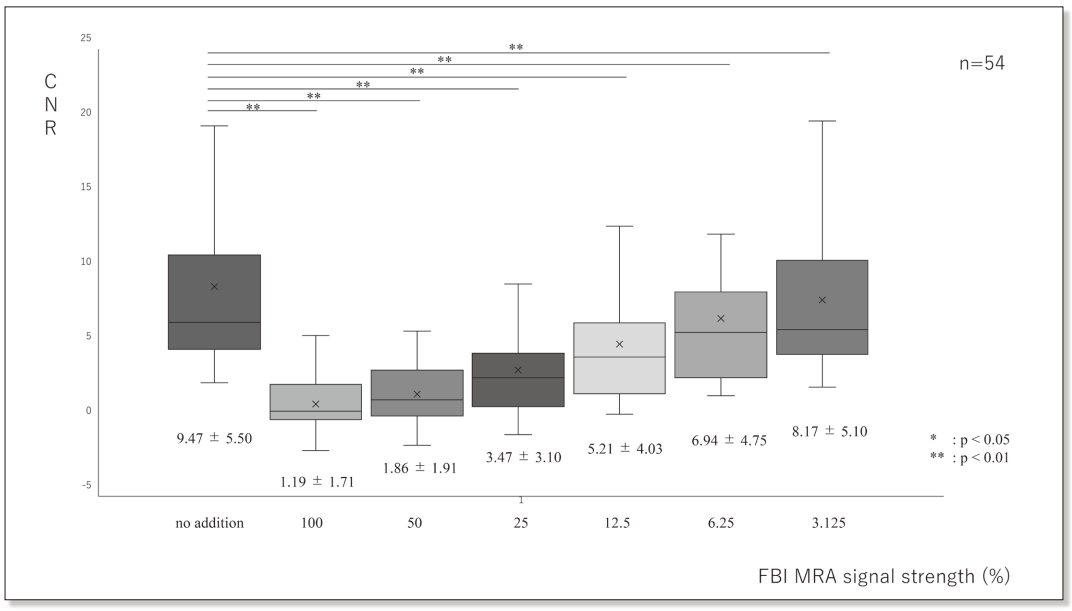

Fig. 5 CNR of the muscle and arterial wall calcification.

CNR, contrast-to-noise ratio

mean CNR value of MR bone imaging without summation was 9.47 ± 5.50, whereas all FBI-MRA summation images exhibited a decrease in the CNR. Statistical testing revealed significant differences among all the combinations. However, lower summation ratios of FBI-MRA resulted in higher CNR values, with the FBI-MRA 3.125% summation image showing a CNR of 8.17 ± 5.10.

The case was analyzed using summation images with inversion processing based on the study results. The patient was an 86-year-old female with aortic and mitral valve stenoses. She first visited our hospital in 2015 because of a cold sensation in her left lower limb, and CTA confirmed the diagnosis of LEAD. She continued treatment at another hospital, but returned to our institution in 2023. Owing to renal function deterioration, MRA was performed instead of CTA. MRA revealed a 4.25 cm-long segment in the left common femoral artery that was not visualized, corresponding to a previously confirmed calcified stenotic lesion on CTA (Fig. 6, arrow).

Fig. 7 shows MR bone images before and after summation at the same site. In MR bone imaging without summation (Fig. 7a), calcification of the left femoral artery was visible; however, its relationship with the artery was unclear. In contrast, in the summation image (Fig. 7b), both the artery and calcifications were clearly visualized, making it easier to assess their positional relationship. Complete arterial occlusion due to calcification (Fig. 7b, arrow) was also confirmed.

Additionally, the ventral slice in Fig. 8 shows the collateral circulation that developed around the calcified segment (Fig. 8a, arrow). This collateral vessel was not observed on the previous CTA (Fig. 8c, arrow), suggesting that it was newly developed.

Summation images of the right femoral artery of the same patient are also presented. The short-axis view of the arterial calcification site

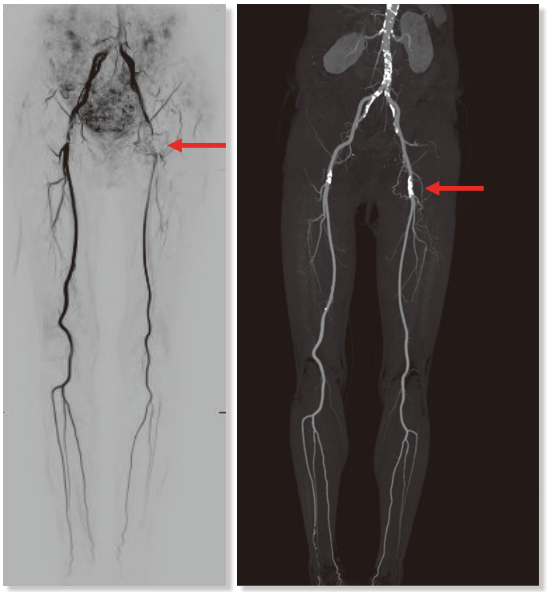

a b

Fig. 6 Overall view of the lower extremity of a patient.

a: Non-contrast FBI-MRA image obtained during examination.
b: Contrast-enhanced CTA image obtained in 2015.

FBI, fresh blood imaging
MRA, magnetic resonance angiography
CTA, computed tomography angiography

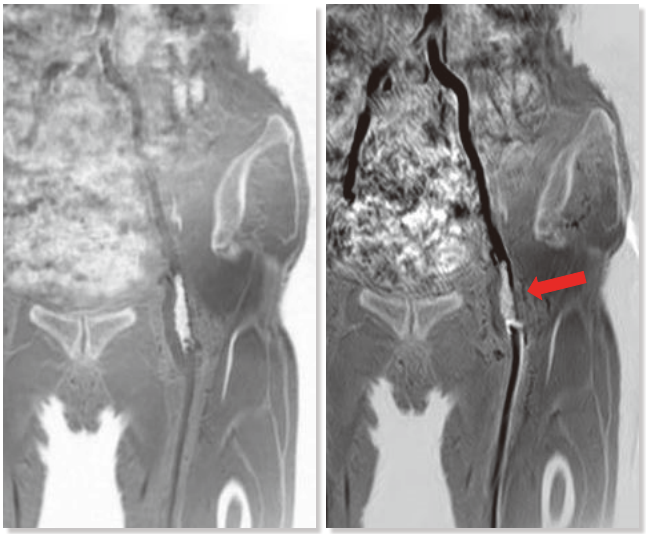

a b

Fig. 7 CPR image of the left femoral artery.

a: MR bone image. b: Additive image.

MR, magnetic resonance

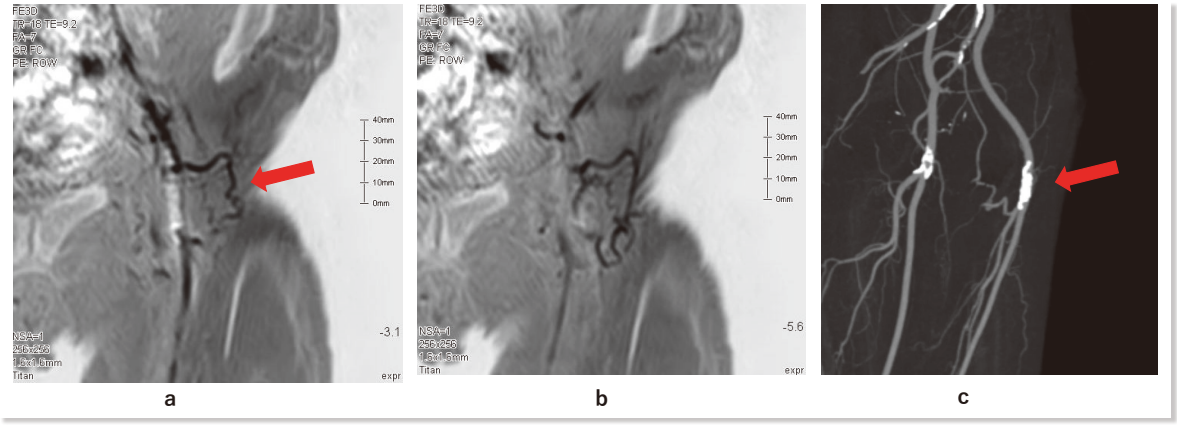

Fig. 8 a, b: Collateral vessels developed by bypassing the calcified left femoral artery.
c: Contrast-enhanced CTA in 2015.
CTA, computed tomography angiography

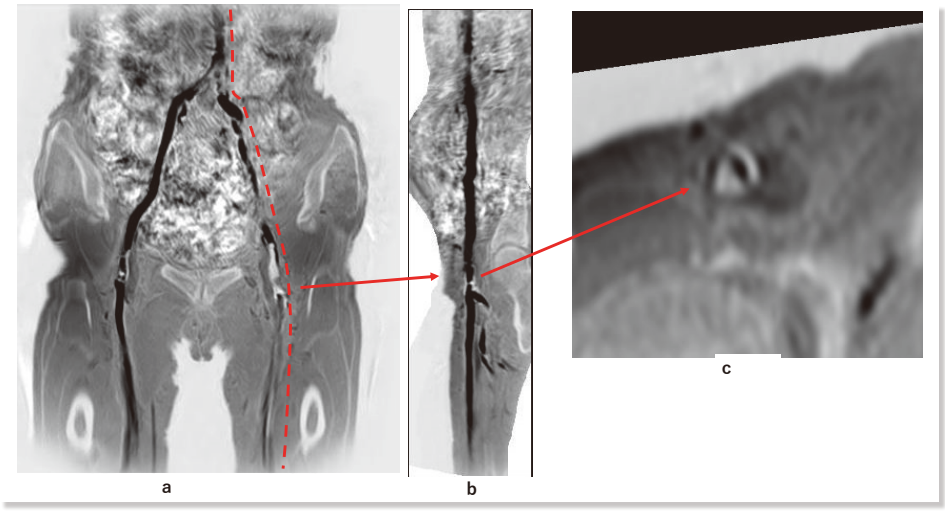

Fig. 9 a: CPR image of the right femoral artery. b: Straight view. c: Axial image.

in the right common femoral artery showed circumferential calcification with an artery running through the lumen, indicating that the vessel was stenotic, but not completely occluded (Fig. 9).

4. Discussion

In this study, the CNR between the arterial lumen, arterial wall calcification site, and muscle was evaluated to determine the optimal summation ratio.

Between the arterial lumen and arterial wall calcification site, the CNR improved in all summation images; however, the changes due to summation ratios were smaller than those observed between the arterial lumen and muscle or between the muscle and arterial wall calcification site. No significant differences were observed between FBI-MRA summation images (100%, 50%, or 25%) and MR bone images without summation. This is likely because MR bone imaging represents calcifications as low-signal regions [12], allowing sufficient CNR between the arterial lumen and calcifications, even without summation.

The CNR between the arterial lumen and muscle increased in all summation images. Lower summation ratios of FBI-MRA resulted in lower CNR values, but even in the FBI-MRA

3.125% summation image (11.27 ± 7.99), the CNR remained higher than that of MR bone imaging without summation (3.59 ± 3.11). Significant differences were observed in all comparisons, likely due to the contribution of arterial signals from FBI-MRA to MR bone imaging [6].

The CNR between the muscle and arterial wall calcification site decreased in all summation images. FBI-MRA extracts arterial signals by subtracting diastolic images from systolic images, canceling out other signals, and making them part of the background signal [16, 17]. Consequently, in summation images with MR bone imaging, non-arterial tissues become part of the background signal. This likely explains why the muscle, when summed with background signals, appeared as a low-signal region, reducing the CNR relative to the arterial wall calcification site, which is already represented as a low-signal region in MR bone imaging. Significant differences were observed in all summation images, with lower summation ratios of FBI-MRA yielding higher CNR values.

Considering these results:

1. Between the arterial lumen and arterial wall calcification site, significant differences in the CNR were observed at FBI-MRA summation ratios of 12.5% or lower.
2. Between the arterial lumen and muscle, higher summation ratios of FBI-MRA resulted in higher CNR values; however, the CNR improved in all summation images.
3. Between the muscle and arterial wall calcification site, lower summation ratios of FBI-MRA resulted in higher CNR values.

Based on these findings, an FBI-MRA summation ratio of 12.5–3.125% was considered as the recommended setting for generating summation images.

However, the optimal FBI-MRA summation ratio may be influenced by factors such as blood flow and the extent of calcification in individual patients. Given the small sample size in this study, it may be necessary to adjust the summation ratio on a patient-by-patient basis.

4.1. Clinical usefulness

This study demonstrated that FBI-MRA summation improved the CNR of arteries. In contrast, for calcifications, the CNR decreased compared with MR bone imaging without summation, suggesting that the original images should also be included in the evaluation.

The limitations of this study include the small sample size and lack of comparison with conventional imaging methods, such as angiography, CTA, or non-summation MRA, for vascular calcification assessment.

4.2. Conclusion

A novel MRA image processing method incorporating calcification information was successfully developed by combining FBI-MRA with MR bone imaging. This technique has the potential to be a new diagnostic option for LEAD.

Conflicts of Interest

The authors declare no conflicts of interest related to this study.

Acknowledgments

We express our gratitude to **Takashi Okikawa (Saiseikai Kumamoto Hospital), Hiroya Aso (Shimane University Hospital), and the organizers of the Tottori BIRT Meeting** for their valuable support and encouragement in publishing this study. *ke to thank Editage (www.editage.jp) for English language editing.*

References

1) The Japanese Circulation Society, The Japanese Society for Vascular Surgery, 2022. Revised Edition of the Peripheral Artery Disease Guidelines. 10. https://www.j-circ.or.jp/cms/wp-content/uploads/2022/03/JCS2022_Azuma.pdf, accessed on 2023-10-13.
2) Mochizuki Y, et al.: Lower extremity occlusive artery disease. Rinsho Zasshi Naika (Journal of Clinical Internal Medicine), 132, 742-743, 2023.
3) Moriya H, et al.: Lower extremity peripheral artery lesions. Jin to Toseki (Kidney and Dialysis), 95, 301-306, 2023.
4) Ohtake T, et al.: Impact of lower limbs' arterial calcification on the prevalence and severity of PAD in patients on hemodialysis. Journal of Vascular Surgery (J Vasc Surg), 53, 676-683, 2011.
5) Osawa S, et al.: Invasive treatment. Rinsho Toseki (Journal of Clinical Dialysis), 31, 937-939, 2015.
6) Nakamura K, et al.: How much can MRA reveal about peripheral arteries? – Comparison with CT and the efficacy of non-contrast MRA. Junkanki Journal, 67, 454, 2019.
7) Omori H, et al.: CT and MRI for cardiovascular diseases related to hemodialysis. Rinsho Gazou (Clinical Imaging), 36, 1151, 2020.
8) The Japanese Circulation Society, The Japanese Society for Vascular Surgery, 2022. Revised Edition of the Peripheral Artery Disease Guidelines. 18. https://www.j-circ.or.jp/cms/wp-content/uploads/2022/03/JCS2022_Azuma.pdf, accessed on 2023-10-13.
9) Yamashita Y: Powerful guide to diagnostic imaging for generalists, 341, Medical Science International, 2014.
10) Nakamura K, et al.: Noncontrast-enhanced peripheral MRA: Technical optimization of flow-spoiled fresh blood imaging for screening peripheral arterial diseases. Magnetic Resonance in Medicine (Magn Reson Med), 65, 595-602, 2011.
11) Hamano Y, et al.: Fundamentals and approach of MR bone imaging based on MR signals. Rinsho Gazou (Clinical Imaging), 39, 435-436, 2023.
12) Ikeda K, MR: Bone imaging – From GRE method to ZTE method. Rinsho Gazou (Clinical Imaging), 39, 442-443, 2023.
13) Araki R: Definitive Edition: Complete MRI 2nd Edition. 613-615, Gakken Medical Shujunsha, 2015.
14) Watanabe M: Fundamental study on the usefulness of non-contrast lower limb MRV using the 2D-spiral GRE method and the effects of different imaging positions on lower limb venous visualization. Nichibo Gijutsu Gaku Shi (Japanese Journal of Radiological Technology), 68, 841-850, 2012.
15) Protocols and test objects for the assessment of MRI equipment. EEC Concerted Research Project. Magnetic Resonance Imaging (Magn Reson Imaging), 6, 195-199, 1988.
16) Miyazaki M, et al.: Peripheral MR angiography: separation of arteries from veins with flow-spoiled gradient pulses in electrocardiography-triggered three-dimensional half-Fourier fast spin-echo imaging. Radiology, 227, 890-896, 2003.
17) Miyazaki M, et al.: Nonenhanced MR angiography. Radiology, 248, 20-43, 2008.

Regulations and Requirements for Submissions to the Journal of the Japan Association of Radiological Technologists

Submission Regulations

Revised: April 1, 2013
October 30, 2013
February 20, 2016
April 20, 2019
October 3, 2020
July 9, 2022
December 3, 2022

Objective

Article 1. These regulations are based on the operations defined in Article 4 of the articles on the incorporation of the Japan Association of Radiological Technologists (hereafter "the Association"). They stipulate the criteria for submissions to the Journal and informational magazines published by the Association (hereafter "the Journal, etc.").

Eligibility

Article 2.

2-1. Only members of this association are allowed to submit articles to the association's journal, etc.

2-2. However, the following requirements must be met in order to submit articles:

(1) Students of radiologic technology schools who have a member of this association as a co-author.

(2) Individuals with a foreign nationality who hold a radiologic technologist license.

(3) Non-members other than the above may submit articles by paying half of the association membership fee per article as a submission fee.

2-3. The submission fee stated in the preceding paragraph 3 will not be refunded regardless of whether the article is accepted or not.

2-4. Co-authors do not need to pay the submission fee.

Copyright

Article 3. The copyright of the published manuscript is based on rules regarding the management of the works of the Society.

Obligations

Article 4.

4-1. The topic of submitted manuscripts must belong to a relevant domain to technologies for prevention, diagnosis, and treatment related to radiation therapy, and manuscripts must be unpublished.

4-2. Submitted papers, whether for fundamental or applied research, must sufficiently consider bioethics, and authors must bear the ultimate responsibility for their content.

4-3. Fabrication, forgery, plagiarism, violation of the law, and other forms of wrongdoing are not allowed in submissions.

4-4. If the author has already reported similar content to that of the published manuscript or submitted it to another journal, the author is required to explain the difference from the manuscript in a separate document.

4-5. The author must disclose all information regarding conflicts of interest.

4-6. The author shall be held accountable for any misconduct regarding the content of the publication, and the Society shall not be involved at all.

Submissions

Article 5. The types of accepted submissions are categorized as follows:

(1) Original articles
Highly original research papers with clear objectives and conclusions.

(2) Review articles
Articles systematically summarizing a specific research domain from a particular perspective.

(3) Rapid communications
Reports of original research that must be published rapidly.

(4) Reports
Surveys of significance to the study of radiological technology or reports of interesting and

important cases.

(5) Notes

Articles on the development or evaluation of new equipment, techniques, products, etc.

(6) Technical material

Compilations of survey data or technical aspects, or anything that can serve as a reference for research and technology.

(7) Overview articles

A compilation of technologies, principles, or basic elements with reference to the literature. However, what was explained in the development and use of equipment and software constitutes a technical explanation.

(8) Miscellaneous

Other items approved by the editorial committee for publication, such as lecture transcripts, courses published as journal articles, and newspaper/magazine articles that were not published in Issues 1–7.

How to submit

Article 6.

6-1. Use the online posting system.

6-2. The author shall save the duplicate data of the submitted manuscript until the publication decision.

Formatting

Article 7. The explanation of the manuscript shall be provided according to the submission procedure specified separately.

Reception of submissions

Article 8. The reception date shall be the date on which the editorial board has determined to comply with this regulation.

Review

Article 9.

9-1. Received manuscripts will be reviewed carefully and impartially by peer-reviewers selected by the editorial committee.

9-2. Peer reviews are limited to two times. However, in the case of Article 5, items 7 and 8, in principle, peer review is not performed.

9-3. The acceptance or rejection of the manuscript will be decided by the editorial committee in consideration of the opinions of the reviewers, and the date will be the final acceptance date.

Corrections

Article 10.

10-1. In principle, the author must proofread the manuscript up to twice and return it by the designated date. If the deadline is breached, the school will be completed with the proofreading of the editorial board.

10-2. The correction of words and plates that were not included in the manuscript is not allowed.

Printing

Article 11.

11-1. 20 copies of the papers published in the Journal, etc., will be presented to their authors as an offprint.

11-2. The authors must bear the expenses of any additional offprints. If additional offprints are required, they must be requested by the time corrections are submitted.

Revision or repeal of regulations

Article 12.

12-1. This regulation will come into effect on April 1, 2012.

12-2. This regulation will come into effect on April 1, 2016.

12-3. This regulation will come into effect on April 20, 2019.

12-4. This regulation will come into effect on October 3, 2020.

12-5. This regulation will come into effect on July 9, 2022.

12-6. This regulation will come into effect on December 3, 2022.

Requirements for Submissions to the Journal of the Japan Association of Radiological Technologists

Revised: February 20, 2016
April 20, 2019
October 3, 2020
July 19, 2023

Based on Article 7 of the Submission Regulations of the Japan Association of Radiological Technologists, the following guidelines must be followed for manuscript submission:

1. How to write original articles, reviews, breaking news, reports, notes, materials, and explanations

1) Title and abstract

Enter the following items in the online posting system.

①List the author's name, institution, affiliation and occupation, and select the field of expertise. The author's qualifications should be as specified in the submission guidelines.

②Select the type of post.

③Provide the title in both Japanese and English, and include information about the co-authors. List the co-authors in the order of authorship. If a co-author is not a radiological technologist, their qualifications should be as specified in the submission guidelines.

④Summarize the abstract in Japanese and English within 300 characters (words).

⑤Enter the keywords in English. Keywords should be in noun forms and should be limited to five.

2) Text and figures/tables

Create the main text, including figures and tables, in a single file. Additionally, prepare figures and tables as separate files and submit them.

①The manuscript should be in Japanese or English.

Create the document using Word with A4 paper size. Use Mincho font for Japanese text and Times font for English text, both at 12 points. Set the line spacing to 18 points. Leave a margin of at least 2 cm on all sides (top, bottom, left, and right).

②The specified number of pages and excess page costs of the manuscript are as shown in the following table.

Type of submission	Number of pages (as published)	Fee for additional pages
Original articles	8	¥10,000 per page
Review articles	8	
Rapid communications	3	
Reports	3	
Notes	8	
Technical material	8	
Overview articles	8	
Technical overview articles	4–6	None
Miscellaneous	2 (strictly enforced)	

③As a general rule, academic terms should conform to Cabinet Notification No. 2 and JIS.

④The unit of quantity is the International System of Units (SI).

⑤Include page numbers and line numbers in the main text.

⑥Use ", " and ". " for punctuation.

⑦Use full-width characters for Katakana and half-width characters for English letters and numbers.

⑧The main text should be structured with headings such as Introduction, Methods, Results, Discussion, Conclusion, and References.

⑨For equipment, include the generic name, model, manufacturer, city, and country.

⑩Number the equations.

⑪The figures and tables created as separate files from the main text are of higher resolution and can be subjected to secondary processing in production.

⑫Number the figures and tables.

⑬Ensure that all figure and table numbers are referenced in the main text.

⑭For academic papers, write the titles of figures and tables, as well as the text within the tables, in English.

⑮Provide Japanese explanations for figures and tables.

⑯When reproducing figures and tables, clearly indicate the source and ensure that the author has obtained permission from the original source.

3) References

References should be listed in the order in which they appear, with the numbers in parentheses at the end of the referenced text.

The notation format is as follows.

①For magazines

Author names: Title (article title) Magazine name (abbreviation), volume, first-last page, year of publication.

②For a book

Author names: Book title, First-last page, publisher, year of publication.

③If there are two or more authors, enter only the first author and enter “other” and “et al.”

4) Trademark name

If a trademark name is required, write the trademark name in both parentheses after the common name and add ®.

5) Acknowledgments

Create a separate file from the main text for the acknowledgments.

2. Submission of copyright transfer agreement

(1) The first author and co-authors must agree to the contents of the copyright transfer agreement as specified in the copyright regulations.
(2) The copyright transfer agreement should be as specified in the copyright regulations, and the designated form available on the society's website must be used.
(3) The copyright transfer agreement must be signed by the first author and co-authors, and provided when the manuscript is submitted.

3. About secondary publication

(1) Obtain approval from the editorial departments of both the first and second journals.
(2) The period until the secondary publication should be decided through discussions between the editorial departments of both parties and the author.
(3) Secondary publications of treatises are intended for different types of readerships.
(4) The secondary publication of a treatise should faithfully reflect the content of the first treatise.
(5) Specify the source of the original treatise.
(6) Specify in the title that it is a secondary publication.

4. About technical commentary requested by the editorial board

The structure of the document should generally follow the sections (1) to (9) below.

(1) Abstract (100-150 words in Japanese and English)
(2) Keywords (3 words)
(3) Introduction:
(4) Purpose of explanation (overview)
(5) Main paper
(6) Comparison and consideration with previous research (development technology)
(7) Clinical usefulness
(8) Conclusion
(9) References

Journal of JART
-English edition 2025-

June 13, 2025

Issuer: Ueda Katsuhiko
Publisher: The Japan Association of Radiological Technologists
22F Mita Kokusai Building. 1-4-28,
Mita, Minato-ku, Tokyo. 108-0073
TEL: +81-3-4226-2211　FAX: +81-50-3153-1519
https://www.jart.jp

・Published by The Japan Association of Radiological Technologists

The Japan Association of Radiological Technologists
https://www.jart.jp